Table of contents

List of figures

List of tables

Notation and Symbols

Symbol/Notation	Meaning	Units
Notation and acronyms		
AOB	Ammonia oxidising bacteria	
AS	Activated sludge	
ATP	Adenosine triphosphate	
BNR	Biological nitrogen removal	
COBRA	Constrained based reconstruction and analysis	
COD	Chemical oxygen demand	mg-O_2/L
DEN	Heterotrophic denitrifiers	
DO	Dissolved oxygen	mg/L or mmol/L
DW	Gram of dry weight biomass	gDW
e^-	Electron	mol
e^-eq.	Electron equivalent	mol
FBA	Flux balance analysis	
FISH	Fluorescent in-situ hybridization	
GC	Gas chromatography	
KEGG	Kyoto encyclopaedia of genes and genomes database	
HRT	Hydraulic retention time	d
IPCC	International panel for climate change	
LP	Linear programming	
MMC	Mixed microbial culture	
MRE	Mean relative error	Analysed variable units
MS	Mass spectrometry	
N_2	Molecular nitrogen	
N_2O	Nitrous oxide	
NADH	Reduced nicotinamide adenine dinucleotide	
NH_2OH	Hydroxylamine	
NH_4^+	Ammonium	
NO	Nitric oxide	
NO_2^-	Nitrite	
NO_3^-	Nitrate	
NOB	Nitrite oxidising bacteria	
NET	Network embedded thermodynamic analysis	
PAPi	Pathway activity profiling algorithm	
PLS-DA	Partial Least Squares Discriminant Analysis	
RS	Monte Carlo random sampling	

RMSE	Root mean squared error	
S_A	PAPi algorithm activity score	
SMN	Stoichiometric metabolic network	
sAUR	Specific ammonium uptake rate	mmol-N/gCOD*h or mmol-N/gDW*h
sN_2OPR	Specific N_2O production rate	mmol-N/gCOD*h or mmol-N/gDW*h
sOUR	Specific oxygen uptake rate	mmol-O_2/gCOD*h or mmol-O_2/gDW*h
SRT	Sludge retention time	d
std	Standard deviation	Same units as data
TSS	Total suspended solids	mg/L
V	Reactor working volume	L
VFA	Volatile fatty acids	
VSS	Volatile suspended solids	mg/L
WWTP	Wastewater treatment plant	
R^2	coefficients of determination	
m	Slope value in linear equation	

Symbols

Q	Inflow rate	L/d
S	Stoichiometric matrix. Has dimensions m rows x n reactions	
n	Number of reactions (columns) in S matrixs	
m	Number of metabolites (rows) in S matrixs	
J	Total number of reactions that consume or/and produce the compound i	
a	element's number of atoms in compound i	
X^k	Biomass concentration of modelled species/guild k	gDW/L, gVSS/L
X_l	Calibration dataset vector from experiment	
x_l	Calibration dataset vector estimated by SMN model	
x_{ij}	Relative abundance of metabolite i in sample j	
$\bar{X}_i$	Mean relative abundance of metabolite i	
l	Variable ID in calibration dataset	
S_i or X_i	Concentration of metabolite i	mmol/L or mg/L
s_{ij}	Stoichiometric coefficient of metabolite i in reaction j	
v	Vector of reaction rates	mmol/h or mmol/gDW*h
v_j	Reaction rate (flux) of reaction j	mmol/h or mmol/gDW*h
α_j	Lower limit of reaction rate (flux) of reaction j	mmol/h or mmol/gDW*h
β_j	Upper limit of reaction rate (flux) of reaction j	mmol/h or mmol/gDW*h
Z	Objective function reaction of optimization problem	
f^k	Fraction of species k in biomass	fraction, from 0 to 1

j	Model's reaction ID	
i	Model's metabolite ID	
k	Model's microbial species/guild ID	
v^k	Vector of fluxes estimated for species/guild k	
P	Matrix of reaction rates estimated with random sampling simulation. Has the dimension n x p	
M	Matrix of v solutions from candidate models. Has dimensions n x d	
d	Number of solutions in M matrix	
n	Number of reactions in sample in RS simulation	
p	Number of samples acquired by random sampling simulation	
[e]	Compound label to indicate its occurrence in extracellular space	
[p]	Compound label to indicate its occurrence in periplasmic space	
[c]	Compound label to indicate its occurrence in cytoplasmic space	
$S_{z_i}^{\sigma}$	Sensitivity coefficient	
σ	Standard deviation in sensitivity test	Same units as data
z_i	Vector of the model's input values for the *i* variable tested in sensitivity test	
Y	Vector of values of estimated calibration variables in sensitivity test	
$\frac{\partial Y}{\partial Z_i}$	Derivative term representing an estimated slope between Y and z_i vectors in sensitivity test	

THE UNIVERSITY OF AUCKLAND
SCHOOL OF GRADUATE STUDIES

Co-Authorship Form

Graduate Centre
ClockTower – East Wing
22 Princes Street, Auckland
Phone: +64 9 373 7599 ext 81321
Fax: +64 9 373 7610
Email: postgraduate@auckland.ac.nz
www.postgrad.auckland.ac.nz

This form is to accompany the submission of any PhD that contains research reported in published or unpublished co-authored work. **Please include one copy of this form for each co-authored work**. Completed forms should be included in all copies of your thesis submitted for examination and library deposit (including digital deposit), following your thesis Acknowledgements.

Please indicate the chapter/section/pages of this thesis that are extracted from a co-authored work and give the title and publication details or details of submission of the co-authored work. Corresponds to Chapter Two, Section 2.8. Perez-Garcia, O., Villas-Boas, S., Singhal, N. 2014. A method to calibrate metabolic network models with experimental datasets. Proceedings of the 8th International Conference on Practical Applications of Computational Biology & Bioinformatics. Springer Series: Advances in Intelligent and Soft Computing 294, 183-190.

Nature of contribution by PhD candidate	Computational techniques development, data analysis and manuscript write-up
Extent of contribution by PhD candidate (%)	85%

CO-AUTHORS

Name	Nature of Contribution
Dr. Silas Villas-Boas	Technical review and advice
Dr. Naresh Singhal	Technical review and advice

Certification by Co-Authors

The undersigned hereby certify that:

- the above statement correctly reflects the nature and extent of the PhD candidate's contribution to this work, and the nature of the contribution of each of the co-authors; and
- in cases where the PhD candidate was the lead author of the work that the candidate wrote the text.

Name	Signature	Date
Dr. Silas Villas-Boas	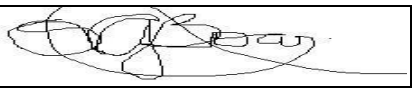	7/08/2014
Dr. Naresh Singhal	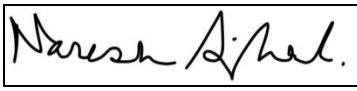	4/08/2014
		Click here
		Click here
		Click here
		Click here

THE UNIVERSITY OF AUCKLAND
SCHOOL OF GRADUATE STUDIES

Co-Authorship Form

Graduate Centre
ClockTower – East Wing
22 Princes Street, Auckland
Phone: +64 9 373 7599 ext 81321
Fax: +64 9 373 7610
Email: postgraduate@auckland.ac.nz
www.postgrad.auckland.ac.nz

This form is to accompany the submission of any PhD that contains research reported in published or unpublished co-authored work. **Please include one copy of this form for each co-authored work**. Completed forms should be included in all copies of your thesis submitted for examination and library deposit (including digital deposit), following your thesis Acknowledgements.

Please indicate the chapter/section/pages of this thesis that are extracted from a co-authored work and give the title and publication details or details of submission of the co-authored work. Corresponds to Chapter Three Perez-Garcia, O., Villas-Boas, S., Chandran, K., Singhal, N. Metabolic network modeling of mixed microbial cultures for environmental biotechnology: applications and modeling approaches

Nature of contribution by PhD candidate	Litterature review and manuscript write-up
Extent of contribution by PhD candidate (%)	80%

CO-AUTHORS

Name	Nature of Contribution
Dr. Silas Villas-Boas	Technical review and advice
Dr. Kartik Chandran	Technical review and advice
Dr. Naresh Singhal	Technical review and advice

Certification by Co-Authors

The undersigned hereby certify that:

- the above statement correctly reflects the nature and extent of the PhD candidate's contribution to this work, and the nature of the contribution of each of the co-authors; and
- in cases where the PhD candidate was the lead author of the work that the candidate wrote the text.

Name	Signature	Date
Dr. Silas Villas-Boas	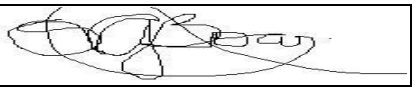	7/08/2014
Dr. Kartik Chandran		3/08/2014
Dr. Naresh Singhal		4/08/2014
		Click here
		Click here
		Click here

THE UNIVERSITY OF AUCKLAND
SCHOOL OF GRADUATE STUDIES

Graduate Centre
ClockTower – East Wing
22 Princes Street, Auckland
Phone: +64 9 373 7599 ext 81321
Fax: +64 9 373 7610
Email: postgraduate@auckland.ac.nz
www.postgrad.auckland.ac.nz

Co-Authorship Form

This form is to accompany the submission of any PhD that contains research reported in published or unpublished co-authored work. **Please include one copy of this form for each co-authored work**. Completed forms should be included in all copies of your thesis submitted for examination and library deposit (including digital deposit), following your thesis Acknowledgements.

Please indicate the chapter/section/pages of this thesis that are extracted from a co-authored work and give the title and publication details or details of submission of the co-authored work. Corresponds to Chapter Four Perez-Garcia, O., Villas-Boas, S., Swift, S., Chandran, K., Singhal, N. 2014. Clarifying the regulation of NO/N2O production in Nitrosomonas europaea during anoxic-oxic transition via flux balance analysis of reconstructed metabolic network model. Water Research 60, 267-277

Nature of contribution by PhD candidate	Simulation study, data analysis and manuscript write-up
Extent of contribution by PhD candidate (%)	80%

CO-AUTHORS

Name	Nature of Contribution
Dr. Silas Villas-Boas	Technical review and advice
Dr. Simon Swift	Technical review and advice
Dr. Kartik Chandran	Technical review and advice
Dr. Naresh Singhal	Technical review and advice

Certification by Co-Authors

The undersigned hereby certify that:

- the above statement correctly reflects the nature and extent of the PhD candidate's contribution to this work, and the nature of the contribution of each of the co-authors; and
- in cases where the PhD candidate was the lead author of the work that the candidate wrote the text.

Name	Signature	Date
Dr. Silas Villas-Boas	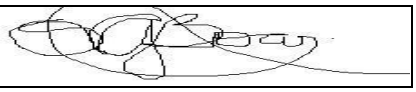	7/08/2014
Dr. Simon Swift	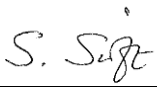	7/08/2014
Dr. Kartik Chandran	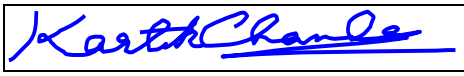	6/08/2014
Dr. Naresh Singhal		4/08/2014
		Click here
		Click here

Last updated: 25 March 2013

THE UNIVERSITY OF AUCKLAND
SCHOOL OF GRADUATE STUDIES

Co-Authorship Form

Graduate Centre
ClockTower – East Wing
22 Princes Street, Auckland
Phone: +64 9 373 7599 ext 81321
Fax: +64 9 373 7610
Email: postgraduate@auckland.ac.nz
www.postgrad.auckland.ac.nz

This form is to accompany the submission of any PhD that contains research reported in published or unpublished co-authored work. **Please include one copy of this form for each co-authored work**. Completed forms should be included in all copies of your thesis submitted for examination and library deposit (including digital deposit), following your thesis Acknowledgements.

Please indicate the chapter/section/pages of this thesis that are extracted from a co-authored work and give the title and publication details or details of submission of the co-authored work. Corresponds to Chapter Five Perez-Garcia, O., Villas-Boas, S., Chandran, K., Singhal, N. Establishing the limits of N2O production in nitrifying mixed cultures using a multispecies metabolic network model

Nature of contribution by PhD candidate	Simulation study, data analysis and manuscript write-up
Extent of contribution by PhD candidate (%)	80%

CO-AUTHORS

Name	Nature of Contribution
Dr. Silas Villas-Boas	Technical review and advice
Dr. Kartik Chandran	Technical review and advice
Dr. Naresh Singhal	Technical review and advice

Certification by Co-Authors

The undersigned hereby certify that:

- the above statement correctly reflects the nature and extent of the PhD candidate's contribution to this work, and the nature of the contribution of each of the co-authors; and
- in cases where the PhD candidate was the lead author of the work that the candidate wrote the text.

Name	Signature	Date
Dr. Silas Villas-Boas	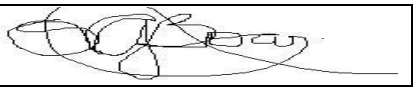	7/08/2014
Dr. Kartik Chandran		3/08/2014
Dr. Naresh Singhal		4/08/2014
		Click here
		Click here
		Click here

THE UNIVERSITY OF AUCKLAND
SCHOOL OF GRADUATE STUDIES

Co-Authorship Form

Graduate Centre
ClockTower – East Wing
22 Princes Street, Auckland
Phone: +64 9 373 7599 ext 81321
Fax: +64 9 373 7610
Email: postgraduate@auckland.ac.nz
www.postgrad.auckland.ac.nz

This form is to accompany the submission of any PhD that contains research reported in published or unpublished co-authored work. **Please include one copy of this form for each co-authored work**. Completed forms should be included in all copies of your thesis submitted for examination and library deposit (including digital deposit), following your thesis Acknowledgements.

Please indicate the chapter/section/pages of this thesis that are extracted from a co-authored work and give the title and publication details or details of submission of the co-authored work. Corresponds to Chapter Six Perez-Garcia, O., Villas-Boas, S., Chandran, K., Singhal, N. Metabolite profiling and metabolic network modeling of denitrifying mixed cultures: analysis of the effect of electron equivalent flow on N2O accumulation

Nature of contribution by PhD candidate	Experimental study, data analysis and manuscript write-up
Extent of contribution by PhD candidate (%)	80%

CO-AUTHORS

Name	Nature of Contribution
Dr. Silas Villas-Boas	Technical review and advice
Dr. Kartik Chandran	Technical review and advice
Dr. Naresh Singhal	Technical review and advice

Certification by Co-Authors

The undersigned hereby certify that:

- the above statement correctly reflects the nature and extent of the PhD candidate's contribution to this work, and the nature of the contribution of each of the co-authors; and
- in cases where the PhD candidate was the lead author of the work that the candidate wrote the text.

Name	Signature	Date
Dr. Silas Villas-Boas	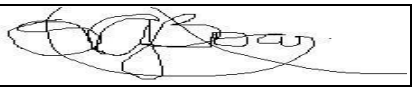	7/08/2014
Dr. Kartik Chandran		3/08/2014
Dr. Naresh Singhal		4/08/2014
Dr. Simon Swift		Click here
		Click here
		Click here

CHAPTER ONE

Introduction and research scope

1.1. Relevance of nitrous oxide (N_2O) in our environment

Nitrous oxide (N_2O) is an atmospheric trace gas that influences the atmosphere's chemistry and the greenhouse gas effect. Biological and chemical processes naturally produce N_2O on the Earth's surface (U.S. EPA, 2010). However, anthropogenic activities over the last 100 years have increased the amount of atmospheric N_2O concentrations by 20%, from 270ppbv to more than 324ppbv (IPCC, 2001; IPCC, 2013), contributing to two negative impacts on the atmosphere (Wuebbles, 2009): a) the greenhouse effect and b) the ozone (O_3) depletion effect. Because of this, monitoring and reduction of N_2O emissions are now part of the legally binding commitments entered into by the governments of many countries, including New Zealand, through international agreements like the Kyoto Protocol (N.Z. MfE, 2013a) within the United Nations Framework Convention on Climate Change (UNFCCC).

N_2O is a potent greenhouse gas. The capacity of one molecule of N_2O to trap heat (i.e. infrared radioactive forcing) is 206 times that of one carbon dioxide (CO_2) molecule (IPCC, 2001). This, together with the long atmospheric lifetime of N_2O (118±25 years), results in the global warming potential of N_2O being 310 times higher than that of CO_2 on a per molecule basis (Schreiber et al., 2012; U.S. EPA, 2014). These features of N_2O result in an overall contribution of 6 to 8% to the atmospheric greenhouse gas effect, despite its relative low atmospheric concentration (in comparison to other atmospheric gases such as CO_2) (IPCC, 2013; U.S. EPA, 2014).

Aside from its greenhouse gas effect, N_2O has been categorized by the International Panel for Climate Change (IPCC) as the "dominant ozone-depleting substance emitted in the 21st Century" (Ravishankara et al., 2009). When

Table 1.1. Nitrous oxide fact sheet

Molecular formula	N_2O
Current global atmospheric concentration (until 2013)	324±1 ppbv
Concentration increase (from 1900 to 2013)	20%
Global warming potential [a] (for a 100-year time scale)	310
Ozone depletion potential [b] (Weighted emission)	150 GgCFC-11 /year
Atmospheric lifetime	~120 years
Overall greenhouse gas effect contribution	6 to 8%
Total global emission (from Earth's surface in 2010)	18.8 TgN/year
Anthropogenic global emission (from Earth's surface in 2010)	6.8 TgN/year
Anthropogenic emission percentage from total emission	36%
Major source (natural and anthropogenic)	Microbial metabolism

[a] Global warming potential (GWP), defined as the ratio of the time-integrated radiative forcing from the instantaneous release of 1 kilogram (kg) of a trace substance relative to that of 1 kg of a reference gas CO_2 (IPCC, 2001).
[b] Ozone depletion potential (ODP), the amount of stratospheric ozone destroyed by the release of a unit mass of chemical at Earth's surface to the amount destroyed by the release of a unit mass of chlorofluorocarbon 11 (CFC-11) (Ravishankara et al., 2009).

reaching the stratosphere, N_2O participates in a set of reactions that transform ozone (O_3) into molecular oxygen (O_2) and lead to ozone layer depletion (Ravishankara et al., 2009; Schreiber et al., 2012), resulting in ozone depletion potential for N_2O that is 150 times higher than that for chlorofluorocarbon 11 (CFC-11), the ODP reference compound (Ravishankara et al., 2009).

Total global N_2O emissions from both natural and anthropogenic sources are estimated to be 18.8TgN annually (U.S. EPA, 2010). Thirty six per cent of this amount (i.e. 6.8 TgN/year) is emitted as a consequence of anthropogenic activities, such as agriculture, fossil fuel combustion and waste treatment (**Figure 1.1**). Anthropogenic N_2O emissions are increasing atmospheric N_2O concentration at a rate of 0.6ppb/year (IPCC, 2001). In New Zealand, anthropogenic N_2O emissions account for 14.7% (0.021 TgN or 10.6 $TgCO_2$-equivalents) of the total greenhouse gasses emitted per year (N.Z. MfE, 2013b). The largest source of N_2O emissions is from agricultural soils, which contribute 95.0% (0.0199TgN) of New Zealand's total N_2O emissions (N.Z. MfE, 2013b).

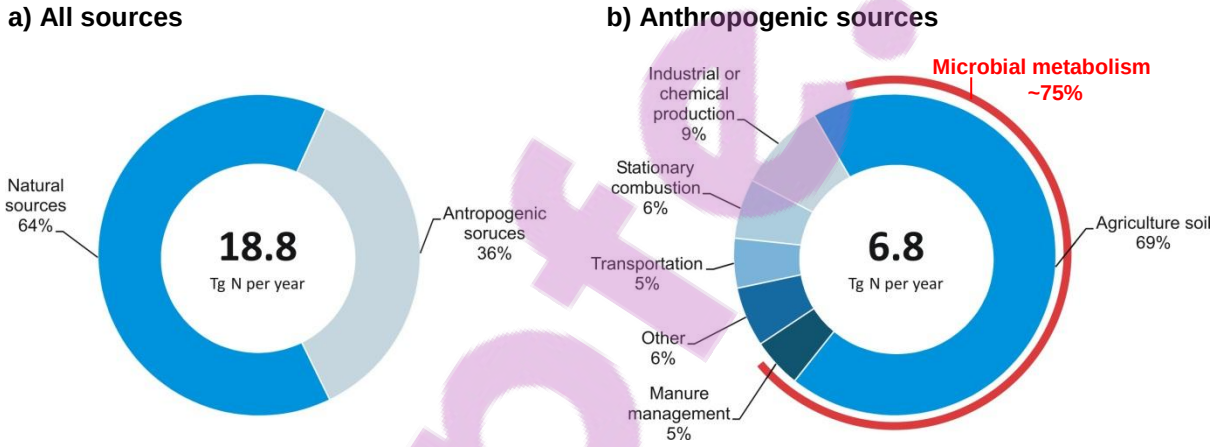

Figure 1.1. Global emissions of nitrous oxide (N_2O): a) all sources and b) anthropogenic sources. The number at the centre of the percentage graphs corresponds to the net amount of N_2O emitted per year in Teragrams of nitrogen (Tg N). One Teragram equals $1x10^{12}$ grams.

1.2. Microbes as the major source of N_2O

Independently of its natural or anthropogenic origin, microbial metabolism accounts for the largest source of N_2O emitted from Earth's surface, reaching between 65 to 80% of total emissions (Schreiber et al., 2012; Stein and Yung, 2003; U.S. EPA, 2010; Wuebbles, 2009). As shown in **Figure 1.1b**, of total anthropogenic emissions, microbial metabolism in agriculture soils and manure management systems is the major source of N_2O, accounting for approximately 75% of these (Wuebbles, 2009). This microbial N_2O production activity in agricultural systems is mostly a consequence of global conversion of land for agriculture, combined with massive usage of nitrogen-based fertilizers (Stein and Yung, 2003; Wuebbles, 2009). Natural sources of N_2O emissions are mainly the result of microbial metabolism in riparian areas, grassy soils and ocean waters (U.S. EPA, 2010). In addition to biological processes, chemical reactions can also produce N_2O. However, they

are not a major contributor to the N_2O production process within natural and anthropogenic systems as they usually only occur at low pH (<4) and high nitrogen loads (Schreiber et al., 2012).

Nitrification and denitrification are the primary biological processes leading to N_2O production and subsequent emission to the atmosphere (Ferguson et al., 2007; Schreiber et al., 2012; Stein and Yung, 2003; Stein, 2010). Nitrification is the biochemical process in which autotrophic microbes metabolically oxidize ammonia (NH_3) (present as ammonium (NH_4^+) in aqueous solution at pH < 8) to nitrite (NO_2^-); and subsequently oxidize nitrite to nitrate (NO_3^-) under aerobic conditions (Tchobanoglous et al., 2003). Denitrification, on the other hand, is the biological process in which heterotrophic microbes metabolically reduce nitrate or nitrate to nitrogen gas (N_2) under anaerobic conditions and use organic carbon compounds as electron donors (Tchobanoglous et al., 2003). Nitrification and denitrification are biochemical processes employed by microbes to metabolically synthesise energy-rich compounds (i.e. ATP and NADH) required for biosynthesis of biomass precursors and cell growth (Arp and Stein, 2003; Hooper et al., 1997; van Spanning et al., 2007).

It is currently recognized that nitrifying and denitrifying microbes are the most important environmental sources of N_2O, specifically autotrophic ammonia oxidizing bacteria (AOB) and heterotrophic denitrifiers organism (DEN) (Schreiber et al., 2012; Stein, 2010; U.S. EPA, 2010). In fact, N_2O is a common sub-product and precursor in nitrification and denitrification performed by AOB and DEN. Other microbial guilds (or ecological functional microbial groups) that can also produce N_2O are: nitrite oxidizing bacteria (NOB), ammonia oxidizing archaea (AOA), anaerobic ammonia oxidizing bacteria (anammox), nitrite dependent methane oxidizers (N-AOM) and dissimilatory nitrite reducers to ammonia (DNRA). However, their contribution to the overall amount of N_2O produced in nitrifying and denitrifying systems has been poorly quantified (Schreiber et al., 2012).

The microbial metabolic pathways that lead to the production of N_2O during nitrification and denitrification in AOB, NOB and DEN are summarized in **Figure 1.2.** The arrows represent biochemical reactions of nitrogenous compounds formed during nitrification (grey background) and denitrification (green background). The different colours of the arrows represent reactions present in the metabolism of different microbial guilds. Nitrification is an oxidation process where the oxidation state of nitrogenous compounds (indicated with roman numbers in parenthesis) increases (from top to bottom). On the other hand, denitrification is a reductive process and, therefore, the oxidation state of nitrogenous compounds decreases (from left to right) (Grady et al., 1999). Catalytic enzymes known to mediate the reaction from one nitrogenous compound to another are indicated was follows: AMO, ammonia monooxygenase; HAO, hydroxylamine oxidoreductase; NXR, nitrite oxidoreductase; NAR, membrane bound nitrite reductase; NirK, copper containing nitrite reductase; NirS, cytochrome cd_1 nitrite reductase; cNor, nitric oxide reductase that accept electrons from c-type cytochromes; qNor, nitric oxide reductase that accept electrons from ubiquinols; Nos, nitrous oxide reductase; C_{P460}, cytochrome P460; C_{c554}, cytochrome c554; Hmp, flavohemoglobins; (Hooper et al., 1997; Schreiber et al., 2012; Stein, 2010; Stein, 2011; Whittaker et al., 2000). Note that biochemical reactions for the

transformation of nitrogenous compounds in AOA, anammox, N-AOM and DNRA microbes are not shown in **Figure 1.2.** The four main N_2O production pathways known to occur in biological nitrifying and denitrifying microbes are listed in **Table 1.2** (Stein, 2011; Wunderlin et al., 2012).

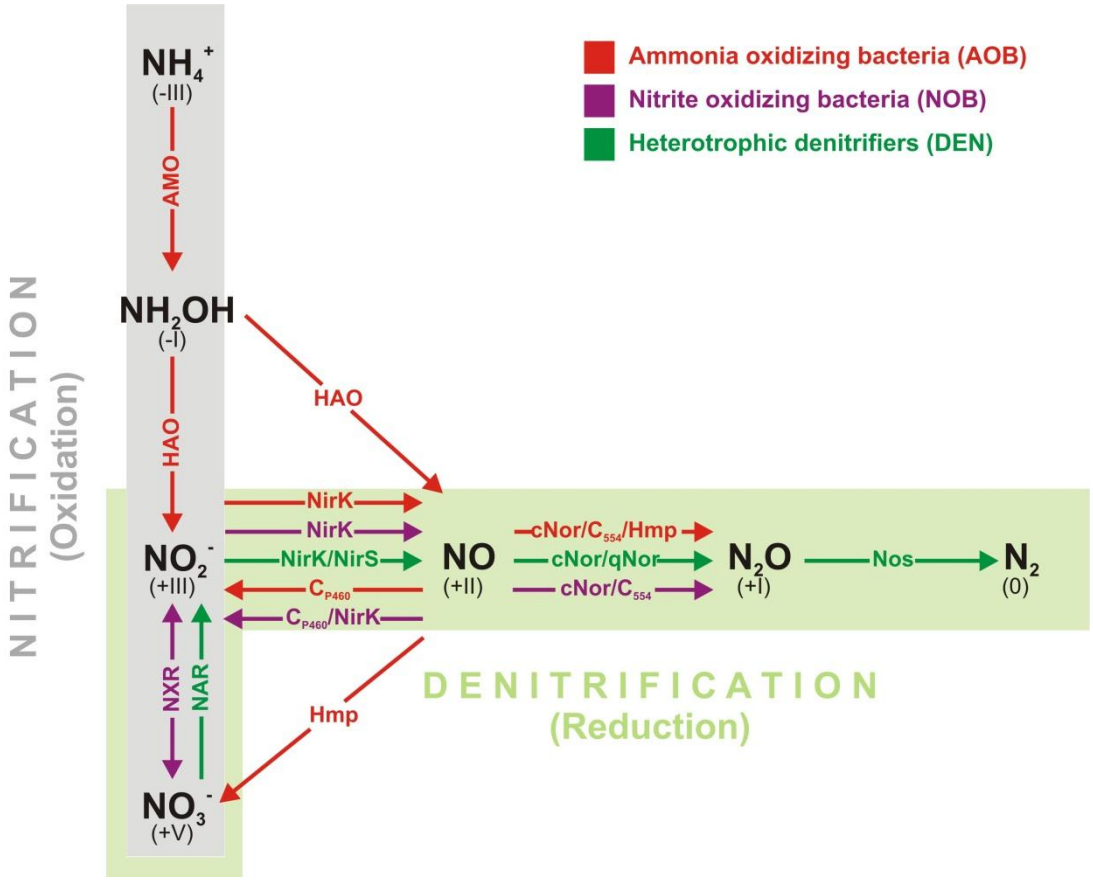

Figure 1.2. Microbial metabolic pathways for NO and N_2O production in nitrification and denitrification processes

Table 1.2. The four main N_2O production pathways in nitrifying and denitrifying microbes

Pathway name	Key mediating enzyme(s)
Aerobic hydroxylamine oxidation pathway in ammonia oxidizers (also known as HAO mediated NO production pathway)	Hydroxylamine oxidoreductase (HAO) and nitric oxide reductase (cNor)
Dissimilatory nitrite reduction pathway in ammonia oxidizers (also known as nitrifier denitrification pathway)	Nitrite reductase (NirK) and nitric oxide reductase (cNor)
Dissimilatory nitrite reduction pathway in denitrifiers (also known as incomplete denitrification)	Nitrite reductases (NirK and NirS) and nitric oxide reductases (cNor and qNor)
NO detoxification pathway	Cytochromes (C_{c554} and C_{P460}) and flavohemoglobins (Hmp)

Of particular relevance in the N_2O production pathways is the fact that homologous enzymes present in different microbial guilds can catalyse the same reaction, as illustrated in **Figure 1.2.** For example, nitrite reductases (NirK) and nitric oxide reductases (cNor) are commonly present in all AOB, NOB and DEN microbes; and all of them can be active in a particular nitrifying/denitrifying system. Moreover, different enzymes with different regulatory and kinetic properties can catalyse for the same reaction (these enzymes are called isozymes). For example, cNor, Cytochrome c554 (C_{c554}) and flavohemoglobins (Hmp) can catalyse the reduction of nitric oxide (NO) to N_2O in AOB. The occurrence of this "parallel pathway", along with the complexity of metabolic reaction modulation and the rapid turnover of NO and N_2O formation (Schreiber et al., 2012), has in the past made analysis extremely difficult. The result has been a gap in knowledge about the rates of the individual metabolic reactions that make up N_2O production pathways in relation to specific environmental factors affecting microbial populations.

1.3. N_2O emission from biological nitrogen removal processes

Nitrous oxide (N_2O) can be produced and directly emitted from wastewater treatment facilities (WWTP) (Ahn et al., 2010; Foley et al., 2010; Kampschreur et al., 2009). N_2O in particular is produced during biological nitrogen removal (BNR), where nitrification and denitrification processes are used to reduce excessive nitrogen concentration in wastewater (Foley et al., 2010; Wunderlin et al., 2012). Excessive nitrogen in untreated wastewater is usually present as NH_4^+. During BNR, aerobic conditions are imposed on the NH_4^+ rich wastewater; then nitrification takes place where NH_4^+ is oxidized to NO_2^- by AOB, and subsequently to NO_3^- by NOB. Afterwards, anaerobic and organic carbon-rich conditions are imposed on the NO_3^- rich wastewater, leading to anoxic conditions, Hence, denitrifying microbes convert nitrate generated during nitrification to nitrogen gas (N_2), thus removing nitrogen from wastewater (Grady et al., 1999; Tchobanoglous et al., 2003).

The amount of N_2O emitted from BNR reactors in wastewater treatment is highly variable. N_2O emission fraction in full scale WWTP ranges between 0 to 25% of the influent N-load, according to the IPCC (Kampschreur et al., 2009). The amount of emission thus expressed is the percentage of nitrogen load in a BNR system, emitted as N_2O. For example, a BNR system with N-load of 50 mg-N/L emitting 1% of N-load as N_2O is releasing 0.5 mg-N of N_2O per litre treated into the atmosphere. Full scale BNR systems have a lower N-load emission percentage (ranging from 0 to 25%) than lab scale systems (ranging from 0 to 95%) (Kampschreur et al., 2009; Rassamee et al., 2011). Extensive measurements from BNR bioreactors in the United States and Australia WWTP indicate an average of between 0.03% and 1.8% of N-load emitted as N_2O (Ahn et al., 2010; Foley et al., 2010). These values may appear low, but emissions as low as 0.5-1% of oxidized nitrogen are of a similar magnitude to greenhouse gases emitted during energy production for aeration (Ni et al., 2013a), which are now acknowledged by water utilities as significant contributors to the carbon footprint of wastewater treatment plants (Ni et al., 2013a).

The WWTP surveys in the US and Australia showed that aerobic zones in BNR processes generally contributed more to N_2O emission than anoxic zones (Ahn et al., 2010; Foley et al., 2010). In fact, N_2O emissions measured from the aerobic zone were always higher than emissions from anoxic zones. This is contrary to previous thinking that denitrification emitted more N_2O than nitrification because N_2O is an obligatory intermediary compound in denitrification. Higher emissions from aerobic zones can be attributed to three possible phenomena: a) increased air-stripping of N_2O; b) N_2O production due to oxygen inhibited denitrification; or c) N_2O production by nitrification during changes in aeration. However, up until now it has not been possible to infer the specific contribution of these phenomena to overall emissions (Ahn et al., 2010; Tallec et al., 2006). Whilst nitrous oxide is emitted predominantly in the aerated zones, it remains unclear as to whether nitrifying or denitrifying microorganisms are the main source of N_2O emissions (Kampschreur et al., 2009).

The most important environmental factors influencing N_2O emissions in BNR nitrification and denitrification processes are dissolved oxygen, nitrite, ammonium and organic carbon concentrations. Low dissolved oxygen and high nitrite accumulation are in effect environmental conditions that trigger N_2O emission during nitrification, as illustrated in **Figure 1.3.** Similarly, a low carbon to nitrogen ratio (COD/N), increased nitrite concentration and high dissolved oxygen are operational parameters leading to N_2O emission during denitrification (Kampschreur et al., 2008; Kampschreur et al., 2009; Rassamee et al., 2011). It has been observed from wastewater treatment laboratory cultures and full scale measurements that N_2O and its precursor NO are generally produced when nitrifying and denitrifying microbes are exposed to quick changes of redox conditions, i.e. aerobic, anaerobic and anoxic (Ahn et al., 2011; Kampschreur et al., 2008; Kampschreur et al., 2009; Law et al., 2012). It can be argued that activated sludge processes that maximize transient or permanent accumulation of ammonium or nitrite, especially in the presence of dissolved oxygen, can be expected to have high N_2O emissions (Ahn et al., 2010; Chandran et al., 2011).

There has been considerable uncertainty as to how BNR operational parameters influence N_2O formation pathways in nitrifying and denitrifying microbes. Certainly, the study of laboratory cultures of these microbes has generated considerable knowledge about reactions, catalytic enzymes and the associated genes involved in N_2O formation (shown in **Figure 1.2.**). However quantification of N_2O producing pathway activity and functional gene detection in regard to specific operational parameters of BNR has been done only in a few studies (Ahn et al., 2011; Pan et al., 2013a; Wunderlin et al., 2013; Yu et al., 2010). Moreover, physiological and ecological feedback can greatly influence the rates of N_2O producing metabolic pathways (Stein and Yung, 2003), which complicates the task of developing strategies to mitigate N_2O emissions from BNR and other anthropogenic sources. It follows therefore that quantitative relationships between N_2O emission, production pathway rates and BNR operational parameters are necessary to be able to define guidelines for emission prevention (Kampschreur et al., 2009).

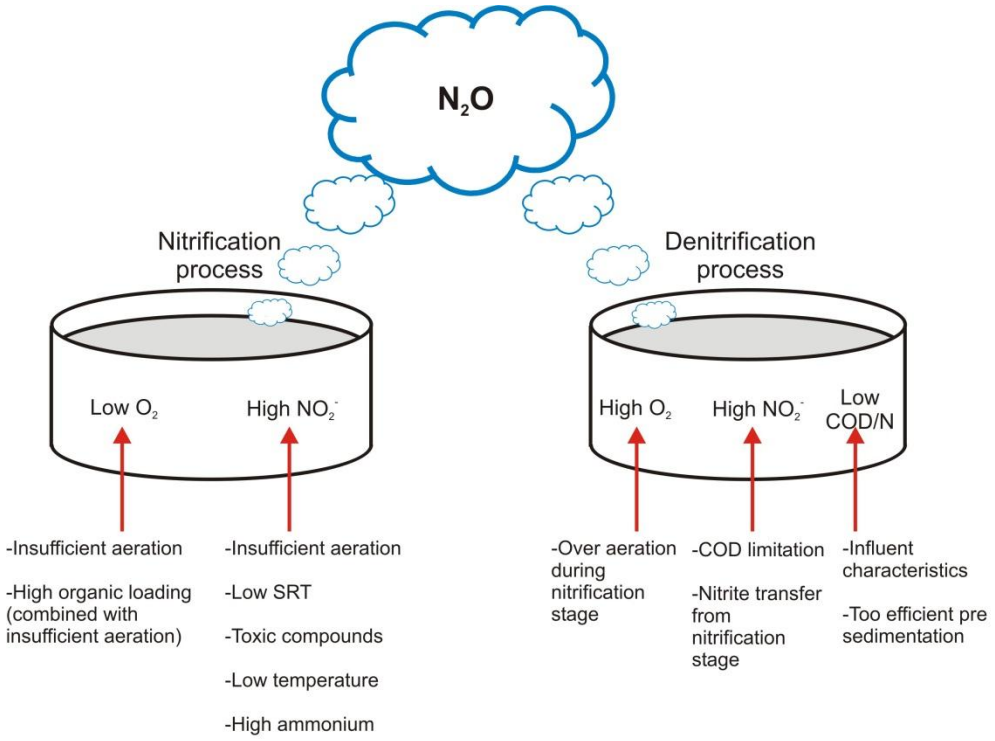

Figure 1.3. Main operational parameters and environmental conditions of BNR processes leading to N_2O emission. Adapted from (Kampschreur et al., 2009)

1.4. Linking N_2O production metabolism with BNR operational parameters through SMN modelling and metabolomics

Characterization of microbial metabolism in BNR processes through stoichiometric metabolic network (SMN) modelling and metabolomics is an ideal way to establish quantitative relationships between observed N_2O emission, reaction rates of microbial N_2O production pathways and BNR operational parameters. By fitting SMN models to data from N_2O producing-BNR bioreactors is possible to develop quantitative hypothesis of the actual molecular mechanisms occurring in nitrifying and denitrifying cells when producing N_2O. Then those hypotheses can be experimentally validated so that the generated knowledge used to design operational guidelines of BNR reactors in order to avoid N_2O emissions. SMN modelling is a computational method within the Bioinformatics and Systems Biology disciplines that uses stoichiometric equations for biochemical reactions taking place in a target organism (or microbial community) to reconstruct a pathway level - or even full cell level - metabolic model (Feist et al., 2009; Thiele and Palsson, 2010). This model can be used to estimate metabolic reaction rates (also called fluxes) simultaneously occurring in cells under a given environmental condition (Becker et al., 2007; Feist et al., 2009). Metabolomics, on the other hand, is an analytical technology that aims to identify and quantify the set of metabolites present in a biological sample from an organism grown under defined conditions (Villas-Bôas et al., 2005; Weckwerth and Morgenthal, 2005). Flux and metabolite profiles of cell cultures (such as those of BNR processes) provide the

most physiologically relevant description of a cells' metabolism, because they represent the final functional output of interactions of all the genetic, transcriptional, protein, enzymatic and signalling activities within the cells (Cascante and Marin, 2008; Chubukov et al., 2014; Kohlstedt et al., 2010; Lee et al., 2006)

The dynamic nature and small spatial scale of NO and N_2O formation (Schreiber et al., 2012) complicates experimental rate measurements. An alternative is to estimate the metabolic reaction rates via SMN modelling and related simulation methods (Feist et al., 2009; Kim et al., 2012; Schellenberger et al., 2011). These computational methods apply the principles of conservation of mass and energy to biochemical networks of metabolic compounds and biochemical reactions to provide 'snapshot' estimations of reaction rates at a specific steady state (Varma and Palsson, 1994a). In this way, the requirement of the model's kinetic parameters, such as maximum reaction rates and affinity constants, can be avoided.

Figure 1.4 illustrates how SMN modelling and metabolomics can be used to quantify the activity of N_2O production pathways in BNR microbes responding to specific operational parameters as follows. For SMN modelling, the organism's DNA contains the information needed to produce specific proteins (A and B) with enzymatic activities. Proteins catalyse for specific reactions where metabolites are used as substrates (x, *a*, *y*) to be transformed into products (z, b, c). Subsequent reactions form metabolic pathways, which constitute the cell metabolism. Each reaction can be represented as a stoichiometric equation (A and B). The conversion of a metabolic reconstruction of an organism into a model requires transformation of the reaction list into a computable, mathematical, matrix format. Thus, the equations' stoichiometric coefficients are arranged in the stoichiometric matrix (S), where S stands for stoichiometric. The rows in the diagram correspond to the network metabolites and the columns to the network reactions (Orth et al., 2010; Varma and Palsson, 1994a). The S matrix contains all the information relating to the reactions modelled for a particular organism. The conversion also includes the imposition of physicochemical and environmental constraints to define systems boundaries (Varma and Palsson, 1994a). In this research, the constraints were microbe substrate uptake rates (measured in BNR bioreactors) and reaction thermodynamic properties (i.e. Gibbs energy of reaction). While a metabolic reconstruction is unique to the target organism, one can derive different, environmental, condition-specific models from a single reconstruction (Thiele, 2009). Once the metabolic network is captured in a matrix S format and condition-specific constraints have been imposed, different mathematical simulations can be performed to estimate flux profiles (rate of metabolic reactions) of cell cultures.

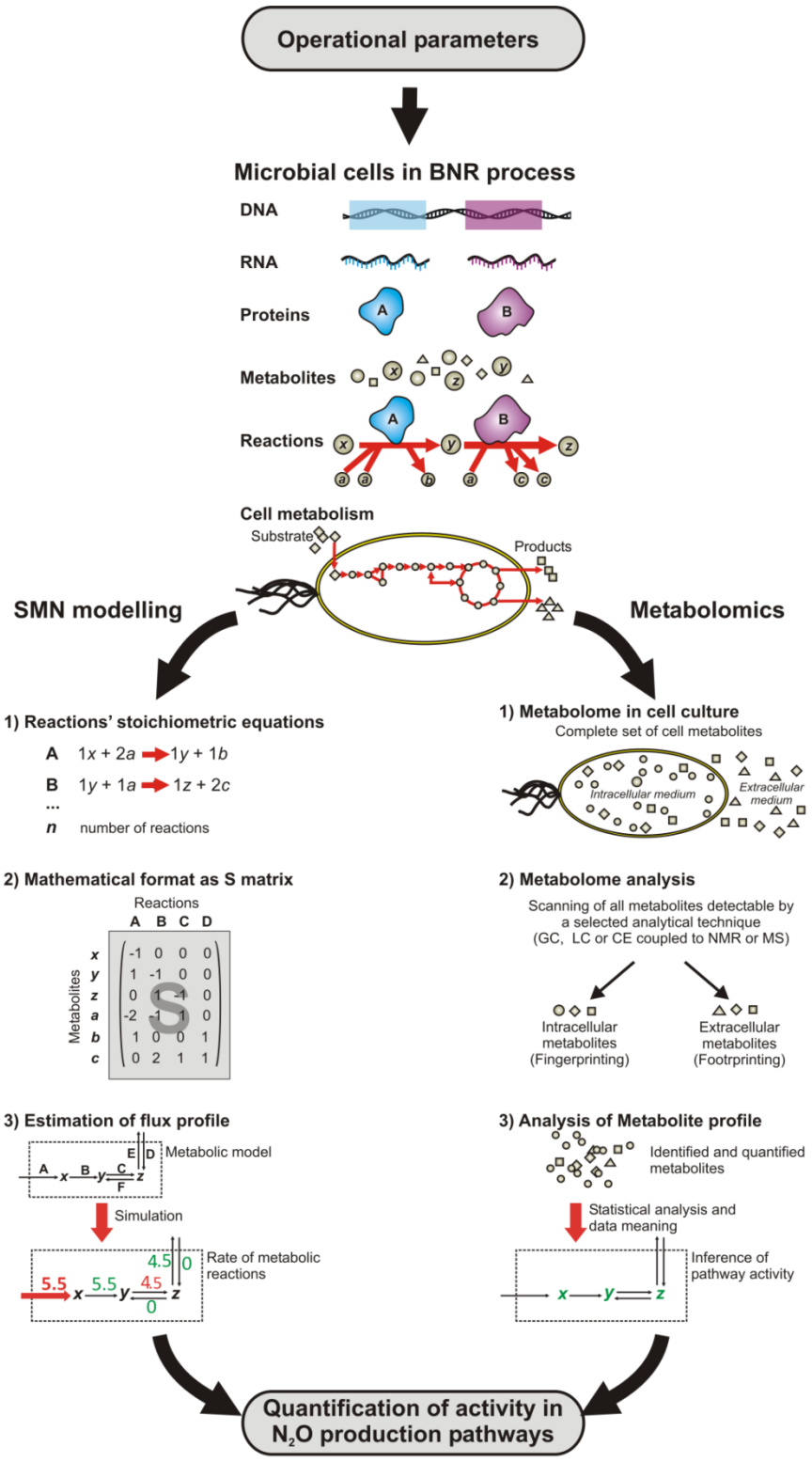

Figure 1.4. Linking operational parameters in BNR process to activity of microbial N_2O production pathway through SMN modelling and Metabolomics

Figure 1.4 also illustrates the basic principle of metabolomics described above. As mentioned above, metabolomics refers to an analysis technology that identifies and quantify sets of metabolites ('metabolome') present in a biological sample from an organism grown under defined conditions. Biomass in cell cultures is sampled to perform a targeted or non-targeted metabolome analysis. Metabolite profiling quantifies metabolites in a non-targeted, non-biased and comprehensive manner using various analytical techniques including nuclear magnetic resonance (NMR) spectroscopy and mass spectrometry (MS). These tools are often combined with different separation techniques including gas chromatography (GC), liquid chromatography (LC) and capillary electrophoresis (CE) (Lee et al., 2006). Once the metabolites in samples are identified and quantified, various statistical and data mining techniques are used to infer activity in metabolic pathways. Being the intermediates of biochemical reactions, metabolites play a very important role in connecting the many different pathways that operate within a living cell. Therefore, the level of metabolites in a cell or tissue represents integrative information of the cellular function and, hence, defines the phenotype of a cell or tissue in response to genetic or environmental changes (Villas-Bôas et al., 2005; Villas-Bôas and Bruheim, 2007).

1.5. Why bring systems biology tools to environmental engineering?

Systems biology tools such as SMN modelling and metabolomics have created the opportunity to develop the next generation of biotreatment and bioremediation models. Nowadays, cheaper molecular biology and genomics, proteomics, and metabolomic techniques allow us to identify and quantify specific microbial species, full genome sequences, gene expression activity and metabolic and biodegradation compounds (Lovley, 2003). In this context, metabolomics can be applied to elucidate biodegradation pathways of contaminate compounds by identifying and quantifying dozens or even hundreds of compounds in a single sample (Villas-Bôas and Bruheim, 2007). Powerful computers are becoming cheaper as well, and new computation algorithms for data mining and model simulation are generated more readily (Lewis et al., 2012).The advantage of SMN models in this context is that they can incorporate the data generated with these new techniques and tools to produce a more accurate and realistic estimation of microbial processes. Therefore deep metabolic models like these can serve as a bridge between molecular/biochemical research and wastewater treatment and bioremediation practices, effectively functioning as a tool that can better link the work of microbiologists and engineers in optimising process operation (Oehmen et al., 2010). SMN modelling and metabolomics are tools with potential to be used by environmental engineers and biotechnologists, not only in research but also as in applications such as process design and optimization through linkages with activated sludge (AS), hydrodynamic and geochemical models. The current research work aspires to advance and consolidate this area of environmental engineering.

1.6. Research aim and objectives

The aim of this research is to establish the relationships between the activity of N_2O production pathways and environmental conditions (e.g. electron donor and acceptor availability) in BNR bioreactors by using SMN modelling and metabolite profiling of nitrifying and denitrifying microbes. To accomplish this, the research is guided by the following objectives:

- To develop a computational platform based on SMN modelling of nitrifying and denitrifying microbes of BNR processes;
- To assess how oxygen and ammonium availability regulates the metabolic pathways of N_2O and NO production of ammonia oxidizing bacteria;
- To determine the rates of N_2O production in nitrifying mixed cultures in response to different concentrations of oxygen and ammonium, and different microbial community compositions; and
- To use metabolite profiling to assess the effect of COD/N ratios and high nitrite concentration on the metabolic mechanism of N_2O accumulation in denitrifying cultures.

1.7. Thesis outline

This doctoral thesis is organised into seven chapters. Chapters Two to Six, which form the body of this thesis, were written as independent peer-reviewed journal manuscripts. At the time of writing this thesis, the manuscripts have been either accepted, submitted or are in review process for publication. Chapters prepared originally as publication manuscripts were slightly modified to maintain coherence and avoid repetition in the current document. **Figure 1.5.** is a diagram of the workflow designed to achieve the research aim. **Table 1.3.** presents an overview of the thesis outline arranged by chapters, research objectives and manuscripts for publication.

The methods employed to develop the computational SMN modelling platform are formally described in Chapter Two. The chapter introduces the twelve SMN models of BNR microbes developed in this research. The twelve models correspond to biochemical reactions and metabolites formed during the nitrogen respiratory metabolism of predominant species of ammonia oxidizing bacteria (AOB), nitrite oxidizing bacteria (NOB) and denitrifying bacteria (DEN). A broad literature review shows that this study is the first to perform the SMN modelling of those organisms. In addition, this chapter presents the computational method developed in this study for calibrating parameters of the SMN models as computational tools to calibrate models using experimental data from BNR processes were lacking.

Chapter Three presents a full literature review of applications and approaches currently used to characterize metabolic activity in engineered environmental bioprocesses using SMN modelling. A review and discussion of these approaches was necessary, as SMN modelling is a technique normally applied to studies with microbial cultures of pure-species. The methods revised during this literature review were further employed during the studies of Chapters Five and Six to produce SMN models nitrifying and denitrifying microbial communities in BNR processes. The review provided the

building block to look beyond this type of study and explore in detail how SMN can be adapted to model mixed-species microbial cultures.

Chapters Four and Five present two independent simulation studies performed to investigate the effect of ammonium and oxygen concentrations on N_2O production in nitrifying processes. Chapter Four looks at the first study, which investigates the basic metabolic modulation mechanism of N_2O and NO (nitric oxide) formation pathways in nitrifying pure cultures of *Nitrosomonas europaea*, an important AOB species in full scale BNR systems. Modulation of N_2O production in *N. europaea* was analysed by fitting a SMN model to data from pure culture studies reported on literature. Further, given that full scale BNR systems employ mixed cultures of microbes, the second simulation study described in Chapter Five investigates N_2O production and NO turnovers in nitrifying mixed cultures in response to ammonium and oxygen concentrations and microbial community structure. In this study, the microbial community structure observed in nine previously published experiments on N_2O production by nitrifying mixed cultures was modelled by adapting eight of the developed SMN models to generate one multispecies SMN.

The research into the relationship between environmental conditions of denitrifying BNR processes and microbial N_2O production metabolism is described in Chapter Six. N_2O formation in denitrifying processes was investigated in an experimental study where laboratory-scale denitrifying batch cultures were run on growth medium with different carbon to nitrogen ratios (COD/N). GC-MS based metabolite profiling analysis of biomass samples from cultures was undertaken to identify pathways of carbon assimilation. Then, a lumped SMN model of denitrifying microbes was used to quantify reaction rates in the pathways identified by the metabolomic analysis.

Chapter Seven is the final chapter of the thesis and contains a summary of conclusions drawn from this doctoral research. This chapter propose a novel integral hypothesis about the mechanism of how electron donor and acceptor availability modulates the rates of NO and N_2O production during both nitrification and denitrification. The chapter also discusses promising avenues for further research and describes a preliminary method to link SMN models of BNR microbes with kinetic models for BNR design and optimisation applications.

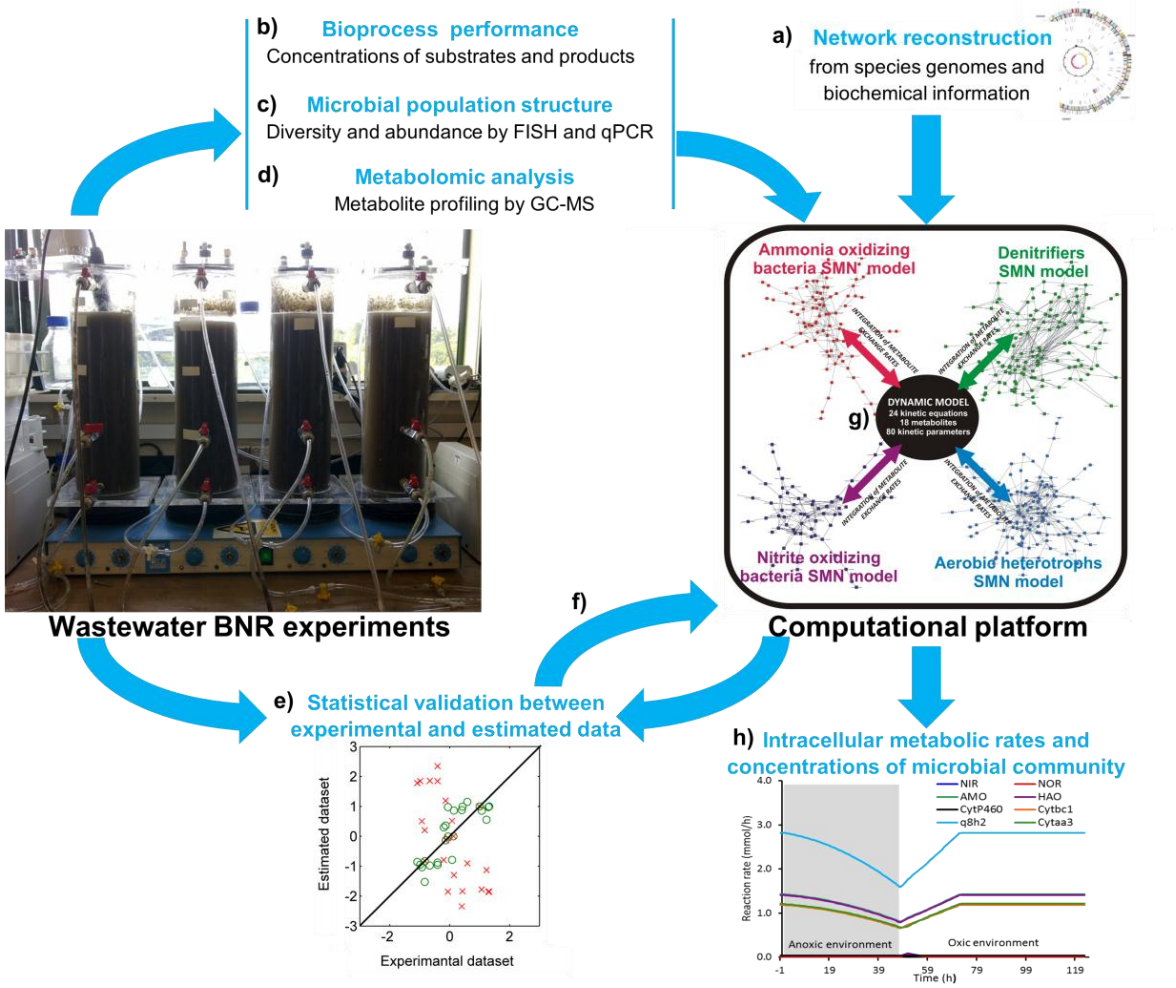

Figure 1.5. Research workflow and thesis outline

a) SMN models are built from stoichiometric equations elucidated from microbial species genomes (Chapters Two and Three); b) BNR process performance data is used as input data for the SMN model to analyse N_2O production in *Nitrosomonas europaea* (Chapter Four); c) Microbial community structure data (FISH and qPCR) from previously published experiments is used to analyse N_2O production in nitrifying mixed cultures (Chapter Five); d) GC-MS-based metabolite profiling is used to analyse metabolic activity in N_2O-producing denitrifying cultures (Chapter Six); e) the model's predictions and experimental data are statistically compared (Chapters Three, Four, Five and Six); f) calibration of the model is repeated until satisfactory prediction accuracy is reached (Chapters Three, Four, Five and Six); g) SMN models can be implemented in activated sludge (AS) models for full process simulation (Chapter Three and Seven); and h) the analytical platform estimates rates of metabolic reactions (Chapters Four, Five and Six).

Table 1.3. Thesis chapters, thesis objectives and written manuscripts for publication

Thesis chapter	Research objective	Outcome as manuscript for publication
One	Introduction and thesis scope	Chapter content not prepared as a publication manuscript
Two	To develop a computational platform based on SMN models of nitrification and denitrification organisms (method development)	*Perez-Garcia, O., Villas-Boas, S., Singhal, N.* 2014. A method to calibrate metabolic network models with experimental datasets. Proceedings of the 8th International Conference on Practical Applications of Computational Biology & Bioinformatics. Springer Series: Advances in Intelligent and Soft Computing 294, 183-190. ***Published***
Three	To develop a computational platform based on SMN models of nitrification and denitrification organisms (literature review for method extension)	*Perez-Garcia, O., Villas-Boas, S., Swift, S., Singhal, N.* Metabolic network modeling of mixed microbial cultures for environmental biotechnology: applications and modeling approaches. Environmental Microbiology. ***In internal review***
Four	To assess how oxygen and ammonium availability regulate the metabolic pathways of N_2O and NO production of ammonia oxidizing bacteria	*Perez-Garcia, O., Villas-Boas, S., Swift, S., Chandran, K., Singhal, N.* 2014. Clarifying the regulation of NO/N_2O production in Nitrosomonas europaea during anoxic-oxic transition via flux balance analysis of reconstructed metabolic network model. Water Research 60, 267-277. ***Published***
Five	To determine the rates of N_2O production in nitrifying mixed cultures in response to different concentrations of oxygen and ammonium and different microbial community compositions	*Perez-Garcia, O., Villas-Boas, S., Chandran, K., Singhal, N.* Establishing the limits of N_2O production in nitrifying mixed cultures using a multispecies metabolic network model. Biotechnology and Bioengineering. ***In internal review***
Six	To clarify the metabolic mechanism of N_2O accumulation in denitrification reactors exposed to nitrite accumulation and different COD:N ratios	*Perez-Garcia, O., Villas-Boas, S., Chandran, K., Singhal, N.* Metabolite profiling and metabolic network modeling of denitrifying mixed cultures: analysis of the effect of electron equivalent flow on N_2O accumulation. Environmental Science and Technology. ***In internal review***
Seven	Conclusions	Chapter content not prepared as a publication manuscript

CHAPTER TWO

Development of SMN models of biological nitrogen removal microbes

This chapter provides a theoretical description of stoichiometric metabolic network (SMN) modelling methods and details of how these methods were applied in this research. The first section explains the research approach aimed at achieving the objectives of this thesis. The research involved the use of SMN to model the metabolism of twelve species of nitrifying and denitrifying microbes. The software packages used to build up these models are specified and the method to formulate them is described. This method is formally referred to as "metabolic network reconstruction. Two model simulation algorithms, flux balance analysis (FBA) and Monte Carlo random sampling (RS), used to simulate the developed models are defined. Lastly, there is a description of the model calibration method developed during this doctoral thesis and routinely used to calibrate the SMN models generated. This calibration method draws on coefficient values that identify the model version that best fits multivariable experimental datasets.

2.1. Research approach overview

The research approach of this thesis focuses on estimating the rates of all metabolic reactions for nitrogen respiration and energy production occurring simultaneously in nitrifying and denitrifying microbial cultures producing N_2O. From this estimations, the operational conditions of these cultures are able to be mechanistically related to reaction rates of NO and N_2O-producing pathways.

The research used SMN modelling to estimate the metabolic reaction rates of nitrifying and denitrifying microbes at specific steady-states, that is, when the microbial cells are producing nitrous oxide in the analysed cultures. This method and related simulation algorithms produce 'snapshot' estimations of the rate of biochemical reactions within the network formed by chemical compounds and sequenced reactions in cell metabolism (Durot et al., 2009; Oberhardt et al., 2009; Orth et al., 2010). The metabolism of twelve microbial species was modelled. These species belong to one of the three microbial guilds (AOB, NOB and DEN) that catalyse nitrification and denitrification processes in BNR systems. These species and their corresponding guilds (also known as ecological functional microbial groups) are specified in **Table 2.1.** The species were selected on the basis of the following criteria:

- Species abundance and relevance in nitrifying and denitrifying BNR cultures; and
- Availability of genome data

Table 2.1. The twelve species modelled with SMN

Microbial guild	Modelled organisms	SMN size
Ammonium oxidizing bacteria (AOB)	*Nitrosomonas europaea*	Rx. 49 Met. 44
	Nitrosomonas eutropha	Rx. 60 Met. 54
	Nitrosococcus oceani	Rx. 62 Met. 58
	Nitrosospira multiformis	Rx. 56 Met. 54
Nitrite oxidizing bacteria (NOB)	*Candidatus* Nitrospira defluvii	Rx. 49 Met. 45
	Nitrobacter hamburgensis	Rx. 47 Met. 43
	Nitrobacter winogradskyi	Rx. 44 Met. 41
	Nitrospina gracilis	Rx. 42 Met. 40
Heterotrophic denitrifiers (DEN)	*Paracoccus denitrificans*	Rx. 485 Met. 351
	Pseudomonas aeruginosa	Rx. 484 Met. 349
	Acidovorax avenae	Rx. 475 Met. 334
	Azoarcus sp. EbN1	Rx. 470 Met. 347

Rx = number of reactions; Met = number of metabolites

The metabolic models developed for these organisms include biochemical reactions of the following metabolic pathways:

- Nitrogen respiration;
- Energy production (electron transport chain (ETC), production of NADH and ATP);
- Maintenance energy consumption;
- Protein and biomass production; and
- Transport and exchange for diffusion of substrates and products across cells membranes and within cells and the extracellular environment.

The developed models specifically included the above pathways and reactions in order to be able to accurately estimate the nitrogen mass balance occurring during cellular metabolic activity. Nitrogen respiration and energy production pathways were modelled in their complete extent by including all the reactions of these pathways according to the genome of the modelled species. Biomass build up

pathways (anabolic pathways) were not modelled in detail –only as two reactions for protein and biomass production– because N_2O is produced during catabolism rather than anabolism. In addition to simulate biomass build up, protein and biomass production reactions were included to capture the effect of nitrogen contents in biomass and protein on the overall metabolic nitrogen mass balance.

The four models of denitrifying microbes included reactions forming the metabolic pathways for organic carbon assimilation. These reactions were included to capture the effect of carbon oxidation and assimilation on N_2O production. Consequently, models of denitrifying microbes were bigger (have higher number reactions and metabolites) than models of nitrifying species. The modelled pathways for organic carbon oxidation and biomass synthesis included in denitrifiers' models are listed below:

- Central carbon (glycolysis and tricarboxylic acids cycle (TCA));
- Amino acid synthesis (for the synthesis of the 20 amino acids -forming proteins) and
- Fatty acid synthesis and degradation (long-chain saturated and unsaturated).

Table 2.2. lists all the experiments analysed with the SMN models developed during this doctoral research. The developed models were fitted to data from those experiments in order to diagnose them and develop quantitative hypothesis of the actual molecular mechanisms occurring in nitrifying and denitrifying cells when producing N_2O. A step out of the scope of this research thesis would be to experimentally validate the herein developed hypothesis and use the generated knowledge to design operational guidelines of BNR reactors in order to avoid N_2O emissions. Further details of these experiments are to be found in Chapters Four, Five and Six. Details of how species SMN were adapted to model mixed species microbial cultures are provided in Chapters Three, Five and Six. The research approach of this thesis is illustrated in **Figures 1.5** and 2.1, and involves four main, consecutive steps:

(i) Model development (formulation, implementation and calibration);
(ii) Experiment data acquisition (from scientific publications or experiments performed as part of the research);
(iii) Model simulation to fit experimental data; and
(iv) Metabolic rate estimation and pathway activity inference.

This chapter focuses on the first step, model development, in which formulation refers to the reconstruction of the stoichiometric metabolic network (SMN); implementation involves the conversion to the SMN into its mathematical form and the application of the corresponding constraints; and calibration is the application of mathematical techniques to compare the model's estimated data with experimental data and thus improve the model's predictions. Steps (ii), (iii) and (iv) describing the simulation studies of microbial cultures are covered in Chapters Four, Five, and Six.

Table 2.2. List of experimental microbial cultures analysed with SMN models and metabolite profiling. Grey boxes indicate the operational parameter used as the experiment's control variable

Process	Experimental culture reference	Culture mode	Operational Parameters of Cultures				Applied SMN model	Metabolites profile
			Oxygen availability	Nitrogenous substrate availability	Carbon substrate availability	Microbial community composition		
NH_4^+ oxidation to NO_2^-	Previously published by (Yu et al., 2010)	Continuous, pure species culture	■	■			*Nitrosomonas europaea* model	Not analysed
	Previously published by (Yu et al., 2010)	Continuous, pure species culture	■	■			*Nitrosomonas europaea* model	Not analysed
	Previously published by (Ahn et al., 2011)	Continuous, mixed species culture	■	■		■	Nitrifiers multi-species model	Not analysed
	Previously published by (Law et al., 2012)	Batch, mixed species culture	■	■		■	Nitrifiers multi-species model	Not analysed
	Previously published by (Law et al., 2012)	Batch, mixed species culture	■	■		■	Nitrifiers multi-species model	Not analysed
	Previously published by (Law et al., 2012)	Batch, mixed species culture	■	■		■	Nitrifiers multi-species model	Not analysed
NH_4^+ oxidation to NO_3^-	Previously published by (Ahn et al., 2011)	Continuous, mixed species culture	■	■		■	Nitrifiers multi-species model	Not analysed
	Previously published by (Ahn et al., 2011)	Continuous, mixed species culture	■	■		■	Nitrifiers multi-species model	Not analysed
	Previously published by (Wunderlin et al., 2013)	Batch, mixed species culture	■	■		■	Nitrifiers multi-species model	Not analysed
NH_4^+ oxidation to NO_2^-	Previously published by (Wunderlin et al., 2013)	Batch, mixed species culture	■	■		■	Nitrifiers multi-species model	Not analysed
NH_2OH oxidation to NO_x	Previously published by (Wunderlin et al., 2013)	Batch, mixed species culture	■	■		■	Nitrifiers multi-species model	Not analysed
NO_3^- reduction to N_2	Experiment performed as part of this doctoral research	Batch, mixed species culture		■	■		Denitrifier models lumped on a single network	Analysed
	Experiment performed as part of this doctoral research	Batch, mixed species culture		■	■		Denitrifier models lumped on a single network	Analysed
	Experiment performed as part of this doctoral research	Batch, mixed species culture		■	■		Denitrifier models lumped on a single network	Analysed
	Experiment performed as part of this doctoral research	Batch, mixed species culture		■	■		Denitrifier models lumped on a single network	Analysed

2.2. Used software

Several software packages were used in this research to build up and simulate SMN models, and to analyse metabolite profile data. **Table 2.3.** lists the software packages and provides details of their application and internet link for download. The majority of these are available at no cost on the corresponding web page. **Figure 2.1.** illustrates the research workflow, the corresponding data resources and the software packages used for each step. In step (i), searches of scientific literature and biochemical databases were undertaken to acquire stoichiometric equations of sequenced biochemical reactions. These equations were entered into an Excel spreadsheet to reconstruct the SMN, which was then loaded into MATLAB® using the COBRA toolbox. A series of simulations were performed to calibrate the SMN structure. Although not used for this part of the research, model loading and simulation can be also done in Optflux. In step (ii), Excel and R software was used to record the compound concentration curves observed in experimental cultures and then calculate specific rates for the production and consumption of culture substrate and products. Values of cultures' yields, elemental mass balances and other variables that describe metabolic performance in experiments were also calculated. AMDIS, R Metab, PAPi and gplots software packages were used to process the data generated in the GC-MS metabolite profile analysis of culture biomass. In step (iii), specific rates of substrate consumption measured in experimental cultures were used as SMN model input data in MATLAB-COBRA toolbox. The model is fitted to datasets observed on cultures. In step (iv), once the model reproduced the observed experimental data, COBRA toolbox was used to estimate metabolic rates; and the effect of operational parameters of experimental cultures on metabolic pathways was inferred from these estimated metabolic rates. Finally network visualisation and network topology analysis can be performed using Cytoscape, CellDesigner and Optflux.

Table 2.3. Software packages used for SMN modelling and metabolite profiling data analysis

Software package	General application	Specific application and software type	Internet URL for download
Excel	SMN modelling	Build-up of SMN reconstruction file. Standalone software	http://office.microsoft.com/en-us/excel/
MATLAB® 7.0 (or above)	SMN modelling	Software and computing environment. Standalone software	http://www.mathworks.com/
COBRA toolbox v2.0	SMN modelling	SMN Modelling and simulation in MATLAB. Free MATLAB toolbox	http://opencobra.sourceforge.net/openCOBRA/Welcome.html
SBML toolbox	SMN modelling	Functions allowing SBML models to be used in MATLAB. Free MATLAB toolbox	http://sbml.org/Software/SBMLToolbox
libSBML 5.5.0	SMN modelling	Programming library to manipulate SBML files. MATLAB library	http://sbml.org/Software/ libSBML
GLPK solver	SMN modelling	COBRA toolbox solver. Free MATLAB solver	http://www.gnu.org/s/glpk/
Tomlab solver	SMN modelling	COBRA toolbox solver. MATLAB solver	http://tomopt.com/tomlab/
Gurobi solver	SMN modelling	COBRA toolbox solver. MATLAB solver	http://www.gurobi.com/
Cytoscape	SMN modelling	Network visualisation. Stand alone and free software	http://www.cytoscape.org/
Optflux	SMN modelling	SMN Modelling and simulation. Standalone and free software	http://www.optflux.org/
CellDesigner	SMN modelling	Pathway graphic reconstruction. Standalone and free software	http://www.celldesigner.org/
anNET	SMN modelling and metabolite profiling	Analysis of metabolites concentrations with SMN models. Free MATLAB toolbox	http://www.imsb.ethz.ch/researchgroup/nzamboni/research
AMDIS	Metabolite profiling	Mass spectral deconvolution and identification. Standalone, free software	http://www.amdis.net/
Metab	Metabolite profiling	AMDIS data treatment. R package	http://www.metabolomics.auckland.ac.nz/index.php/home-top
PAPi	Metabolite profiling	Data meaning of metabolite profiles. R package	http://www.metabolomics.auckland.ac.nz/index.php/home-top
gplots	Metabolite profiling	Graphical and heatmap plotting. R package	http://cran.r-project.org/web/packages/gplots/index.html
R	SMN modelling and metabolite profiling	Data analysis, statistics and graphic plotting. Stand alone, free software	http://www.r-project.org/

NOTE: At least one solver (GLPK, Tomlab or Garubi) is required to run COBRA toolbox. However, several solvers can be installed into MATLAB.

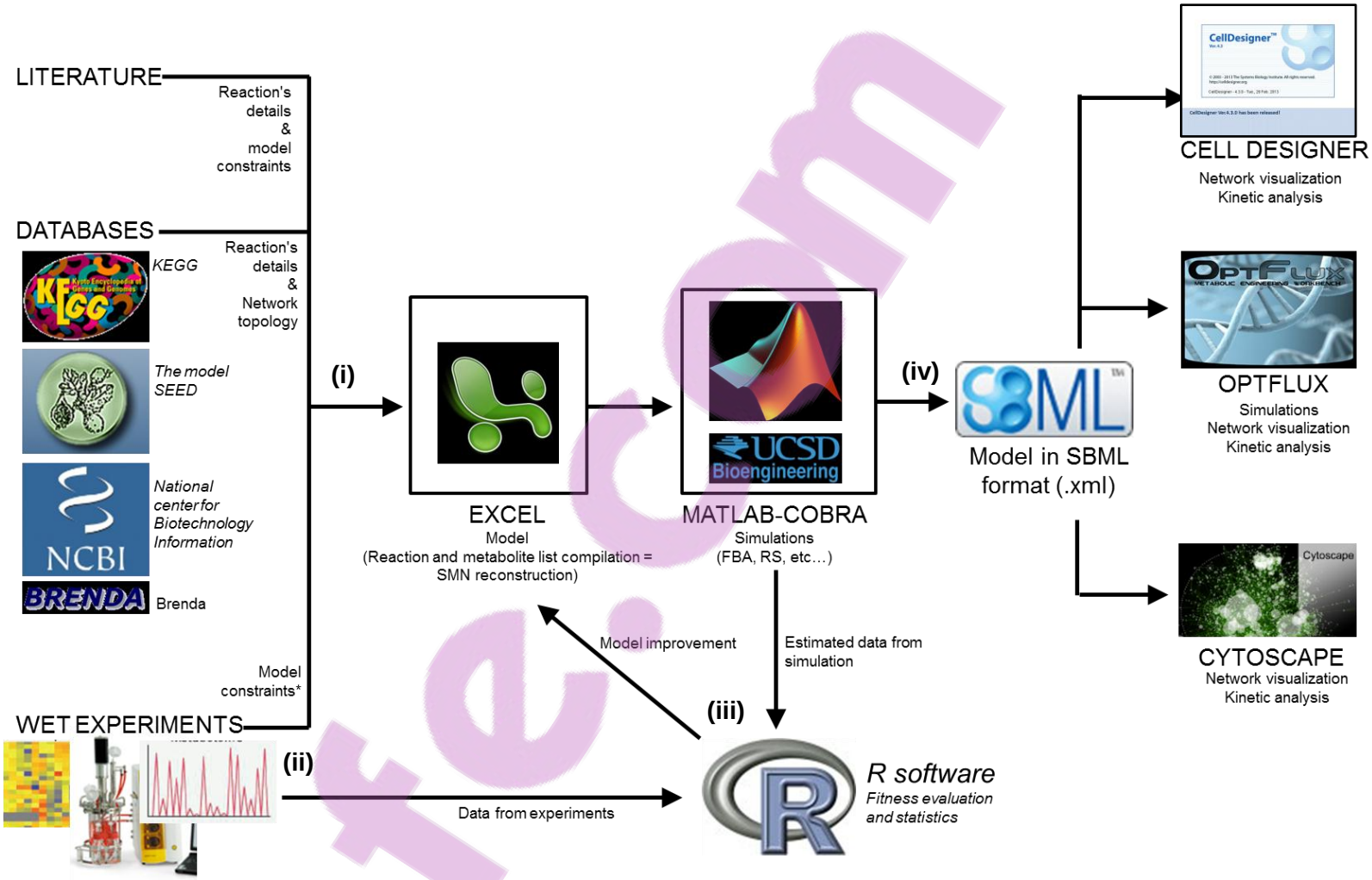

Figure 2.1. Research workflow and corresponding software packages

2.3. Concept of SMN modelling

Stoichiometric Metabolic Network (SMN) modelling is a metabolic modelling method applied to quantify rates of metabolic reaction and in this way describe the metabolic state of cells (Ishii et al., 2004a; Kitano, 2002; Palsson, 2009; Varma and Palsson, 1994b). SMN modelling - also known as metabolic network modelling or genome-scale metabolic modelling - is a data analysis technique particular to Bioinformatics and Systems Biology disciplines. The aim of these disciplines is to investigate and understand the systematic relationships between genes, molecules and organisms. They are particularly concerned with computational modelling of cells and are therefore heavily rely upon computer science and modelling methods (Endler et al., 2009; Kell, 2006; Kitano, 2002; Park et al., 2008).

SMN modelling focuses on predicting **steady state fluxes,** i.e. reaction rates, rather than time-dependent metabolite concentrations and kinetic equations (Klitgord and Segrè, 2010). SMN models utilise the principle of mass conservation within metabolism, to provide a 'snapshot' estimation of the rate of all network reactions simultaneously operating under a specific environmental or physiological state (Orth et al., 2010; Varma and Palsson, 1994b). A set of specific reaction rates estimated at a specific steady state is called flux distribution (Orth et al., 2010; Varma and Palsson, 1994b) These reaction rates are generally expressed in units of micro moles (mmol) of compound produced or consumed per unit of biomass per hour (h). Biomass is commonly expressed as grams of dry weight (gDW)). Specificity of mole identity is given by the compounds involved on the reaction. The reaction rates are expressed as follow:

$$\frac{mmol}{gDW * h}$$

In an SMN model, the cell can be imagined as a set of pipes with metabolites flowing through each pipe and biochemical conversions taking place at junctions between pipes. Some metabolites can also be exchanged with the environment, flowing in or out of the system through dedicated pipes that can be opened or shut, and may have upper bounds to their throughput. The cell must achieve a balance between production and consumption of all the intermediate substrates and products involved in its metabolism. In other words, what flows in through a junction must flow out (Durot et al., 2009).

2.4. Stoichiometric metabolic network reconstruction

For each microbial species modelled, an initial metabolic network was generated from gene-annotation data found in the internet biochemical databases KEGG, Model SEED and NCBI. As illustrated in **Figure 2.2**, the networks of biochemical reactions were reconstructed from existing knowledge of which genes are present in each species, as well as the function of genes. Network reconstruction was done on Excel spreadsheets following the (Thiele and Palsson, 2010) protocol.

The network consisted of mass and charge-balanced stoichiometric biochemical reactions that were classified as either reversible or irreversible (Savinell and Palsson, 1992; Thiele and Palsson, 2010).

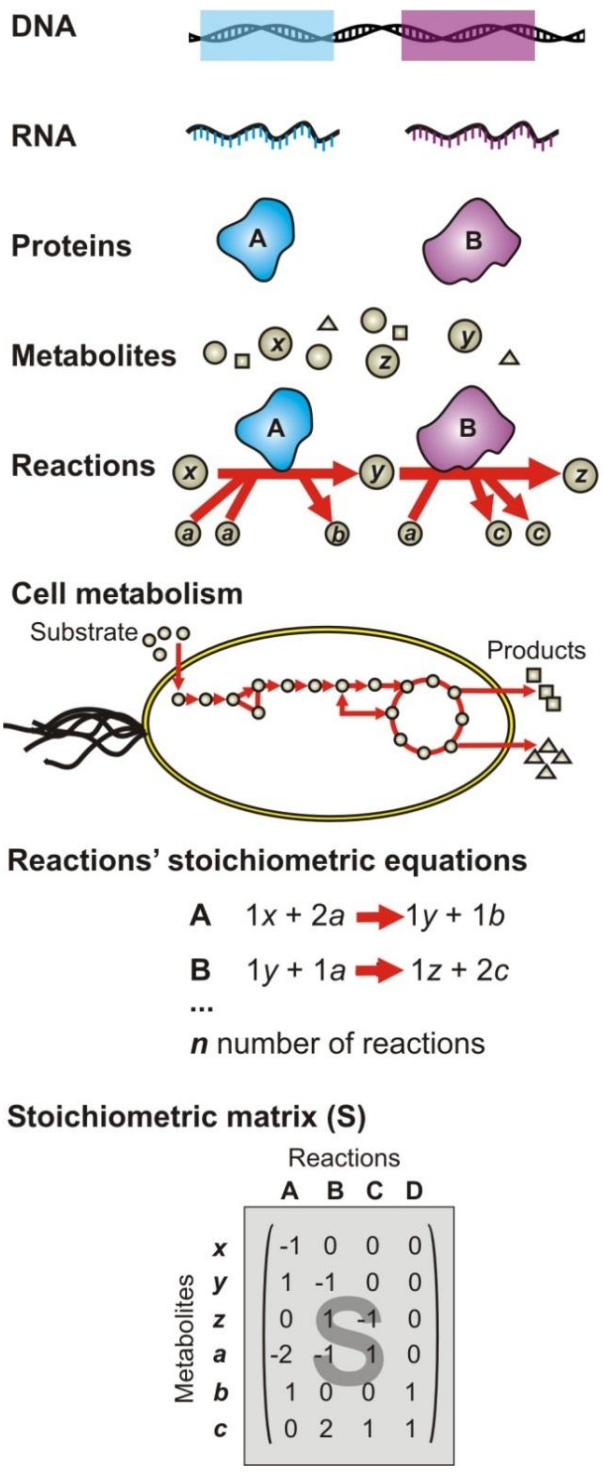

Figure 2.2 Formulation of stoichiometric metabolic network (SMN) using genomic information

Figure 2.2. depicts the SMN reconstruction process as follows: the organism's DNA encodes information to synthesise specific proteins with enzymatic activities (A and B); proteins catalyse for specific reactions where metabolites are used as substrates (x, *a*, *y*) to be transformed into products (z, b, c); subsequent reactions form metabolic pathways, which constitute cell metabolism; each reaction is represented as a stoichiometric equation (A and B);. the equations are then compiled in an extensive list of reactions involved in the modelled pathways.

2.4.1. Metabolic network compartmentalisation

The reactions of nitrifier and denitrifier species were modelled as occurring in three cellular compartments: extracellular, periplasmic and cytoplasmic spaces (Chain et al., 2003). Labels [e], [p] and [c] have been assigned to metabolic compounds to indicate their occurrence in extracellular, periplasmic and cytoplasmic compartments, respectively (**Figure 2.3.**). The metabolite a[e] is thereby differentiated from a[p]. The diffusion between extracellular and periplasmic spaces is simulated as a[e] ←→ a[p]. All reconstructed metabolic networks had stoichiometric equations to represent three types of biochemical reactions (**Figure 2.3.**):

- Exchange reactions
- Transport reactions
- True metabolic reactions (inferred from organism genomes)

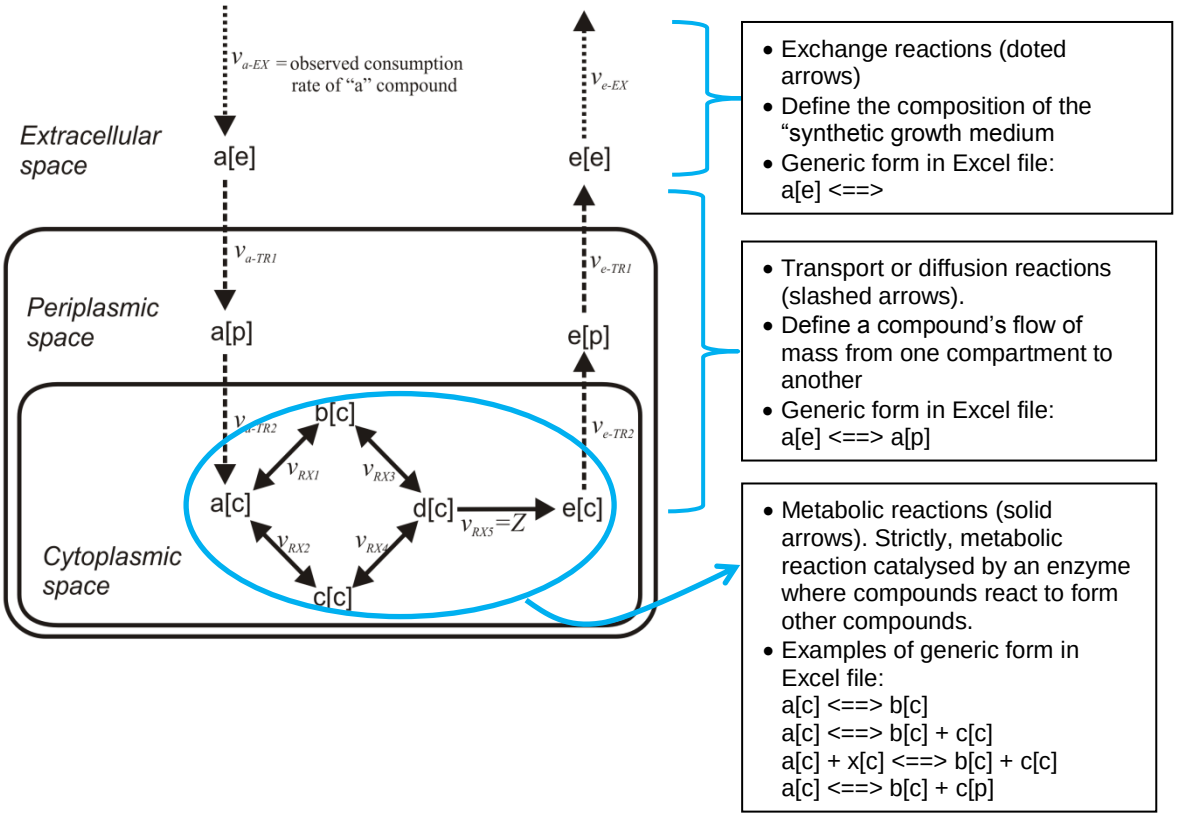

Figure 2.3. Types of biochemical reactions and network compartments

The system boundaries of the metabolic network need to be defined. Specifically, for all metabolites in the model that can be consumed or secreted by cells, a so-called exchange reaction needs to be added to the reconstruction. The exchange reactions were employed in later simulations to define environmental conditions, e.g., carbon source or oxygen availability.

2.4.2. Metabolic network size

The metabolic network size of each of the microbial species modelled is specified in **Table 2.1.** The SMN formulated for each species contained the reactions of the nitrogen respiration and energy production pathways. The modelled metabolic networks also contained reaction equations for maintenance energy consumption, protein production and biomass production, as well as for transport and exchange reactions of consumed and secreted compounds. (See Section 2.1.)

The SMNs reconstructed for the modelled organisms are considered pathway-scale due the amount metabolic pathways included in the reconstructed networks. This scale was chosen for two main reasons:

- To improve predictive accuracy of rates of the mechanism of concern, i.e. N_2O production in nitrifiers and denitrifiers and their relationship to the consumption of nitrogenous compounds, electron donors and electron acceptors; and
- To facilitate the upscale from single species models to multi-species models, as multi species models are necessary to capture the metabolic behaviour of mixed species microbial cultures.

Depending of the number of reactions they contain, SMN models may be classified into two general scales, i.e. the pathway-scale or the genome-scale. Pathway-scale models contain reaction equations for specific and essential metabolic pathways. The size of this model ranges from a few dozen to three hundred reaction equations. Genome-scale models (GEMs) contain reaction equations for all metabolic pathways occurring in an organism, according to the catalytic enzymes encoded in its genome. The size of genome-scale models can go from a few hundred, for models of bacteria and archaea organism with small genomes, to a couple of thousand for eukaryotic organism models (Kim et al., 2012). Genome-scale modelling involves the inclusion of full biosynthetic pathways and expands the range of substrates and potential secreted products. Although expansion of the model may improve the fitness to experimental data, it also presents additional difficulties, such as: a) the tendency to overestimate the rate of reactions in pathways that may only have low flow of metabolites due SMN models assume that all enzymes in pathway are present active (unless explicit experimental evidence); b) the uncertainty of stoichiometric details of many reactions; or c) uncertainty of network topology (Feist et al., 2009).

2.4.3. The biomass production reaction

Biomass production is mathematically represented by adding an artificial 'biomass reaction' — that is, an extra column of coefficients in the stoichiometric matrix — that consumes precursor metabolites at a stoichiometry that simulate biomass production. To generate a biomass reaction, the dry weight cellular composition of the organism of interest needs to be obtained from experimental literature or estimated using data from highly related organisms. Cellular composition refers to the percentage of proteins, RNA, DNA, carbohydrate, lipids, polyamines and other constituents of a given cell. This reaction is scaled in the modelling so that the flux through it is equal to the growth rate (μ) of the organism (Oberhardt et al., 2009; Orth et al., 2010).

2.4.4. Data sources for network reconstruction

Two main sources of stoichiometric equations and network topology were used to reconstruct the metabolic networks, i.e. internet databases and scientific literature containing metabolic and biochemical information of the modelled species.

Table 2.4. Internet databases of biochemical reactions and metabolic pathways

Database	Application	Internet URL
KEGG. Kyoto encyclopaedia of genes and genomes	Very useful database with detailed information of enzymes, pathway reactions and compounds.	http://www.genome.jp/kegg/
The Model SEED	Very useful database where complete genome scale models can be downloaded.	http://seed-viewer.theseed.org/seedviewer.cgi?page=ModelView
NCBI. National centre for biotechnology information	Detailed information about literature, genomes, genes, proteins and compounds.	http://www.ncbi.nlm.nih.gov/
BRENDA.	Specific detailed information on enzymes and reactions	http://www.brenda-enzymes.info/
Metacyc	Specific detailed information of pathways and reactions	http://metacyc.org/
GOLD. Genomes on line database	Specific detailed information of genomes, genes	http://www.genomesonline.org/index.htm
BioModels database	Curated models of biological systems	http://www.ebi.ac.uk/biomodels-main/
BiGG database	Curated genome scale models	http://bigg.ucsd.edu/

Specialised biochemistry literature was used to obtain details of reaction stoichiometry, cofactors and by-products. Biochemical databases sourced from the internet were used to obtain complete sets of stoichiometric equations to reconstruct complete pathways. **Table 2.4.** below provides details of those databases found to be most useful in reconstructing the metabolic networks.

The metabolic reactions of the modelled organisms were mapped based on genome sequence and other physiological and biochemical data from the literature. For instance, **Figure 2.4**. is a screen shot of the KEGG database with a metabolic network map of the nitrogen metabolism of *Nitrosomonas europaea*. The green boxes indicate the presence of reactions identified with Enzyme Commission (EC) numbers, according to the *N. europaea* sequenced genome.

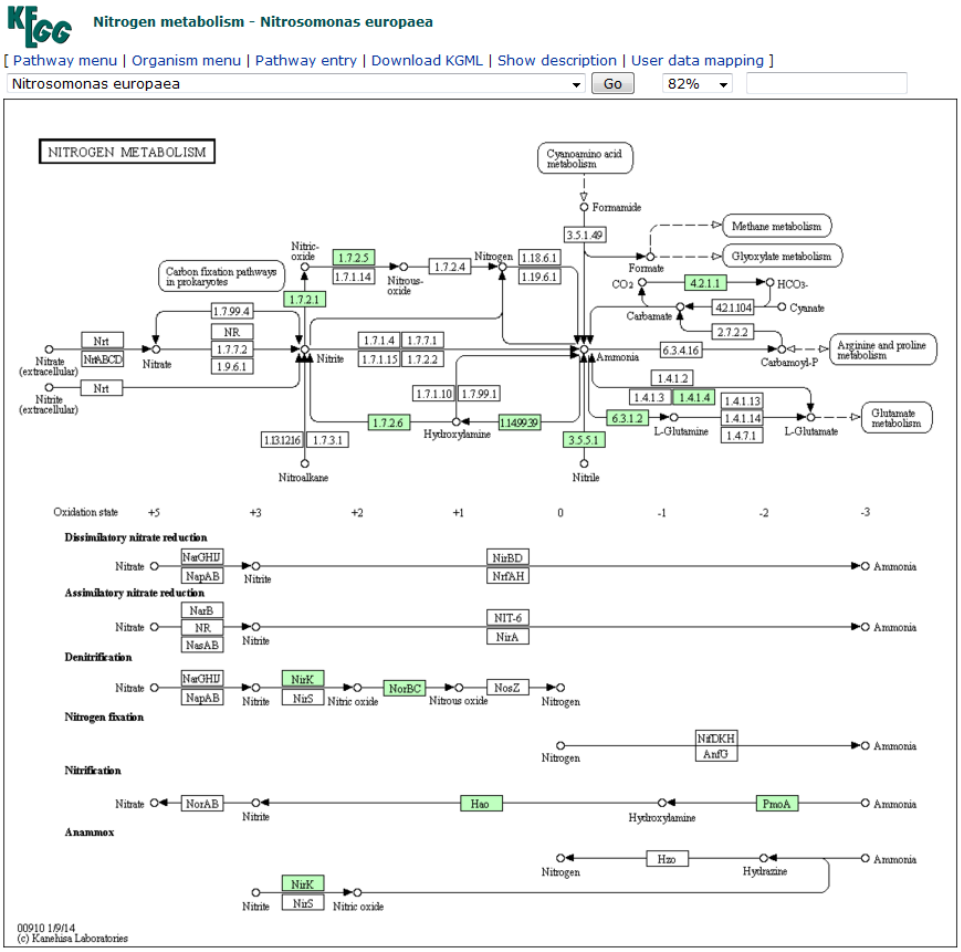

Figure 2.4. Screenshot of KEGG database displaying the metabolic network of *N. europaea* nitrogen metabolism

2.5. Conversion of reconstructed SMN into a mathematical model

The conversion of an SMN reconstruction of an organism into a model requires transformation of the reaction list into a mathematical matrix format. Thus, the equations' stoichiometric coefficients are arranged in the **stoichiometric matrix (*S*),** which size is m x n. Every row of this matrix represents a unique compound i (for a system with m number of compounds); and every column represents a reaction j (for a system with n number of reactions) (**Figure 2.2.**). S stands for stoichiometric. For example, an entry s_{ij} in the matrix is a stoichiometric coefficient of metabolite i in reaction j. A negative entry on the S matrix indicates that the corresponding compound is consumed in the reaction. Conversely, a positive entry indicates that the corresponding compound is produced in the reaction. A stoichiometric coefficient of zero is used for every metabolite that does not participate in a particular reaction. The S matrix contains all the information relating to the reactions modelled for a particular organism (Orth et al., 2010; Varma and Palsson, 1994a).

The metabolic reconstruction is converted into an *in silico* model by mathematically describing the reactions within the S matrix and by imposing physicochemical and environmental constraints to the network, so that system boundaries are defined (Varma and Palsson, 1994a). An illustration of the concept of network system boundaries is presented in **Figure 2.5.** The constraints can be grouped into any one of four categories (Oberhardt et al., 2009):

(i) Physicochemical (e.g., conservation of mass. Defined in the S matrix);

(ii) Topological (e.g. compartmentalisation and spatial restrictions associated with metabolites/enzymes. Defined in the S matrix);

(iii) Environmental (e.g. media composition, pH, temperature. Defined in the model as reaction rates lower ($\propto_j$) and upper (β_j) bounds); and

(iv) Thermodynamic (e.g. Gibbs energy of reaction. Defined in the model as reaction reversibility).

Mathematically, these constraints define a multidimensional solution space of allowable reaction flux distributions. The solution space is where the actual cell's flux state resides. In the same way that a cell is unique in having one genome and many phenotypes, a metabolic reconstruction is unique for its target organism. From this reconstruction, context-specific models can be derived by changing the constraint values, with each context-specific model representing cellular functions under different environmental conditions (Thiele, 2009). The environmental constraints applied to the reconstructed SMN models were the microbial uptake rates for oxygen, nitrogenous compounds and carbonaceous substrates measured on the analysed cultures listed in **Table 2.2.**

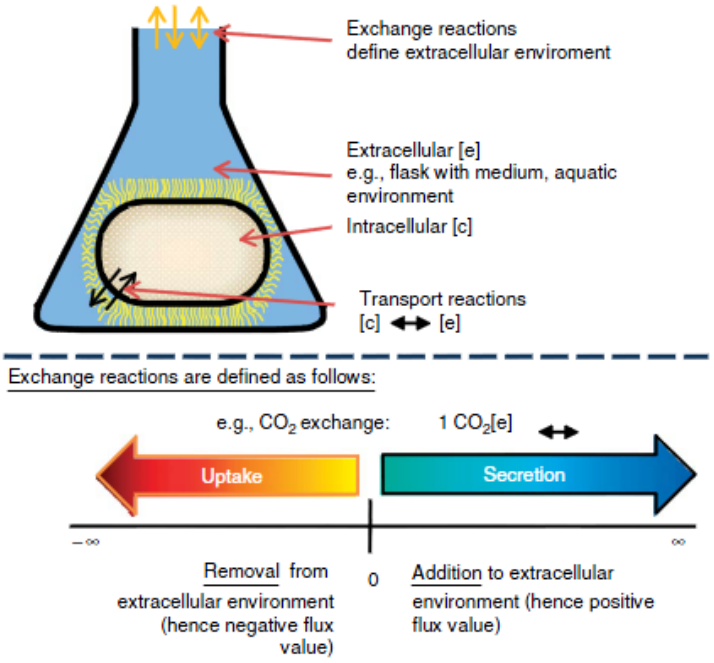

Figure 2.5. Conceptual scheme of system (model) boundaries
[Reprinted by permission from Macmillan Publishers Ltd: Nature Protocols (Thiele and Palsson, 2010), copyright 2010. See Appendix Five]

2.6. Model simulation

Once the metabolic network is captured in a matrix format, different mathematical analyses on properties of the modelled metabolism can be performed. These mathematical analyses have been reviewed in recent publications Durot et al., (2009); Kim et al., (2012); Lewis et al., (2012) and are commonly referred to under the generic name of "constrained-based reconstruction and analysis" (COBRA) methods. **Figure 2.6.** from Lewis et al., (2012) presents an overview of the different COBRA methods and their applications. These applications include modelling genetic perturbations, *in silico* design of mutant strains and modelling regulatory and signalling networks. However the above applications are beyond the scope of this research thesis and will not be discussed further. In general, COBRA methods follow two main categories, biased methods formulated as optimisation problems and unbiased methods formulated to characterise network solution space. Hence, biased COBRA methods include the optimisation of an objective function to identify physiologically relevant flux distributions; and unbiased methods describe all steady-state flux distributions, including reaction sets that function together.

Two COBRA methods were applied in this research to simulate the metabolic behaviour of nitrifying and denitrifying microbes, these methods were:

- Flux balance analysis (FBA) and
- Monte Carlo random sampling (RS)

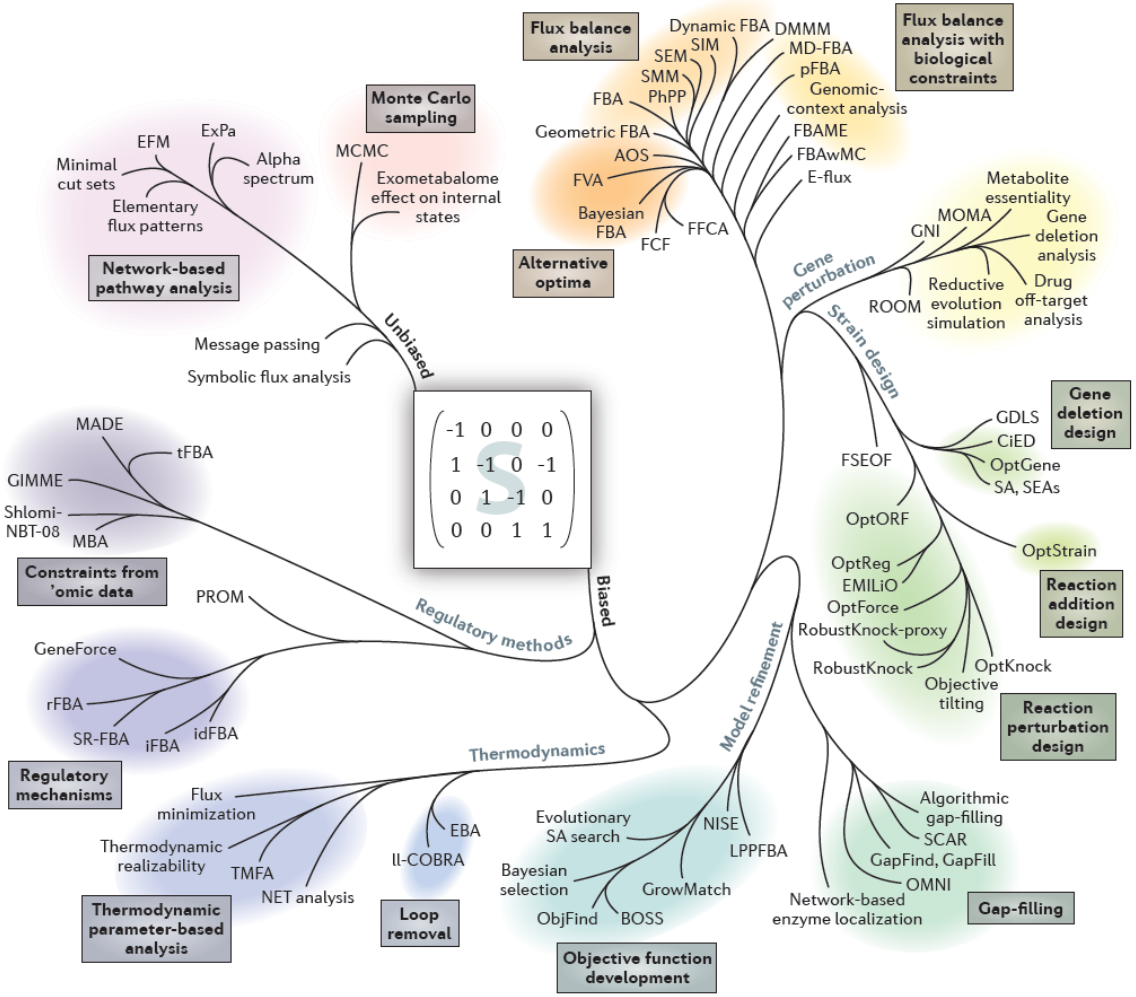

Figure 2.6. "Phylogeny" of simulation algorithms and applications of SMN modelling
[Reprinted by permission from Macmillan Publishers Ltd: Nature Review Microbiology (Lewis et al., 2012), copyright 2012. See Appendix Five]

FBA was used to estimate flux distributions of the NO and N_2O production pathways in the analysed microbial cultures. While RS was used to identify the values for N_2O production rates that can occur in nitrifying microbial communities when exposed to different environmental conditions.

FBA is the most basic and commonly-used biased method for simulating SMN models and is effective in making quantitative predictions of flux distributions using a few governing constraints on the model (Feist et al., 2009; Oberhardt et al., 2009; Orth et al., 2010). RS is an unbiased method used to characterise all feasible flux values in the network, thus providing a probability distribution of feasible fluxes for each reaction under user-provided growth conditions (Price et al., 2004; Schellenberger and Palsson, 2009). A description and mathematical formalisation of FBA and RS methods is provided in the following sections.

2.6.1. Flux balance analysis

Flux balance analysis (FBA) is a formalism in which a reconstructed network is framed as a linear programming (LP) optimisation problem, where a specific objective function, e.g. growth or by-product secretion, is maximised or minimised to calculate network reaction rates. Constraints in network reaction rates for uptake of substrates are added to the optimisation problem to represent a given environmental condition (Edwards et al., 2001; Oberhardt et al., 2009; Orth et al., 2010), such that estimated metabolic reactions rates are related to a culture's operational parameters.

FBA employs a mathematical formalism derived from the mass action expression. The dynamic mass-balance for each compound in the network is represented by the system of equation:

$$\frac{dX}{dt} = S \bullet v \tag{2.1}$$

where X is the vector of metabolite concentrations, t is time, S is the stoichiometric matrix with size m x n and v is the vector of metabolic fluxes through all network's reactions (Orth et al., 2010; Savinell and Palsson, 1992).

Transients in metabolism are typically on the order of a few minutes, which is much faster than cellular growth rates and other dynamic changes in the microorganism's environment. Therefore FBA is performed on metabolic networks at steady-state. Accordingly, the FBA assumes that metabolic fluxes are in a pseudo-steady-state relative to growth and process transients (Varma and Palsson, 1994a). By definition, the change in concentration of metabolites over time is equal to zero when a system is at steady-state:

$$\frac{dX}{dt} = 0 \tag{2.2}$$

The set of possible steady-state flux distributions through the metabolic network is represented as the vector v in the Equation 2.3.

$$S \bullet v = 0 \tag{2.3}$$

The equation (2.3) constitutes the main constraint set representing a biochemical network in FBA, and implies that the formation fluxes of a metabolic compound i are balanced with its degradation fluxes, the sum of fluxes therefore equalling zero. The steady-state condition $S \bullet v = 0$ defines a system of linear equations, as shown in **Figure 2.7.**

A precise definition of the boundary of the system to be modelled is also needed to formulate an explicit mathematical representation. A specific environmental or phenotypic condition (described in section 2.5.) is included in a model's constraints by adding constraints on the reaction rates of the vector with the following form:

$$\alpha_j \leq v_j \leq \beta_j \tag{2.4}$$

where α_j and β_j represent the lower and upper bounds for reaction rate v_j. Lower bound (α) and an upper bound (β) are in fact set to every reaction in the system. These bounds are represented by column vectors, with coefficients representing minimum and maximum fluxes for the corresponding reaction j. Bounds for exchange reactions represent the flow of nutrients into and out of the biochemical system; while bounds for transport reactions (occurring across cell and subcellular compartment membranes) and metabolic reactions (occurring within the confines of the cell membrane) represent physicochemical constraints on reaction rates due to thermodynamics or maximal uptake rates (Orth et al., 2010).

SMN are underdetermined systems, i.e. there are more reactions than there are compounds (n > m). Therefore there is no unique flux distribution that satisfies the system of equations. Thus, the underdetermined system of linear equations can be formulated as an optimisation problem, in which the solution algorithm finds the optimal flux distribution that minimises or maximises a particular objective defined by the user (Varma and Palsson, 1994a). The mathematical representation of this objective is called **objective function (Z).** The rationale behind selecting a particular objective function is based on the fact that an organism will maximise its performance under conditions to which it is adapted (Park et al., 2009; Schuetz et al., 2007). Typically, this is set to maximise the rate of the biomass production reaction ($Z = v_{Biomass}$), although other choices, such as minimisation of resource utilisation and maximisation of ATP production, have been reported (Schuetz et al., 2007). FBA seeks to maximise or minimise the objective function Z, which is a linear combination of fluxes. Optimisation of such system is accomplished with **linear programming (LP)**. The output of FBA is a particular flux distribution that maximises or minimises the objective function (Oberhardt et al., 2009; Orth et al., 2010). **Figure 2.7.** presents the generalised concept of FBA, where the observed consumption rate

and objective function criteria - to maximise/minimise the rate a specific reaction - are used to find the rate values of the rest of the network reactions.

A mathematical formalism for FBA optimisation problems states as follows:

$$max(v_{Biomass})$$

$$s.t. \begin{cases} S \bullet v = 0 \\ \alpha_j \leq v_j \leq \beta_j \\ v_{SubstarteUptake} = Upateke\ measured\ on\ experiment \end{cases}$$

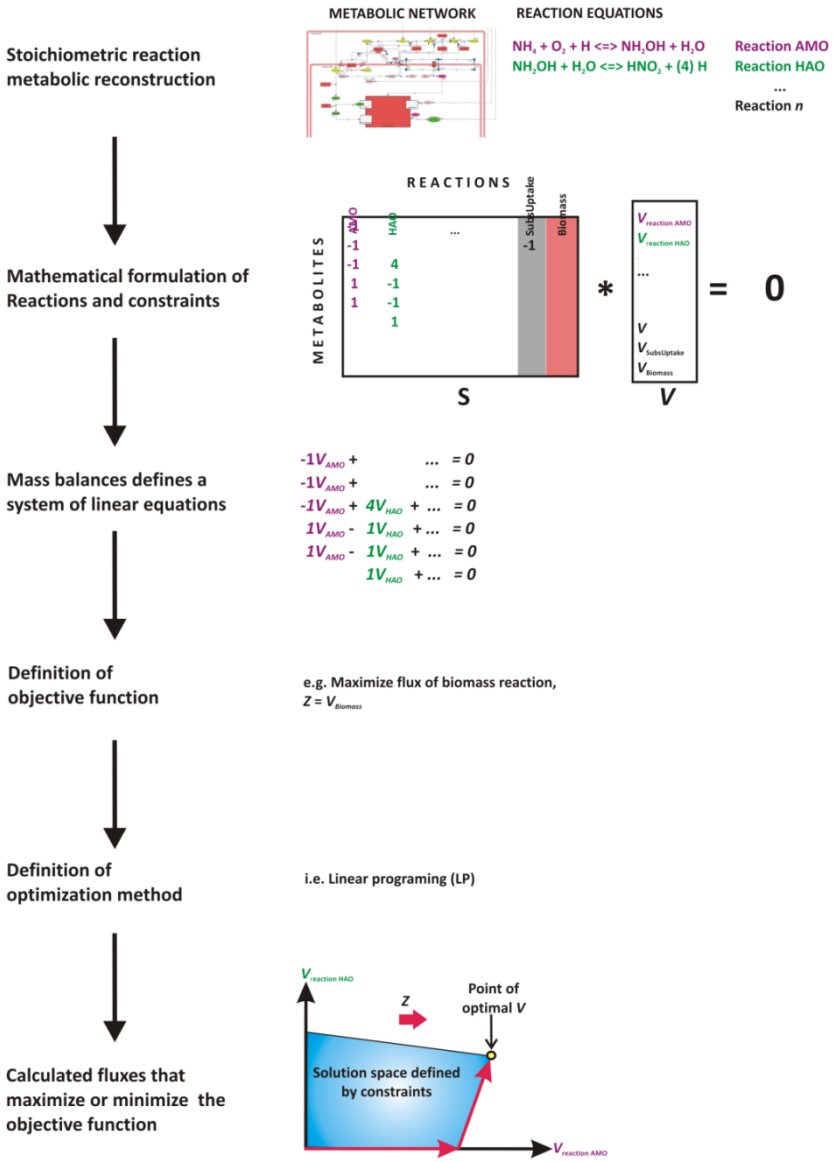

Figure 2.7. Formulation of a FBA problem

A key question in FBA approach is whether intracellular fluxes in metabolic steady state can be predicted from network stoichiometry alone by invoking optimality principles. Since no single objective can predict experimental data from a cell culture under all possible environmental conditions, then the pivotal element is to identify the most relevant objective for each condition. For instance, for cultures under unlimited growth conditions, the best objective function appears to be nonlinear maximization of the ATP yield per unit of flux, which is a combination of the linear maximization of overall ATP yield and minimization of the overall flux. For cultures under nutrient scarcity the linear maximization of ATP or biomass yield is clearly superior (Schuetz et al., 2007).

2.6.2. Monte Carlo random sampling (RS)

FBA only returns a single optimal point as a solution and thus yields little information about the variability of possible solutions within the solution space. The existence of a solution space means that many conceivable flux distributions can satisfy the steady-state condition and constraints (Schellenberger and Palsson, 2009). An alternative method to FBA is to characterise the solution space using Monte Carlo random sampling (RS) (Schellenberger and Palsson, 2009). Uniform random sampling of the solution space in any environmental condition is a rapid and scalable way to characterise the structure of the allowed space of metabolic fluxes (Becker et al., 2007). But most importantly, RS provides a set of rate values for each reaction so that descriptive statistics, such as mean, median, standard deviation and range, can be estimated (Schellenberger and Palsson, 2009). This makes flux estimations more robust than those calculated with FBA.

RS of reconstructed SMN was performed using the random walk algorithm, artificial cantering hit-and-run (ACHR), encoded in the COBRA toolbox v2.0 (Thiele et al., 2005). The algorithm involves three steps (Thiele et al., 2005): (i) identification of initial point within the solution space; (ii) 'warm-up' point calculation using iterations of basic hit-and-run algorithms; warm up points are stored in a matrix W; and (iii) sample point calculation using the W matrix as a reference for sampling with each iteration

The ACHR algorithm produces a valid solution point for every sampling iteration. An initial valid point is moved repeatedly inside the space according to probabilistic rules (Schellenberger and Palsson, 2009). Each iteration provides a flux value for each reaction, such that several iterations will provide a set of flux values. This is illustrated in **Figure 2.8.**, where FBA and RS solution concepts are compared. All possible rate values of the two given network reactions (v_1 and v_2) lie in the solution space (dark grey area) defined by the reactions' lower (α) and upper (β) rate limits. FBA finds a single rate value for each reaction (white circle) that maximises (or minimises) the value of a given objective function. RS, on the other hand, obtains rate values sampled from the entire solution space (black crosses) to produce a dataset that can be statistically analysed.

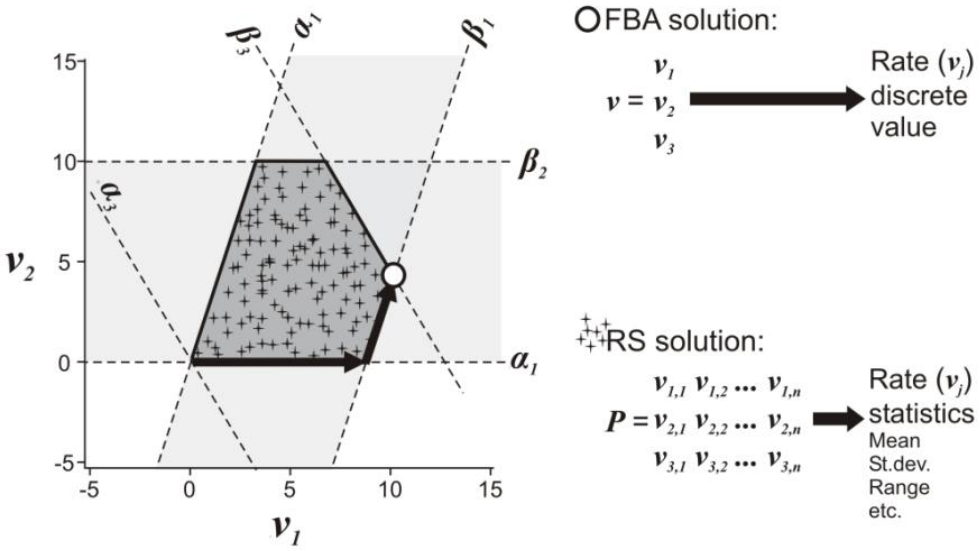

Figure 2.8 Concept of FBA and RS simulations of metabolic networks

2.7. Simulation software

FBA and RS of the reconstructed SMN models were performed using COBRA toolbox v2.0 (Schellenberger et al., 2011) running in MATLAB® (The MathWorks Inc, Massachusetts, USA). The COBRA toolbox (Becker et al., 2007) is a set of COBRA methods encoded in MATLAB software format. COBRA toolbox v2.0 was also used to convert the SMN reconstruction file into its mathematical form, as well as for network evaluation and debugging. A list of COBRA toolbox v2.0 functions routinely used during this research is presented in **Table 2.5.** The MATLABS's COBRA toolbox is available without cost on "The open COBRA project" website (URL: http://opencobra.sourceforge.net/openCOBRA/Welcome.html).

Table 2.5.: List of COBRA toolbox 2.0 functions used to evaluate, debug and simulate SMN models

Function	Function's command syntax
Load model	>>model=xls2model('reconstructionfile.xls','reconstructionfile.xls')
Run standard FBA	>>solution=optimizeCbModel(model)
Matrix verification	>>spy(model.S)
Detect network's dead ends	>>outputMets=detectDeadEnds(model)
Find all gaps	>>[allGaps,rootGaps,downstreamGaps]=gapFind(model)
Dynamic simulation	>>substrateRxns={EX_o2(e)} >>initConcentrations=x >>initBiomass=0.035 >>timeStep=.25; nSteps=100 >>dynamicFBA(model, substrateRxns, initConcentrations, initBiomass, timeStep, nSteps,plotRxns)
Flux variability analysis	>>[minFlux,maxFlux]=fluxVariability(model,optPercentage)
Robustness analysis	>>robustnessAnalysis(model,'controlreaction',numberofpoints)
GeometricFBA	>>flux=geometricFBA(model)
RS of solution space	>>[modelSampling,samples]=sampleCbModel(model,'WarmPointsFile')
Scatter plot of sampled solution space	>>sampleScatterMatrix(rxnNames,modelSampling,samples)
Convert COBRA model to sbml model	>>sbmlModel = convertCobraToSBML(model)
Save the sbml model into a .xml file	>>OutputSBML(sbmlModel,'NewFileName.xml')

2.8. Model calibration

The accuracy of SMN models in estimating observations within real cells relies on rigorous model calibration (Edwards et al., 2001). Model calibration involves comparing the model's estimated values with experimental data obtained from measurements in real systems. This allows the model's structure and parameter values to be refined until differences between the datasets are minimal (Feist et al., 2009).

On the context of SMN modelling, structure (also known as network topology) refers to which biochemical reactions are included on the model. Model structure is defined by two criteria: a) the purpose of the model and therefore the pathways to be modelled, and b) the catalytic capabilities of enzymes encoded on the genome of the modelled organism. Wrong genome annotations and

uncertainty on presence or activation of catalytic enzyme introduce the necessity to calibrate the structure of models. The structure of SMN models developed during this doctoral thesis sticks to metabolic pathways of N_2O transformation experimentally proven to exist on the modelled microbes.

On other hand, there are two kinds of parameters that can be calibrated on SMN models: a) stoichiometric coefficients (s_{ij}) of compounds in reaction equations; and b) lower and upper bound values of reaction rates (respectively α_j and β_j). Values of stoichiometric coefficients are defined by the catalytic capabilities of enzymes and in principle they don't need to be calibrated. However the catalytic capabilities of some enzymes can be not well defined and consequently being unknown the exact stoichiometry of the reaction they catalyse; therefore, generating the necessity to calibrate the unknown value of reaction's stoichiometric coefficients. Further, given the fact that the big majority of α_j and β_j values of metabolic reactions are unknown, the general consensus is to assign them a value that do not constraint the free flux of metabolites through the network, unless explicit experimental data indicate the contrary (Thiele and Palsson, 2010). For instance if the maximum reaction rate (μ^{max}) of given enzyme is measured experimentally, then this value can be assigned to the β_j parameter of the corresponding model reaction. Reaction's α_j or β_j values require to be calibrated when a specific constraint is to be placed and there is uncertainty on the specific value to be assigned.

The following sections describe a method developed to calibrate structure and parameters values of SMN models. The method principle is based on minimize relative errors of predicted metabolic metrics against values of those metrics observed experimentally. The metabolic metrics (also known as process variables) may be culture yields, compound uptake and production rates, and other variable describing the steady state metabolism of the cellular culture under specific experimental conditions. This type of multivariate experimental dataset is used to measure the accuracy of model simulations using various scores of goodness of fit. The example described on the following sections specifically focuses on the calibration of stoichiometric coefficients values related to uncharacterised or lumped reactions of SMN models. However, the method is also applicable to calibrate model structure and upper and lower bounds of reaction rate.

2.8.1. Develop method for model calibration

When experimental data is limited or does not contain information appropriate for model calibration, it can limit the ability of SMN models to produce relevant and accurate estimates. Lack of experimental data for model calibration is a common problem in SMN modelling. For example, the general procedure for SMN model calibration involves comparing estimated and experimental growth rates observed under different organic carbon sources (Durot et al., 2009; Edwards et al., 2001). Thus, de facto, this approach may not be applicable to calibrating models of organism or microbial communities that do not use organic molecules to grow, i.e. autotrophs. Another possible scenario is to use 13C-flux analysis, which provides metabolic reaction rate measurements that can be directly compared

with FBA simulations. However, experimental data is limited by the cost of this technique and its limited scope in that it can provide rate measurements only for the central carbon pathway (Sauer, 2006).The most valuable experimental data for model calibration and validation comes from transcriptomic, proteomic and metabolomic analysis (Kümmel et al., 2006a; Kümmel et al., 2006b; Lewis et al., 2010). Unfortunately, this requires pre-existing analytical and expertise capability to obtain relevant omic data. Due to these limitations, it is sometimes necessary to employ computational methods to calibrate SMN models using common bioprocess performance data.

2.8.1.1. Metabolic network

The metabolic network developed to model *Nitrosomonas europaea* metabolism was used to develop the calibration method. The metabolic network, constructed using (Thiele and Palsson, 2010) protocol, consisted of 44 metabolites, 49 stoichiometric reactions and 3 compartments. The COBRA toolbox 2.0 (Schellenberger et al., 2011), together with the GLPK solver running in MATLAB®7 R2010b software (MathWorks Inc., Natick, MA, USA), was used to convert the metabolic network into its mathematical form and perform FBA simulations. Mathematically, the network was represented as a stoichiometric matrix, $S\ (m \times n)$, of m metabolites and n reactions. A non-zero entry $s_{i,j}$ in S indicates the participation of metabolite i in reaction j. All reactions within the network were mass-balanced, such that $S * v = 0$, where v is a vector of reaction rates - or fluxes (Feist et al., 2009; Varma and Palsson, 1994a). The reaction rate limits - or constraints - were defined in the form $\alpha_j \leq v_j \leq \beta_j$, where α_j and β_j are the lower and upper limits placed on the reaction rate v_j (Varma and Palsson, 1994a).

The metabolic network of *N. europaea* respiration pathways had to be calibrated (curated) as it contained four reactions involving compounds with undetermined stoichiometric coefficients. These four reactions, presented in **Table 2.6.**, corresponded to electron transport chain reactions that translocate protons across the cellular membrane and the ATP stoichiometric coefficient in the biomass reaction. The precise stoichiometry of these reactions was found to be either ambiguous or simply not present in the scientific literature.

2.8.1.2. Generation of model versions and simulations

Candidate stoichiometric coefficients were defined in the four reactions presented in **Table 2.6.**, so that mass and energy balance was preserved. Although **Table 2.6.** shows that fraction values were not assigned to candidate coefficients, these can be assigned directly if needed without method modification.

Table 2.6. Reactions of the SMN model calibrated in this study

Reaction ID	Stoichiometric equation	Candidate coefficients "s"	Number of coefficients
A	nh3[p] + o2[p] + q8h2[c] + ***s*** h[c] → nh2oh[p] + h2o[c] + q8[c] + ***s*** h[p]	0, 1, 2	3
B	q8h2[c] + 2 cyt552[p] + ***s-2*** h[c] → ***s*** h[p] + q8[c] + 2 cyt552e[p]	2, 4	2
C	atp[c] + 10 nadh[c] + 0.25 protein[c] + ***s*** m[c] ←→ adp[c] + 10 nad[c] + pi[c] + 0.26 h[c] + biomass[c]	From 0 to 50 each 5	20
D	***s*** atp[c] + 10 nadh[c] + 0.25 protein[c] + m[c] ←→ ***s*** adp[c] + 10 nad[c] + ***s*** pi[c] + ***s*** h[c] + biomass[c]	From 0 to 100 each 10	11

By systematically combining the candidate stoichiometric coefficients for each reaction with those for the remaining three reactions, we obtained a total of 1320 combinations (3 x 2 x 20 x 11 = 1320), which gave 1320 model versions. These model versions and their corresponding FBA simulations were automatically generated with the following MATLAB® script:

```
%% Run a FBA simulation for all model versions generated by changing the S
matrix.
%Define column vectors "coeffsA", "coeffsB", "coeffsB" and "coeffsD" of
coefficient values of each reaction. All column vectors must be of the same
length.
coeffsA=[];
coeffsB=[];
coeffsC=[];
coeffsD=[];
%Assign the values of "coeffs" to the corresponding stoichiometric
coefficient with coordinates (i,j) in model.S matrix and run a FBA
simulation. Values of column vectors are assigned row by row until the
length of "coeff1". Store the solution on the matrix "M"
for j=1:length(coeff1);
    model.S(43,50)=coeff1(j);
    model.S(42,50)=coeff2(j);
    model.S(26,50)=coeff2(j);
    model.S(11,50)=coeff2(j);
    model.S(11,33)=coeff4(j);
    model.S(20,33)=coeff5(j);
    model.S(11,41)=coeff6(j);
    model.S(20,41)=coeff7(j);
    solution=optimizeCbModel(model);    %FBA simulation
    M(:,j)=solution.x          %Generation of "M" matrix
end
```

The above script generated an M matrix of n number of reactions and d number of FBA solutions (d=1320). Note that FBA simulations can be substituted by other methods to estimate network fluxes, such as random sampling or extreme pathways.

Alternatively, the following MATLAB® script can be used to iteratively assign candidate values to upper or lower bounds (α_j and β_j) to a single reaction and then run FBA simulations:

```
%% Run a FBA simulation for all model versions generated by changing the
lower bounds (alfa) to a single reaction
%Define a list with the name of the reaction to be constrain and the
rxnNameList1=[]
%Define candidate the values to be placed in that reaction. The variables
"rxnNameList1" and "values1" must be of the same length
values1=[]
%%Assign the values of "values1" to the corresponding reaction on
"rxnNameList1" and run a FBA simulation. Store FBA solution on the matrix
"M". Iteratively run the above steps until the length of "values1"
for j=1:length(values1)
    model=changeRxnBounds(model,rxnNameList1(j),values1(j),'l');
    solution=optimizeCbModel(model);            %FBA simulation
    M(:,j)=solution.x;                          %Generation of "M" matrix
end
surf(M)                                         %Surface plot of "M"
```

The above script can be used to generate candidate models and their solutions in order to calibrate model structure and reaction's constraints.

2.8.1.3. Defining experimental datasets for calibration

Compound concentration curves, biomass concentration, reactor volume, inflow rate of growth medium and other biochemical information is reported in previously published experiments on *N. europaea* growing in aerobic conditions without oxygen and ammonium substrate limitation) (Grady et al., 1999; Vadivelu et al., 2006; Whittaker et al., 2000). Data from these experiments was used to define an experimental dataset X_l of 28 mean values of l variables, which describe the metabolism of these organisms under specified conditions. **Table 2.7.** defines the categories to which the 28 variables of the experimental dataset belong.

The 28 variables apply to the same specific steady-state condition of *N. europaea* growth. In the case of experiments with batch cultures, a steady-state was assumed for time periods where the change in substrate and product concentrations maintained a linear trend, indicating a constant rate of consumption and production of compounds. The rate variables were normalised by the total biomass in the bioreactor, expressed as grams of dry weight (gDW)).

Table 2.7. Definition of variables of calibration datasets.
Including number of variable values in dataset found in previously published experiments

Variable category	Formula for variable estimation with model simulation results	Number of dataset variables
Growth rate	$= v_{biomass}$	1
Specific substrate uptake rate	$= v_{substrate}$	2
Specific compound production rate	$= v_{product}$	2
Molar yield ratio of product	$= \frac{v_{product}}{v_{substrate}}$	4
Net amount of compound used in reaction	$= v_j * s_i$	2
ATP molar yield ratio	$= \frac{\sum_{j=1}^{J}(v_{ATP\ consumption} * s_{ATP})_j}{\sum_{j=1}^{J}(v_{ATP\ synthezis})_j}$	2
Proton translocation yield ratio	$= \frac{\sum_{j=1}^{J}(v_{H+\ produced} * s_{H+})_j}{v_{substrate}}$	2
Pivot compound reaction yield ratio	$= \frac{v_{consumption\ of\ i\ in\ reaction\ j}}{v_{synthezis\ of\ i}}$	6
Percentage yield ratio of element	$= \frac{v_{production\ of\ i} * s_i * a}{v_{consumption\ of\ i} * s_i * a} * 100$	4
Element mass balance	$= \sum_{j=1}^{J}(v_j * s_i * a)_j$	3
TOTAL		28

Note: v_j is the rate of reaction j; s_i is the stoichiometric coefficient of compound i; J is the total number of reactions that consume or/and produce the compound i; and a is the element's number of atoms in compound i.

2.8.1.4. Evaluation of goodness to fit

The goodness of fit of a model describes the degree to which model predictions fit experimental data (Makinia, 2010). Goodness of fit was evaluated after data transformation in the following way. The 28 variables were estimated using the simulation results of the M matrix and applying the generic formulas presented in **Table 2.7.** to produce a x_l dataset for each of the 1320 model versions. Experimental and estimated datasets (X_l and x_l, respectively) were $\log_{10}$ or auto-scale transformed, as dataset values had a different order of magnitude and dimensions, e.g. $v_{O2\ uptake}$ = 2.5mmol/gDW*h while the $v_{biomass}/v_{O2\ uptake}$ yield = 0.012gDW/mmol-O_2. Data transformation was necessary to capture the deviation between the observed and estimated values in absolute terms, and to minimise the effect of varying scales for different variables (Schuetz et al., 2007; van den Berg et al., 2006).

The overall fitness between experimental and estimated datasets was evaluated using the fitness scores presented in **Table 2.8.** The model version with lower fitness scores was considered to have the highest accuracy in reproducing the experimental data and to therefore yield a calibrated model.

Table 2.8. Some formulas to evaluate goodness to fit of a model. Modified from (Makinia, 2010)

Fitness score	Formula
Mean relative error (MRE)	$MRE = \frac{1}{n}\sum_{l=1}^{n}\frac{\lvert(X_l - x_l)\rvert}{X_l}$
Mean absolute error (MAE)	$MAE = \frac{1}{n}\sum_{l=1}^{n}\lvert(X_l - x_l)\rvert$
Root mean squared error (RMSE)	$RMSE = \sqrt{\frac{1}{n}\sum_{l=1}^{n}(X_l - x_l)^2}$
Root mean squared scaled error (RMSSE)	$RMSSE = \sqrt{\frac{1}{n}\sum_{i=1}^{n}\frac{m_l(X_l - x_l)^2}{(std)_l^2}}$

Note: n is the total number of variables in both observed and estimated datasets; X_l is the observed data (measured in experiments) in variable l; x_l is the estimated data (estimated in simulations) in variable l; m_l is the number of data points contributing to X_l; and std is the standard deviation of the observed data in variable l.

2.8.2. Results

The graphs to the left of **Figure 2.9.** present the fitness scores obtained for each of the 1320 model versions. The plots on the right show the same scores, but the scores for each version are sorted from lowest to highest. Both MRE and RMSSE scores for fitness of model versions identified version number “757” as showing the best fitness to experimental data. Version “757” had the following stoichiometric coefficient values: free protons generated on AMO reaction ($s_{i,A}$) = 1, protons translocated during ubiquinone-8 oxidation ($s_{i,B}$) = 2, number of ATP moles on maintenance reaction ($s_{i,C}$) = 5, and number of ATP moles on biomass production reaction ($s_{i,D}$) = 80. On other hand, MRE and RMSSE scored model version “24” as having the worst fitness to the experimental data. MAE and RMSE scores ranked the versions differently from each other, as well as from MRE and RMSSE.

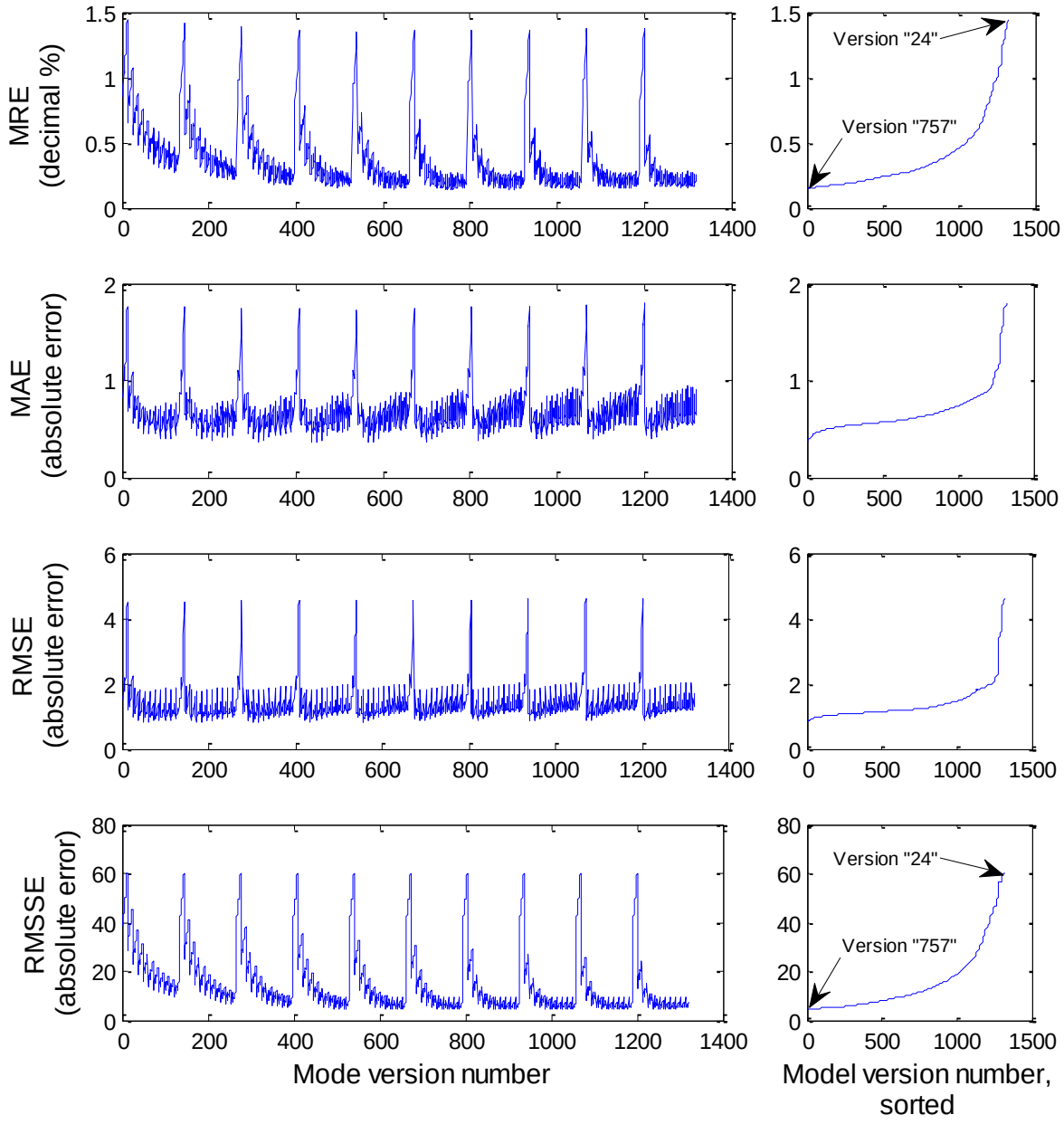

Fig. 2.9. Plots of fitness scores obtained for the 1320 model versions.

Figure 2.10. shows calibration curves generated by plotting experimental and estimated datasets for model versions “24” and “757”. The diagonal line represents a perfect fit between experimental and estimated datasets. “X” markers represent the estimated dataset of model version “24”. “O” markers represent the estimated dataset of model version “757”. Also shown is the effect of both log transformed and auto-scaled datasets. Without transformation, the deviation between estimated and experimental datasets cannot be visually evaluated during calibration because of the significant variation in the scale of different variables. The Log_{10} transformed and auto-scaled data gave less noisy calibration curves, because all variables were re-scaled to the same units.

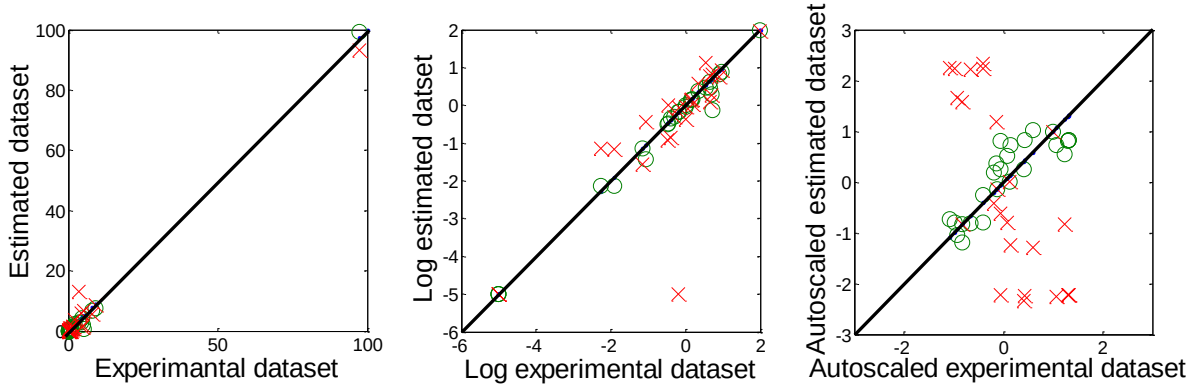

Figure 2.10. Model calibration curves generated without treatment, log[10] transformed treatment and auto-scaled treatment of datasets.

The calibration curves in **Figure 2.10.** show similar results to those obtained for fitness scores, especially with auto-scaled data. Model version fitness can therefore be evaluated both ways, i.e. either with fitness scores or visually using calibration curves. MRE and RMSEE scores provided the most meaningful fitness scores for two reasons: i) they corrected differences in the scales or units of variables; and ii) they better reflected small deviations between experimental and estimated datasets. However, MRE is a more meaningful score as error is measured on a scale from 0 to 1, with 0 representing a perfect fit. This allows the percentage of accuracy to be determined directly with the formula: $accuracy\ (\%) = ((1 - MRE) * 100)$. Auto-scaled transformations provided the best way of visually representing the deviations of estimated datasets from experiments, because auto-scaled datasets are more sensitive to numerical differences between the two.

2.8.3 Summary of calibration methods

The method presented in the above sections is an easy-to-implement way of calibrating stoichiometric coefficients in SMN models. The essence of the method is to find those coefficients that produce a model version that best fits experimental data. In this sense, the SMN model structure (coefficients of the S matrix) is defined by experimental data and this ensures realistic estimates for intracellular reaction rates. Model calibration should be done against various experimental datasets produced under different environmental conditions in order to obtain a non overfitted model. Extracting as much information as possible on values of variables from experiments or scientific literature is essential to produce a robust experimental dataset with a large number of variables l, and thereby improve the fitness scores. This method can be applied to evaluate the fitness of multiple metabolic reaction constraints. It can also be extended to fit models to transcriptomic or metabolomic data by using the model simulations algorithms of parsimonious enzyme usage FBA (pFBA) (Lewis et al., 2010) or network embedded thermodynamic (NET) analysis (Kümmel et al., 2006a). Nonetheless, these applications were beyond the scope of this research.

2.9. Conclusions

The research approach of this thesis focuses on estimating rates of all the metabolic reactions for nitrogen respiration and energy production simultaneously occurring in nitrifying and denitrifying microbial cultures producing N_2O. Thus, operational conditions of cultures can be mechanistically related to reaction rates of NO and N_2O-producing pathways. The research approach involves four main steps: (i) development of SMN models of BNR microbes to include formulation, implementation and calibration; (ii) experiment data acquisition from scientific publications or from experiments performed; (ii) model simulation to fit experimental data; and (iv) metabolic rate estimation and pathway activity inference. This chapter described the model development and provided detailed theoretical information about SMN modelling. Steps two to four are covered in the methods section of Chapters Four, Five and Six describing formal simulation studies of experimental cultures.

In short, the primary objective of this doctoral thesis was to develop a computational platform to be able to estimate the rates of reactions forming the biological pathways for N_2O and NO production. This platform was based on SMN models of nitrifying and denitrifying microbes. The metabolism of twelve species of BNR microbes was modelled. Four of those species belong to the ammonia oxidizing bacteria (AOB) guild, another four to the nitrite oxidizing bacteria (NOB) guild and the last four to the heterotrophic denitrifying bacteria (DEN) guild. The species were selected on basis of their abundance and relevance in full scale and laboratory-scale BNR microbial cultures. SMN formulation, i.e. SMN reconstruction, was based on biochemical and metabolic information on the species found in scientific literature and biochemical databases, such as KEGG. SMN reconstructions were done in Excel spreadsheets, following the protocol described in (Thiele and Palsson, 2010). The MATLAB COBRA toolbox v2.0 was used to convert reconstruction files into mathematical models and to perform SMN evaluation, debugging and simulation. The COBRA toolbox was the modelling software of choice because the MATLAB environment allowed flexible model modification, calibration method implementation and other statistical analysis.

The computational platform also included methods for model simulation and calibration, as well as for processing experimental data. This was to provide for comparison with the model simulation results. The model simulation methods used from the COBRA toolbox were FBA and RS. The model calibration methods developed during this research involved the generation of candidate models with a novel MATLAB script and the generation of calibration datasets using equations developed in this research. These new equations were also used to generate experimental datasets for fitness evaluation. Finally, different fitness evaluation scores were assessed. Results highlighted that mean relative error (MRE) is the most practical and meaningful score to evaluate fitness between model estimations and experimental datasets, as its scale from 0 to 1 makes it easier and faster to interpret.

CHAPTER THREE

SMN modelling of mixed microbial cultures: approaches and applications

This chapter presents a full review of applications and approaches used to characterize metabolic activity in environmental bioprocesses using Stoichiometric Metabolic Network (SMN) modelling. The review and discussion of these approaches is necessary as SMN modelling is a technique normally applied to studies of pure species cultures. Further, this review seeks to provide in some detail how SMN modelling can be adapted for metabolic characterization of mixed species microbial cultures (MMC). SMN modelling has successfully been applied to the design and optimization of antibiotic, alcohol and amino acid production processes. It has however been less than successfully applied in the analysis of engineered environmental processes, such as biological nutrient removal or methanogenic anaerobic digestion. Poor applicability occurs due to the fact that the catalytic activity in environmental processes is provided by an actual microbial community, which complicates the model development process considerably. SMN modelling of the environmental bioprocesses required to simulate microbial communities must include multiple species metabolism and their ecological relationships. This review chapter presents and discusses recent approaches to modelling microbial communities using SMN modelling and the applications of those models to Omic data interpretation, process optimization and biochemical pathway design.

3.1. Environmental biotechnology

Environmental biotechnology aims to develop, use and regulate biological systems for remediation of contaminated environments (land, air, water) and for sustainable and “clean” manufacturing of goods (Kleerebezem and van Loosdrecht, 2007; Vallero, 2010). Moreover, environmental biotechnology aims to consolidate biobased economies. Our current society depends on many natural resources, and the availability of these natural resources (minerals, fossil fuels) is becoming more and more limited. The challenge of a sustainable and biobased economy is to develop innovative technologies to recover and reuse minerals and energy-rich compounds from waste streams and non-food agricultural crops. Environmental biotechnology combines traditional elements from environmental engineering in terms of cleaning of waste streams with process engineering aimed at product manufacturing maximization. Environmental engineering is a broad field, including both abiotic and biotic solutions to pollution and environmental problems. In this context, environmental biotechnology focusses on the development and use the biotic solutions applied by environmental engineering.

3.2. Mixed microbial cultures in environmental bioprocesses

The aim of environmental biotechnology is relevant to applications in the fields of wastewater treatment, soil bioremediation, marine bioremediation, bioplastic production, biofuel production and more (Agler et al., 2011; Marshall et al., 2013). These applications require the use of mixed microbial cultures (MMC) to deliver the required good or service (Miller et al., 2010). A mixed microbial culture consists of a microbial community stabilized by selecting the source of the natural inoculum and by controlling the bioprocess conditions so that a natural/ecological selection can be promoted in the microbial population (Kleerebezem and van Loosdrecht, 2007; Rodríguez et al., 2006). This stabilized microbial community has the required metabolic capacities to control the rate of chemical conversions in the mixed microbial culture (Miller et al., 2010). The microbial community is composed of groups of organisms that exploit the same class of environmental resources in a similar way. These groups of similar organisms are called microbial guilds or an ecological functional microbial group (EFMG). A particular mixed microbial culture can be dominated by one or many guilds (Begon et al., 2005). In the case of biological nitrogen removal systems, the microbial community is dominated by the guilds of ammonia and nitrite oxidizers or by denitrifiers. **Table 3.1.** contains a list of common bioprocesses performed by MMC for environmental applications.

Table 3.1. Common environmental processes performed by mixed microbial cultures

Catalytic microbial guild	Biochemical process	Environmental application
Heterotrophs	Organic carbon degradation (suspended C to soluble C)	Organic matter removal
	Organic carbon oxidation (soluble C to CO_2)	Organic matter removal
	Ammonification (organic N to NH_4^+)	Organic matter removal
	Fermentation (soluble C to VFA)	Volatile fatty acids (VFA) production
	Denitrification (NO_3^-/ NO_2^- reduction to N_2)	Biological nitrogen removal
	Anaerobic digestion (organic C to CH_4)	Methane production
Autotrophic nitrifiers (AOB and NOB)	Nitritation (NH_4^+ oxidation to NO_2^-)	Biological nitrogen removal
	Nitratation (NO_2^- oxidation to NO_3^-)	Biological nitrogen removal
Phosphate accumulating organisms. (PAOs)	Phosphorus release (VFA uptake, PHA storage)	Biological phosphorus removal
	Phosphorus uptake (PHA degradation)	Biological phosphorus removal
	Phosphorus release (VFA uptake, PHA storage)	Polyhydroxyalkanoates (PHA), production
Microalgae	Nutrient assimilation (soluble N & P to organic molecules)	Biological nutrient removal
	Carbon assimilation (storage compound build up)	Lipids/biofuel production

3.2.1. Advantages of mixed microbial cultures

In the context of environmental biotechnology and engineering, bioprocesses based on MMC have four clear advantages over bioprocesses based on traditional pure cultures (Kleerebezem and van Loosdrecht, 2007; Marshall et al., 2013; Rodríguez et al., 2006). They are:

- no sterilization requirements and subsequent reduction of operational cost;
- the capacity to use mixed substrates;
- adaptive capacity owing to microbial diversity; and
- the possibility of a robust process (able to maintain high yields and productivities under on highly variable environmental conditions), e.g. wastewater biotreatment.

MMC are especially attractive for the production of bulk-chemicals, because they reduce the costs associated with culture contamination and work in strictly sterile conditions. For example, the high cost of substrate and equipment required for aseptic operation are the main factors responsible for the high selling price of polyhydroxyalkanoates (PHA), polyesters used for bio-plastic production. The use of open mixed cultures and waste materials as substrate can therefore substantially decrease the cost of PHA and increase their market potential (Dias et al., 2005).

MMC do not require expensive substrates compared to pure culture fermentations, which generally require the use of pure - and therefore more expensive - substrates. In MMC, the use of waste products and less-pure substrates is possible, and has subsequent cost and environmental implications (Rodríguez et al., 2006). The production of energy carriers or other valuable products by mixed culture fermentation finds a use for what were previously considered useless wastes or by-products; and also enables interesting downstream integrations (Rodríguez et al., 2006). Anaerobic digestion is a classic example of a process that combines the objectives of elimination of organic compounds from a waste stream with the generation of a valuable product in the form of methane-containing biogas (Kleerebezem and van Loosdrecht, 2007). Another example is the use of fermented agro-industrial wastes as low-cost substrates for PHA production (Pardelha et al., 2012).

When targeting industrial applications, bioprocess robustness and reproducibility are highly desirable. Bioprocesses based on MMC exhibit these attributes (Allison and Martiny, 2008; Werner et al., 2011). The physicochemical properties of bioreactor feed select the most efficient and effective microbial catalysts and even lead to the evolution of a more stable and productive microbial community (Marshall et al., 2013). Because mixed microbial cultures have a diverse microbial community with multiple metabolic capabilities, they can be resilient to adverse conditions and recover rapidly following an environmental upset. For instance, biological wastewater treatment by activated sludge can operate continuously for years. Similarly, it has been demonstrated that under adequate operational conditions, PHA can be produced by MMC continuously for two years in the same bioreactor, achieving high and stable production rates and yields (Dias et al., 2005).

3.2.2. Limitations of mixed microbial cultures

Despite the above-mentioned advantages MMC did not find wide application at industrial scale – except for waste and wastewater biotreatment applications – as this technology still presents significant limitations. The products formed by MMC vary in amount and composition (Agler et al., 2011). The control of the optimum balance among the microorganisms is not straightforward and requires a better understanding of microbial community behaviour (Agler et al., 2011). Many of the final products of MMC bioprocesses have a low market value, like anaerobic fermentation methane production from waste, which has limitations owing to the low price of natural gas (US$ 0.5 per kg) (Kleerebezem and van Loosdrecht, 2007). In some MMC processes the observed yields are much lower than the ones observed from pure cultures and/or expected from the theoretical process reaction stoichiometry. For example, in bio-hydrogen production from carbohydrates by anaerobic MMC, the measured hydrogen production per mole glucose is much lower (two moles) than the theoretical four mol-H/mol-Glucose yield expected from the bioprocess reaction stoichiometry (Li and Fang, 2007). Another disadvantage is that metabolic routes for waste degradation or product formation can be undefined, therefore complicating the definition of operation strategies. For example, the main limitation of the fermentative hydrogen production process is that no generally accepted selection criterion for the most favourable fermentative hydrogen production route is available (Li and Fang, 2007; Rodríguez et al., 2006). N_2O production in wastewater BNR also faces the problem of the many pathways of N2O production due the diversity of microbial guilds and metabolic routes. The outcome of all of these limitations is that designing process operation strategies to avoid the emission of this green-house gas and ozone depleting substance is difficult.

3.3. SMN modelling of environmental bioprocesses

3.3.1. Bioprocesses modelling and metabolic modelling

Engineered environmental bioprocesses are complex systems that depend on external chemical and physical processes to achieve the desired goals. Due to complex bioprocess behaviour, environment variability, biological population diversity and operation strategy diversity, it is not always possible to estimate how changing any operational parameter will affect the desired outcome. The problem of complexity can be addressed with mathematical models that enable simulation of a process; and estimating the impact that changing parameters will have on its effectiveness in delivering the service or product (Makinia, 2010). Mathematical modelling of environmental bioprocesses is a common practice in environmental biotechnology and engineering. For instance, the Activated Sludge Models (ASMs) (Kaelin et al., 2009; Makinia, 2010) is a family of bioprocess models widely used by researchers and wastewater treatment facility operators. The main applications of ASM models are listed below (van Loosdrecht et al., 2008):

- to gain insight into process performance;
- to evaluate possible scenarios for upgrading;
- to evaluate new WWT plant design;

- to support management decision-making; and
- to develop new control schemes

The bioprocess model is only a part of full treatment or remediation technology. For example, a model of a full wastewater bio treatment technology based on activated sludge has the following hierarchy of sub models (Makinia, 2010):

Hydraulic process model (describes the hydraulics of each unit operation and their connections)

1. Influent wastewater characterization model
2. Sedimentation model
3. Reactor model (A mass balance equation is applied to each reactor)
    - 3.1. Temperature model
    - 3.2. Oxygen transfer model
    - 3.3 Hydrodynamic mixing model, e.g. CSTR or plug flow. (Mixing and mass transfer characteristics and reactor mass balance equation)
    - 3.4. Bioprocesses model (e.g. ASM)
        - 3.4.1. Kinetic model
            - 3.4.1.1. Metabolic model (e.g. metabolic control analysis (MCA))
        - 3.4.2. Stoichiometric model
            - 3.4.2.1. Metabolic model (e.g. SMN modelling)

The organogram above shows that metabolic models are extensions of bioprocess models developed and used when it is necessary to do more detailed research into microorganism physiology, or when overproduction of a useful or undesired metabolic intermediate is sought (Ishii et al., 2004a). The metabolic modelling approach relies on the concept of metabolic pathways as sequences of specific enzyme-catalysed reaction steps converting substrates into cell products. Despite the existence of accurate bioprocess models, such as ASM, this kind of model does not contain detailed information on cellular behaviour and metabolic pathways. The inclusion of metabolic information is essential for deeper bioprocess understanding and operation improvement. Metabolic models commonly have the following applications (Oehmen *et al.*, 2010):

- as an analytical tool to generate mechanistic hypothesis from experimental observations;
- to improve process efficiency by providing quantitative basis for process design, control and optimisation;
- as a numeric method to estimate the activity of a specific microbial guild; and
- as a tool to investigate the involvement of a specific metabolic pathway in observed process.

Metabolic models have a bright future as both state-of-the-art research tools and for practical applications through linkages with bioprocess models such as ASM (Oehmen *et al.*, 2010). In this way metabolic models can serve as a bridge between molecular/biochemical research and environmental

engineering practice, functioning as a tool that can better link the work of microbiologist and engineer in optimising a particular environmental bioprocess (Oehmen *et al.*, 2010).

3.3.2. Stoichiometric metabolic network modelling

SMN modelling is a cutting edge metabolic modelling method used to quantify metabolic reaction rates and in this way describe the metabolic state of cells (Ishii et al., 2004b; Kitano, 2002; Palsson, 2009; Varma and Palsson, 1994). Metabolic network modelling is a data analysis technique of the new branches of biological sciences: Bioinformatics and Systems Biology. These disciplines are involved particularly in computational modelling of cells with a view to investigating and understanding the systematic relationships between genes, molecules and organisms (Endler et al., 2009; Kell, 2006; Kitano, 2002; Park et al., 2008).

SMN models have become an important tool for characterizing the metabolic activity of cells in biotechnological process and have huge potential to assist in the analysis and understanding of MMC (Lovley, 2003; Zengler and Palsson, 2012). The explosion in the number of new SMN models for up to 200 different organisms over the last few years highlights the increasing popularity of this approach in the pharmaceutical, chemical, and environmental industries (Kim et al., 2012; Park et al., 2008). This usefulness relies on their application as a computational tool to address questions that cannot be easily addressed experimentally.

3.4. Approaches to modelling MMC with SMN modelling

While several aspects of microbial metabolism can be fruitfully addressed by studying pure cultures of individual microbial species, many environmental bioprocesses require an understanding of how microbes interact with each other (Klitgord and Segrè, 2010; Lovley, 2003; Zengler and Palsson, 2012). Lack of information about environmental factors controlling the growth and metabolism of microorganisms in polluted environments often limits the implementation of biodegradation strategies (Lovley, 2003). Only a detailed understanding of the functioning and interactions within microbial populations will allow a rational manipulation for the purpose of optimizing bioremediation efforts (Vilchez-Vargas et al., 2010). Within this context, SMN modelling may be especially relevant to the analysis of environmental and industrial bioprocesses based on MMC (Miller et al., 2010).

Environmental bioprocesses have the peculiarity of being open systems where the catalytic activity is provided by microbial communities instead of single species populations (Grady et al, 1999; Comeau, 2008). Interaction between organisms may be especially important in microbial communities where multiple species are involved in degrading substrates available on the environment (Stolyar et al., 2007). The development of more sophisticated metabolic network modelling methods for interacting species will enable increasingly realistic prediction of communal phenotypes (Stolyar et al, 2007; Oberhardt et al, 2009). These developments will allow SMN models that include metabolic information

from different species to quantify rates of exchange of compounds between different species populations (Lovley, 2003; Stolyar et al, 2007). The model can be applied to simulate cellular metabolism of a homogenous mixture of bacterial cells in suspension (completely mixed system in stirred tank reactor). However, it can be extended to simulate cellular metabolism in a biofilm or flocculated system by implementing reaction–diffusion equations (Rodríguez et al., 2006).

The stoichiometric metabolic modelling approach has been used since 1999 to understand the behaviour of biological systems in complex environments and to model organisms relevant to engineering environmental bioprocesses, when Pramanik and co-workers (Pramanik et al., 1999) developed a SMN model of phosphate accumulating organisms. This study was the first attempt to adapt SMN to model a MMC. Professor Derek R. Lovley from University of Massachusetts was one of the first researchers to present a coherent framework to use omics techniques, computational biology and metabolic network modelling to study engineered environmental processes (Lovley, 2003). However, as shown in **Table 2.2.**, literature reviewed up until 2014 indicates that SMN modelling has been applied to quantify metabolic rates in engineered environmental bioprocesses in only a few studies, including modelling studies by (Poughon et al., 2001) on nitrification.

Table 2.2. also shows that four approaches have been developed to model microbial communities in mixed cultures using SMNs. These SMN modelling approaches are described above and in the following sections:

- Lumped network
- Compartment per guild network (also known as multi-compartment)
- Dynamic-SMN (also known as hybrid) and
- Bi-level simulation

A conceptual scheme for each modelling approach is illustrated in **Figure 3.1.**

Table 3.2. Approaches and applications for SMN modelling of environmental bioprocesses

Modelling approach	Environmental bioprocess	Modelled organisms/guilds	Model application	Reference
Lumped	Enhanced biological phosphorus removal (EBPR)	Mixed population of Phosphate accumulating organisms	Description of how carbon, energy and redox potential are channelled through metabolic pathways	(Pramanik et al., 1999)
	Nitrification	*Nitrosomonas* sp. and *Nitrobacter* sp.	Description the redox reactions of the electron transport chain	(Poughon et al., 2001)
	Anaerobic fermentation of carbohydrates to various alcohols and carboxylic acids	Mixed population of anaerobic fermentative organisms	Link of operation parameters (feeding composition, gas partial pressure and pH) to product formation	(Rodríguez et al., 2006)
	Growth of phototropic microbial mat and toxin production	*Synechococcus* spp, *Chloroflexus* spp, and sulphate reducing bacteria	Description of metabolic mechanism behind the observed biomass productivity, relative abundance and toxin productivity	(Taffs et al., 2009)
	Subsurface anaerobic organic matter fermentation	*Clostridium cellulolyticum*, *Desulfovibrio vulgaris*, and *Geobacter sulfurreducens*	Description of substrate consumption routes in microbial community	(Miller et al., 2010)
	fermentative anaerobic production of H_2 and acetate	Community enriched with *Clostridium* sp, *Lactobacillus sp* and *Seleomanas* sp	Description of metabolic routes for product degradation	(Chaganti et al., 2011)
Lumped-dynamic	Waste sugars fermentation to PHA	Mixed population of PHA producing organisms	Linking operation parameters (feeding regime) to product formation	(Dias et al., 2008)
			Linking operation parameters (feed composition) to product formation	(Pardelha et al., 2012)
			Assessing single population contribution to process performance	(Pardelha et al., 2013)
Compartment per guild network	Methanogenic fermentation	*Desulfovibrio vulgaris* and *Methanococcus maripaludis*	Description of metabolic mechanism behind the association of organisms	(Stolyar et al., 2007)

	Growth of phototropic microbial mat	*Synechococcus* spp, *Chloroflexus* spp, and sulphate reducing bacteria	Description of metabolic mechanism behind the observed biomass productivity, relative abundance and toxin productivity	(Taffs et al., 2009)
	Commensalism and mutualism between pairs of organisms	Pairs of seven different bacteria[+]	Novel process development. Identifying new environmental conditions that support specific ecological interactions	(Klitgord and Segrè, 2010)
Dynamic-SMN	*In situ* Uranium bioremediation by microbial reduction and precipitation	*Geobacter sulfurreducens*	Description of metabolic mechanisms in ground water bodies, Hydrodynamic-SMN model	(Scheibe et al., 2009)
	In situ Uranium bioremediation by microbial reduction and precipitation	*Geobacter sulfurreducens* and *Rhodoferax ferrireducens*	Description of metabolic mechanisms in ground water bodies, Monod-SMN	(Zhuang et al., 2011)
Bi-level simulation	Growth of phototropic microbial mat	*Synechococcus* spp, *Chloroflexus* spp, and sulphate reducing bacteria	Description of metabolic mechanism behind the observed biomass productivity, relative abundance and toxin productivity	(Taffs et al., 2009)
		Synechococcus spp, *Chloroflexus* spp, and sulphate reducing bacteria	Assessing the effect microbial community structure on the total community biomass.	(Zomorrodi and Maranas, 2012)
	Methanogenic fermentation by mutualistic community	*Desulfovibrio vulgaris* and *Methanococcus maripaludis* synthorphic association	Linking the effect of microbial community composition to process performance	(Zomorrodi and Maranas, 2012)
	Subsurface anaerobic organic matter fermentation	*Clostridium cellulolyticum*, *Desulfovibrio vulgaris*, and *Geobacter sulfurreducens*	Description of substrate consumption routes in microbial community	(Zomorrodi and Maranas, 2012)

[+] = genome scale models of *Escherichia coli, Helicobacter pylori, Salmonella typhimurium, Bacillus subtilis, Shewanella oneidensis, Methylobacterium extorquens,* and *Methanosarcina barkeri*.

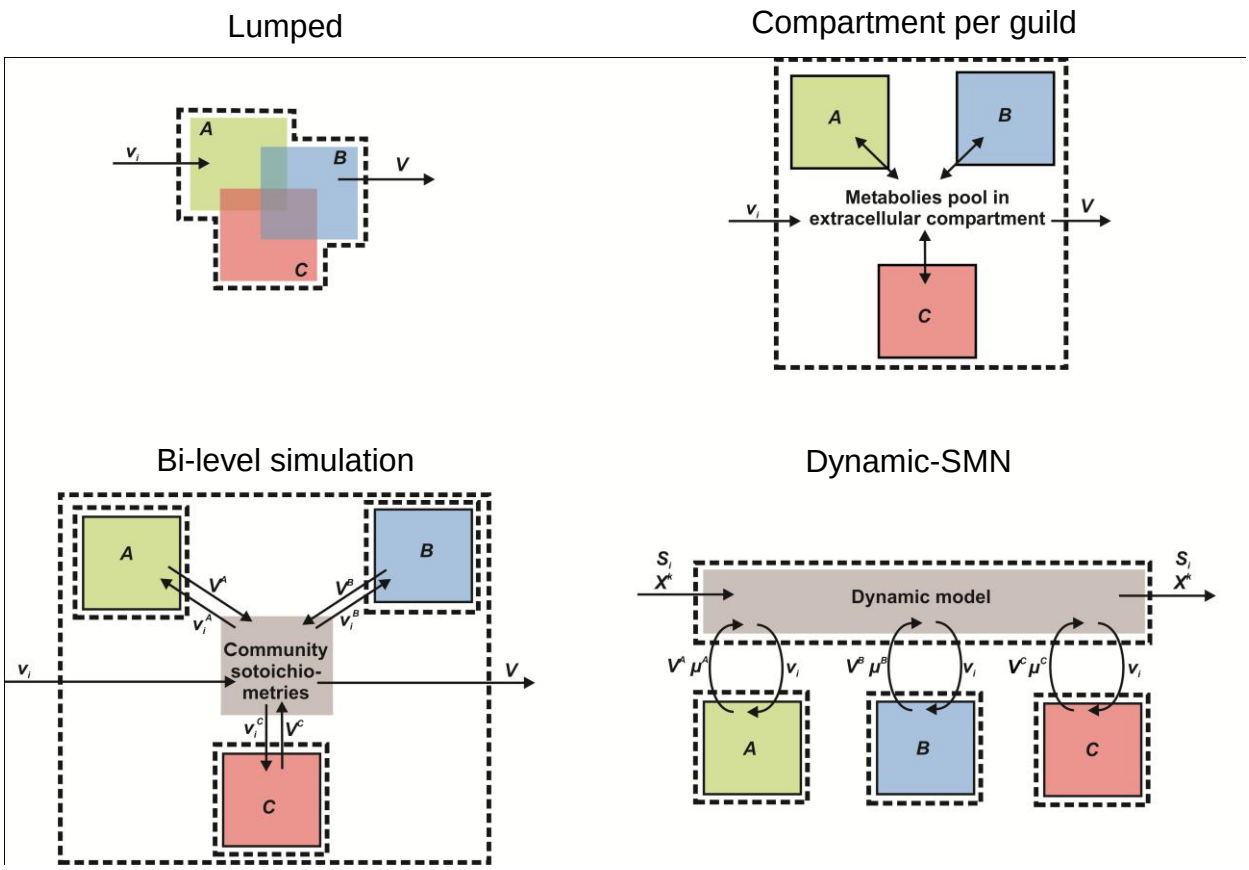

Figure 3.1. Conceptual scheme of the four approaches to model mixed microbial cultures using stoichiometric metabolic networks

In all figures boxes *A*, *B* and *C* represent sets of equations of metabolic reactions occurring in organisms/guilds *A*, *B* and *C*, respectively These sets of reactions can have any number of sub compartments, i.e. extracellular space and organelles; dashed lines indicate model (system) boundaries; solid lines indicate guild boundaries; v_j is the flux of metabolite in reaction j; v is the vector of fluxes estimated by the model; v^k is the vector of fluxes estimated by the model of species/guild k (*A*, *B* or *C*) ;S_i is the concentration of metabolite i; and X^k is the biomass concentration of modelled species/guild k (*A*, *B* or *C*).

3.4.1. Lumped approach

In this approach the community is modelled as a single entity in which all metabolic reactions and metabolites from the guilds are combined into a single set of reactions. A metabolic network of the whole mixed culture is built up by simply inventorying the most common catabolic reactions, i.e. electron transport chain, glycolysis, tricarboxylic acid cycle (TCA) and amino acid synthesis; and later lumping multiple subsequent reactions of specific pathways into a single reaction that represents the overall pathway (Rodríguez et al., 2006). Reactions catalysed by more than one guild are only considered once. The method captures the metabolic constraints of the overall matter and energy transformations without the need for detailed knowledge of every organism in the community (Taffs et al., 2009).

This modelling approach is based on the assumption that all the organisms in the community have reactions in common. It treats the MMC or microbial community as a single virtual microorganism catalysing the most common pathways (Rodríguez et al., 2006). The product spectrum is obtained by maximizing the biomass growth yield which is limited by catabolic energy production. The virtual microorganism proposed here should be regarded as a representation of the different microbial strains involved in the bioprocess. Microbial diversity and the dynamics of the process are neglected at this stage (Rodríguez et al., 2006). Ignoring microbial diversity and assuming a virtual microorganism able to carry out the most common fermentative conversions is acceptable in steady state conditions (Rodríguez et al., 2006). thus, simplifying the processes of model development and calibration.

The lumped network approach is ideally suited for investigating the metabolic potential of a community based solely on metagenomic data as the assignment of each reaction to a constituent guild is unnecessary. The approach is quite flexible and can be scaled to different levels of detail. An additional advantage of the lumped approach is the reduction of computational burden. With these advantages, the method is uniquely suited for initial and exploratory analyses of diverse or poorly understood communities (Taffs et al., 2009). A weakness in the lump reactions is that the model's output does not specify which guilds employ a particular enzyme or produce biomass and maintenance ATP. Instead, the results describe potential performance of the microbial community or MMC. The method also neglects the logistics associated with transferring metabolites between organisms, including conversion of the relevant metabolite into one for which transporters are available (Taffs et al., 2009)

3.4.2. Compartment per guild approach (multi-compartment)

In a compartment per guild network, each organism or guild is modelled as a distinct compartment and exchangeable metabolites are transferred through an extra compartment representing the extracellular environment (Klitgord and Segrè, 2010; Stolyar et al., 2007; Taffs et al., 2009). The

approach is implemented by assigning reactions and metabolites to a network representing each guild, with suffixes on metabolite identifiers preventing sharing of compounds common to the metabolism of multiple guilds. Explicit transport reactions accounting for the exchange of metabolites between guild members and the extracellular space are defined (Taffs et al., 2009). This approach introduces a fictitious compartment that represents the extracellular environment shared by the microbial species in addition to the original extracellular spaces for individual models (Klitgord and Segrè, 2010). The compartments represented by different microbial species are separated spatially by the extracellular medium. Consequently, the presence or absence of a single transporter in one species may greatly affect the behaviour of other species in the system (Stolyar et al., 2007).

The compartment per guild modelling approach has the advantage of conceptual tractability. Dividing the community into guild-level compartments linked by transferred metabolites, e.g. oxygen, is an intuitive way to represent interactions within a community. It is also an ideal method for understanding which guild performs a particular metabolic transformation. For example, it is easy to estimate the fraction of total biomass (carbon moles) or total maintenance ATP (used to account for energy-dependent cellular processes other than growth) produced by each guild (Taffs et al., 2009). Using a multi-compartment approach, (Klitgord and Segrè, 2010) developed the Search for Exchanged Metabolites (SEM) algorithm to verify potential interactions between a pair of organisms and produce a list of putatively exchanged metabolites. Selected carbon and nitrogen sources are then combined in all possible ways to give rise to a set of putative media that can sustain growth of the join pair model (Klitgord and Segrè, 2010). In this way, The Search for Interaction-Inducing Media (SIM) algorithm identifies the set of media that support growth of multi-species co-cultures and predicts the class of interaction they induce (Klitgord and Segrè, 2010)

One drawback of this approach is that the size of the resulting network can lead to a 'combinatorial explosion' of new pathways composed by reactions from different guilds (Klamt and Stelling, 2002). To address this limitation, the models for each guild member can be constructed to only capture the necessary metabolic capabilities while maintaining computational tractability (Taffs et al., 2009). A second drawback of this approach is the requirement for significant *a priori* information or assumptions, as reactions must be assigned to each individual guild (Stolyar et al., 2007).

3.4.3. Dynamic-SMN (hybrid)

This approach couples the rate predictions of SMN models with differential equations that capture the dynamic response of the biological process with respect to substrate concentrations, temperatures or pH. Differential equations have been coupled to single species SMN (Çalik et al., 2011; Hjersted et al., 2005; Mahadevan et al., 2002) or to various SMNs to yield a multispecies model (Scheibe et al., 2009; Zhuang et al., 2011). The main attribute of hybrid models is that they can predict reaction rates and compound (metabolite) concentrations across a time interval.

Dynamic-SMN captures both metabolic complexity and metabolic dynamism. Because the majority of environmental bioprocesses are in fact dynamic systems, this approach has the potential to truly capture the behaviour of these systems. The constraint-based modelling approach may be particularly well suited to modelling microorganisms in heterogeneous environments, as it does not assume constant yield coefficients and has been shown to account for the changes in the metabolic network in response to nutrient limitations (Schuetz et al., 2007).

Models that can accurately predict microbial growth and activity are particularly important when dealing with the dynamic conditions expected in wastewater biotreatment and soil bioremediation. For instance, in (Scheibe et al., 2009), a genome-scale SMN model of the metabolism of *Geobacter sulfurreducens* was coupled to a soil reactive transport model (HYDROGEOCHEM). The objective was to model operations of *in situ* bioremediation of uranium spills in soil.. By discretizing an aquifer as a numeric grid, the hybrid model simulates hydrologic, geochemical and metabolic processes in the spill are. At each time step, the SMN model estimates microbial mediated metabolic reaction rates of the simulated geochemical conditions in each grid element at that time. These fluxes then feed back to the reactive transport model as reaction rates for the current time step. The reactive transport model is stepped forward one time interval, after which the process is repeated. The step that involves referencing the metabolic model from the reactive transport model can take one of two forms: (i) concurrent execution of the metabolic model through a direct subroutine call from the reactive transport model; or (ii) selection of metabolic fluxes at each time step of the reactive transport simulation from a large set of pre-calculated metabolic model solutions covering the expected range of environmental conditions. In this study, researchers chose an example of *in situ* subsurface bioremediation application that is essentially catalysed by one microbial genus in an initial attempt to apply SMN modelling to bioremediation. The coupled SMN and reactive transport model predicted acetate concentrations and U(VI) reduction rates in a field trial of *in situ* uranium bioremediation that were comparable to the predictions of a calibrated conventional model, but without the need for empirical calibration other than specifying the initial biomass of *Geobacter*. The results from this study suggest that coupling SMN models with reactive transport models may be a worthwhile approach to developing models that can be truly predictive (Scheibe et al., 2009).

3.4.4. Bi-level optimization approach

The approaches described above rely on either a single objective function to describe the entire community (Stolyar et al., 2007) or separate optimization problems for each microorganism (Tzamali et al., 2011). Bi-level optimization integrates both species and community-level fitness criteria into a multi-level/objective framework. The bi-level optimization approach is based on the assumption that a universal community-specific fitness criterion does not exist (Zomorrodi and Maranas, 2012). The bi-level simulation approach uses successive rounds of simulations to analyse potential interactions within a community. A first round of simulations is applied to each modelled guild in isolation. The output data are mined for ecologically relevant interactions. The selected interactions are then

compiled and used to define new stoichiometric reactions that are used in a second round of simulations to examine the potential for interactions between guilds. Conceptually, the first round of simulations provides guild-level stoichiometry relating substrates to products. This stoichiometry can be further processed to consider intra-guild interactions (Taffs et al., 2009)

The bi-level optimization approach, like that developed as the OptCom algorithm (Zomorrodi and Maranas, 2012), postulates a separate biomass maximization problem for each species as inner problems. The inner problems capture the driving forces of species-level fitness, demonstrated by the maximization of individual species biomass production. Inter-species interactions are modelled with appropriate constraints in the outer problem representing the exchange of metabolites among different species. The inner problems are subsequently linked with the outer stage through inter-organism flow constraints and optimality criteria, so at a community-level (i.e. overall community biomass) objective function is optimized (Zomorrodi and Maranas, 2012). OptCom incorporates all available experimental data for the entire community (i.e. community biomass composition) as constraints in the outer problem and all data related to individual species as constraints in the respective inner problems, while allowing the biomass flux of individual species to fall below (or rise above) the maxima ($vopt^{k}_{biomass}$) of the inner problems. OptCom can capture various types of interactions among members of a microbial community. Symbiotic interactions between two or more populations can be such that one or more species benefits from the association (positive interaction), is negatively affected (negative interactions), or is a combination of both. Mutualism, synergism and commensalism are examples of positive interactions, whereas parasitism and competition are examples of negative interaction. OptCom can be used for assessing the optimality level of growth for different members in a microbial community and subsequently making predictions regarding metabolic trafficking (predictive mode) given the identified optimality levels. An advantage of the bi-level optimization approach is that it can also be coupled with differential equations to generate dynamic hybrid models (Zomorrodi et al., 2014).

The bi-level simulation approach allows the analysis of more complex metabolic networks and larger communities than the compartment per guild approach, because each guild is initially considered separately. It also has the advantage of retaining guild-specific output, information which is lost using the lumped approach. The manual selection of specific modes permits a community analysis based on ecological strategies of interest for each guild. Results can then be re-examined in light of the selection criteria used, relating community stoichiometry and guild (Taffs et al., 2009). The bi-level simulation approach has the disadvantage of requiring two rounds of data processing and simulation. In addition, manual selection of ecologically interesting modes from individual models requires a priori knowledge and can significantly influence the solution. Finally, intermediate processing introduces some rounding error (Taffs et al., 2009).

3.4.5. Comparing approaches

Table 3.3. lists the advantages and disadvantages of each of the simulation approaches. The approaches can be compared in terms of their ability to describe and explain the flows of carbon, nitrogen and energy through the community (Taffs et al., 2009). This is important because potential applications include more diversified communities and more complex cellular metabolisms (Taffs et al., 2009).

Table 3.3. Advantages and disadvantages of modelling approaches

Approach	Advantages	Disadvantages
Lumped	• Easy to implement • Direct implementation of metagenomic data • Do not require deep knowledge of the metabolic network • Suitable to model not characterized microbial communities	• Less detailed • Loss of ecological information • Overestimation of metabolic potential
Compartment per guild	• Easy to implement • Captures exchange of compounds between guilds • Provides information about metabolic behaviour of each modelled guild	• Limited to simulate steady states • Computationally heavy • A priori knowledge of exchangeable compounds between guilds • Not scalable to communities with many guilds
Dynamic-SMN	• Process prediction • Dynamic simulation • Estimations of concentrations and reaction rates • Linkable to hydrodynamic or geochemical models	• Design of differential equations • Calibration of unknown kinetic parameters (i.e. maximum reaction rates v_{max} and affinity constants K_m) • Computationally heavy
Bi-level simulation	• Guild level rate estimations • Community level rate estimations • Definition of ecological relationships • Scalable to communities with large number of guilds • Able to be upgraded to a dynamic model	• Difficult implementation for non-experts • Required a priori calibration of guild model • Computationally heavy

The lumped approach models the community metabolic potential by treating all enzymatic activities and metabolites as residents of the same physical space without membrane boundaries. The lumped reactions approach represents the coarsest scale methodology, requires the least a priori information and is easier to implement than alternative approaches. The pooled approach can often be used

when other approaches cannot (due to complexity) or should not (due to lack of detailed data). These advantages are balanced against a tendency to overestimate the metabolic potential. This is unsurprising, as real communities are not super-organisms. Individuals are membrane-separated and must contend with the logistics associated with matter and energy transport. The lumped technique is best for initial work on 'poorly' characterized systems (Taffs et al., 2009).

The compartmentalized community analysis method has the advantage of intuitive tractability and separates activity and function by guild, but requires substantially more knowledge of the community than the pooled reactions approach. The compartmentalized method also lends itself uniquely to investigation of the robustness of specific consortium interaction types (Taffs et al., 2009).

The bi-level simulation approach has properties very similar to the compartment per guild approach, but with the important advantage of easy scalability achieved by concatenating multiple rounds of simulations. The approach also provides additional ecological insight into the competitive strategies underlying each guild's function. The bi-level simulation approach also easily captures interactions between different guilds as well as between members of the same guild expressing different physiologies.

3.5. Applications of SMN modelling of MMC

As more metabolic models of different organisms become available, the modelling of microbial communities becomes more feasible and relevant. SMN modelling has four applications for the analysis MMC and environmental bioprocesses (**Figure 3.2.**):

- inference of metabolic mechanisms from observed data;
- bioprocess optimization;
- high throughput (omics) data analysis and interpretation; and
- discovery and design of novel catalytic pathways and microbial associations

The above applications are described in the following sections.

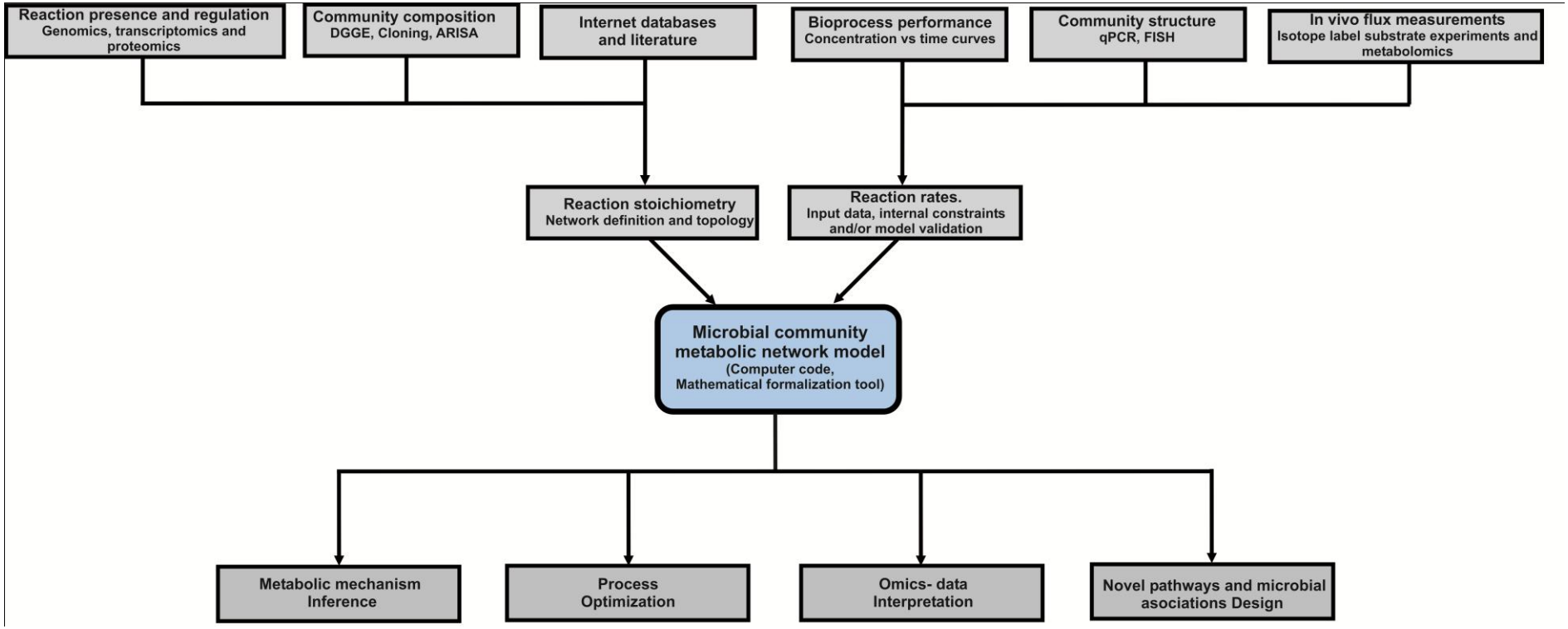

Figure 3.2. Applications of SMN models of MMC

3.5.1. Inference of metabolic mechanisms from observed data

In this application, experimental data is acquired and used as model input to generate estimations of metabolic behaviour. Experimental behaviour is then contrasted and interpreted under the light of model predictions (Chaganti et al., 2011; Pramanik et al., 1999). Because the SMN model includes detailed information of metabolic pathways, a mechanistic interpretation of the results obtained from experiments is possible (Rodríguez et al., 2006). In addition, SMN modelling can be used to infer ecological relationships in complex microbial communities, especially with regard to mechanisms of mass and energy transfer between guilds, and the relationship between species presence and its function in the community (Stolyar et al., 2007; Taffs et al., 2009). In the (Stolyar et al., 2007) study, simulations helped reveal and clarify essentiality of substrate assimilatory pathways and reaction stoichiometry by comparing simulation results with growth rates of experimental data.

3.5.2. Bioprocess optimization

The increasing availability of the genome sequences of microorganisms involved in important engineered environmental processes makes it feasible to consider developing metabolic models that can aid prediction of the likely outcome of potential operation strategies (Scheibe et al., 2009). It is recognized that the investigation of the optimal process operating strategy can be most effectively performed by adopting a model-based methodology (Dias et al., 2005). This application generates a model-driven experimental hypothesis. In this application the model suggests experiments to confirm the use of a specific or relevant metabolic pathway and the presence of points of metabolic regulation and modulation (Pramanik et al., 1999). Intracellular flux distributions for different environmental scenarios can be calculated and culture feeding scenarios can be optimized with simulations targeting maximal compound productivity and/or desired composition (Dias et al., 2008). This is particularly useful for linking specific operational parameters to bioprocess product formation. For instance, (Dias et al., 2005; Pardelha et al., 2012) developed a process model based on MNM to optimize the PHB productivity by mixed cultures. These studies aimed to explore the optimal carbon sources and ammonia-feeding strategies that maximize both the final intracellular PHB content as well as the volumetric productivity (Dias et al., 2005).

3.5.3. High throughput (omics) data analysis and interpretation

Metabolic network models have successfully helped in the interpretation of transcriptomic, proteomic and metabolomic data from single culture experiments (Lewis et al., 2010; Oberhardt et al., 2009). Recent advances in the use of high-throughput sequencing and whole-community analysis techniques, such as meta-genomics and meta-transcriptomics, are making genomic information available from microbial communities. However, due to the lack and complexity and low reliability of meta-omics data, the information generated may remain without meaning or usefulness. SMN models are beginning to be used to analyse and interpret this kind of data. Proteomic and transcriptomic data have been successfully interpreted and used as constraints of SMN models through the Parsimonious

FBA (pFBA) algorithm (Lewis et al., 2010). In a similar way, metabolomics data can be interpreted in the light of SMN models through the Network Embedded Thermodynamic (NET) analysis (Kümmel et al., 2006).

3.5.4. Discovery and design of novel catalytic pathways and microbial associations

The most innovative application of metabolic network modelling of MMC is their capacity to discover and design novel microbial associations and catalytic pathways within a microbial community. The real power of computational biology techniques relies on their ability to rapidly test thousands of metabolic variations or combinations without developing wet experiments or generating mutants. For instance, it is possible to computationally generate artificial microbial ecosystems without re-engineering microbes themselves, but rather by predicting their growth on appropriately designed media. This approach is of particular relevance to environmental biotechnology, given the restrictions on the use of genetically modified organisms in bioremediation strategies. SMN models can be used to identify environmental conditions that can sustain growth for a combination of defined species, but which fail to do so for one or both individual species, thereby inducing putative symbiotic interactions (Klitgord and Segrè, 2010; Stolyar et al., 2007). This analysis is based on the assumption that, given two arbitrary organisms, it is possible to identify environmental conditions that induce a mutualistic or commensal interaction. SMN modelling opens up the possibility of identifying these conditions. For example, in the study done by (Klitgord and Segrè, 2010), 21 models were generated using pair combinations of seven SMN models of different species. From the simulations of these paired models, several putative growth media were identified to induce novel commensalism or mutualism relationships between the species. Naturally, further experimentation is required to confirm the model's predictions, but these experiments would be based on a robust hypothesis generated a priori. In another relevant *in silico* study by (Taffs et al., 2009), three species-based SMN models were used to map the novel pathways generated by the metabolic networks of each species connected to each other via the exchange of substrate and products. In terms of metabolic engineering, using the enzymatic potential of multiple interacting species can greatly expand the solution space of process optimization possibilities. Generating novel pathways by inducing interactions between different organisms rather than - or in addition to - genetically modified organisms has several benefits. Firstly, one could use the metabolic potential of organisms that may be hard to genetically manipulate. Secondly, communities may be inherently more stable than individual modified species, in which specific mutations could potentially revert. In this sense, symbiotic interactions, e.g. to biodegrade a pollutant, may arise more readily through environmental fluctuations than genetic modifications (Klitgord and Segrè, 2010)

2.4. Conclusions

SMN modelling and systems biology can contribute to a comprehensive understanding of microorganisms, their interaction with other species in a community and their interplay with their environment. Meaningful insight into the interaction of microorganisms with other organisms and the environment has often been hampered by the fact that microbial communities are extremely complex (Zengler and Palsson, 2012). Thus far, SMN modelling approaches have been restricted to metabolic function. However, it is likely that most interactions between different microorganisms will have an influence on metabolism, making SMN modelling well suited for accurately elucidating the major interactions in microbial communities.

Identification of the most important microbial guilds involved in the performance of a given mixed microbial culture is a prerequisite to characterising it in an SMN model. Once the functional guild or species is identified, whole-genome sequences, in conjunction with detailed physiological experiments, enable SMN models to be generated for the identified organisms. Species-specific SMN models are then used to build up community models using one of the four modelling approaches. Mixed microbial populations can be modelled with the lumped approach. These populations are composed of multiple species, but with all the species belonging to the same guild and exploiting a given environmental resource using the same metabolic pathways. In contrast, microbial communities with more than one guild are best modelled with the multi-compartment and bi-level optimization approaches. These approaches capture ecological interactions between different species and guilds. Finally, MMC process dynamics can be captured using the dynamic-SMN modelling approach. However differential and kinetic equations need to be further derived and added to the SMN model of the microbial community. Modelling of microbial communities requires the description of molecular mechanisms that describe species interactions, such as competition, commensalism and mutualism. For instance, AOB and NOB microbes in nitrifying communities compete for oxygen but establish a mutualistic relationship through nitrite production-consumption.

The successful application of SMN modelling to environmental engineering and biotechnology requires recognising and modelling several abiotic factors influencing process performance. The chemical factors of the process include nutrients, electron donors/acceptors and stressors. The physical factors are those imposed by the micro/macrogeography of microbe location and include, for example, humidity, conductivity, temperature, pressure texture, matric conditions and redox (O2) status (de Lorenzo, 2008). As this complexity increases, there is a need to develop a new set of fundamental principles and concepts, and algorithms that will allow the secrets of microbial and cellular communities to be unravelled (Zengler and Palsson, 2012). SMN modelling of microbial communities and subsequent computer simulations are tools that can lead to a better understanding of the microbial cell and will undoubtedly contribute significantly to the field of environmental engineering.

CHAPTER FOUR

Effect of aerobic and anoxic conditions on N_2O and NO production pathways in ammonia oxidizing bacteria

This chapter describes a simulation study performed to characterize how dissolved oxygen and ammonium concentration in nitrification process influence the NO and N_2O production pathways in ammonia oxidizing bacteria (AOB). The metabolic mechanism regulating the production pathways of NO and N_2O was characterized by applying the developed computational platform to analyse previously published data from experiments of *Nitrosomonas europaea* cultures producing N_2O. The simulation study of *N. europaea* cultures exposed to oxic-anoxic-oxic transition indicated that NO and N_2O production primarily resulted from an intracellular imbalance between the production and consumption of electron equivalents during NH_3 oxidation, and that NO and N_2O are emitted when the sum of their production rates is greater than half the rate of NO oxidation by cytochrome P460.

4.1. Background

AOB produce NO and N_2O during nitrification and autotrophic denitrification in wastewater treatment BNR processes (Ahn et al., 2010; Foley et al., 2010; Kampschreur et al., 2009). The operational conditions of wastewater treatment processes that lead to NO and N_2O production by AOB are related to changes in the concentration of electron donors (NH_4^+ and NH_2OH) and acceptors (O_2 and NO_2^-) (Chandran et al., 2011; Kampschreur et al., 2008). However, despite the availability of extensive information on nitrogen respiration and energy production in AOB, the metabolic triggers and modulatory mechanisms controlling NO and N_2O production are not well understood.

NO/N_2O production in AOB occurs via two pathways (Cabail and Pacheco, 2003; Stein, 2010; Stein, 2011; Wunderlin et al., 2012) (**Figure 4.1.**):

(i) The aerobic hydroxylamine oxidation pathway mediated by hydroxylamine oxidoreductase (HAO); and

(ii) The nitrifier denitrification pathway mediated by nitrite reductase (NirK) and nitric oxide reductase (cNor) enzymes

From pure cultures of *Nitrosomonas europaea*, a model AOB species constantly and abundantly (high fraction of AOB dry weight biomass) detected in full scale nitrification processes (Wagner et al., 2002), it is known that these two pathways are part of the nitrogen respiration, electron transport chain, and energy generation mechanism of AOB ((Hooper et al., 1997; Whittaker et al., 2000; Yu et al., 2010). As a result, activation of the HAO mediated pathway leads to generation of electron

equivalents and activation of the NIR mediated pathways implies a consumption of electron equivalents. However, details of how the availability of electron donors (NH_4^+ or NH_2OH) and acceptors (O_2 or NO_2^-) influences the activity of these pathways remain unclear.

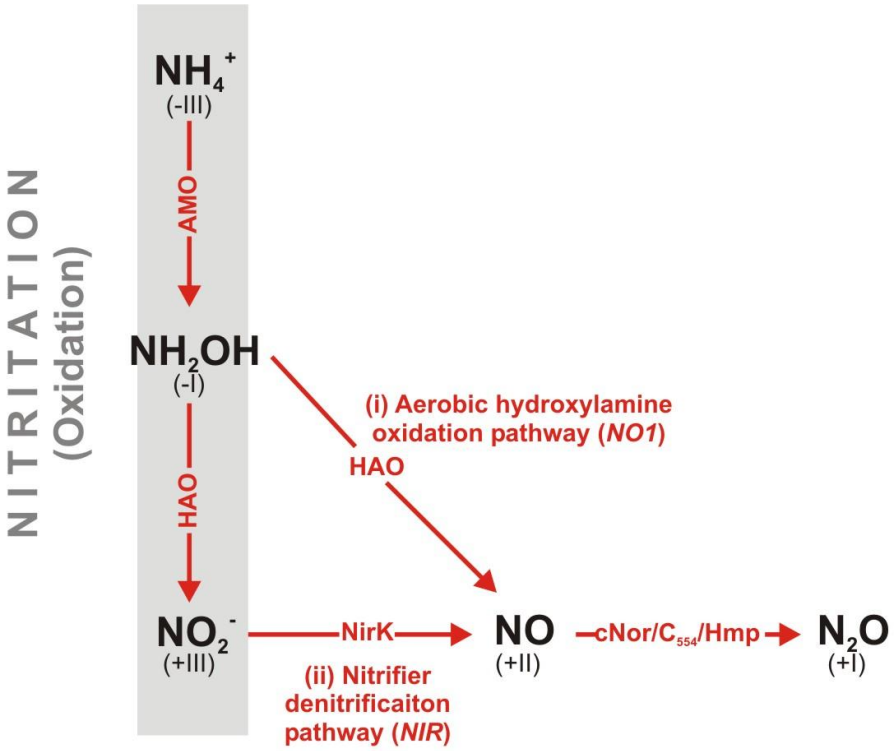

Figure 4.1. Pathways of NO and N_2O production in AOB

Activated Sludge (ASM) models have been modified to dynamically predict NO and N_2O production under different environmental conditions by linking NO and N_2O production to the respiratory activity and the responsible metabolic pathway (Kampschreur et al., 2007; Ni et al., 2011; Ni et al., 2013b; Pan et al., 2013b; Yu et al., 2010). This approach however does not clarify why these gases are produced, as NO and N_2O production has largely been described as being decoupled from the cell's energy metabolism. Furthermore, different routes for production or consumption of electron equivalents are ignored. A different approach taken by (Wunderlin et al., 2013) involving the use of isotope signatures of N_2O produced by mixed microbial populations could quantify the contribution of each of the two N_2O production pathways under different environmental conditions. However, the method provides no explanation for what activated the dominant pathway. Added to this, the difficulty and expense of such isotopic signature based experiments could limit their wide adoption in understanding the behaviour of laboratory or full scale systems.

Stoichiometric metabolic network (SMN) modelling and flux balance analysis (FBA) are emerging techniques in systems biology that could be used to quantify the rate of reactions within the network formed by chemical compounds and sequenced chemical reactions in cells' metabolism (Durot et al.,

2009; Oberhardt et al., 2009; Orth et al., 2010). FBA provides a 'snapshot' estimation of reaction rates in the metabolic network at a specific metabolic steady state (Orth et al., 2010), therefore we applied it to quantify the simultaneous activity in the hydroxylamine mediated and nitrifier denitrification pathways during NO and N_2O production by AOB. In this study *Nitrosomonas europaea* served as a model AOB as its metabolism as well as the pathways for ammonium oxidation and production of energy, NO and N_2O, are known (Poughon et al., 2001; Sayavedra-Soto and Arp, 2011; Stein, 2010). Furthermore, its genome has been sequenced, which allows the reconstruction of its entire complement of metabolic pathways (Chain et al., 2003). We constructed a SMN model based on *Nitrosomonas europaea* energy production metabolism and enzymology, and used it in combination with FBA to quantify the metabolic rates of NO and N_2O production pathways during oxic-anoxic-oxic transitions of *N. europaea* cultures. The obtained metabolic rates were used to infer the physiological mechanisms responsible for the modulation of pathways leading the production of these gases.

4.2. Materials and Methods

4.2.1. *Nitrosomonas europaea* SMN model

A metabolic network model for biochemical reactions and metabolites formed during *N. europaea* energy production metabolism was constructed by following the procedure described by in Chapter two and using organism-specific genomic and biochemical information from literature (**Table 4.1.**) and the metabolic pathway databases KEGG and MetaCyc (respectively accessible at http://www.genome.jp/kegg/ and http://metacyc.org/).

The reactions for energy production in *N. europaea* cells are modelled as occurring in three cell compartments: extracellular, periplasmic and cytoplasmic spaces (Chain et al., 2003); labels [e], [p] and [c] have respectively been assigned to metabolic compounds to indicate their occurrence in extracellular, periplasmic and cytoplasmic compartments (**Figure 4.2.A**). The metabolite NH_4^+[e] is thereby differentiated from NH_4^+[p] and the exchange between extracellular and periplasmic spaces can be simulated as NH_4^+[e] ←→ NH_4^+[p]. Further information about network compartmentalization can be found in Chapter two. The constructed *N. europaea* model consists of 44 metabolites and 49 stoichiometric reactions categorized as follows (all reaction IDs are showed with italicized text): 11 exchange reactions representing the flow of metabolic compounds in and out of the cell (IDs of these reactions have the extension "*-Ex*"); 4 reactions representing the consumption and production of metabolic compounds from intracellular pools (IDs of these reactions have the extension "*-Pool*"); 17 reactions representing the transport or diffusion of metabolic compounds between compartments [e], [p] and [c]; 14 reactions for *N. europaea* energy production metabolism catalysed by enzymes, including ammonia respiration, NO and N_2O production, and energy production; and 3 biomass synthesis reactions. The network formed by these reactions and metabolites, produced with Cytoscape 3.0.1 software (Cytoscape consortium, San Diego, USA), is shown in **Figure 4.1.B.** where nodes represent reactions and metabolites; the external branches are the 11 exchange reactions; and the most highly connected nodes are lumped in the central region of the network.

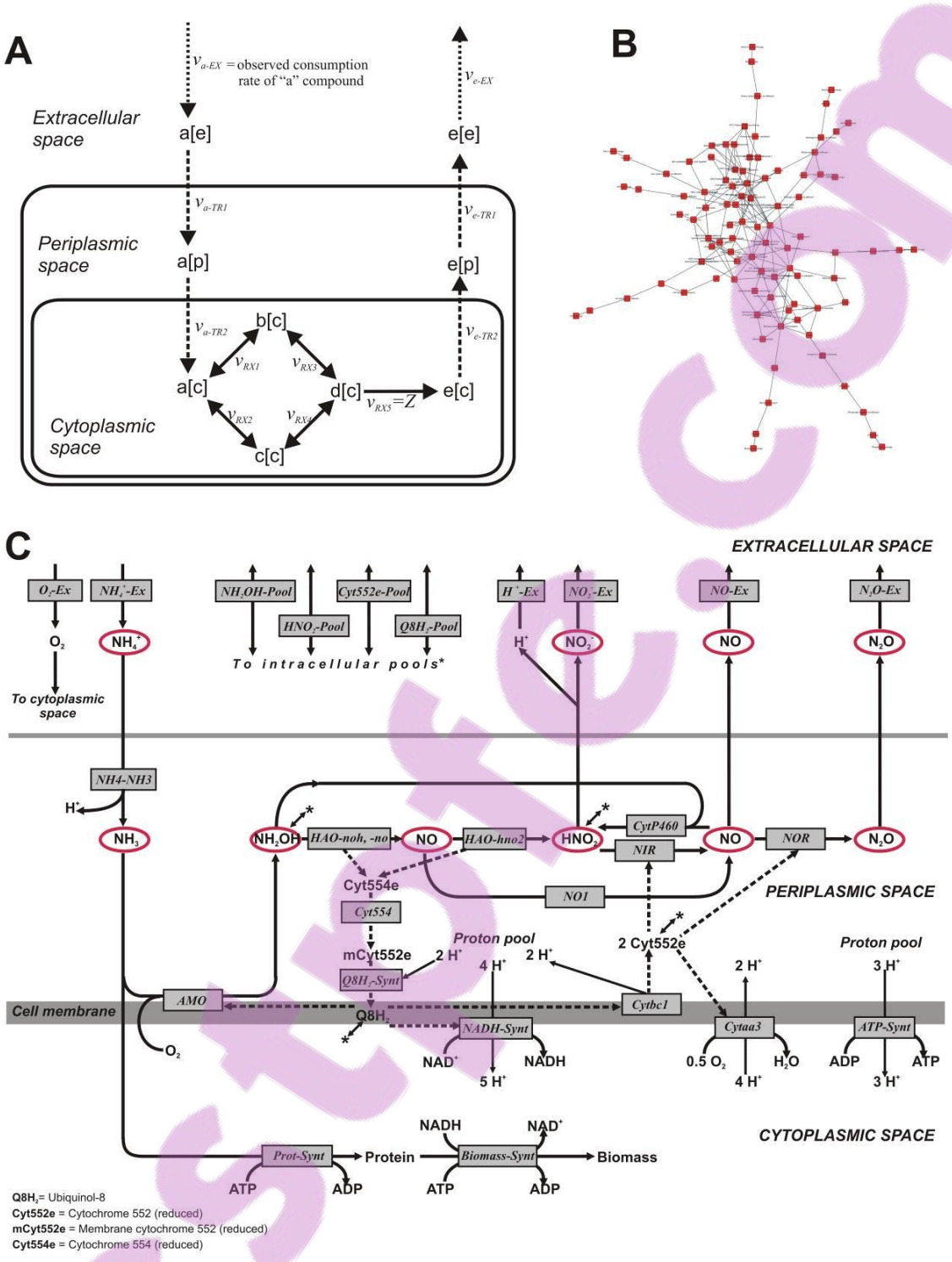

Figure 4.2. The SMN-AOB model developed in this study

(A) The conceptual scheme of FBA in the metabolic network. The conceptual scheme of FBA in the metabolic network. Metabolites "a" to "e" are shown in extracellular, periplasmic, or cytoplasmic compartments using labels [e], [p] or [c]; doted, dashed and solid arrows respectively represent exchange, transport/diffusion, and metabolic reactions (B) Visualization of the SMN-AOB model created using Cytoscape in which nodes represent reactions as well as metabolites. (C) Schematic representation of reactions and metabolic compounds considered in the AOB-SMN model. Black arrows represent metabolic reactions with their ID name shown in grey boxes and dashed lines represent the pathways of electron exchange. Ovals show the main nitrogenous compounds.

Table 4.1. Energy production reactions of the SMN model based on *N. europaea* genomic and biochemical information. Stoichiometric equations are those obtained from the calibration process.

Reaction ID	Reaction description	Reaction stoichiometric equation	Catalyst	References
AMO	AMO Ammonia oxidation to hydroxylamine	$NH_3[p] + O_2[p] + Q8H_2[c] \rightarrow NH_2OH[p] + H_2O[p] + Q8[c]$	Ammonia monooxygenase	1, 2, 3, 4
HAO-noh	HAO Hydroxylamine oxidation to nitroxyl	$NH_2OH[p] + Cyt554[p] \rightarrow NOH[p] + Cyt554e[p] + 2\ H^+[p]$	Hydroxylamine oxidoreductase	1, 2, 3, 4, 5, 6, 7, 8
HAO-no	HAO nitroxyl oxidation to nitric oxide	$NOH[p] + 0.5\ Cyt554[p] \rightarrow NO1[p] + 0.5\ Cyt554e[p] + H^+[p]$	Hydroxylamine oxidoreductase	1, 2, 3, 4, 5, 6, 7, 8
HAO-hno2	HAO nitric oxide oxidation to nitrous acid (protonated nitrite)	$NO1[p] + 0.5\ Cyt554[p] + H_2O[p] \rightarrow HNO_2[p] + 0.5\ Cyt554e[p] + H^+[p]$	Hydroxylamine oxidoreductase	1, 2, 3, 4, 5, 6, 7
C_{c554}	ETC split of electron flow by cyt554	$Cyt554e[p] + Cyt552m[c] \rightarrow Cyt552me[c] + Cyt554[p]$	CytochroneC-m552	1, 2, 9, 10, 12
Q8H2-Synt	ETC Ubiquinone to ubiquinol for AMO	$Q8[c] + Cyt552me[c] + 2\ H^+[p] \rightarrow Q8H_2[c] + Cyt552m[c]$	Ubiquinol-8	1, 2, 9, 10
NADH-Synt	ETC NADH production by NADH-ubiquinone reductase using ubiquinol	$NAD^+[c] + Q8H_2[c] + 4\ H^+[p] \rightarrow NADH[c] + Q8[c] + 5\ H^+[c]$	NADH-ubiquinone reductase. COMPLEX I	9, 6, 1, 2, 10
Cytbc1	ETC proton pump by CytCbc1 reductase using ubiquinol-8	$Q8H_2[c] + 2\ Cyt552[p] \rightarrow 2\ H^+[p] + Q8[c] + 2\ Cyt552e[p]$	Cytochrome bc1 COMPLEX III	9, 6, 1, 2, 10
Cytaa3	ETC proton pump by Cytaa3, Oxygen as final electron acceptor OXIC	$0.5\ O_2[c] + 4\ H^+[c] + 2\ Cyt552e[p] \rightarrow H_2O[c] + 2\ H^+[p] + 2\ Cyt552[p]$	Cytochrome aa3 COMPLEX IV	9,6, 1, 2, 10
CytP460	NO_2 synthesis from NH_2OH + NO	$0.5\ NH_2OH[p] + 0.5\ NO[p] + 2.5\ Cyt552[p] + H_2O[p] \rightarrow HNO_2[p] + 2.5\ Cyt552e[p] + 2.5\ H^+[p]$	Cytochrome P460	11, 13, 14
NO1	Leak of NO from *HAO_no*	$NO1[p] \rightarrow NO[p]$	Hydroxylamine oxidoreductase	7, 8
NIR	Nitrite reduction to nitric oxide	$HNO_2[p] + Cyt552e[p] + H^+[p] \rightarrow NO[p] + Cyt552[p] + H_2O[p]$	Nitrite reductase	5, 15, 16, 17
NOR	Nitric oxide reduction to nitrous oxide	$NO[p] + Cyt552e[p] + H^+[p] \rightarrow 0.5\ N_2O[p] + Cyt552[p] + 0.5\ H_2O[p]$	Nitric oxide reductase	11, 5, 15, 18
ATP-Synt	ETC ATP trans membrane synthesis (four protons per ATP)	$ADP[c] + Pi[c] + 3\ H^+[p] \rightarrow ATP[c] + H_2O[c] + 3\ H^+[c]$	ATP synthase	9, 1, 2, 4, 19
Prot-Synt	Protein synthesis using ammonia and ATP	$8.9\ ATP[c] + 4\ NH_3[c] + 16\ CO_2[c] + 62\ H[c] \rightarrow 8.9\ ADP[c] + 8.9\ pi[c] + 8.9\ h[c] + Protein[c] + 19\ H_2O[c]$		20, 21
ATP-Man	Non-growth associated energy consumption (Maintenance ATP consumption)	$ATP[c] + H_2O[c] \rightarrow ADP[c] + Pi[c] + H^+[c] + m[c]$		22, 23, 24
Biomass-Synt	Biomass synthesis ATP consumption	$15\ ATP[c] + 12\ NADH[c] + 0.31\ Protein[c] + 32\ m[c] \leftrightarrow 15\ ADP[c] + 10\ NAD^+[c] + 15\ Pi[c] + 15\ H^+[c] + Biomass[c]$		22, 21

[p] = metabolite in periplasmic space, [c] = metabolite in cytoplasmic space, [e] = metabolite in extracellular space.

References: 1=(Whittaker et al., 2000), 2=(Ferguson et al., 2007), 3=(Colliver and Stephenson, 2000), 4=(Arp et al., 2002), 5=(Stein, 2011), 6=(Poughon et al., 2001), 7=(Kostera et al., 2008), 8=(Cabail and Pacheco, 2003), 9=(Chain et al., 2003), 10=(Arp and Stein, 2003), 11=(Chandran et al., 2011), 12=(Hooper, 1991), 13=(Hooper et al., 1997), 14=(Elmore et al., 2007), 15=(Yu et al., 2010), 16=(Beaumont et al., 2002), 17=(Cantera and Stein, 2007), 18=(De Vries et al., 2007), 19=(Kumar and Nicholas, 1982), 20=(Grady et al., 1999), 21=(Terry and Hooper, 1970), 22=(Thiele and Palsson, 2010), 23=(Tchobanoglous et al., 2003), 24=(Vadivelu et al., 2006)

A scheme of the primary reactions and metabolites considered in the model is illustrated in **Figure 4.2.C.** The figure includes the exchange of compounds between cellular and extracellular spaces, oxidation and reduction of nitrogenous compounds in the periplasmic space, and protein and biomass synthesis in the cytoplasmic space, along with the electron transport chain. The complete list of reaction equations and metabolic compounds that form the complete SMN model can be found in the Appendix One of this document.

Table 4.1. presents a list of model's primary metabolic reactions, their stoichiometric equations, the associated reaction's catalyst enzyme and associated references and **Table 4.2.** lists model's metabolic compounds forming the reaction equations of **Table 4.1. Table 4.2.** also shows the number electron equivalents carried by the reduced form of the metabolic compound and midpoint redox potential values (at pH = 7; Pi = 1atm). Metabolic compounds redox potential values were taken from (Grady et al., 1999) and (Poughon et al., 2001).

Table 4.2. Metabolic compounds and their redox couple of the *N. europaea* SMN model.

Compound name of redox pair	Reduced form in equations	Oxidized form in equations	# of electrons	Redox potential (mV)
Ammonium/Ammonia	NH_4^+	NH_3	0	0
Ammonia/Hydroxylamine	NH_3	NH_2OH	2	+900
Hydroxylamine/Nitroxyl	NH_2OH	NOH	2	-81
Nitroxyl/Nitrite	NOH	NO_2^-	2	+335
Nitroxyl/Nitric oxide	NOH	NO	1	+270
Nitric oxide/Nitrite	NO	NO_2^-	1	+400
Nitrite/Nitrate	NO_2^-	NO_3^-	2	+408
Hydroxylamine/nitrite	NH_2OH	NO_2^-	4	+127
Reduced/Oxidized Nicotinamide adenine dinucleotide	NADH	NAD^+	2	-320
Water/Oxygen	2 H_2O	O_2	4	+815
Ubiquinonol-8/Ubiquinone-8	$Q8H_2$	Q8	2	+60
Hydrogen/proton	H_2	2 H^+	2	-420
Ferrocytochrome c554/ Ferricytochrome c554	Cyt554e	Cyt554	2	+254
Membrane Ferrocytochrome c552/Ferricytochrome c552	Cyt552me[c]	Cyt552m[c]	2	+254
Periplasmic Ferrocytochrome c552/ Ferricytochrome c552	Cyt552e[p]	Cyt552[p]	1	+254

Reduced form = oxidized form + #[electrons]

The metabolic network incorporates three compartments: cytoplasmic space, periplasmic space and extracellular space represented as [c], [p] and [e], respectively (**Table 4.1.**). Periplasmic space was included as it plays a critical role as several key respiratory reactions that occur in this compartment

((Whittaker et al., 2000). The model includes exchange reactions ("-*Ex*") for NH_4^+, NO_2^-, NO, N_2O, H^+, O_2, PO_4^{3-} and biomass (as Cell-N) compounds that define the extracellular space environment. Compartment exchange reversible reactions were included to simulate the diffusion of compounds between extracellular space and periplasmic space. Proton exchange between the periplasmic space and other compartments occurs via specific proton translocation and transport reactions. In the periplasmic space, nitrite and ammonia are assumed to protonate to nitrous acid (HNO_2) and ammonium (NH_4^+) due to the lowering of pH by respiration ((Sayavedra-Soto and Arp, 2011).

The oxidation of ammonia by AMO (Reaction ID: *AMO*) can occur in the periplasmic space or in the cytoplasmic space (Ferguson et al., 2007). However, it is not known with any certainty whether ammonium deprotonation to ammonia contributes to periplasmic proton gradient. Both scenarios were tested with the model's calibration procedure. Hydroxylamine oxidation by HAO is modelled as three consecutive reactions (Reaction IDs: *HAO-noh*, *HAO-no*, and *HAO-hno2*) involving hydroxylamine oxidation to nitroxyl (NOH), nitroxyl oxidation to nitric oxide (NO) and nitric oxide oxidation to nitrous acid (HNO_2) (**Table 4.1.**).

NO and N_2O production in *N. europaea* occurs via two routes, the hydroxylamine oxidoreductase (HAO) mediated aerobic hydroxylamine oxidation pathway (Reaction IDs: *HAO-noh* and *NO1*) and the nitrite reductase (NirK) mediated nitrifier denitrification pathway (Reaction IDs: *NIR* and *NOR*) (Ni et al., 2011; Stein, 2010; Stein, 2011). The reconstruction of the HAO mediated NO/N_2O production pathway involved partitioning the HAO reaction into three steps (reactions *HAO-noh*, *HAO-no*, and *NO1* in Table 4.1.), with the production of HNO and NO as intermediates (Cabail and Pacheco, 2003; Kostera et al., 2008; Poughon et al., 2001), and subsequent production of N_2O from NO via *NOR* reaction (catalysed by nitric oxide reductase (cNor)). The nitrifier denitrification NO/N_2O production pathway uses HNO_2 and NO as final electron acceptors in two reductive reactions (*NIR* and *NOR*) catalysed by NirK and cNor with cytochrome c552 oxidoreductase activity (Ni et al., 2011; Stein, 2010; Stein, 2011). Thus, the *NIR* and *NOR* reaction are assumed to use reduced periplasmic Cytochrome c552 (Metabolite ID: Cyt552e) as the electron donor. Ubiquinol-8 ($Q8H_2$) and reduced cytochrome 552 (Cyt552e) play a particularly significant role in the modelled electron transport chain by acting as pivot compounds that distribute the flow of electrons to different electron acceptors (**Figure 4.2.C**).

The model includes the reaction catalysed by cytochrome P460 (Reaction ID: *CytP460*) as *N. europaea* cells use it to reduce NO accumulation, which appears to lower the toxic effects of NO, via comproportionation of NO and NH_2OH to NO_2^- (Chandran et al., 2011; Stein, 2011). The cytochrome P460 has a 40-fold lower Cytochrome 552 oxidoreductase activity than the HAO reaction (Numata et al., 1990) This information is used in the model to define a maximum rate (upper bound) in the *CytP460* reaction as: $0 \leq v_{CytP460} \leq (\frac{v_{HAO-noh}}{40})$, where $v_{CytP460}$ is the estimated flux value of the reaction *CytP460* and $v_{HAO-noh}$ is the flux value of reaction *HAO-noh*.

Nitrous oxide reductase activity (N_2O reduction to N_2) as not included in the model as the *N. europaea* genome does not contain genes encoding this enzyme or homologs.[9] It is generally accepted that N_2O reduction to N_2 does not occur in AOB and is an attribute of true denitrifiers only ((Stein, 2010).

Included in the model were all the electron transport chain reactions found in *N. europaea*, including the reactions for the production of ubiquinol-8 and NADH (Reaction ID: *Q8H2-Synt* and *NADH-Synt*) as well as reactions catalysed by the proton pump cytochrome bc1 (Reaction ID: *Cytbc1*) and the terminal oxidase proton pump cytochrome aa3 (Reaction ID: *Cytaa3*) (**Figure 4.2.** and **Table 4.1.**). It was assumed that cytochrome 554 was not able to deliver electrons to periplasmic cytochrome 552 ((Stein, 2011), and in this way open another route of electrons towards acceptors molecules. **Table 4.2.** shows the electron equivalents and redox potential of the redox couples of the *N. europaea* electron transport chain used to balance the stoichiometric equations. ATP synthesis by a 3 proton ATP synthase was included in agreement with (Chain et al., 2003).

Four exchange reactions were incorporated into the model to mimic the production or consumption of intracellular pools of hydroxylamine, nitrous acid, ubiquinonol-8 ($Q8H_2$) and reduced cytochrome 552 (Reaction ID's: *NH_2OH-Pool, HNO_2-Pool, $Q8H_2$-Pool* and *Cyt552e-Pool*, respectively). These reactions were maintained with infinite upper and lower bounds.

Reactions for protein production, non-growth associated ATP consumption and biomass production (Reaction ID's, *Prot-Synt; ATP-Man* and *Biomass-Synt*) were included following the (Thiele and Palsson, 2010) protocol. The number of moles of ATP required for the synthesis of one mole of protein or nucleic acids in *Prot-Synt* and *Biomass-Synt* reactions was estimated as 8.9 mmol-ATP per mole of protein in *Prot-Synt* reaction and 15 mmol-ATP consumed in *Biomass-Synt* reaction, following (Thiele and Palsson, 2010) calculus method using the macromolecule composition of *N. europaea* presented in (Terry and Hooper, 1970). The protein production reaction was emulated by the consumption of NH_3 and ATP to produce a hypothetical protein molecule with molecular composition $C_{16}H_{24}O_5N_4$ defined by (Grady et al., 1999). The biomass production reaction emulated the consumption of biomass precursors (including ATP) to produce one gram of biomass dry weight with a hypothetical molecular formula of $C_5H_7O_2N$. A non-growth associated ATP consumption reaction (ID: *ATP-Man*) was included to emulate the consumption of ATP associated with cellular processes that do not produce biomass. and to account for biomass yield from NH_4^+ and experimental observations of 65% non-growth associated energy consumption (Poughon et al., 2001; Tchobanoglous et al., 2003; Vadivelu et al., 2006).

4.2.2. FBA Model simulations

FBA was applied to estimate the unknown rates of network reactions by using values of consumption rates of substrates (i.e. oxygen and ammonium) as model input. The unknown rates (or fluxes) were found by optimizing with linear programing an objective function (*Z*) subject to the specified substrate uptake rates as described in Chapter 3 (Becker et al., 2007; Orth et al., 2010; Varma and Palsson, 1994a).

4.2.3. Model calibration

The draft reconstructed network contained seven reaction's stoichiometric coefficients not defined on the literature or databases. To find the unknown values of those coefficients a model calibration process was therefore required. Calibration of the metabolic network was performed to estimate the stoichiometric coefficients of reactions by minimizing the mean relative error (MRE) (Chapter two) between model predictions and reported values of 17 yield ratios (**Table 4.3.**) for *N. europaea* metabolism under unlimited electron donor (NH_4^+) and acceptor (O_2). Results of model's FBA simulations were applied in the equations presented in **Table 4.4.** to estimate the 17 yield ratios. Estimations of the 17 yield rations were performed repeatedly using different model's variants until reach the minimum average MRE score, as described in Chapter 3.

Maximizing biomass production as the objective function has been reported to give accurate estimates of cellular phenotypes (Orth et al., 2010; Schuetz et al., 2007); however, to confirm this we evaluate various objective functions involving maximization of biomass production ($Z = v_{Biomass-Synt}$), electrons produced by HAO reaction ($Z = v_{HAO-hno2}$), ATP synthesis ($Z = v_{ATP-Synt}$), electron equivalents production by cytochrome bc1 ($Z = v_{Cytbc1}$), NO_2^- detoxification through *NIR* reaction ($Z = v_{NIR}$), and periplasmic proton potential by cytochrome aa3 ($Z = v_{Cytaa3}$). The best fitting objective function was the one that gave the lowest average MRE. No further recalibration of model's stoichiometric coefficients is required for different environmental conditions as a variation in metabolic state only influences the rates of reactions but not reaction stoichiometry ((Becker et al., 2007; Orth et al., 2010).

4.2.4. Modulatory reactions of NO and N_2O production

To assess metabolic modulation of production of NO/N_2O, a sensitivity analysis was performed for the five reactions directly involved in their production, i.e. *NO1*, *NIR*, *NOR, NO-Ex* and *N_2O-Ex*. A Latin-Hypercube approach was adopted to perform 12,000 simulations using random values between 0 and 1 for specific rates v_j of the reactions involved in consumption of substrates, intracellular pools of electron carriers, and energy production metabolism, along with FBA to estimate the rates of the *NO1*, *NIR*, *NOR, NO-Ex* or *N_2O-Ex* reactions. The reaction sensitivity was assessed by calculating sensitivity coefficient $\left(S_{z_i}^{\sigma}\right)^2$, as described bellow.

Table 4.3. Seventeen molar yield ratios that describe energy generation metabolism in *N. europaea*. Equations to estimate the rate values using the AOB-SMN model are specified in **Table 4.4.**

Yield numbe	Yield ratio	Description of Yield ratio	References	Units	Reported value in literature	Estimated rate values (RE scores)		
						$Z = v_{Biomass-Synt}$	$Z = v_{ATP-Synt}$	$Z = v_{Cytaa3}$
1	$\frac{O_2}{NH_4^+}$	Overall stoichiometry of ammonium oxidation to nitrite	1, 2	$\frac{mol\ O_2}{mol\ N}$	1.5	1.43 (0.047)	1.43 (0.047)	1.5 (0)
2	$\frac{NO_2^-}{NH_4^+}$	Overall stoichiometry of ammonium oxidation to nitrite	1, 2	$\frac{mol\ N}{mol\ N}$	1	0.99 (0.009)	0.99 (0.009)	1 (0)
3	$\frac{Biomass^{\#}}{NH_4^+}$	Overall stoichiometry of ammonium oxidation to nitrite	1, 2, 3	$\frac{mol\ N}{mol\ N}$	0.012	0.0095 (0.205)	0.0095 (0.205)	0 (1)
4	$\frac{H_2O}{NH_4^+}$	Overall stoichiometry of ammonium oxidation to nitrite	1, 2	$\frac{mol\ H_2O}{mol\ N}$	1	1.088 (0.088)	1.088 (0.088)	1 (0)
5	$\frac{NO_2^-}{NH_4^+}$	Overall stoichiometry of ammonium oxidation to nitrite	3	$\frac{mol\ N}{mol\ N}$	0.011	0.010 (0.37)	0.010 (0.37)	0 (1)
6	$\frac{ATP_{Biomass}}{ATP_{Synthetized}}$	Growth associated ATP consumption	2, 3, 4	$\frac{mol\ ATP}{mol\ ATP}$	0.35	0.357 (0.021)	0.357 (0.021)	NA
7	$\frac{ATP_{Manteinance}}{ATP_{Synthetized}}$	Maintenance associated ATP consumption	4	$\frac{mol\ ATP}{mol\ ATP}$	0.65	0.643 (0.011)	0.643 (0.011)	NA
8	$\frac{\rightarrow H^+}{NH_4^+}$	Total protons translocated per mol of ammonium oxidised	3, 5	$\frac{mol\ H}{mol\ N}$	9	8.54 (0.051)	8.54 (0.051)	9 (0)
9	$\frac{\rightarrow H^+}{NH_2OH}$	Total protons translocated per mol of hydroxylamine oxidised	3, 5	$\frac{mol\ H}{mol\ N}$	8	7.54 (0.057)	7.54 (0.057)	8 (0)
10	$\frac{\rightarrow H^+}{NH_4^+ * O}$	H^+/O yield from ammonium oxidation	5	$\frac{mol\ H}{mol\ O}$	3.4	6 (0.764)	6 (0.764)	3 (0.765)
11	$\frac{\rightarrow H^+}{NH_2OH * O}$	H^+/O yield from hydroxylamine oxidation	5	$\frac{mol\ H}{mol\ O}$	4.4	4 (0.090)	4 (0.090)	3 (0.091)

12	$\frac{O_{2\ AMO}}{O_2}$	Oxygen consumption ratio by AMO reaction	6	$\frac{mol\ O_2}{mol\ O_2}$	0.66	0.69 (0.0411)	0.69 (0.0411)	0.67 (0.001)
13	$\frac{O_{2\ Cytaa3}}{O_2}$	Oxygen consumption ratio by Cytaa3 reaction	6	$\frac{mol\ O_2}{mol\ O_2}$	0.33	0.31 (0.079)	0.31 (0.079)	0.33 (0.001)
14	$\frac{H^+_{Leaked}}{\rightarrow H^+}$	Proton gradient dissipation not associated to ATP production	3	$\frac{mol\ H}{mol\ H}$	4.5	2.28 (0.493)	2.28 (0.493)	0 (1)
15	$\frac{Q8H_{2\ used\ by\ AMO}}{Q8H_{2\ Synthetized}}$	Ubiquinol-8 (q8h2) oxidation ratio by AMO reaction	7	$\frac{mol\ Q8H_2}{mol\ Q8H_2}$	0.5	0.51 (0.02)	0.51 (0.02)	0.5 (0.000)
16	$\frac{Q8H_{2\ used\ by\ Cytbc1}}{Q8H_{2\ Synthetized}}$	Ubiquinol-8 oxidation ratio by Cytochrome bc1 reaction	7	$\frac{mol\ Q8H_2}{mol\ Q8H_2}$	0.4125	0.442 (0.02)	0.442 (0.02)	0.5 (0.214)
17	$\frac{Q8H_{2\ used\ by\ NADHSynt}}{Q8H_{2\ Synthetized}}$	Ubiquinol-8 oxidation ratio by NADH synthesis reaction	7	$\frac{mol\ Q8H_2}{mol\ Q8H_2}$	0.08754	0.058 (0.22)	0.058 (0.22)	0 (1)
	Average MRE (% of error)					**0.152^{A}**	**0.152^{A}**	**0.338^{B}**

References: 1 = (Grady et al., 1999), 2 = (Tchobanoglous et al., 2003), 3 = (Poughon et al., 2001), 4 = (Vadivelu et al., 2006), 5 = (Hollocher et al., 1982) 6 = (RW.ERROR - Unable to find reference:174), 7 = (Whittaker et al., 2000).
^{A} or ^{B} = Values detonated with different letters differ significantly according to one way ANOVA test at $P < 0.05$.
NA = A flux is not available to estimate yield ratio.
$^{\#}$ = biomass as a molecule with the standard formula $C_5H_7O_2N$.

Table 4.4. Equations to estimate the 17 calibration yield ratios using the FBA results of the *N. europaea* SMN model. v_j is the rate value of reaction j and s_i is the stoichiometric coefficient value of metabolic compound i in reaction j.

#	Yield ratio	Equation
1	$\frac{O_2}{NH_4^+}$	$= \frac{v_{O2-Ex}}{v_{NH4-Ex}}$
2	$\frac{NO_2^-}{NH_4^+}$	$= \frac{v_{NO2-Ex}}{v_{NH4-Ex} * -1}$
3	$\frac{Biomas}{NH_4^+}$	$= \frac{v_{Biomass-Ex}}{v_{NH4-Ex} * -1}$
4	$\frac{H_2O}{NH_4^+}$	$= \frac{v_{H2O-Ex}}{v_{NH4-Ex} * -1}$
5	$\frac{NO_2^-}{NH_4^+}$	$= \frac{v_{O2-Ex}}{v_{NO2-Ex}}$
6	$\frac{ATP_{Biomass}}{ATP_{Synthetized}}$	$= \frac{(v_{Prot-Synt} * s_{ATP[c]}) + (v_{Biomass-Synt} * s_{ATP[c]})}{v_{ATP-Synt}}$
7	$\frac{ATP_{Manteinance}}{ATP_{Synthetized}}$	$= \frac{v_{ATP-Man}}{v_{ATP-Synt}}$
8	$\frac{\rightarrow H^+}{NH_4^+}$	$= \frac{(v_{NH4-NH3} * s_{H[p]}) + (v_{AMO} * s_{H[p]}) + (v_{HAO-noh} * s_{H[p]}) + (v_{HAO-no} * s_{H[p]}) + (v_{HAO-hno2} * s_{H[p]}) + (v_{Cytbc1} * s_{H[p]}) + (v_{Cytaa3} * s_{H[p]})}{v_{NH4-NH3}}$
9	$\frac{\rightarrow H^+}{NH_2OH}$	$= \frac{(v_{AMO} * s_{H[p]}) + (v_{HAO-noh} * s_{H[p]}) + (v_{HAO-no} * s_{H[p]}) + (v_{HAO-hno2} * s_{H[p]}) + (v_{Cytbc1} * s_{H[p]}) + (v_{Cytaa3} * s_{H[p]})}{v_{HAO-noh}}$
10	$\frac{\rightarrow H^+}{NH_4^+ * O}$	$= \frac{(v_{NH4-NH3} * s_{H[p]}) + (v_{AMO} * s_{H[p]}) + (v_{HAO-noh} * s_{H[p]}) + (v_{HAO-no} * s_{H[p]}) + (v_{HAO-hno2} * s_{H[p]}) - (v_{Q8H2-Synt} * s_{H[p]}) + (v_{Cytbc1} * s_{H[p]}) + (v_{Cytaa3} * s_{H[p]})}{v_{Cytaa3}}$
11	$\frac{\rightarrow H^+}{NH_2OH * O}$	$= \frac{(v_{AMO} * s_{H[p]}) + (v_{HAO-noh} * s_{H[p]}) + (v_{HAO-no} * s_{H[p]}) + (v_{HAO-hno2} * s_{H[p]}) - (v_{Q8H2-Synt} * s_{H[p]}) + (v_{Cytbc1} * s_{H[p]}) + (v_{Cytaa3} * s_{H[p]})}{v_{Cytaa3}}$

12	$\frac{O_{2\ AMO}}{O_2}$	$= \frac{v_{AMO}}{v_{O2-Ex}}$
13	$\frac{O_{2\ Cytaa3}}{O_2}$	$= \frac{v_{Cytaa3} * 0.5}{v_{O2-Ex}}$
14	$\frac{H^+_{Liked}}{\rightarrow H^+}$	$= \frac{(v_{ATP-Symt} * 7.5) - (v_{ATP-Synt} * 3)}{(v_{NH4-NH3} * s_{H[p]}) + (v_{AMO} * s_{H[p]}) + (v_{HAO-noh} * s_{H[p]}) + (v_{HAO-no} * s_{H[p]}) + (v_{HAO-hno2} * s_{H[p]}) - (v_{Q8H2-Synt} * s_{H[p]}) + (v_{Cytbc1} * s_{H[p]}) + (v_{Cytaa3} * s_{H[p]})}$
15	$\frac{Q8H_{2\ used\ by\ AMO}}{Q8H_{2\ Synthetized}}$	$= \frac{v_{AMO}}{v_{Q8H2-Synt}}$
16	$\frac{Q8H_{2\ used\ by\ Cytbc1}}{Q8H_{2\ Synthetized}}$	$= \frac{v_{Cytbc1}}{v_{Q8H2-Synt}}$
17	$\frac{Q8H_{2\ used\ by\ NADHSyn}}{Q8H_{2\ Synthetized}}$	$= \frac{v_{NADH-Synt}}{v_{Q8H2-Synt}}$

$\rightarrow H^+$ = proton translocation (exchange) between periplasmic and cytoplasmic spaces

Each of the five sensitivity analysis consists of 12000 FBA simulations performed assigning random combinations of six different rate values (0, 0.2, 0.4, 0.6, 0.8 and 1) over 17 of the model's reactions that represent the consumption of substrates, intracellular pools and energy production metabolism. Constraint rate values were chosen to simulate a full range of reaction flux from zero to one. The 17 randomly constrained reactions were: consumption of ammonium (*NH_4-Ex*), consumption of oxygen (*O_2-Ex*), consumption of nitric acid intracellular pool (*HNO_2-Pool*), consumption of hydroxylamine intracellular pool (*NH_2OH-Pool*), consumption of reduced periplasmic cytochrome-552 intracellular pool (*Cyt552e-Pool*), consumption of ubiquinonol-8 intracellular pool (*$Q8H_2$-Pool*) and the reactions of the energy production metabolism, *AMO, HAO-noh, HAO-no, HAO-hno2, Cyt554, $Q8H_2$-Synt, NADH-Synt, Cytbc1, Cytaa3, CytP460,* and *ATP-Synt*. FBA simulations were performed using $Z = v_{Biomass-Synt}$ given that this objective function proved to accurately represent the AOB metabolism based on MRE scores obtained in the calibration step. The sensitivity coefficients were estimated with the Equation 4.1. (Saltelli et al., 2008):

$$S_{z_i}^{\sigma} = \frac{\sigma_{z_i} \partial Y}{\sigma_Y \partial z_i} \qquad (4.1.)$$

where $S_{z_i}^{\sigma}$ is the estimated sensitivity coefficient based on standard deviations σ; z_i is a vector of the model's input values for the *i* variable - in this case the *i* variables are the tested stoichiometric coefficients; Y is the vector of estimated values by the model using the z_i vector in this case Y represents one of the estimated calibration variables; and the derivative term $\frac{\partial Y}{\partial z_i}$ represents an estimated slope between Y and z_i vectors.

4.2.5. Estimating metabolic reactions rates in experiments

The rates of reactions in the metabolic pathways of energy, NO, and N_2O production were estimated for two previous experiments on nitrification by *N. europaea* reported by (Yu et al., 2010). The first experiment involved exposing the cell culture in chemostats to oxic-anoxic-oxic transition under a constant influent ammonium concentration of 20mM during, while the second experiment involved subjecting the cell culture to the transition with the influent ammonium concentration maintained at 20 mM during the oxic periods but lowered from 20mM to 10mM during the anoxic period.

The complete reference where experiments results were originally published is following presented:

> Yu R, Kampschreur MJ, Van Loosdrecht MCM, Chandran K. 2010. Mechanisms and specific directionality of autotrophic nitrous oxide and nitric oxide generation during transient anoxia. Environmental Science and Technology 44:1313-1319.

Both experiments were conducted in bioreactors with 4 litters of working volume with *N. europaea* concentrations of 2.4±0.5x10^8 cells/mL during the entire experiment. Each experimental chemostat culture of was operated at constant pH of 7.5 and temperature of 21ºC. Dissolved oxygen was maintained at 6 mg-O_2/L during the aerobic period and at 0 mg-O_2/L m during the anoxic period of experiments. Influent feed had 20mM of NH_4^+ as energy source and did not contain other nitrogenous

compounds. Chemostat performance was monitored by measuring specific oxygen uptake rate and effluent concentrations of NH_4^+, NH_2OH, NO_2^-, and cells. Experiment's liquid phase N_2O concentration was reported directly on (Yu et al., 2010) publication and NO liquid phase concentrations were calculated from gaseous ppm(v) data (obtained by (Yu et al., 2010)) by applying Henry's law of gases. The experimental rates of production of nitrogenous compounds observed at different instants of time were used as model's input and calibration data as described in the next paragraphs.

Experimental rates were estimated as follow: The 135 hour duration concentration curves of nitrogenous compounds reported for each of the analysed experiments were split into 135 hourly intervals. For each interval, metabolic compounds were assumed to be at pseudo-steady state (Mahadevan et al., 2002a) to obtain 135 data points corresponding to the measured bioreactor's concentrations of nitrogenous compounds. Each concentration data was used together with influent concentrations and chemostat liquid flow rate along the Equation 4.2. to calculate 135 experimental rates for each compound.

$$v_i = \left(X_i^{OUT} - X_i^{IN}\right) * Q \qquad (4.2.)$$

where v_i is the experimental consumption (negative symbol) or production (positive symbol) rate of the i^{th} compound; X_i^{OUT} is the concentration of the compound in chemostat; X_i^{IN} is the concentration of the compound in chemostat influent and; Q is the liquid flow chemostat rate (0.075L/h).

To estimate the metabolic reaction rates of each experiment,135 FBA simulations were performed using the experimental ammonium consumption rate of each interval as constraint of model's *NH_4-Ex* reaction. Additionally, in each FBA simulation, the rate value v_{Cytaa3} of the terminal oxidase (*Cytaa3*) was specified to fit the rate of N_2O production; in a similar way the rate value $v_{HAO-hno2}$ of hydroxylamine oxidoreductase (*HAO-hno2*) reaction was specified to fit the rate of NO production. Maximum rate values $\beta_{CytP460}$ = 0.037 mmol/h and β_{NO1} = 0.05 mmol/h were maintained constant during the 135 FBA simulations in agreement with maximum rate values of cytochrome P460 and HAO enzymes reported by (Numata et al., 1990) and (Sayavedra-Soto and Arp 2011). Preliminary simulation provide computational evidence to support the measured cytochrome P460 hydroxylamine oxidation activity 40 times lower than the activity of hydroxylamine oxidoreductase (HAO) suggested by (Numata et al., 1990) and a limited amount of NO leaked from HAO reaction suggested by (Sayavedra-Soto and Arp, 2011). Otherwise, if the maximum rate value of *CytP460* and *NO1* reaction are as high as the one for *AMO* or *HAO* reactions, half of the electron equivalents (as Cyt552e) would be produced by *CytP460* without activation of the electron transport chain, and the values of proton translocation ($\rightarrow H^+/O$) and Ubiquinol-8 consumption yields measured by (Whittaker et al., 2000) and (Hollocher et al., 1982) would be impossible to observe. Therefore, during these simulations of experiments, the upper bound of the *CytP460* reaction ($\beta_{CytP460}$) was constrained to 0.037mmol/h to correspond to obtain the proportion $v_{CytP460} = v_{HAO\_hno}/40$ suggested by (Numata et al., 1990). Similarly, following (Sayavedra-Soto and Arp, 2011) observation, the upper bound of the *NO1*

reaction (β_{NO1}) was constrained to the rate value of 0.05mmol/h to assume a limited amount of NO released by hydroxylamine oxidoreductase.

Finally, the accuracy of the model's estimations was assessed using coefficients of determination (R^2), slope values (m) and root mean square errors (RSME) (Equation 4.3.) between experimental and estimated rates of production of NO_2^--N, NO-N, N_2O-N and cell-N (i.e., nitrogen incorporated in biomass). RSME were estimated with the Equation 4.3. (Makinia, 2010):

$$RMSE = \sqrt{\frac{\sum_{i=1}^{n}(X_l^i - x_l^i)^2}{n}} \qquad (4.3.)$$

where $RMSE$ is the root mean square error for value; X_l^i is the i^{th} observed value (from the experiments) of variable l; x_l^i is the i^{th} estimated (predicted by model) value of variable l; and n is the number of data points.

4.3. Results

4.3.1. Metabolic network calibration

The objective functions for maximizing biomass production ($Z=v_{Biomass\text{-}Synt}$) and maximizing ATP synthesis ($Z=v_{ATP\text{-}Synt}$) gave the same lowest average MRE of 0.152 (**Table 4.3.**), interpreted as a percentage of accuracy of 84.8% (from (1 – MRE)*100) to fit the 17 observed yield values. As the estimated molar yields and MRE values obtained with $Z=v_{Biomass\text{-}Synt}$ and $Z=v_{ATP\text{-}Synt}$ were identical, FBA of *N. europaea* metabolism can be performed using either of these objective functions as biomass synthesis is inherently linked to ATP synthesis. Therefore, consistent with literature (Orth et al., 2010; Schuetz et al., 2007), $Z=v_{Biomass\text{-}Synt}$ was adopted as the objective function for FBA in this study. The stoichiometric equations obtained by calibrating the model (i.e. corresponding to the lowest average nRSE using $Z=v_{Biomass\text{-}Synt}$) are presented in **Table 4.1.**

The rates for the energy production metabolism of *N. europaea* operating under non-limiting oxygen and ammonium concentrations, estimated using the calibrated model, are shown in **Figure 4.3.** According to this calibration *N. europaea* cells take up 1.012 moles of nitrogen per mole of NH_3-N oxidized by *AMO* (mol-N/mol-N_{AMO}). Thus, one mol-N as NH_3 is oxidized to NH_2OH and 0.012 mol-N are assimilated into cell biomass. In the AMO reaction producing NH_2OH 0.999 mol-N is oxidized to HNO_2 through the *HAO-noh*, *HAO-no* and *HAO-hno2* reactions and 0.001 mol-N 'leaks' as NO via the *NO1* reaction to extracellular space. *CytP460, NIR* and *NOR* reactions remain inactive under non-limiting oxygen and ammonium conditions, and no N_2O is produced. The yield coefficient for nitrogen assimilation into biomass is estimated as 0.012 mol-N/mol-N_{AMO}, consistent with the reported value of 0.15 g-COD/g-N (0.013mol-N/mol-N_{AMO}) (Grady et al., 1999).

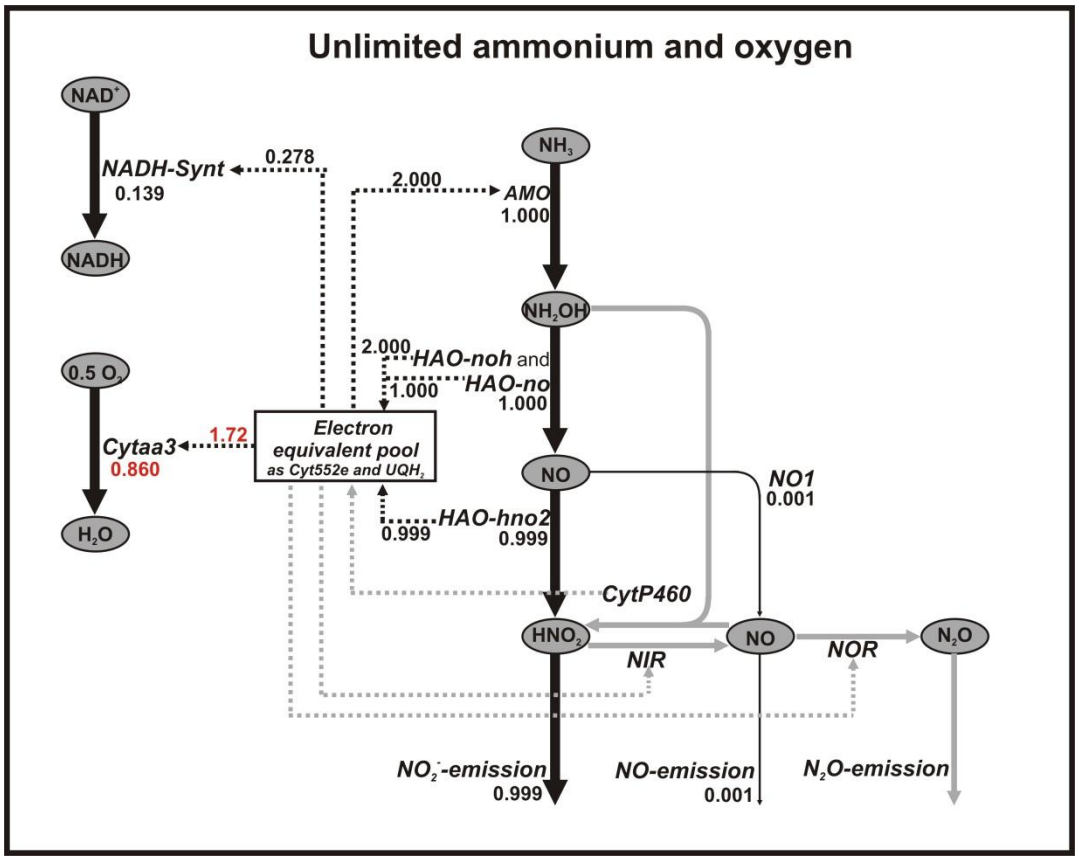

Figure 4.3. FBA analysis of *N. europaea* energy production metabolism operating under non-limiting oxygen and ammonium concentrations. Solid lines show the flow of metabolic compounds, while dotted lines represent the flow of electron equivalents. All showed rates were normalized by 1 mmol of NH_3 oxidized by AMO

4.3.2. Modulatory reactions of NO and N_2O production

The sensitivity analysis identified the reactions catalysed by the terminal oxidase cytochromes aa3 (*Cytaa3*), the cytochrome P460 (*CytP460*) and the third step of the hydroxylamine oxidation reaction (*HAO-hno2*) as having a prominent effect on the rates of N_2O and NO exchange and production via reactions *NO-Ex*, *N_2O-Ex*, *NO1*, *NIR,* and *NOR.* **Figure 4.4.** presents the results of FBA simulations of the *N. europaea* SMN randomly constrained using the Latin-Hypercube approach. In this figure, only 600 out of 1200 FBA simulation results are displayed to don't overload the figure with data. Sensitivity coefficients $\left(S_{z_i}^{\sigma}\right)^2$ were estimated form data such as the one depicted in **Figure 4.4.** **Figure 4.5.** shows the largest sensitivity coefficients $\left(S_{z_i}^{\sigma}\right)^2$ for *Cytaa3* and *CytP460* reactions obtained in five sensitivity analyses. The sensitivity coefficients of each analysis were obtained from randomly and independently constrained 17 reactions (X axis) in the AOB-SMN model. The sensitivity coefficients of *NO1*, *NIR* and *NOR* reactions indicate that NO/N_2O production by nitrifier denitrification and/or hydroxylamine oxidoreductase mediated pathways is governed by *Cytaa3* and *CytP460* reactions (with $\left(S_{z_i}^{\sigma}\right)^2$ coefficients ranging between 0.1 - 0.35), as cytochromes -aa3 and -P460 determine the availability of electrons equivalents (as periplasmic cytochrome 552) for *NIR* and *NOR* (**Figure 4.2.C.**). Similar sensitivity coefficients for the 17 constrained reactions suggest that *N_2O-Ex* is fully governed by the *NOR* reaction (sub-figures "*NOR*" and "*N_2O-Ex*" of **Figure 4.4.**). In contrast, *NO-*

Ex was governed by the *CytP460* and *HAO-hno2* reactions but not by *Cytaa3* (sub-figure "*NO-Ex*" of Fig. 2). *NIR*, *NOR* and *N_2O-Ex* reactions showed sensitivity to the rates of consumption of intracellular hydroxylamine with $\left(S_{z_i}^{\sigma}\right)^2$values between 0.07 and .09 but not to the rates of consumption of intracellular nitrous acid, reduced periplasmic cytochrome 552, and ubiquinol-8 ($\left(S_{z_i}^{\sigma}\right)^2$= 0).

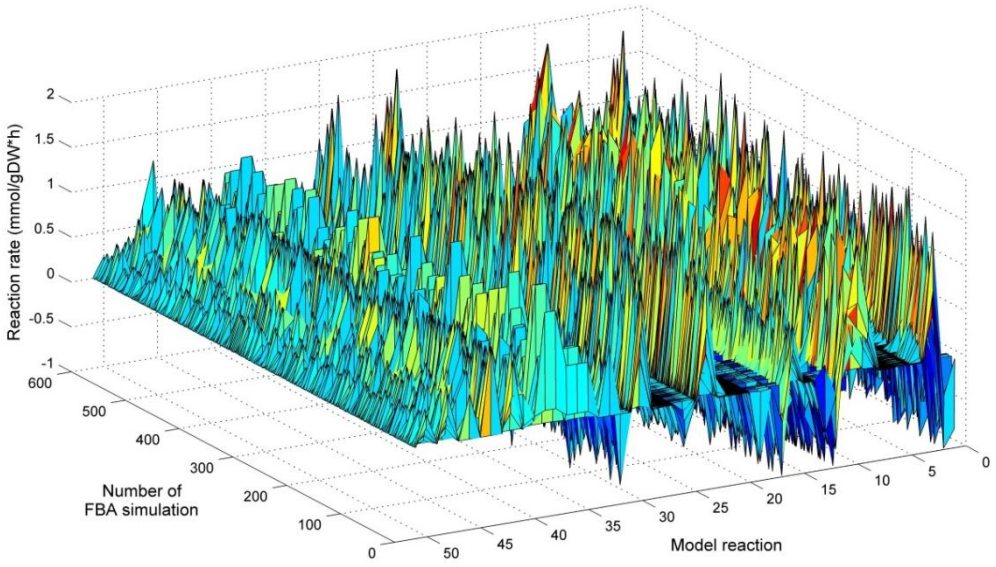

Figure 4.4. Results of FBA simulations of the *N. europaea* model randomly constrained. The figure shows the estimated rates for all the reactions in model

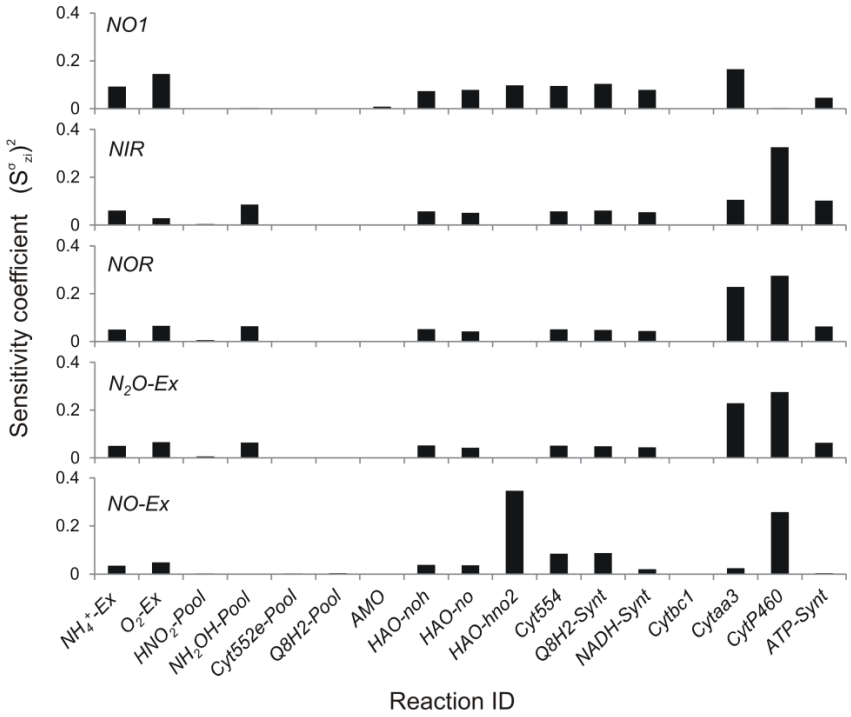

Figure 4.5. Five independent sensitivity analysis performed to NO and N_2O exchange and production reactions. The sensitivity coefficients of each analysis were obtained from randomly and independently constraint 17 reactions (X axis) of the AOB-SMN model

4.3.3. Metabolic reaction rate estimation from NO/N_2O production experiments

Figure 4.6. shows bioreactor's experimental and predicted rates of *N. europaea* nitrification process exposed to oxic-anoxic-oxic transition. In all graphics, the X axis represents time; the anoxic period is shown with grey background and starts at time zero. Sub figure A shows the data for oxic-anoxic-oxic transition with non-limiting influent ammonium concentration of 20 mM. Sub figure B shows the data for oxic-anoxic-oxic transition with lowered influent ammonium concentration of 10 mM during the anoxic period. Red vertical lines on the metabolic-reactions graphics indicate the time for which data was analysed in **Figure 4.7.**

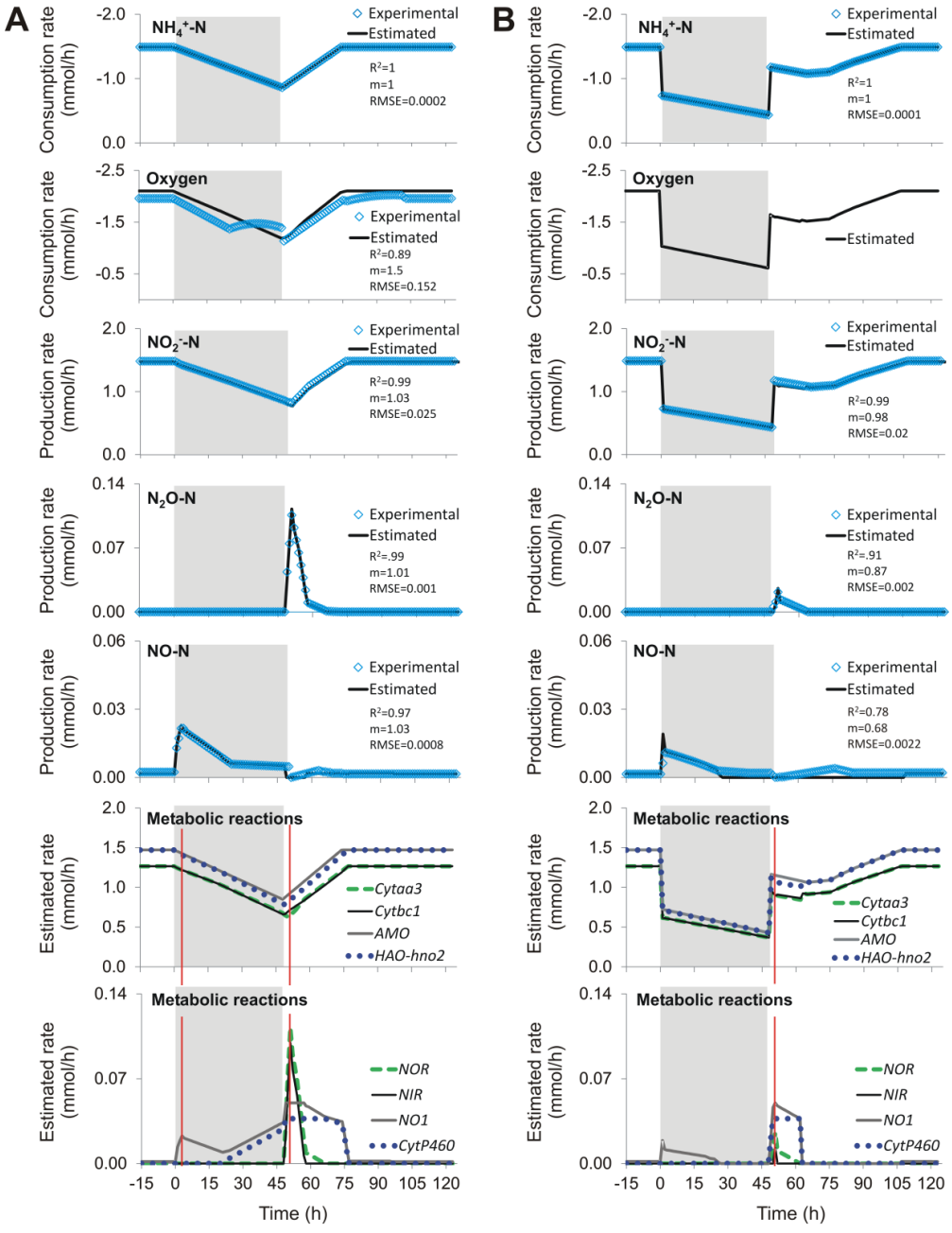

Figure 4.6. Bioreactor's experimental and predicted rates of *N. europaea* nitrification process exposed to oxic-anoxic-oxic transition

Figure 4.6.'s R^2, slope (m), and RMSE for observed versus fitted values indicate that the SMN model adequately estimates the rates of production of nitrogenous compounds and metabolic reactions for the experiments reported by (Yu et al., 2010)

Figures 4.7. to **4.9.** show an scheme of the routes for electron flow through *N. europaea*'s energy and NO/N_2O production pathways along. As well, these figures show the estimated metabolic rates (normalized with the *AMO* reaction rate) under unlimited ammonium and oxygen, and during peak NO and N_2O emission in oxic-anoxic-oxic transition. Solid lines show the flow of metabolic compounds, while dotted lines represent the flow of electron equivalents. All shown rates were normalized by 1 mmol of NH_3 oxidized by AMO. **Figure 4.7.** depicts the estimated rates at the time of transition to anoxic condition with constant ammonium from Figure 4.6.; **Figure 4.8.** depicts the estimated rates at the time of peak of N_2O production in experiment from **Figure 4.6.A.**; and **Figure 4.9.** depicts the estimated rates at the time of peak of N_2O production in experiment from **Figure 4.6.B.**

For the experiment with constant ammonium concentration (20mM), following the transition to anoxia, NO was emitted via the HAO mediated pathway *NO1* (Figure. 4.7.). In this case NO was emitted only when the rate of *NO1* reaction exceeded that of *CytP460* reaction. At peak N_2O emission following the recovery to oxia (**Figure 4.8.**) the *HAO-hno2* rate was slightly lower than that for *AMO* reaction. Similarly, the *Cytaa3* rate was slightly lower than the *Cytbc1* rate. In this circumstances, NO 'leaked' through the *NO1* reaction, however NO was majorly produced through the *NIR* reaction. More over the coordinated rates for *NOR* and *NIR* reactions at the time of peak N_2O production indicate that 66% of the N_2O emission could be attributed to nitrifier denitrification pathway (*NIR* reaction) (Figures. 4.6.A. and 4.8.).

Figures. 4.6.B. and **4.9.** show that following the transition to anoxia in the experiment with a lower influent ammonium concentration of 10 mM during the anoxic phase, the *NIR* reaction rate was estimated as zero and entire NO production occurred via the HAO mediated pathway *NO1*. As in previous experiment, during recovery following the transition to oxia from anoxia there was a coordinated increase of *NOR* and *NIR* reactions rates at the same time as the N_2O emission peak (Figure 4.6.B.). The maximum *CytP460* rate of 0.037 mmol/h was maintained due to a demand for electron equivalents to keep running the flow of electrons through the electron transport chain and produce ATP to sustain cell growth. The peak rates for *NOR* and *NIR* of 0.022 and 0.011 mmol/h, respectively, are lower than *NO1* (0.043 mmol/h) and indicate that only 20% of the peak N_2O emission may be attributed to nitrifier denitrification (**Figure 4.8.**).

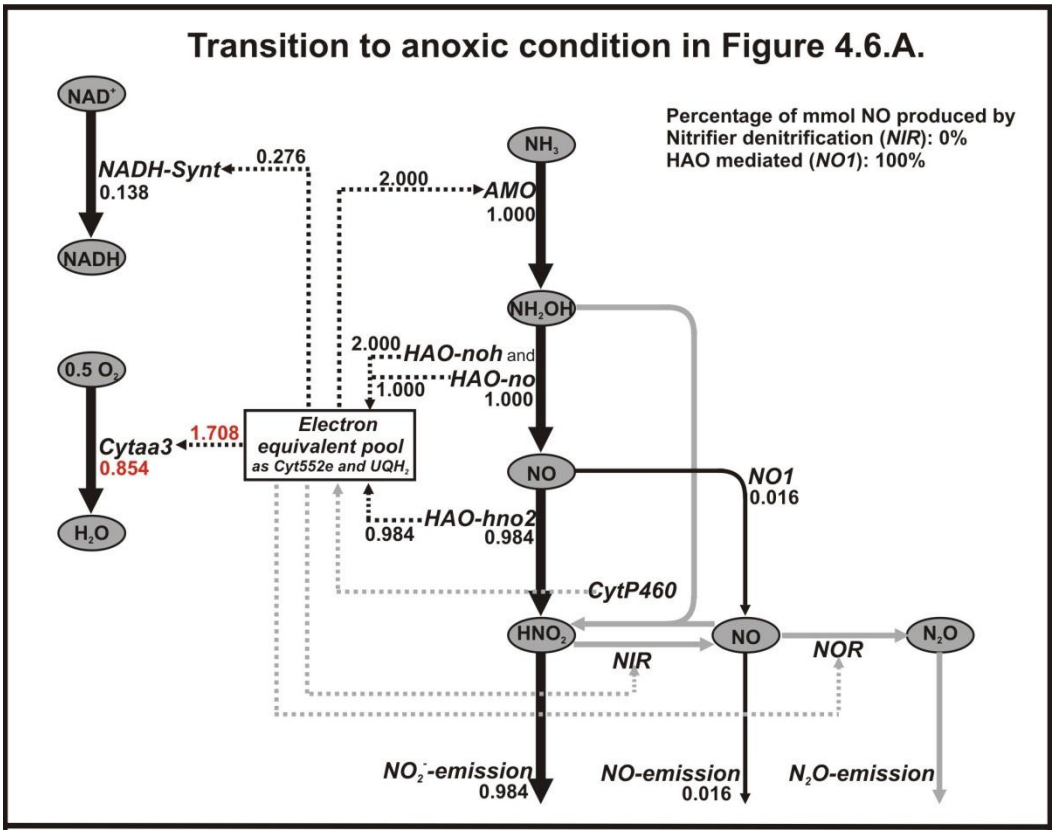

Figure 4.7. Estimated rates in the transition to anoxic condition. In Figures 4.7., 4.8. and 4.9., solid lines show the flow of metabolic compounds, while dotted lines represent the flow of electron equivalents. All showed rates were normalized by 1 mmol of NH_3 oxidized by AMO

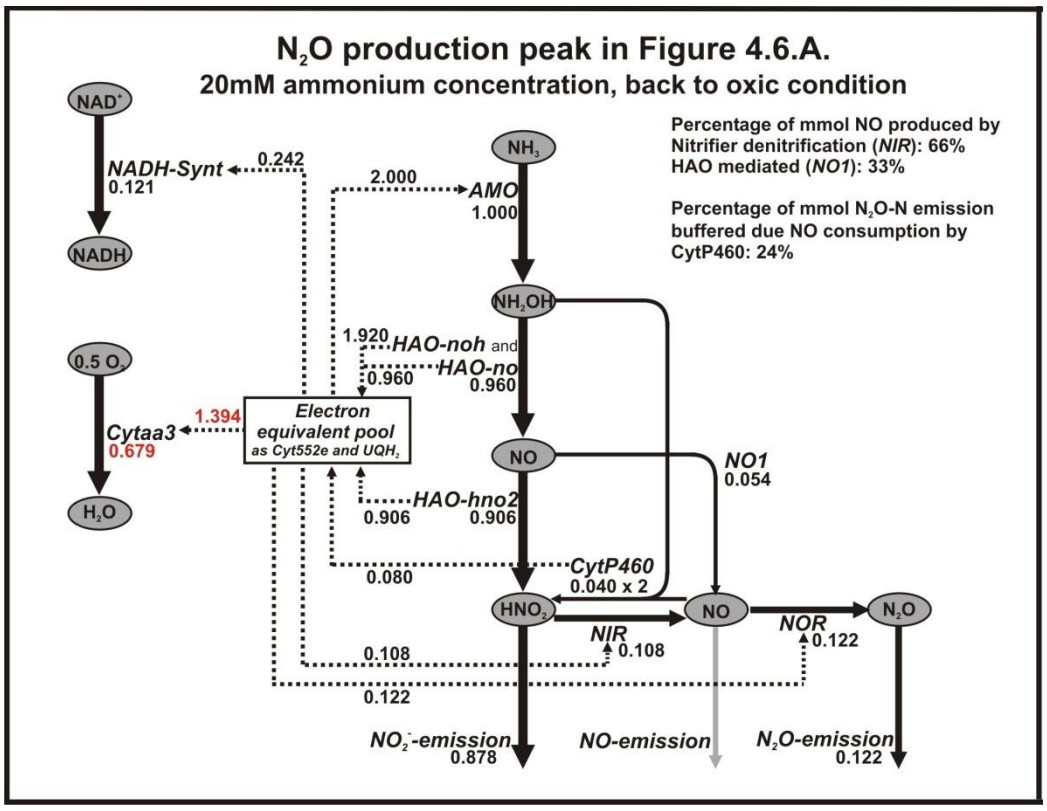

Figure 4.8. Estimated rates for experiment in constant 20mM ammonium concentration, after returning to oxic condition

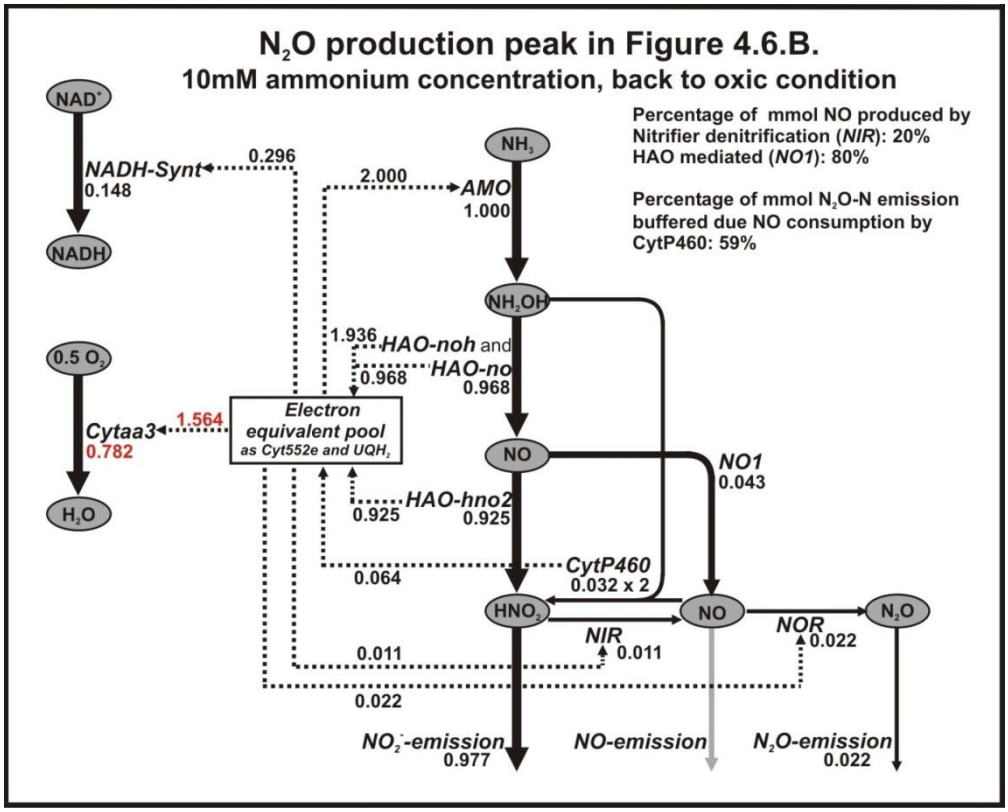

Figure 4.9. Estimated rates for experiment in constant 10mM ammonium concentration, after returning to oxic condition

4.4. Discussion

4.4.1. *N. europaea* metabolic network for energy and NO/N_2O production

The reconstruction of NO and N_2O production pathways was based on metabolic reactions experimentally shown to be active in *N. europaea* metabolism (references cited in **Table 4.1.**). Alternative NO and N_2O production/consumption reactions such as chemo-denitrification or N_2 production from N_2O ((Schmidt, 2008) were not included in the reconstruction as *N. europaea* does not have the genomic potential to perform these reactions. Two reactions catalysed by the cytochromes c'-beta and c554 that could produce N_2O in *N. europaea* (Chandran et al., 2011; Stein, 2010) were ignored as the reactions catalysed by these enzymes use the same substrate and have a similar reaction mechanism to *NOR* (Schmidt, 2008) and due to a lack of sufficient biochemical information on these reactions in the literature. Nitrite and nitrous oxide reductases have cytochrome c oxidoreductase activity and Cyt552e satisfies the mass and charge balances for these reactions (Stein, 2010, 2011); therefore our model uses reduced periplasmic cytochrome 552 (Cyt552e) as the electron donor in *NOR* and *NIR* reactions. Model calibration results support the hypothesis by Whittaker et al. (2000), Arp and Stain (2003) and Ferguson et al. (2007) about an AMO enzyme having catalytic activity on the periplasmic space. When adopting this configuration, the obtained values of proton translocation coefficients and ATP yield per NH4 oxidised were slightly closer to the experimental values than when assuming AMO activity on cytoplasm.

The AOB-SMN model ignored anabolic pathways, such as the Calvin-Benson-Bassham cycle, central carbon reactions and amino acid synthesis because the rates of production of nitrogenous compounds can be accurately estimated without considering these pathways by calibrating the protein and biomass synthesis reactions against experimental biomass yield. Moreover nitrogen assimilation into biomass accounts for less than 2% of total NH_4^+-N consumed by AOB ((Tchobanoglous et al., 2003),Therefore the maximum possible error in model's nitrogen mass balance by excluding anabolic reactions would be 2%.

Model performance was assessed for six different objective functions. The developed model was capable of reproduce experimental datasets only if maximization of growth or ATP production were set as objective functions. These results suggest that *N. europaea* metabolism is geared towards the maximization of growth even under various environmental conditions. The good fitness obtained between model estimations using growth as objective function and experimental datasets of *N. europaea* cultures under oxic-anoxic-oxic transition suggests that growth remains as a mayor driven of cell metabolism under changing environmental conditions. This implies that particular biomass and product formation rates observed during a change of environmental conditions are a result of cells adaptation to keep producing biomass using the resources available under the new environmental conditions. Nevertheless it is important to acknowledge that the achieved good fitness was result of a combination between the optimization criteria (to maximize growth) and the setting of additional constraints (i.e. placed on the Cytaa3, HAO-hno2 and CytP460 reactions).

The values of parameters $\beta_{CytP460}$, β_{NO1} and $\beta_{ATP-Man}$ were taken from experimental observations reported on various references, although the value of these parameters can vary depending on the experiment's environmental conditions. During this study the value of those parameters was maintained constant across all simulations and provided accurate estimations of production rates of nitrogenous compounds. However further model refinements should consider to perform sensitivity analysis of these parameters in order to obtain rate estimations that consider parameter variability.

4.4.2. Modulatory mechanism of NO and N_2O production

The model presented herein is an investigative tool to gain knowledge of the basic mechanism involved in NO/N_2O production by AOB cells. In this sense, we found that the activation of N_2O production pathways is a mechanism of dissipation of electron equivalents promoted by imbalanced electron donor (NH_4^+) and acceptor (O_2) uptake rates; details of this mechanism are described in following paragraphs. Given the facts that *N. europaea* is commonly and abundantly found in full scale nitrification processes (Wagner et al., 2002) and that AOB species have similar N_2O production mechanism (Stein, 2011), the findings of this study are applicable to a wide range of scenarios. Nevertheless, the model developed in this study is a first step towards the modelling and quantification of complete NO/N_2O production pathways in wastewater treatment systems. The following thesis chapter, addresses the development of a multispecies model.

The high R^2 and slope, and low RMSE, between the estimated and observed production and consumption rates of nitrogenous compounds (**Figure 4.6.**) suggests that NO and N_2O production was accurately modelled and that the estimated intracellular rates appropriately quantify the rates of metabolic reactions. FBA indicates that the activation of *NIR* and *NOR* reactions is a consequence of electron overproduction (as Cyt552e) by *Cytbc1* and *CytP460* relative to the capacity of terminal oxidase *Cytaa3* to use the produced electrons. Electron availability results in activating *NIR* and *NOR* reactions and the consequent production of NO and N_2O. This overproduction of electrons is the consequence of either a lack of oxygen as the final electron acceptor or an excess of the electron donors NH_4^+ and/or NH_2OH. The *CytP460* reaction buffers against the emission of NO and N_2O by oxidizing NO back to HNO_2. Under non-limiting oxygen and ammonium all of the reduced cytochrome c552 produced by NH_4^+ oxidation is used to reduce oxygen by *Cytaa3* and while NO is continuously produced by HAO, its emission through the *NO1* pathway is less than 0.001 mmol-N/mmol-N_{AMO} (**Figure 4.3.**). Therefore, during this circumstance, NO would be a by-product "leaked" from HAO reaction given the three-step nature of this reaction. During the anoxic phase *CytP460* activity results from availability of NO and NH_2OH, and because this reaction is energetically favoured in cells as it produces reduced periplasmic cytochrome 552 (Cyt552e). Consequently, *CytP460* served dual roles of NO detoxification and producing electron equivalents as cytochrome c552. Our analysis suggests that NO and N_2O are emitted when the sum of the rates of *NIR* and *NO1* reactions exceeds half the of *CytP460* rate.

The FBA estimates that around 70% of the peak N_2O-N emitted during transition to oxia under non-limiting ammonium concentration could be attributed to nitrifier denitrification (**Figures 4.6.A.** and **4.8.**). This result agrees with observations in experiments performed under similar conditions on the fraction of N_2O produced through nitrifier denitrification (Wunderlin et al., 2013) and increased *nirK* gene expression (Yu et al., 2010), which encodes for the copper containing nitrite reductase that catalyse *NIR* reaction. For the experiment with lowered ammonium concentration during the anoxic phase, only 0-20% of N_2O production during transition to oxia could be attributed to nitrifier denitrification while the rest resulted from the *NO1* pathway (**Figure 4.6.B.** and **4.9.**). This is attributed to the electron equivalents generated by cytochromes bc1 and P460 as being insufficient to activate the *NIR* reaction, consistent with observations during the recovery period of decreased *nirK* gene expression compared to the experiment with elevated ammonium concentration (Yu et al., 2010). In similar experiments involving the use of isotope signatures, all emitted N_2O was attributed to production via the HAO mediated pathway (Wunderlin et al., 2013). Thus, it is possible that N_2O can be produced without involving the *NIR* reaction. However, **Figure 4.7.** suggests that net N_2O emission under this scenario would be expected to be small. FBA of the anoxic phases receiving 20 mM and 10 mM influent ammonium concentrations gave zero rates for the *NIR* reaction and NO production via the *NO1* pathway for both cases (**Figures. 4.7.**). While these findings contradict observations of increased *nirK* gene expression in *N. europaea* during anoxia ((Yu et al., 2010), the FBA indicates that increased *nirK* expression may not have been accompanied with an increase of NirK protein catalytic activity.

4.5. Conclusions

This chapter describes the application of stoichiometric network modelling with flux balance analysis was to improve the understanding of NO and N_2O production in response to changes of ammonium and oxygen concentrations in during ammonia oxidation to nitrite process of BNR. As far of author's knowledge it is the first time that *N. europaea* metabolism is modelled using SMN. The SMN model developed during this research is computational tool to generate mechanistic hypothesis of *N. europaea* metabolism based on quantifications of biochemical reactions of nitrogen respiration and energy generation pathways. The model was used to generate a hypothesis about how environmental changes on ammonia and oxygen availability modulate the flow of compounds through the two pathways producing NO and N_2O. The develop SMN model open the possibility to generate model driven analysis of experimental data such as gene expression and metabolites profiles. The key research findings of the study are:

- The modulation mechanism of NO and N_2O production pathways is related to an imbalance between production and consumption of electron equivalents caused by changes in the environmental availability of electron donors and acceptors.

- The transition to anoxic conditions results in a leak of NO from HAO mediated reaction due to limited availability of electron acceptors to completely oxidize NO to HNO_2.

- The unlimited availability of electron donors combined with a lack of electron acceptors triggers nitrifier denitrification as an electron sink pathway. When electron donor depletion is accompanied with a decrease in electron acceptor concentration so that the intracellular electron equivalents generated are not enough to activate nitrifier denitrification pathway, NO/N_2O production through the hydroxylamine oxidoreductase pathway can be expected.

- The transition from anoxic to oxic conditions causes baseline N_2O production via the hydroxylamine oxidoreductase pathway, but the amount of N_2O emission is dependent upon activation of the nitrifier denitrification pathway.

- NO and N_2O emissions are partially mitigated by the NO oxidation to NO_2^- reaction catalysed by cytochrome P460.

CHAPTER FIVE

N_2O production in nitrifying mixed cultures: Effect of NO turnovers, oxygen and ammonium concentrations and microbial community structure

The previous chapter describes how SMN modelling was used to quantify reaction rates of N_2O production pathways in AOB cells (i.e. *N. europaea* cells*)* exposed to changes of aerobic and oxic conditions. In this chapter a similar simulation study is described however the analysis is extended to mixed microbial cultures with different microbial community structures. In this sense, the analysis and results presented in this chapter are more relevant in the context of real wastewater treatment. In this study eight of the developed species specific SMN models were modified to generate a multi-species metabolic network model. The modelled species correspond to eight nitrifying bacteria species abundantly detected in nine previously published experiments on N_2O production by nitrifying mixed cultures with different populations of ammonia and nitrite oxidizing bacteria (AOB and NOB). Model simulations of cell metabolism observed in those experiments showed that observed values of N_2O production rate in ammonium oxidation to nitrite or nitrate processes can only be predicted if NO oxidation reactions are included in model formulation, thus contributing to decrease N_2O production rate by 60% to 86%. In contrast occurrence of NO oxidation reactions did not improve model fitness to reproduce data of experiments of hydroxylamine and nitrite oxidation. Decreasing N_2O production effect was further evaluated for nitrification processes with populations of AOB and NOB and only AOB, at various oxygen and ammonium concentrations. For all tested conditions, model predicted a N_2O production rate that follows the trend of experimental observations only if NO oxidation reactions are included in model structure. Resulting that, for processes with AOB and NOB the estimated range of N_2O production rate was lower (from 0 to 0.02 mmol-N/gCOD*h) than the estimated for processes with only AOB (from 0 to 0.13 mmol-N/gCOD*h). These results highlight that NO oxidation and microbial community composition are factors that can determine N_2O production in nitrifying mix cultures.

5.1. Background

As investigated on the previous chapter, N_2O is a nitrification by product formed in AOB cells through two different pathways: (i) the hydroxylamine oxidoreductase (HAO) mediated pathway and (iii) the nitrite reductase (NirK) mediated pathway (also known as nitrifier denitrification) (Kampschreur et al., 2009; Schreiber et al., 2012; Stein, 2010; Yu et al., 2010). Both pathways involve the initial formation of nitric oxide (NO) and then its reduction to N_2O. However, genomes of AOB and NOB species indicate the potential for the existence of other NO transformation routes that can be affecting the overall amount of N_2O produced and eventually emitted from BNR nitrification.

Specifically, genomes of both AOB and NOB species (such as *Nitrosomonas europaea, Nitrosomonas eutropha, Nitrosococcus oceani*, *Nitrospira defluvii*, *Nitrobacter winogradskyi* and *Nitrobacter hamburgensis*) indicate the potential to synthetize enzymes such as cytochrome P460 (C_{P460}), flavohemoglobin (Hmp) and nitrite oxidoreductase (NirK) that can oxidize NO to nitrite (NO_2^-) or nitrate (NO_3^-) (Chain et al., 2003; Lücker et al., 2010a; Schreiber et al., 2012; Starkenburg et al., 2011; Stein, 2010; Stein, 2011; Whittaker et al., 2000), thereby potentially influencing net N_2O production during nitrification processes that trend to produce NO, such as those of ammonium oxidation to nitrite or nitrate operating at low oxygen concentrations and high ammonium loads. C_{P460} purified from *N. europaea* cultures has NO and NH_2OH oxidation activity and its gene sequence is common among genomes of AOB species (Elmore et al., 2007; Numata et al., 1990). Hmp is widely distributed among bacteria (AOB, NOB and heterotrophic denitrifying bacteria) and plays an important role mediating nitrosative stress functioning as NO dioxygenase or reductase (Stein, 2010). Nevertheless expression of C_{P460}, Hmp and oxidative NirK genes has not been confirmed in N_2O producing nitrifying cultures.

Moreover, in addition to AOB mediated pathways, the genomes of NOB species such as *Nitrospina gracilis* and *Nitrobacter hamburgensis* suggest that N_2O can as well be formed in NOB through NO reduction reactions catalysed by cytochrome c554 (C_{c554}) and cNor (Lücker et al., 2013; Starkenburg et al., 2008a). The above mentioned genomic routes of NO and N_2O production/consumption in AOB and NOB are illustrated in **Figure 5.1.**

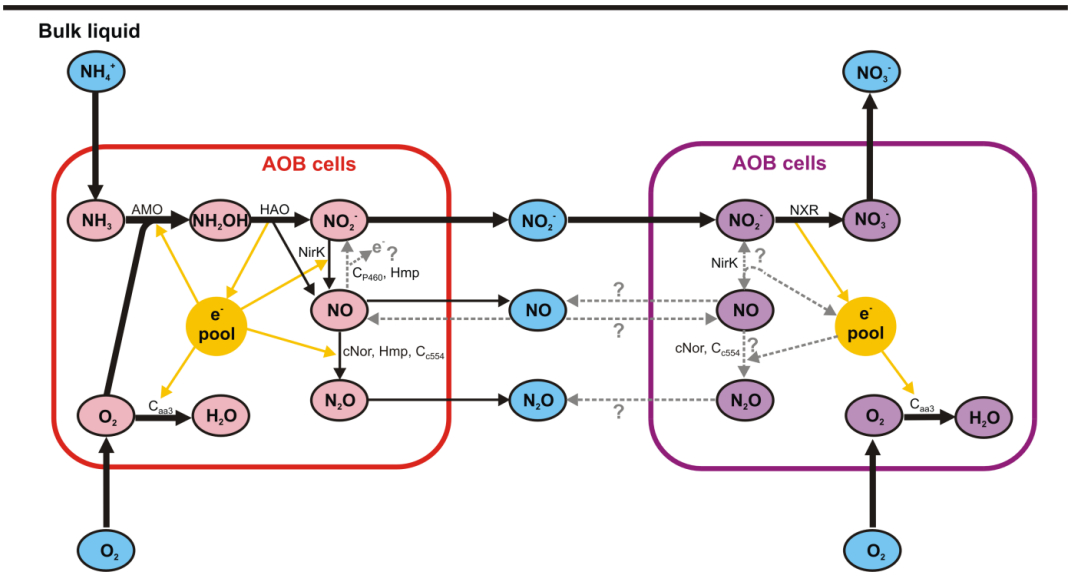

Figure 5.1. Scheme of genomic routes for production and consumption of NO and N_2O in nitrifying microbial communities

Figure 5.1. shows that the contribution of NO oxidation reactions and N_2O production by NOB to the net NO and N_2O emitted in nitrifying mixed cultures is unknown. Nodes represent chemical compounds; thick arrows represent the main route of ammonium (NH_4^+) oxidation to nitrite (NO_2^-) by AOB and from NO_2^- to nitrate (NO_3^-) by NOB. Yellow arrows represent routes of electron flow from or heading nitrogen transformation reactions; dashed arrows represent possible NO oxidation or reduction routes. Encoded enzymes in AOB and NOB genomes are depicted as follow: AMO,

ammonia monooxygenase (genes *amoABC*); HAO, hydroxylamine oxidoreductase (genes *haoAB*); NXR, nitrite oxidoreductase (gene *nxrA-K*); NirK, cooper-containing nitrite reductase (gene *nirK*); C_{P460}, Cytochrome P460 (gene *cyp*); C_{aa3}, terminal oxidase cytochrome aa3 (genes *cox*); cNor, nitric oxide reductase (genes *norABC*); C_{c554}, cytochrome c554 (gene *cyc*); Hmp, flavohemoglobins (gene *hmp*).

The contribution of the putative reactions for NO oxidation and NO reduction by NOB to overall N_2O production and eventual emission from nitrifying mixed cultures has not been investigated. To assess this contribution the rates of redox reactions of the nitrogen respiratory pathways in ammonia oxidizers and nitrite oxidizers need to be quantified. The dynamic nature and small spatial scale of NO and N_2O formation (Schreiber et al., 2012) complicates experimental rate measurements. An alternative is to estimate the metabolic reaction rates via stoichiometric metabolic network (SMN) modelling, flux balance analysis (FBA) and Monte Carlo random sampling (RS) of network's solution space (Feist et al., 2009; Kim et al., 2012; Schellenberger et al., 2011). These computational techniques apply the principles of conservation of mass and energy to biochemical networks of metabolic compounds and biochemical reactions (Varma and Palsson, 1994a) to provide a 'snapshot' estimate of reaction rate at a specific metabolic steady state (Orth et al., 2010). While SMN modelling has been generally applied to estimate metabolic reaction rates within cells of single species, the technique can be adapted to simultaneously analyse reaction rates within cells of different species constituting a microbial community as described in Chapter 2 (Chaganti et al., 2011; Dias et al., 2005; Pardelha et al., 2012; Stolyar et al., 2007).

The objective of this research was to develop and use a multispecies SMN model to evaluate the effect of NO oxidation and NO reduction by NOB on the amount of N_2O produced in nitrifying processes operated under different ammonium and oxygen concentrations and microbial community structures. This effect was assessed by estimating specific N_2O production rates (sN_2OPR) and other variables using different model variants (i.e. including and excluding NO oxidation and NO reduction by NOB reactions and using various microbial community structures) and comparing those estimations to data observed in nine experiments of N_2O production by nitrifying mixed cultures. Model variant that gave a better fit to experimental observations was considered to more accurately represent the mass and energy balance occurring within the microbial community metabolism, therefore providing insights of the effect of NO oxidation; NO reduction by NOB and operational conditions on N_2O production during nitrification.

5.2. Materials and Methods

5.2.1. Analysed experiments

The effect NO oxidation and NO reduction by NOB on N_2O production during nitrification was assessed by modelling and simulating the microbial metabolism observed in nine experiments on N_2O production by nitrifying mixed cultures. The analysed experiments were reported on publications by

Ahn et al., (2011); Law et al., (2012); Wunderlin et al., (2013) and corresponded to one following nitrification processes:

- ammonium oxidation to nitrate by AOB and NOB (full nitrification);
- ammonium oxidation to nitrite by AOB (nitritation);
- nitrite oxidation to nitrate by NOB (nitratation) and;
- hydroxylamine (NH_2OH) oxidation to nitrite and nitrite (NOx) by AOB and NOB.

The nine analysed experiments had different operational concentration of ammonium and dissolved oxygen among them, as well as different microbial community structure. **Table 5.1.** summarizes the nine analysed experiments, their corresponding publication reference and their most relevant operational condition. **Table 5.1.** also presents the specific oxygen and ammonium uptake rates (sOUR and sAUR respectively) and N_2O production rates (sN_2OPR) observed when the experiments had their highest N_2O productivity. These rate values (along with all the reaction rates values specified in this chapter) were normalized by the total amount of biomass in bioreactors (expressed as grams of chemical oxygen demand (COD), a standard variable to measure biomass and organic carbon in wastewater treatment).

Experiments' nitrifying bacterial community structure is presented in **Table 5.2.** In this study, community structure is expressed in terms of fraction (f) of species (k) per unit of biomass. f^k values were calculated according to the community composition and species concentrations reported on each experiment publication. The values were calculated only those AOB and NOB species with highest biomass dry weight percentages on each analysed experiment. Measurements errors from experimental biomass concentration and species fraction on biomass were not considered for model simulations. The fraction of biomass composed by heterotrophic species was not included on analysis due the null nitrifying activity of these species.

For each of the nine analysed experiments, a dataset ($\hat{X}$) composed of variables (t) characterizing the metabolism of experiments' microbial community at a specific steady state period (i.e. when the community had the highest N_2O productivity) was calculated. Datasets $\hat{X}$ were calculated using the following information specified on the publications: (i) the reported concentration curves of substrates and products; (ii) bioprocess working volumes; (iii) influent flow rates and; (iv) microbial cell concentrations. The full definition of dataset variables t and their values in the nine analysed experiments ($\hat{X}_t$) are specified in **Table A4.1.** of the Appendix Four of this thesis document. Experiments' details used to calculate $\hat{X}$ datasets are described as well on Appendix Four. Each dataset $\hat{X}$ have different number (M) of variables t because not all variables could be calculated form the information present on publication. Dataset values $\hat{X}_t$ were posteriorly used as numerical reference to evaluate model's simulation accuracy as further described in section 5.2.4. **Table 5.3.** presents a definition of the variables and symbols used in this research. In addition, **Figure 5.2.** presents an overview of data process workflow described in this materials and methods section.

Table 5.1. Published experiments modelled and analysed as the multispecies SMN model
sOUR, sAUR, and sN_2OPR refer to specific uptake and production rates observed in experiments at the moment of maximum N_2O productivity.
Details of the experimental conditions can be found in Appendix Four.

Process	Experiment ID	Publication	Operational substrate concentrations	Specific rates. Mean±std		
				sOUR ($mmol\text{-}O_2/gCOD*h$)	sAUR ($mmol\text{-}N/gCOD*h$)	sN_2OPR ($mmol\text{-}N/gCOD*h$)
Ammonia oxidation to nitrate by AOB and NOB 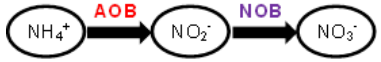	A	(Ahn et al., 2011)	Dissolved oxygen=3.7 mg/L. Influent NH_4^+-N=500mg-N/L	2.82±0.35	2.44±0.81	0.004±0.0028
	B	(Ahn et al., 2011)	Dissolved oxygen =1.1 mg/L. Influent NH_4^+-N=500mg-N/L	2.81±0.32	1.44±0.11	0.071±0.025
	C	(Wunderlin et al., 2013; Wunderlin et al., 2012)	Dissolved oxygen=1.9 mg/L Initial NH_4^+-N=2.5 mg-N/L	0.26±0.003	0.1±0.01	0.002±0.002
Ammonia oxidation to nitrite by AOB 	D	(Ahn et al., 2011)	Dissolved oxygen =1.1 mg/L. Influent NH_4^+-N=500mg-N/L	2.13±0.84	2.72±1.6	0.017±0.014
	E	(Law et al., 2011; Law et al., 2012)	Dissolved oxygen =0.55 mg/L Initial NH_4^+-N=500mg-N/L pH=7	10.2±0.106	5.43±0.33	0.010±0.0017
	F	(Law et al., 2011; Law et al., 2012)	Dissolved oxygen=0.55 mg/L Initial NH_4^+-N=500mg-N/L pH=8	10.25±0.049	6.7±0.54	0.021±0.0013
	G	(Law et al., 2011; Law et al., 2012)	Dissolved oxygen=1.25 mg/L Initial NH_4^+-N=500mg-N/L pH=8	11.73±0.042	11.28±1.12	0.062±0.01
Nitrite oxidation to nitrate by NOB 	H	(Wunderlin et al., 2013; Wunderlin et al., 2012)	Dissolved oxygen=1.1 mg/L Initial NO_2^--N=15.5 mg-N/L	0.06±0	0.09±0.01 as nitrite	0.007±0.0002
Hydroxylamine oxidation to NOx by AOB and NOB 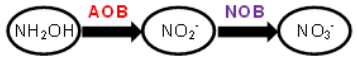	I	(Wunderlin et al., 2013; Wunderlin et al., 2012)	Dissolved oxygen=1.1 mg/L Initial NH_2OH-N=9.8 mg-N/L	0.04±0.004	0.03±0.013 as hydroxylamine	0.002±0.004

Table 5.2. Fractions of nitrifying bacteria species in biomass (f^k) of the nine analysed experiments

Species name	Species ID (*k*)	Experiment								
		A	B	C	D	E	F	G	H	I
Nitrosomonas europaea	neu	0.730	0.730	0.200	0.600	0.80	0.80	0.80	0.200	0.200
Nitrosomonas eutropha	net	0	0	0	0.303	0.05	0.05	0.05	0	0
Nitrosospira multiformis	nmu	0	0	0.300	0	0.05	0.05	0.05	0.300	0.300
Nitrosococcus oceani	noc	0	0	0	0	0.05	0.05	0.05	0	0
Nitrospira defluvii (candidatus)	nde	0	0	0.250	0	0.01	0.01	0.01	0.250	0.250
Nitrobacter winogradskyi	nwi	0.135	0.135	0.125	0.045	0.01	0.01	0.01	0.125	0.125
Nitrobacter hamburgensis	nha	0.135	0.135	0.125	0.045	0.01	0.01	0.01	0.125	0.125
Nitrospina gracilis	nsp	0	0	0	0	0.01	0.01	0.01	0	0
Species detection and quantification method		*	*	**	*	***	***	***	**	**

* = 16S rRNA clone libraries, denaturing gradient gel electrophoresis (DGGE) and sequencing targeting the subunit A of AMO gene (*amoA*), ammonia oxidation (amoA), nitrite reduction (nirK) and NO reduction (norB) q-RT-PCR (reverse transcriptase quantitative polymerase chain reaction);
** = Inferred from nitrogen isotope signatures associated to species;
*** = Fluorescent in-situ hybridization (FISH) used with probes for detection of *Nitrosomonas* sp., Beta-proteobacterial AOB, *Nitrosospira* sp., *Nitrobacter* sp., *Nitrospira* genera and for all true bacteria.

Table 5.3. Chapter's list of variables and parameters and their symbols

Symbol	Definition
$\hat{X}$	Dataset from experiment
X	Dataset estimated with model
$\hat{X}_t$	Value of variable t in data set from experiment
X_t	Value of variable t in dataset estimated with model
M	Number of variables in dataset
f^k	Species k fraction in biomass
v_j^k	Model's rate of reaction j in species k
α_j^k	Lower limit for rate v_j^k
β_j^k	Upper rate limit for rate v_j^k

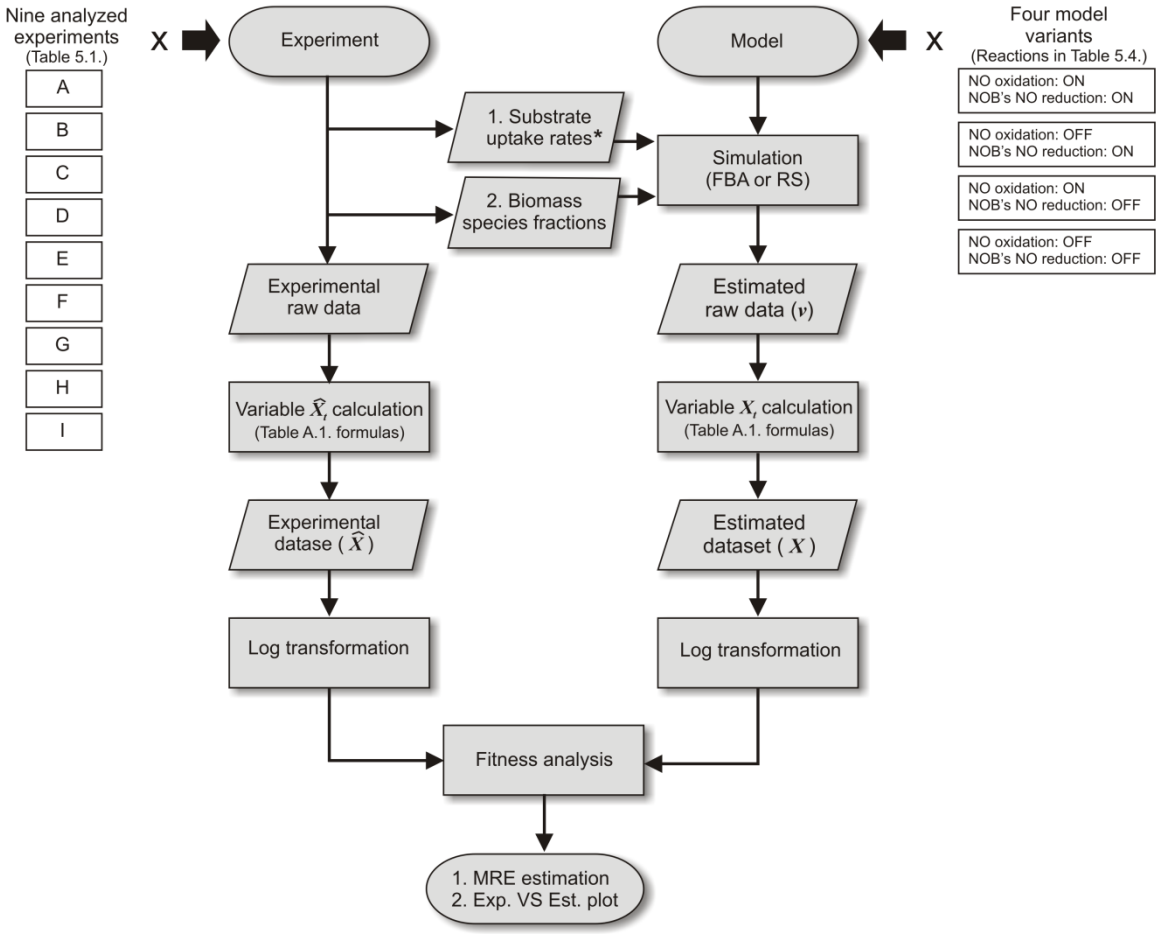

Figure 5.2. Research work flow for fitness analysis
*Substrate uptake rates are determined experimentally or from kinetic equations.

5.2.2. Model development

The metabolism of the microbial community detected in the analysed experiments was modelled using a multispecies stoichiometric metabolic network (SMN). The SMN model was formulated to simultaneously capture nitrogen respiration and energy production (ATP and NADH) by AOB and NOB, as well as the exchange of nitrogenous compounds between different AOB and NOB species in a given nitrifying community. Eight microbial species –four AOB and four NOB– were included in the multispecies model to cover the diversity of respiratory redox reactions involving nitrogenous compounds within experiments' nitrifying microbial communities. The species were selected on the basis of: (i) species abundance in experimental nitrifying microbial communities; and (ii) availability of genome data. The four AOB species selected were *Nitrosomonas europaea*, *Nitrosomonas eutropha*, *Nitrosospira multiformis* and *Nitrosococcus oceani*, and the four NOB species selected were *Candidatus* Nitrospira defluvii, *Nitrobacter winogradskyi*, *Nitrobacter hamburgensis* and *Nitrospina gracilis*.

To develop the multispecies SMN, firstly a metabolic network for each modelled microbial species was formulated as specified in chapter two, then these networks were combined in single network using a multi-compartment approach (see chapter three) (Klitgord and Segrè, 2010; Stolyar et al., 2007; Taffs et al., 2009). In this modelling approach the network of reactions and metabolites developed for each species was assigned to an independent compartment to obtain a single model with eight species-specific compartments, as shown in **Figure 5.3.** An additional ninth compartment representing the microbial community was added to the model (peripheral box in **Figure 5.3.**), and connected to species-specific compartments through exchange reactions accounting for the uptake or secretion of metabolites. Each of the eight species-specific compartments was divided into two sub-compartments to separate the reactions occurring in cell's periplasm from cytoplasm. Transport reactions were added to connected metabolite pools modelled in different compartments (or sub-compartment).

The species specific SMNs were constructed according to the procedure of Thiele and Palsson (Thiele and Palsson, 2010) using organism-specific genomic and biochemical information from the literature and the internet biochemical databases KEGG, NCBI and MetaCyc (http://www.genome.jp/kegg/, http://www.ncbi.nlm.nih.gov/ and http://metacyc.org/, respectively). This procedure is described in Chapters 2 and 4. These metabolic networks consisted of reactions and metabolites for: (i) respiration of nitrogenous compounds (specified in **Table 5.4.**); (ii) electron transport chain, including ATP and NADH synthesis; and (iii) production of protein and biomass using ATP and NADH.

The complete multispecies SMN model contains 407 reactions and 380 metabolic compounds distributed across 25 compartments/sub-compartments. A network of the reactions and metabolites considered in the model was produced using Cytoscape 3.0.1 (Cytoscape consortium, San Diego, USA) and is shown in **Figure 5.4.** This network is formed with 787 nodes representing 407 reactions and 380 metabolic compounds. Species-specific nodes form clusters (eight) around community nodes. Nodes of species-specific metabolic networks form clusters around the nodes represent exchange

reactions and metabolites occurring in the community compartment. Big nodes at the periphery of the network represent the exchange reactions for uptake and secretion of compounds outside of the community.

All model's reaction equation were elementally and charge-balanced, and thermodynamically classified as reversible or irreversible (Kümmel et al., 2006b; Savinell and Palsson, 1992; Thiele and Palsson, 2010). The complete list of reaction equations and metabolic compounds that form the complete SMN model can be found in the Appendix Two of this document.

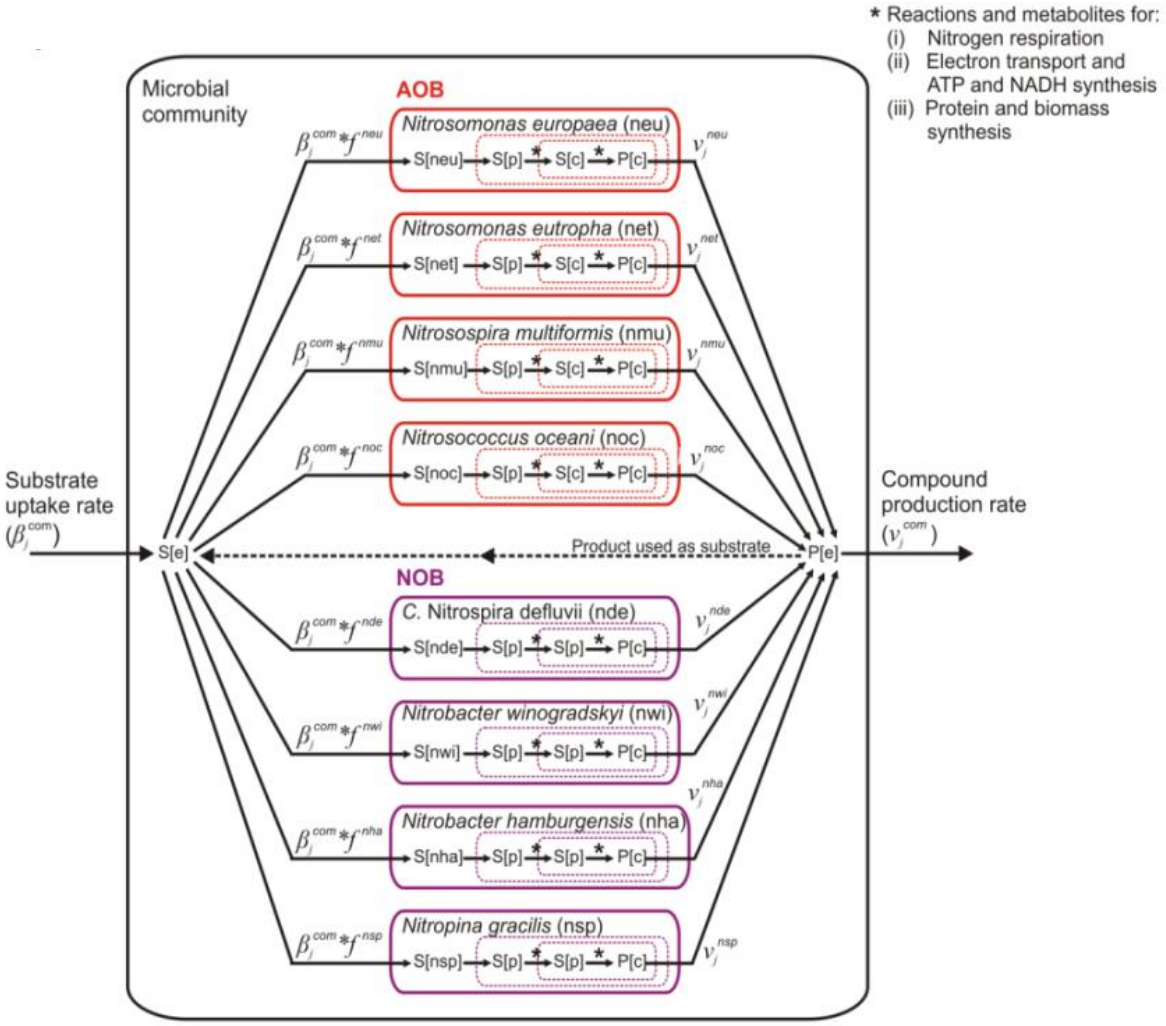

Figure 5.3. Diagram of the multi-compartmentalized structure of the multispecies SMN
Each species is modelled as a compartment (horizontal boxes) of the same model which contains a species-specific metabolic network distributed in two sub-compartments (dashed line boxes) that represent cell's periplasmic [p] and cytoplasmic [c] spaces. Each species-specific compartment exchange substrate and product compounds with a "microbial community" compartment [e] (peripheral box). Rate limits of substrate uptake for the community β_j^{com} are corrected with f^k values (fraction of species *k* per gram of community biomass) to obtain substrate uptake rates of each species.

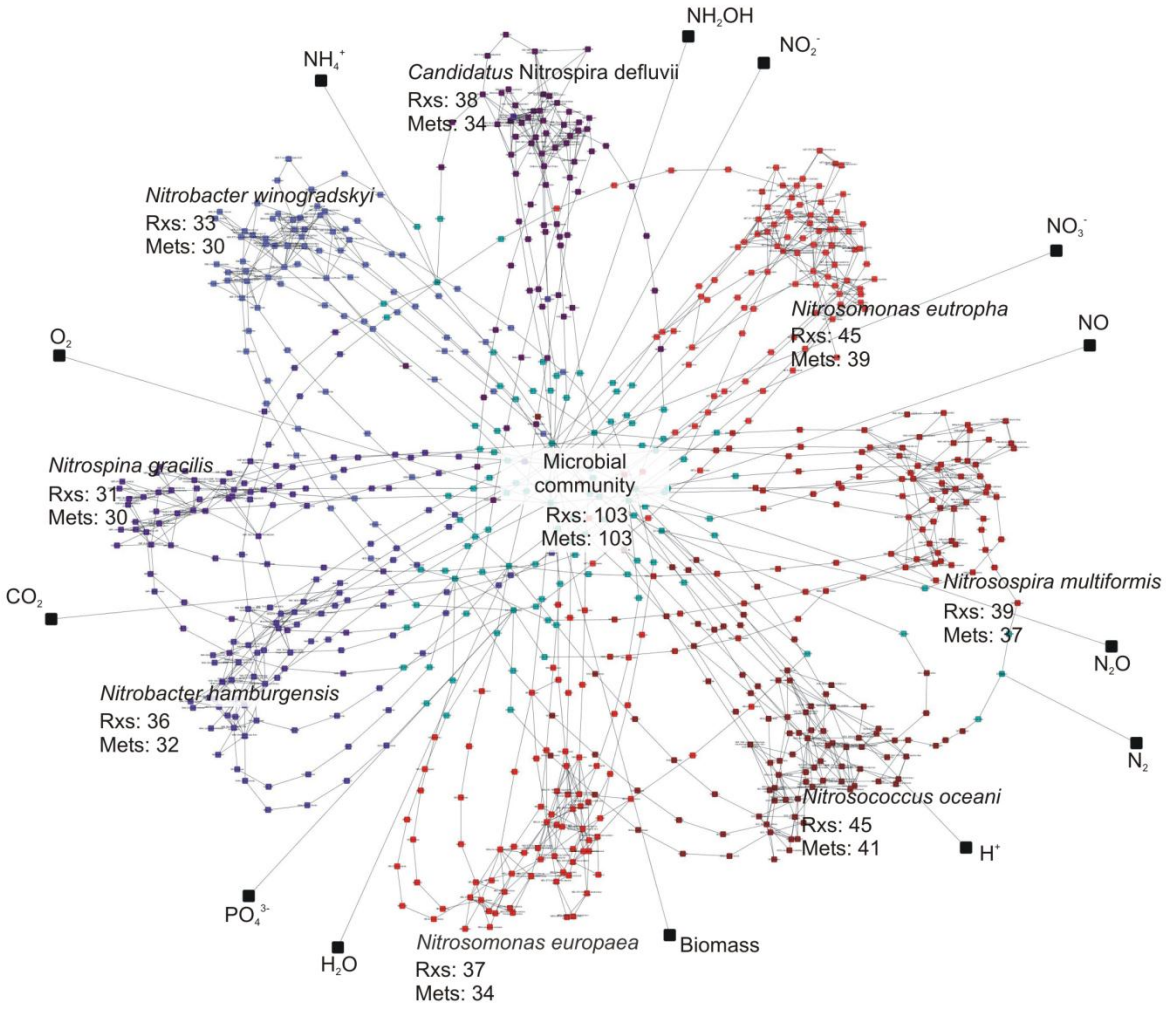

Figure 5.4. Complete nitrifying community metabolic network

Table 5.4. Bacterial species and nitrogen respiration reactions included in the nitrifying community network model.
Grey boxes indicate presence of genes encoding for the reaction's catalytic enzyme in the genome of the corresponding species.

Enzyme name abbreviation		Stoichiometric equation of model's nitrogen respiration reactions	Genes encoding for reaction's catalytic enzyme	Modelled species: AOB: *Nitrosomonas europaea*	AOB: *Nitrosomonas eutropha*	AOB: *Nitrospira multiformis*	AOB: *Nitrosococcus oceani*	NOB: *C. Nitrospira defluvii*	NOB: *Nitrobacter winogradskyi*	NOB: *Nitrobacter hamburgensis*	NOB: *Nitrospina gracilis*
AMO	**	$NH_3[p] + O_2[c] + Q8H_2[c] \rightarrow NH_2OH[p] + Q8[c] + H_2O[c]$	*amoABC*	■	■	■	■				
AMO		$NH_3[p] + N_2O_4[p] + Q8H_2[c] \rightarrow NH_2OH[p] + H_2O[c] + Q8[c] + 2\ NO[p]$	*amoABC*		■						
HAO		$NH_2OH[p] + Cyt554[p] \rightarrow NOH[p] + Cyt554e[p] + 2\ H^+[p]$	*haoAB*	■	■	■	■				
HAO		$NOH[p] + 0.5\ Cyt554[p] \rightarrow NO[p] + 0.5\ Cyt554e[p] + H^+[p]$	*haoAB*	■	■	■	■				
HAO		$NO[p] + 0.5\ Cyt554[p] + H_2O[p] \rightarrow HNO_2[p] + 0.5\ Cyt554e[p] + H^+[p]$	*haoAB*	■	■	■	■				
C_{aa3}	**	$0.5\ O_2[c] + 4\ H^+[c] + 2\ Cyt552e[p] \rightarrow H_2O[ac] + 2\ H^+[p] + 2\ Cyt552[p]$	*coxABC*	■	■		■				
C_{aa3}		$HNO_2[p] + 3\ H^+[c] + 3\ Cyt552e[p] \rightarrow 0.5\ N_2[p] + 2\ H_2O[p] + 3\ Cyt552[p]$	*coxA2*			■	■				
C_{P460}	*	$0.5\ NH_2OH[p] + 0.5\ NO[p] + 2\ Cyt552[p] + H_2O[p] \rightarrow HNO_2[p] + 2\ Cyt552e[p] + 4\ H^+[p]$	*cyp*	■	■					■	■
NirK		$HNO_2[p] + Cyt552e[p] + H^+[p] \rightarrow NO[p] + Cyt552[p] + H_2O[p]$	*nirK*	■	■	■	■				
cNor	+	$NO[p] + Cyt552e[p] + H^+[p] \rightarrow 0.5\ N_2O[p] + Cyt552[p] + 0.5\ H_2O[p]$	*norABC*	■	■	■	■			■	
Hmp	+	$NO[c] + H^+[c] + 0.5\ NADH[c] \rightarrow 0.5\ N_2O[c] + 0.5\ H_2O[c]$	*hmp*		■		■				
Hmp	*	$NO[c] + O_2[c] + 0.5\ NADH[c] \rightarrow NO_3[c] + 0.5\ NAD[c] + 0.5\ H^+[c]$	*hmp*		■		■				
C_{c554}	+	$NO[p] + H^+[p] + 0.5\ Cyt554e[p] \rightarrow 0.5\ N_2O[p] + 0.5\ Cyt554e[p] + 0.5\ H_2O[p]$	*cycA*	■							■
cNXR		$NO_2^-[c] + 2\ Cyt550[c] + H_2O[c] \leftrightarrow NO_3^-[c] + 2\ Cyt550e[c] + 2\ H^+[c]$	*nxrA-K*						■	■	
pNXR		$NO_2^-[p] + 2\ Cyt550[c] + H_2O[p] \rightarrow NO_3^-[p] + 2\ Cyt550e[c] + 2\ H^+[p]$	*nxrACB*					■			■
C_{aa3}		$0.5\ O_2[c] + 4\ H^+[c] + 2\ Cyt550e[c] \rightarrow H_2O[c] + 2\ H^+[p] + 2\ Cyt550[c]$	*cydABC*						■	■	■
C_{aa3}		$0.5\ O_2[c] + 2\ H^+[c] + 2\ Cyt550e[c] \rightarrow H_2O[c] + 2\ Cyt550[c]$	*cydABC*					■			
NirK	*	$NO_2^-[p] + Cyt550e[c] + 2\ H^+[p] \rightarrow NO[p] + Cyt550[c] + H_2O[p]$	*nirK*					■	■	■	■
NirK		$NO[p] + 0.5\ NAD[c] + H_2O[c] \rightarrow NO_2^-[p] + 0.5\ NADH[c] + 1.5\ H^+[p]$	*nirK*						■		
pNXR		$NO_3^-[p] + NADH[c] + H^+[c] \rightarrow NO_2^-[p] + NAD[c] + H_2O[c]$	*nxrAB*					■	■	■	
NAR		$NO_3^-[p] + Q8H_2[c] \rightarrow NO_2^-[p] + Q8[c] + H_2O[c]$	*narGHIJ*						■		
NirB		$NO_2^-[c] + 4\ H^+[c] + 3\ NADH[c] \rightarrow NH_3[c] + 2\ H_2O[c] + 3\ NAD[c]$	*nirB*					■	■	■	
NirA		$NO_2^-[c] + 6\ Fee[c] + 7\ H^+[c] \leftrightarrow NH_3[c] + 2\ H_2O + 6\ Fe[c]$	*nirA*					■		■	■
		Genome publication reference		1	2	3	4	5	6	7	8

(**) = O_2 consumption reactions in AOB
(*) = NO oxidation reactions (not associated with hydroxylamine oxidoreductase (HAO))
(+) = Reactions for NO reduction to N_2O
[p] = metabolic compound in periplasmic space sub-compartment, [c] = metabolic compound in cytoplasmic space sub compartment.
References: 1 = (Chain et al., 20(Chain et al., 2003), 2 = (Stein et al., 2007), 3 = (Norton et al., 2008), 4 = (Klotz et al., 2006), 5 = (Lücker et al., 2010b), 6 = (Starkenburg et al., 2006), 7 = (Starkenburg et al., 2008b), 8 = (Lücker et al., 2013).

5.2.3. Model simulation

The COBRA toolbox 2.0 (Schellenberger et al., 2011) along with the linear programming solver GLPK (GNU project, Moscow, Russia) within MATLAB®7 R2010b software (MathWorks Inc., Natick, MA, USA) was used to convert the SMN reconstruction file to its mathematical form and to run model simulations, as described in Chapter Two. The microbial community metabolic network model was mathematically represented by a stoichiometric matrix, S. A non-zero $s_{i,j}$ entry in S indicates the stoichiometric coefficient of metabolite i participating in reaction j. The conservation of mass balance in the network is achieved by imposing the condition $S * v = 0$, where v was the vector of reaction rates v_j^k (fluxes) (Feist et al., 2009; Varma and Palsson, 1994a). v was constrained using conditions of the form $\alpha_j^k \leq v_j^k \leq \beta_j^k$, where α_j^k and β_j^k are the lower and upper limits placed on the reaction rate v_j^k (Varma and Palsson, 1994b) and k refers to the modeled bacterial species or the entire microbial community.

The simulation algorithms Flux balance analysis (FBA) (Varma and Palsson, 1994a) and uniform Monte-Carlo random sampling (RS) of metabolic network's solution space (Price et al., 2004; Schellenberger and Palsson, 2009) were used to estimate the steady state rates of model's reactions. As illustrated in **Figure 5.5.**, both simulation algorithms, FBA and RS, estimate unknown rate values (v_j^k) of reactions j forming the metabolic network; however FBA gives a discrete rate value for each reaction by optimizing a defined objective function, while RS provides a set of rate values for each reaction so that they can be statistically analysed. FBA and RS simulations were launched respectively using the COBRA toolbox commands "optimizeCbModel()" and "sampleCbModel()"; details of parameters used in FBA and RS simulation algorithms are specified on section A.1.5. of Appendix Four.

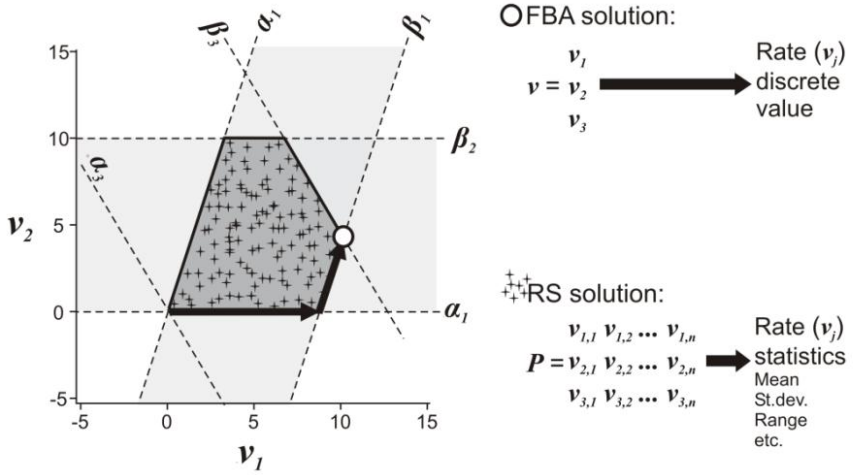

Figure 5.5. Concept of FBA and RS simulations of metabolic networks
All possible rate values of two given networks' reactions (v_1 and v_2) lie in the "solution space" (dark grey area) defined by the reactions' lower (α) and upper (β) rate limits. FBA finds a single rate value for each reaction (withe circle) that maximizes (or minimizes) the value of a given objective function, while RS obtains rate values sampled from the entire solution space (black crosses) to produce a dataset that can be statistically analysed. Figure adapted from (Price et al., 2004).

5.2.4. Role of reactions for NO oxidation and NO reduction by NOB

The effect of NO oxidation and NO reduction by NOB on overall N_2O production by nitrifying communities was assessed by comparing the goodness of fit of simulations from different model variants to the experimental datasets $\hat{X}$. Four model variants where generated by systematically unconstraint (β_j = 1000) or completely constraint (β_j = 0) the rate of all NO oxidation reactions (in both AOB and NOB, indicated with a star symbol (*) on **Table 5.4**) and the rate of NO reduction by NOB reactions (indicated with a plus symbol (+) on **Table 5.4**) as showed in **Figure 5.2.** Model variant that provided estimations with no significant differences to experimental sN_2OPR and minimum error to reproduce experimental datasets values was considered to more closely represent cells metabolism, therefore providing a quantification of the effect of NO oxidation and NO reduction by NOB during nitrification.

The sOUR and sAUR values observed in each experiment, as well as its species abundance fractions, were used as input data to launch a RS simulation of each model variant. sOUR and sAUR values (specified on **Table 5.1.**) were used as values of the following models' parameters: community's maximum oxygen and ammonium uptake rate (β_{O2-Ex}^{com} and β_{NH4-Ex}^{com}); the applied input values corresponded to the sum of the observed mean plus the standard deviation in order to obtain a simulation solution that including the observed variability. Abundance fractions of modelled species (f^k) (values provided on **Table 5.2.**) were used to define values of parameters: k specie's maximum oxygen and ammonium uptake rate (β_{O2-Ex}^{k} and β_{NH4-Ex}^{k}). The value of these parameters was calculated with the formula:

$$\beta_{j-Ex}^{k} = \beta_{j}^{com} * f^k \qquad (5.1.)$$

where β_{j-Ex}^{com} is the experiment's sOUR or sAUR uptake and f^k is the observed abundance fraction of the species k (as shown in **Figure 5.3.**). All input rates were expressed in mmol/h and normalized with experiment's total amount of biomass expressed as chemical oxygen demand (COD) (One gram of biomass dry weight equals 1.42 grams of COD (Grady et al., 1999)). After setting up models' constraints, RS simulations were run; the obtained network fluxes (mean v_j^k values) were used on the formulas provided in **Table A4.1.** of Appendix Four to estimate the datasets X that were used to evaluate model fitness. RS simulations were used to obtain a robust frequency distribution for each estimated metabolic rate, thus significant differences against experiment data can be assessed (Schellenberger and Palsson, 2009; Thiele et al., 2005).

Overall fit between models-estimated and experimental datasets was evaluated using accuracy percentages based on mean relative error (MRE) (Makinia, 2010) of log transformed datasets. This fitness measurement was selected to capture the deviation between estimated and experimental datasets in absolute terms (from 1 to 0 where zero is a perfect fit) and to minimize the scale effect of

different variables (Schuetz et al., 2007; van den Berg et al., 2006); MRE scores were calculated using and derived accuracy percentages were estimated as previously described in Chapter 3.

5.2.5. Effect of oxygen and ammonium concentrations

The effect of NO oxidation on N_2O production during nitrification processes operated at different oxygen and ammonium concentration was analysed by using two model variants -one including and another excluding NO oxidation reactions- to predict sN_2OPR at various combinations of ammonium and oxygen concentrations. Then those predictions were compared with experimental sN_2OPR values from processes of ammonium oxidation to nitrate (experiments A, B and C) and ammonium oxidation to nitrite (experiments D, E, F and G).

Ammonium and oxygen concentration of nitrification processes where related through Michaelis-Menten (Monod) kinetic equations to the rate of models' reactions associated to ammonia monooxygenase (AMO) and terminal oxidase Cytochrome aa3 (C_{aa3}) (reactions indicated with a ** symbol in **Table 5.4.**); who catalyse for reactions of oxygen and ammonium respiration and electron flow in AOB and NOB cells (Arp and Stein, 2003; Whittaker et al., 2000). A matrix of paired values of ammonium and oxygen concentrations (S_{NH4} and S_{O2} respectively) was generated by systematically combining eleven discrete values of ammonia concentration (ranging from 0 to 50 mg-N/L) with seventeen discrete values of oxygen concentration (ranging from 0 to 8 mg-O_2/L). Each pair of S_{NH4} and S_{O2} values was used on the following Monod kinetic Equations to obtain specific rates for AMO and C_{aa3} reactions for each modelled species (i.e. model's parameters β_{AMO}^{k} and β_{cytaa3}^{k} respectively):

$$\beta_{AMO}^{k} = V_{AMO}^{max}\left(\frac{S_{NH4}}{S_{NH4}+K_{NH4}}\right)\left(\frac{S_{O2}}{S_{O2}+K_{O2,AMO}}\right)f^{k} \quad (5.2.)$$

$$\beta_{Cytaa3}^{k} = V_{Cytaa3}^{max}\left(\frac{S_{O2}}{S_{O2}+K_{O2,Cytaa3}}\right)f^{k} \quad (5.3.)$$

where V_{AMO}^{max} and V_{Cytaa3}^{max} are the maximum rates for AMO and C_{aa3} reactions with values 14.74 and 13.42 mmol/gDW*h respectively (Law et al., 2012); $K_{NH4,AMO}$, $K_{O2,AMO}$ and $K_{O2,Cytaa3}$ are affinity constants of ammonium and oxygen in AMO or C_{aa3} reactions with values 0.0017 mmol/L, 0.0019 mmol/L and 0.0019 mmol/L, respectively (Law et al., 2012). f^{k} is the fraction of species k observed in experiment A (ammonium oxidation to nitrate) or in experiment D (ammonium oxidation to nitrate). β_{AMO}^{k} and β_{cytaa3}^{k} parameters were expressed mmol/gCOD*h units.

5.3. Results

5.3.1. Effect of NO oxidation reactions on N_2O formation

A comparison between estimated specific N_2O production rates (sN_2OPR) and accuracy percentages obtained from simulations of the nine experiments with the four model variants highlights that community metabolism (defined with $\hat{X}_t$ values) and sN_2OPR observed in experiments can only be predicted with the multispecies SMN model if reactions for NO oxidation by cytochrome P460 (C_{P460}), flavohemoglobins (Hmp), and nitrite oxidoreductases (NirK) are included in model formulation. Therefore according to model simulations the real mass and energy balance occurring in experiments can only be satisfied if NO oxidation is occurring in AOB and NOB cells.

The result described on the previous paragraph is inferred from **Figure 5.6.** This figure presents model's calibration curves; fitness scores (MRE) and estimated sN_2OPR values for the nine experimental datasets. Only data for model variant with highest accuracy (i.e. lowest MRE) in each experiment is shown. In these calibration curves, circles represent values of experimental $\hat{X}$ (X axis) VS estimated X (Y axis) log transformed datasets; a perfect fitness between both datasets is shown with a diagonal line. Simulation fitness was quantified with mean relative errors (MRE), M is the number of variables in dataset. In N_2O production rates graphs, bars indicate mean values, whiskers indicate standard deviations from the mean and (*) symbols indicate significant differences between experimental and estimated rate values according to one tailed t-test with $\alpha = 0.05$.

As shown in **Figure 5.6.**, no significant differences (according to t-test at $\alpha = 0.05$) were found between specific N_2O production rate from experiments and those estimated with models including NO oxidation reactions, except for experiments of nitrite oxidation to nitrate by NOB (experiment H) and NH_2OH oxidation to NOx by AOB and NOB (experiment I). In contrast, all N_2O production rates estimated with the model without NO oxidation reactions were significantly higher to their corresponding experimental rate value; except for NH_2OH oxidation to NOx experiment (experiment I), where no significant differences were found. By comparing sN_2OPR estimated with model variants including and excluding NO oxidation reactions it can be estimated that NO oxidation by C_{P460}, Hmp, and NirK could be reducing the net N_2O formed during ammonia oxidation to nitrite and nitrate by 60% to 86.4% however not affecting N_2O formation in processes of NH_2OH and nitrite oxidation. Interestingly, ^{15}N experiments by Wunderlin et al., (2013) showed that only when NH_2OH is supplied as electron donor at non-limiting oxygen concentrations, N_2O is mainly produced through hydroxylamine oxidation pathway. Consequently it is expected that NO oxidation reaction would be active under this this circumstances due high NH_2OH and NO availability however our results did not showed that effect.

Figure 5.6. shows as well that model's highest accuracy to reproduce datasets of ammonia oxidation to nitrate and ammonia oxidation to nitrite processes (59±19.8% and 63.5±17% respectively) was achieved with model including NO oxidation. For nitrite oxidation to nitrate, highest accuracy (79±0%) to reproduce dataset values was independent of the inclusion or exclusion of NO oxidation on model

formulation. Highest accuracy percentages values may appear not high, however the most commonly obtained accuracy percentage for single species metabolic network models oscillates between 60% and 95% when estimating one to ten variables (Schuetz et al., 2007; Stolyar et al., 2007). In this study, models' accuracy is assessed with 22 to 37 distinct variables (M value in **Figure 5.6.**). Thus, estimated values for metabolic rates reflected the metabolic behaviour of real nitrification processes operated under different conditions of ammonium, nitrite and oxygen availability and with different microbial community structures.

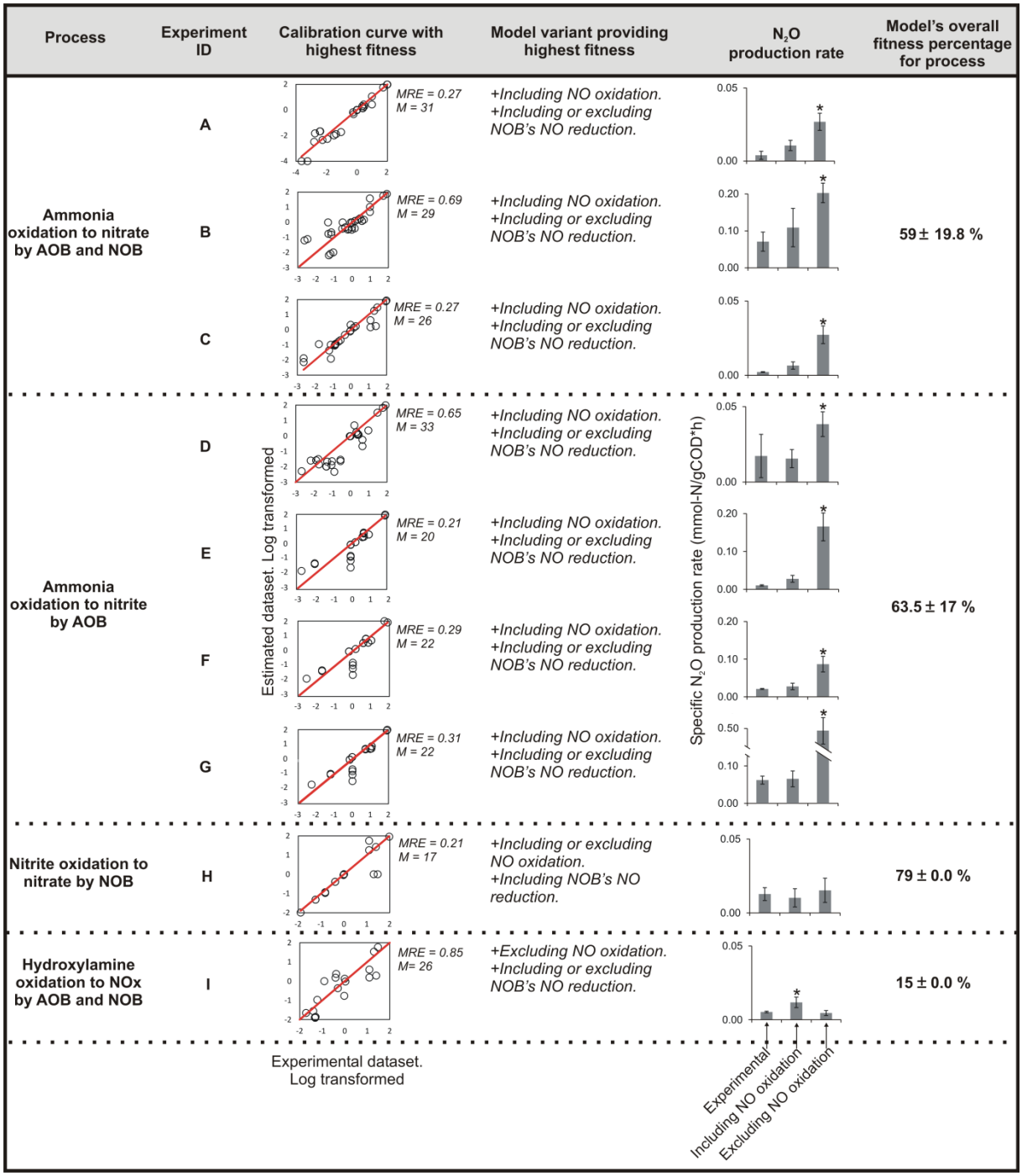

Figure 5.6. Model's calibration curves, fitness scores (MRE) and estimated N_2O production rate (bar graphs) for nine experimental datasets (letters A to I).

sN_2OPR estimated with the SMN models linked to Monod equations across all the tested combinations of ammonium and oxygen concentrations are presented in **Figure 5.7.** N_2O production rates were estimated from the network model's FBA simulations using the rate limits β^k_{AMO} and β^k_{cytaa3} obtained from the Monod kinetic Equations 5.2. and 5.3. Only processes of ammonium oxidation to nitrite and ammonium oxidation to nitrate were analysed using this simulations procedure because are the most relevant for real wastewater treatment.

Figure 5.7. illustrates the same result as **Figure 5.6.**, only models including NO oxidation were able to reproduce N_2O production rates within the range of experimental value. sN_2OPR estimated with model including NO oxidation reactions (**Figures 5.7.A.** and **5.7.B.**) ranged from 0 to 0.13mmol-N/gCOD*h, and were lower than those estimated with model excluding NO oxidation (**Figures 5.7.B.** and **5.7.D.**) that ranged from 0 to 1mmol-N/gCOD*h. Simulations reproducing ammonium oxidation to nitrate processes including NO oxidation reactions (**Figure 5.7.A.**) showed that N_2O production is only expected at DO concentrations below 1.2 mg-O_2/L, having a maximum amount of 0.02 mmol-N/gCOD*h when ammonium concentration is above 35mg-N/L. On the other hand, N_2O production estimated for the same process excluding NO oxidation ranged from 0.05 to 0.8 mmol-N/gCOD*h in all tested DO concentrations occurring in combination with ammonium concentrations above 10mg-N/L (**Figure 5.7.C.**). When NO oxidation reactions were included in the analysis, N_2O production in ammonium oxidation to nitrite processes was estimated to range from 0 to 0.13 mmol-N/gCOD*h at DO concentrations below 1.2 mg-O_2/L, having a maximum N_2O production at ammonium concentrations above 30mg-N/L (**Figure 5.7.B.**). In contrast, estimations excluding the participation of NO oxidation for processes of ammonia oxidation to nitrite resulted in sN_2OPR values much higher than the ones observed in experiments ranging from 0.3 up to 0.8 mmol-N/gCOD*h. Under these circumstances, if NO is not oxidized to NO_2^- or reduced to N_2O it is expected to observe mayor NO concentration in liquid phase and reactor's off gas. Occurrence of NO oxidation reactions would imply rates in oxidative (HAO) and reductive (NirK) NO production reactions of approximately the double of the observed sN_2OPR value. We speculate that NO oxidation reactions play a major role in ammonia oxidation to nitrate processes than in ammonia oxidation to nitrite processes because lack of nitrite accumulation thermodynamically favors NO oxidation to NO_2^-.

5.3.2. Effect of NO reduction by NOB on N_2O production

With respect to NO reduction to N_2O by NOB species, simulations for experiments of ammonium oxidation to nitrate (A, B and C) resulted in rates of N_2O production by NOB species of zero independently if those reactions were included or excluded on the analysis. The above indicates that on the basis of mass and energy balance, it is unlikely that NOB cells were producing N_2O in the analyzed experiments, which contradicts the presence of this capability suggest by their genomes. In contrast, as showed in **Figure 5.6.** experiment H, NOB cells can produce N_2O in nitrite oxidation to nitrate processes. Model simulations agree these experimental observations (with 79±0% of

accuracy), as expected only models with NO reduction by NOB reactions (i.e. NOB N_2O production) were able to reproduce the experimental sN_2OPR values without significant differences. Estimated sN_2OPR values including and excluding NO oxidation for nitrite oxidation nitrate processes were not significantly different from the experimental rate value, suggesting lack oxidation of NO by NOB cells and indicating that N_2O is produced by sequential reduction of NO_2^- and NO.

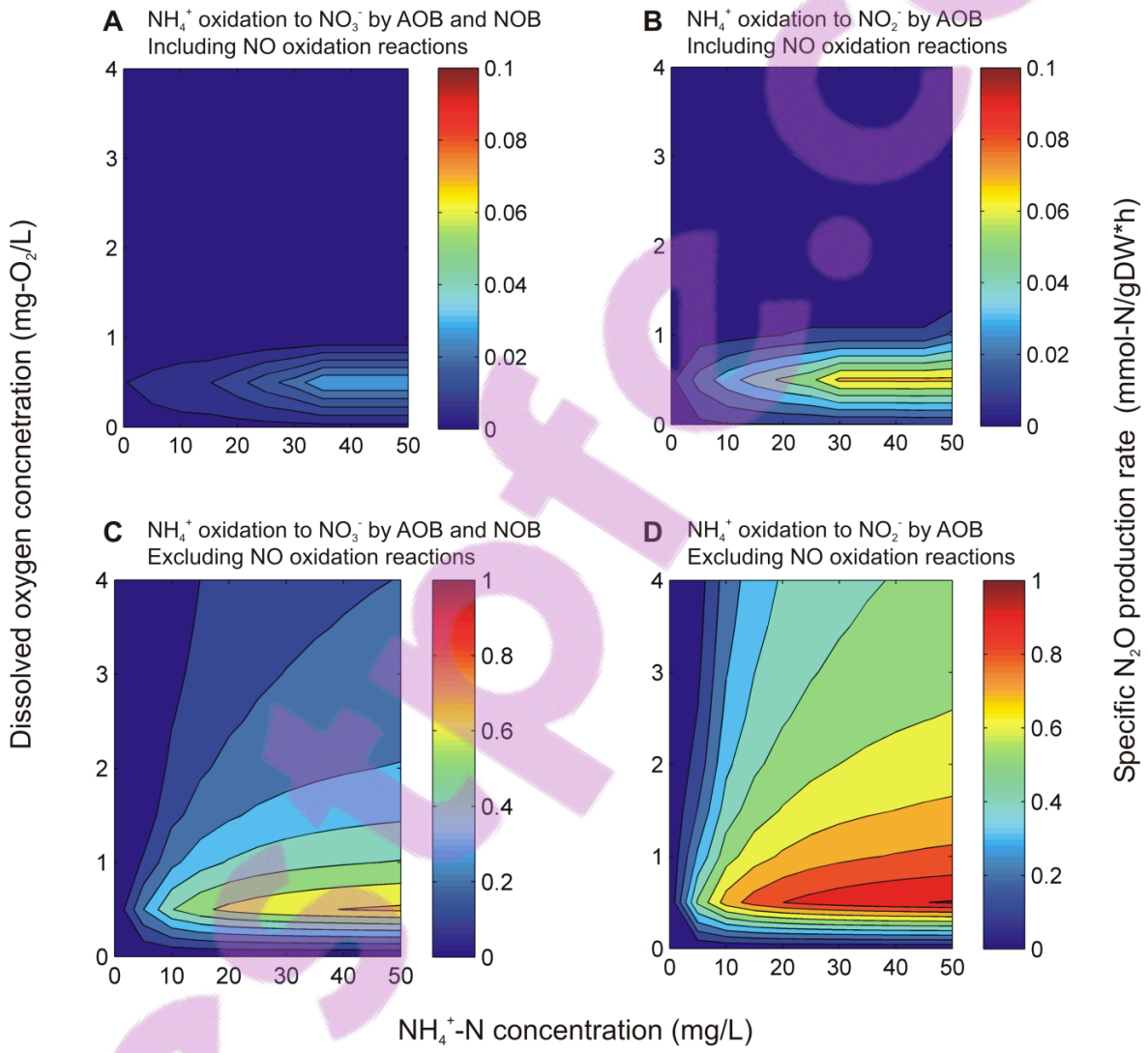

Figure 5.7. Colour maps of the estimated N_2O production rate by AOB species across combinations of ammonium and dissolved oxygen concentrations.

5.3.3. Effect of community composition on N_2O production

Estimated sN_2OPR values show that abundance profile of AOB and NOB populations in microbial community can influence the amount of N_2O produced because different species define different combinations of production/consumption pathways of NO and N_2O. Specifically, nitrifying cultures with AOB and NOB populations produce less N_2O than cultures with only AOB population. For instance, independently of the model used (including or excluding NO oxidation reactions), estimated sN_2OPR values for ammonium oxidation to nitrate by AOB and NOB species (**Figures 5.7.A.** and **5.7.C.**) were lower than those estimated for ammonia oxidation to nitrite by AOB (**Figures 5.7.B.** and **5.7.D.**). Simulations with models ignoring NO oxidation were overestimating sN_2OPR values, therefore results these simulations will not be discussed further.

The 3-D plots of **Figures 5.8.A.** and **5.8.B.** present comparisons between estimated sN_2OPR (as a mesh) and experimental sN_2OPR values (as solid dots, specified in **Table 5.1.**) in relation to sOUR and sAUR values. Estimated and experimental sN_2OPR values were compared in relation to sOUR and sAUR instead of in relation to oxygen and ammonium concentrations to be able to compare all the datasets using a uniform criterion of metabolic activity measurement. In these figures, estimated sN_2OPR plotted as a 3-D mesh was produced with FBA simulations of model including NO oxidation reactions. These estimated sN_2OPR where found by applying the β_{AMO}^{k} and β_{cytaa3}^{k} rate limits from Monod kinetic Equations (1) and (2). Filled green dots and letters represent the experimental values shown in **Table 5.1.**, letters with star symbol (*) represent data from of NH_4^+ oxidation to NO_3^- experiments; the rest of letters represent data from NH_4^+ oxidation to NO_2^- experiments.

A comparison between model's solution mesh and experimental data points reflect that estimated sN_2OPR follows the trend of experimental data points for both processes: ammonium oxidation to nitrate by AOB and NOB (**Figure 5.8.A.** mesh and data points A and B) and to nitrite only by AOB (Fig. 6B mesh and data points D, E, F and G). For processes of ammonium oxidation to nitrate by AOB and NOB (**Figure 5.8.A.**), model estimates that N_2O production is expected at sOUR between 0 and 5 mmol-O_2/gCOD*h. At this range, sN_2OPR does not correlates sAUR and reached a maximum value of 0.01 mmol-N/gCOD*h. On the other hand, for processes of ammonium oxidation to nitrite (**Figure 5.8.B.**), sN_2OPR was estimated to occur at sOUR values between 0 and 18 mmol-O_2/gCOD*h reaching a maximum value of 0.13 mmol-N/gCOD*h at 2 mmol-O_2/gCOD*h; estimated sN_2OPR values had positive and linear correlation with sAUR, however the line formed with this correlation has an intercept value inversely dependent on the sOUR, as represented by the tetrahedron shaped mesh of **Figure 5.8.B.** For instance, the larger the sOUR observed, the highest sAUR required to start observing N_2O production.

Data from experiment B, i.e. ammonium oxidation to nitrate in transition to oxidation to nitrite was considered an outlier and was excluded from **Figure 5.8.** 3-D plots. The above may be due dataset B reflect a condition of transition from partial to full nitrification.

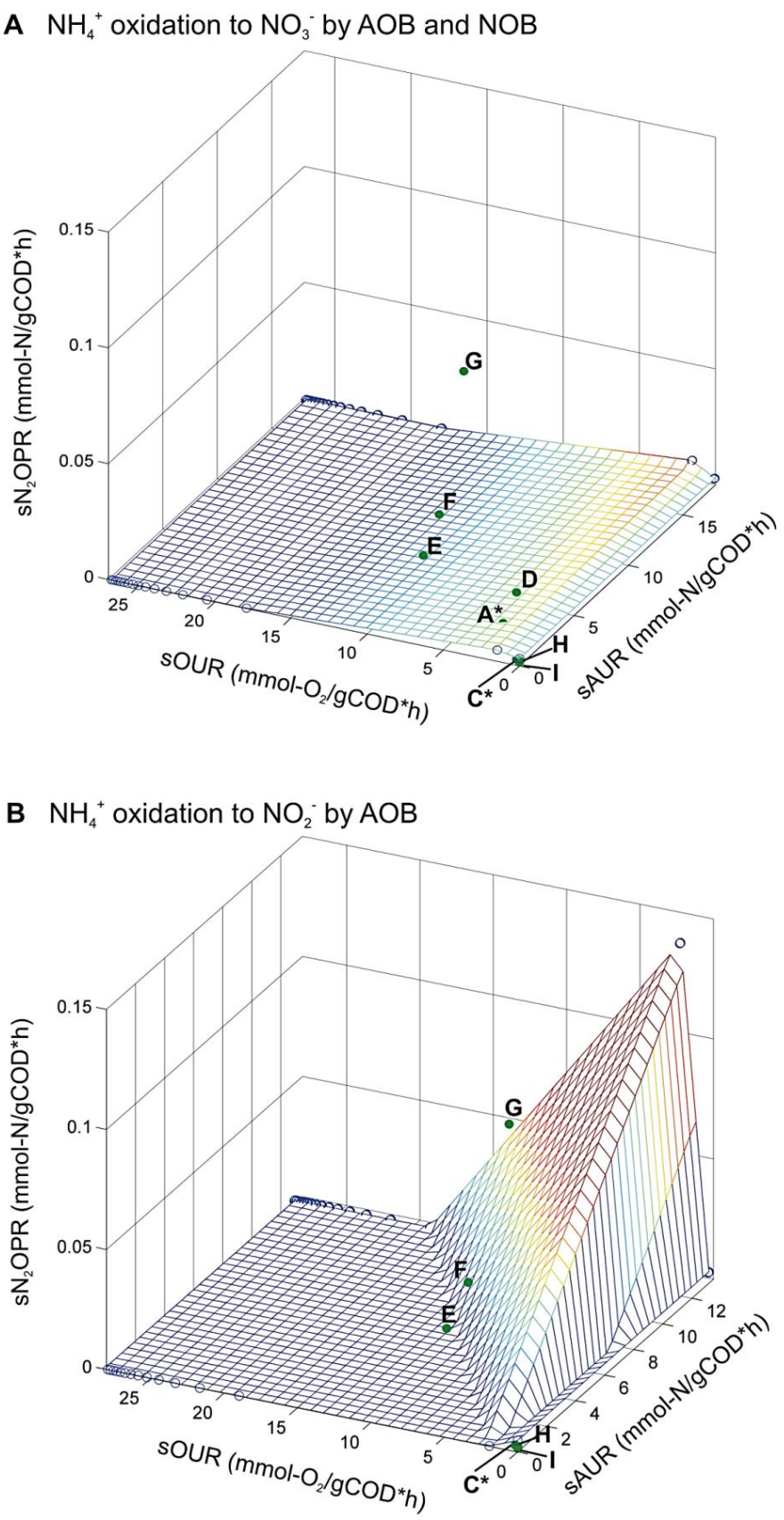

Figure 5.8. 3-D plots of experimental and estimated N_2O production rates in relation to oxygen and ammonium uptake rates. Started letters correspond to complete nitrification cultures

5.4. Discussion

5.4.1. NO oxidation to NO_2^- in AOB and NOB cells

In agreement with (Ahn et al., 2010; Rodriguez-Caballero et al., 2013; Yu et al., 2010), model's simulation estimated higher amounts of NO and N_2O produced from ammonium oxidation to nitrite (**Figure 5.8.B.**) in comparison to ammonium oxidation to nitrate processes (**Figure 5.8.A.**). It has been postulated by (Ahn et al., 2010; Kampschreur et al., 2009; Schreiber et al., 2012) that ammonium oxidation to nitrite process produce more N_2O than ammonium oxidation to nitrate process due NO_2^- accumulation and low dissolved oxygen concentrations (from 0.5 to 1.2mg/L) trigger the use of NO_2^- and NO as terminal electron acceptors in reaction catalysed by nitrite and nitric oxide reductase (NirK and cNor) with the subsequent production of N_2O. In addition to this mechanism, our simulations illustrate that in ammonium oxidation to nitrate processes is possible for NOB cells to be oxidizing NO molecules produced by AOB cells (**Figure 5.9.**). This reaction would be catalysed by NOB's nitrite oxidoreductase (NirK). NOB's NO oxidation would be reducing overall N_2O production by decreasing the amount of substrate available for cNor. As well, NO can be oxidised by AOB as a detoxification mechanism in reactions catalysed by cytochrome P460 (C_{P460}), flavohemoglobins (Hmp). Nevertheless this suggested mechanism requires experimental verification.

In a complete mixed nitrifying culture mutualistic NO oxidation is possible since diffusion of soluble NO from AOB cells to NOB cells would be almost instantaneous. NO can easily diffuse through cell membranes due to its hydrophobicity and small size (Rocha et al., 2010) therefore it can be exchanged between cells without mass transfer restrictions or delay. Also, AOB and NOB populations grow in close proximity in nitrifying flocs and biofilms, as shown in the images depicted in **Figure 5.10.** (Daims et al., 2006; Kindaichi et al., 2004), with the implication that NO can quickly diffuse between populations with minimal exposition to extracellular environment. It is known that instantaneous diffusion of soluble compounds occurs at distances below 100 µm (Jorgensen, 2000). NO chemical oxidation is prompt to happen in aerobic conditions such as the ones presented in nitrifying cultures, however the low dissolve oxygen condition (from 0.5 to 1.5 mg/L) that promotes NO and N_2O production in AOB cells facilitates the accumulation of soluble NO by decreasing its chemical oxidation rate (Thomas et al., 2001). In fact NO accumulation in this conditions has been documented in many nitrification experiments (e.g. Schmidt, (2008) and Yu et al., (2010)), therefore indicating that soluble NO can be available to be oxidized by the biological reactions catalysed by C_{P460}, Hmp or NirK enzymes in AOB and NOB cells. The occurrence of NO oxidation reactions in AOB and NOB cells would represent an advantage to extract electron equivalents (as reduced cytochromes) from NO substrates while reducing toxic damage by this molecule. In our simulations NO oxidation activity in NOB species was related to a null activity of NO_2^- reduction to NO by nitrite reductase enzymes (data not shown) suggesting a complete oxidative metabolism of nitrogen substrates in NOB cells. As far of the best authors' knowledge, experimental detection of NO oxidation reactions has not been evaluated in nitrification experiments of N_2O producing, however their occurrence and control could yield process operation strategies to mitigate N_2O production by microbial communities.

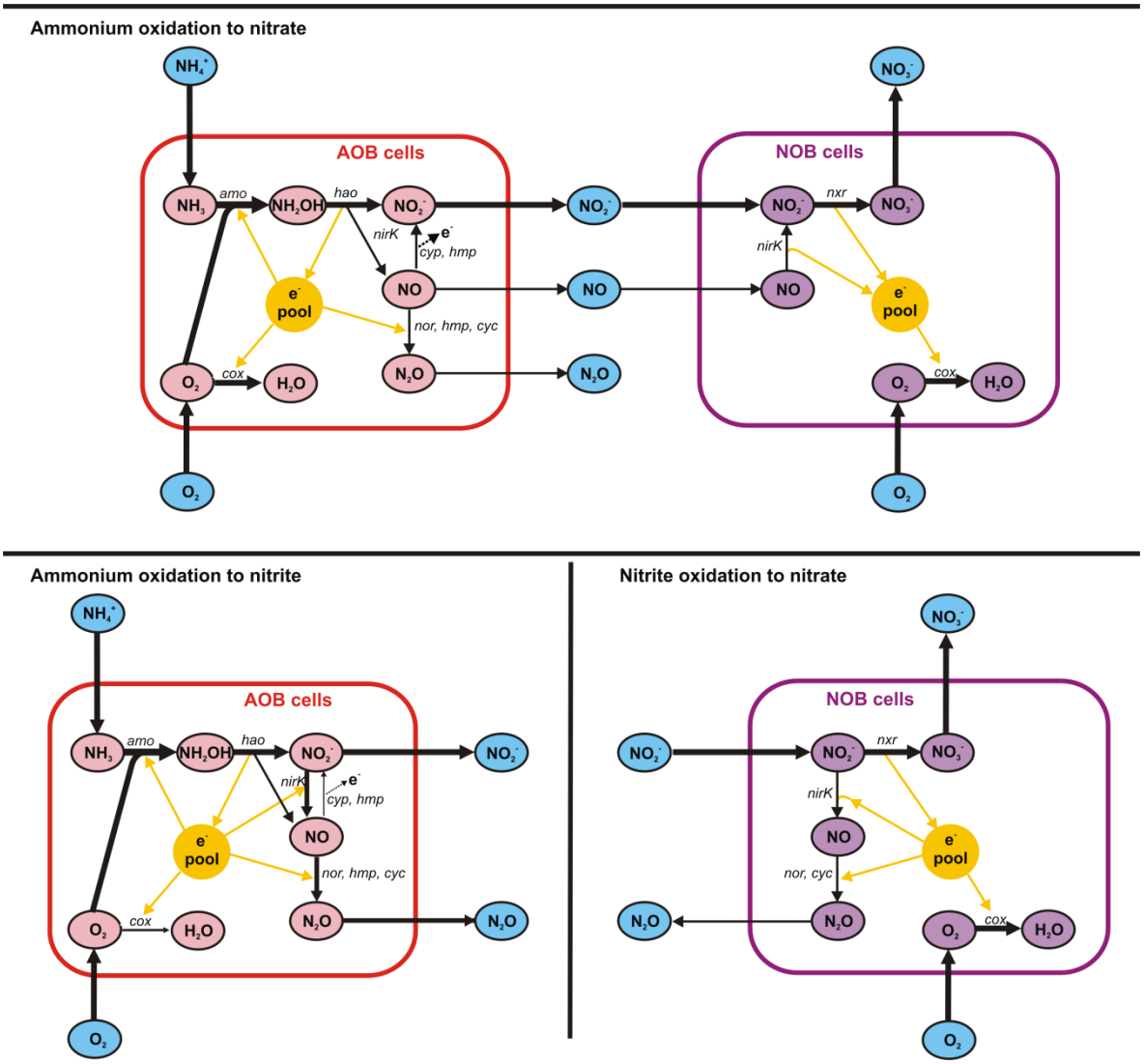

Figure 5.9. Mechanisms of NO and N_2O production in nitrification processes

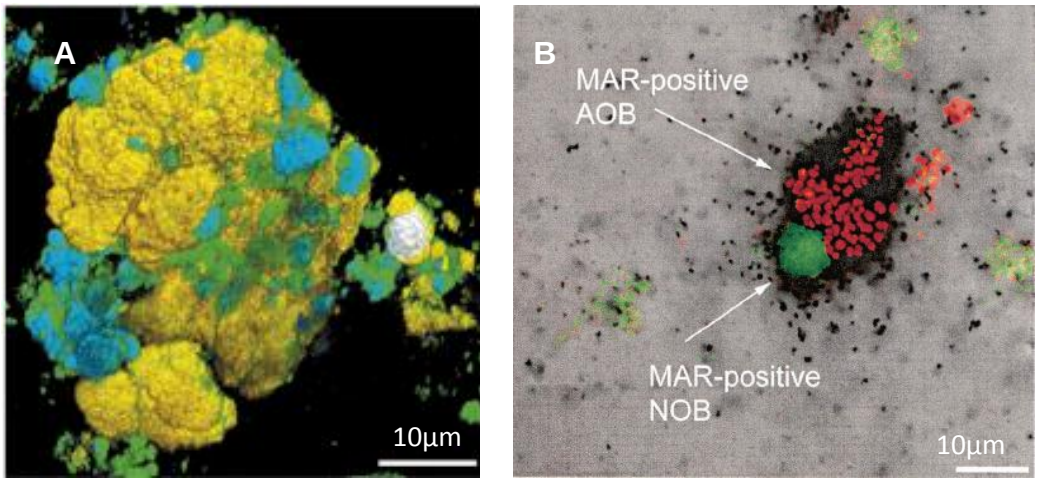

Figure 5.10. Proximity of AOB and NOB populations in nitrifying biofilms, confocal microscope images (A) AOB in blue; NOB in yellow; confocal micrograph bacteria of detected with FISH. (B) AOB in red; NOB in green; confocal laser scan microscope MAR-FISH images [Respectively taken from (Daims et al., 2006; Kindaichi et al., 2004)]

In this specific study, cells acclimation was not playing a crucial role given that all analysed experimental data was taken from cultures at the moment of a steady state. However acclimation would be playing a key role, mainly in the adjustment of the electron donor and acceptor imbalances and therefore the duration of N_2O production peak. Again substrate affinity constants of enzymes would be playing a deterministic role in acclimation phenomenon; I don't think acclimation would come from gene regulation

5.4.2. Microbial community structure

AOB and NOB species profile of a microbial community can influence the amount of N_2O produced not only because homologue enzymes from different species have different enzymatic properties (V^{max} and K_s) but as well because present of different AOB and NOB species define different combinations of production/consumption pathways of NO and N_2O. This is because each species has particular nitrogen transformation reactions, as shown in **Table 5.4.** For example, nitrifying microbial communities dominated by *Nitrosomonas eutropha* can potentially produce more N_2O than ones dominated by *Nitrosomonas europaea*, because *N. eutropha* is able to oxidize ammonia consuming nitrite (as N_2O_4) as an electron acceptor to produce NO in a reaction catalysed by ammonia monooxygenase (Schmidt, 2008). In this sense, RS simulations estimated that in experiment D 50% of N_2O were produced by *N. eutropha* cells, which had a lower biomass abundance fraction (0.3) than *N. europaea*, which produced the complementary 50% of N_2O molecules having a biomass abundance fraction of 0.6. Adding to this, biokinetic analysis of nitrifying mixed cultures suggests that *N. eutropha* has lower half saturation constant (K_s) for NH_4^+ than *N. europaea* (Ahn et al., 2008); which would imply *N. eutropha* growing at maximum sAUR across a broad range of NH_4^+ concentrations and presenting high susceptibility to produce N_2O per unit of biomass.

In another example, microbial communities with higher concentrations of NOB affiliated with *N. hamburgensis* would mitigate better N_2O emission in ammonium oxidation to nitrate processes because the metabolism of this species contains two reactions for the oxidation of NO to NO_2^- that can potentially produce more electron equivalents than other NOB species when AOB cells are producing NO. This mitigation mechanism would be particularly important in wastewater streams with high nitrogen loads as *Nitrobacter*-like bacteria dominate the NOB populations in these environments (Daims and Wagner, 2010). Nonetheless, expression of genes encoding for enzymes catalysing NO oxidation to NO_2^- in AOB and NOB must be experimentally detected in order to establish the occurrence of this N_2O mitigation mechanism.

5.4.3. Modelling approach

The model's multi-compartmentalized structure used together with the observed fraction values of microbial species per unit of biomass (f^k) allowed to perform steady state mass and energy balances for each of the analyzed experiments. Importantly, these balances were performed at both, species population and whole community levels. As well, this approach allowed reproducing different species richness and abundances of the modeled nitrifying microbial communities. Nevertheless, the values of f^k parameters have a degree of uncertainty given that: a) the analyzed experiments were not specifically designed to quantify biomass of AOB and NOB species on nitrifying cultures; and b) the inherent limitations and error of experimental methods to identify and quantify species their abundance. Therefore multispecies SMN models would be strongly beneficiated by uncertainty analysis of f^k values parameters. Further, application of f^k values assumes that the metabolic activity of a species population is directly and only proportional to species abundance. In real cells, substrate concentrations, enzymes V^{max} and K_s values, and gene expression levels also influence metabolic activity (Ahn et al., 2008; Daims and Wagner, 2010; Foladori et al., 2010; Wagner and Loy, 2002; Yu and Chandran, 2010). Therefore, model improvements involves the incorporation of information of expression levels of relevant genes and proteomics data through the parsimonious FBA (pFBA) algorithm (Lewis et al., 2010) and the incorporation of metabolite concentration measurements through Network Embedded Thermodynamic (NET) computational analysis (Kümmel et al., 2006a; Kümmel et al., 2006b). In addition to this biological data, model improvement would involve the inclusion of: gas-liquid mass transfer coefficients for oxygen, NO and N_2O; processes for cell decay and lysis and; differential equations to predict dynamic behaviors across time period.

5.5. Conclusion

During this simulation study - for the first time - the diversity of biochemical reactions for NO and N_2O formation/consumption was modelled; moreover their influence on the net amount of N_2O formed on nitrifying cultures was systematically assessed. The development of this genome informed metabolic model resulted on the finding that previously ignored biochemical reactions for NO oxidation can play a deterministic role on the net amount of N_2O formed in AOB and NOB cells. Nevertheless this role stills need to be assessed and validated experimentally. The multispecies SMN modelling approach also provided the quantitative background to develop a new hypothesis about the role of NOB species as oxidizers of NO molecules on full nitrification processes; consequently helping to reduce N_2O emissions during nitrification processes. In addition, inclusion of metabolic pathways of various AOB and NOB species on a single metabolic model was done for the first time as best of author's knowledge. This multispecies SMN model opens further possibilities to computationally assess N_2O formation and nitrogen respiration of specific species populations within nitrifying communities. The results found in this simulation study illuminate various aspects about SMN modelling approach and N_2O production in nitrifying mixed cultures:

- The metabolism of cells in nitrifying microbial communities can be modelled and simulated using genome-informed multi-species metabolic network models achieving a satisfactory accuracy.

- Nitrifying microbial communities have the genomic potential to oxidize NO to NO_2^-. The activation of NO oxidation reactions can satisfy the mass balance and energy balance of nitrifying mixed cultures performing ammonia oxidation to nitrate and to nitrite.

- Ammonium oxidation to nitrite process has higher potential to produce N_2O in comparison to ammonium oxidation to nitrate process. The range of N_2O production rate estimated for ammonia oxidation to nitrate processes is from 0 to 0.02 mmol-N/gCOD*h, maximum value can be expected only at NH_4^+ concentration above 35 mg-N/L. The range of N_2O production rate estimated for ammonia oxidation to nitrite processes is from 0 to 0.13 mmol-N/gCOD*h, maximum value can be expected only at NH_4^+ concentration above 30 mg-N/L.

- In ammonia oxidation to nitrite processes, N_2O production rate is correlated in a positive linear fashion to cell's ammonium uptake rate. However, the intercept value of the line formed with this correlation is inversely related to oxygen uptake rates, meaning that oxygen uptake rate affect this correlation by modifying the minimum value of ammonium uptake rate required to start observing N_2O production.

- By consuming NO_2^- and NO produced by AOB, NOB cells would have the ability to contribute to reduce of N_2O formation; in this case, both molecules would be used as electron donors in NOB metabolism.

- Independently of process operation conditions, AOB and NOB species richness and abundance profiles can affect the amount of N_2O produced in a given nitrification process.

CHAPTER SIX

N_2O accumulation in denitrifying mixed cultures: Influence of medium COD/N ratio and high nitrite concentration

This chapter describes a research on the pattern of N_2O production during the denitrification process. Analysis of N_2O production and accumulation in denitrification was undertaken as a series of experiments running and monitoring laboratory-scale denitrifying mixed microbial cultures operated in batch mode. In denitrifying cultures the growth medium carbon to nitrogen ratio (COD/N) along with high nitrite concentrations are operational parameters affecting N_2O production and accumulation. These parameters were examined under four experimental conditions: 1) high COD/N ratio, 2) high COD/N ratio plus high nitrite concentration, 3) low COD/N ratio and 4) low COD/N ratio plus high nitrite concentration. Metabolite profiling of culture biomass samples was undertaken to infer metabolic routes of organic carbon degradation. Software programmes Pathway Activity Profiling (PAPi) algorithm and Flux Balance Analysis (FBA) were used to analyse the metabolite profiles of the cultures as a means to quantify metabolic activity in denitrifying cells. Results from these experiments showed that denitrifying cultures operated at a low COD/N ratio produced more N_2O, and for longer periods of time, than cultures operated at a high COD/N ratio. A low COD/N ratio minimized amino and fatty acid concentration in denitrifying cells, showing that under this condition cells are depleted of carbon-rich metabolites and therefore of electron equivalent donors. It can be concluded from this study that denitrifying cultures operated at a low COD/N ratio are likely to produce N_2O after an environmental perturbation due a lack of electron equivalents to completely reduce NO_3^- to N_2.

6.1. Background

Chapter One has explained that microbial nitrification and denitrification processes occurring in agricultural soils, manure management systems and biological wastewater treatment produce between 65 and 75% of anthropogenic nitrous oxide (N_2O) emissions (Schreiber et al., 2012; Stein and Yung, 2003). N_2O is a major greenhouse gas and ozone depleting substance (IPCC, 2013; Ravishankara et al., 2009) and its emission from human-related activities must be identified and ways found to minimise it.

Microbial heterotrophic denitrification is commonly used during biological nitrogen removal (BNR) from wastewater, where soluble nitrate (NO_3^-) is converted to nitrogen gas (N_2), which results in the removal of nitrogen from wastewater. As an intermediate molecule in the denitrification process, N_2O can accumulate under specific conditions (explained in Chapter One) and then be emitted into the atmosphere (Kampschreur et al., 2009). This N_2O production pathway in denitrification is known as

the "dissimilatory nitrite reduction pathway in denitrifiers" or "incomplete denitrification". Preliminary estimations suggest that the carbon footprint of a typical biological nitrogen removal wastewater plant would increase by approximately 30% when just 1% of denitrified nitrogen is emitted as N_2O (de Hass and Hartley, 2004; Pan et al., 2013b).

Heterotrophic denitrification consists of four consecutive reduction steps catalysed by the enzymes nitrate reductase (NAR), nitrite reductase (NirK), nitric oxide reductase (cNor) and nitrous oxide reductase (Nos) (van Spanning et al., 2007), (**Figure 6.1.**). These enzymes produce nitrite (NO_2^-), nitric oxide (NO), nitrous oxide (N_2O) and nitrogen gas (N_2), respectively (van Spanning et al., 2007). The availability of a carbon source is regarded as an important factor affecting N_2O accumulation during denitrification in wastewater treatment (Lu and Chandran, 2010; Lu et al., 2014; Pan et al., 2012; Pan et al., 2013a); since the four denitrification reduction steps require electrons to be produced during the oxidation of organic carbon (**Figure 6.1**)., (Ferguson, 1998; Richardson et al., 2009; van Spanning et al., 2007).

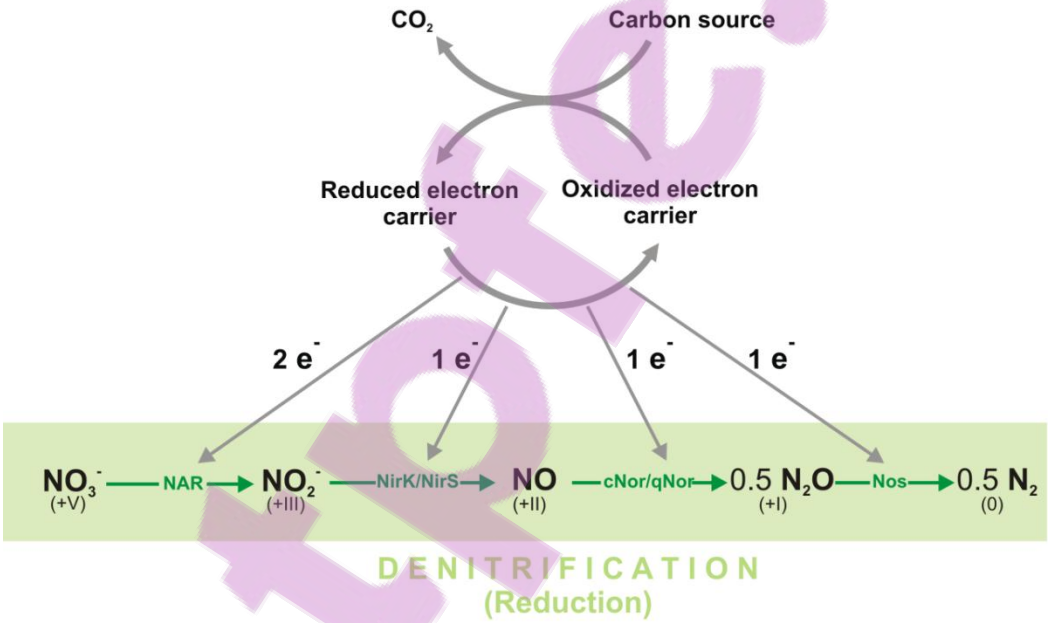

Figure 6.1. The denitrification process and its four main reduction reactions

In particular, the COD/N ratio of growth medium, i.e. the proportion of carbon substrate concentration measured as chemical oxygen demand (COD), to nitrate substrate concentration has been reported to significantly influence N_2O accumulation during denitrification (Hanaki et al., 1992; Kishida et al., 2004; Pan et al., 2013a). Pan, et al., (2013a) showed that low COD/N ratios in growth medium enhance competition for electron equivalents between the four denitrification reductase enzymes, consequently limiting the proportion of electrons distributed to the Nos enzyme, thus promoting N_2O accumulation. Differences in enzyme affinity constants for electrons would be the determining factor of electron distribution (Pan et al., 2013b).

Previous studies that implicate COD/N limitation in N_2O emission inherently assume that the electron affinity of the upstream nitrogen reduction steps is higher than the affinity of N_2O reductase. In such a case, the upstream nitrogen reductases would be more competitive to accepting the electrons from a given electron donor. However electron competition occurs not only under carbon-limiting but also in carbon-abundant conditions (Lu and Chandran, 2010; Pan et al., 2013a), meaning that the upstream electron supply reactions forming the carbon oxidation and electron transport chain pathways also influence the distribution of electron delivery to the four main denitrification reactions. Intracellular carbon storage compounds (i.e. poly-β-hydroxybutyrate (PHB) and long chain fatty acids) with relatively low biodegradability can be used as electron donors for denitrification (Kampschreur et al., 2009; Schalk-Otte et al., 2000). This indicates that not only the activity of the nitrogen reduction pathways but also the activity of carbon oxidation pathways influences electron distribution and N_2O production during denitrification. For example, Schalk-Otte et al, (2000) observed that as soon as PHB became the growth substrate due to COD limitation, N_2O started to accumulate. Moreover, electron equivalents in cells of common species of denitrifier organisms, like *Paracoccus denitrificans* and *Pseudomonas aeruginosa,* can be supplied to the electron transport chain through different metabolic compounds, i.e. NADH, lactate, succinate, $FADH_2$, glycerol-P and glycolate (Ferguson, 1998; Richardson et al., 2009). These metabolites are an indication as to which carbon oxidation pathways could potentially affect the rate of electron supply into denitrification reactions.

As mentioned in Chapter One, two complementary approaches show promise in tracing the activity of cellular carbon oxidation pathways and detecting carbon assimilation intermediates. This is achieved through metabolite profiling and then the estimation the rate of reactions in those pathways through SMN modelling (Becker et al., 2007; Kümmel et al., 2006). Metabolite profiling and SMN modelling are beginning to gain recognition as useful approaches to describe metabolic pathways in waste treatment bioprocesses (Stolyar et al., 2007; Villas-Bôas and Bruheim, 2007). For example, metabolite profiling based on high pressure liquid chromatography coupled with mass spectrometry (HPLC-MS) was successfully used to identify transformation products from micropollutant biodegradation in laboratory scale wastewater treatment bioreactors (Helbling et al., 2010). In addition, a simulation approach through SMN modelling was recently employed to estimate rates of electron consumption by N_2O producing reactions in *Nitrosomonas europaea* laboratory scale cultures (Perez-Garcia et al., 2014).

The goal of the present study is to identify the carbon oxidation pathways of denitrifying cultures producing N_2O as a consequence of exposure to the COD/N ratio of different growth media by performing metabolite profiling and metabolic network modeling of biomass in denitrifying batch cultures. It is hypothesized that cultures with a low COD/N ratio will lead to a higher N_2O production rate than cultures with a high COD/N ratio because carbon substrate unavailability will promote the activation of storage compound oxidation pathways, which in turn will affect electron delivery to denitrification reactions and, consequently, the N_2O production-consumption balance. Even that this hypothesis is conventional, the effect of COD/N ratios on N_2O production-consumption balance has

not being assessed using biomass metabolite profiling and intracellular metabolic reaction rates calculations.

In this research denitrifying batch cultures with different COD/N rate were run in a laboratory environment. The COD/N ratio of cultures was modified by changing carbon source concentration and adding nitrite pulses to mixed liquor. Carbon oxidation pathways were identified by measuring relative abundances of metabolites in cultures, using GC-MS based metabolite profiling (Smart et al., 2010). Metabolite relative abundances were then used to create pathway activity profiles (PAPi) (Aggio et al., 2010) and estimate fluxes in carbon oxidation pathways, employing an SMN model of denitrifying microbes.

6.2. Materials and Methods

6.2.1. Denitrification batch experiments

Denitrifying batch cultures were grown in two lab-scale bioreactors with a working volume of 3 litres seeded with activated sludge from a domestic wastewater treatment plant in Auckland, New Zealand. The photograph in **Figure 6.2**. shows the full scale activated sludge BNR reactor from which the seeding sludge was taken. **Figure 6.3**. is a diagram of the experimental setup installed at the Environmental Engineering Laboratory of The University of Auckland to analyse N_2O production in nitrification and denitrification. Nevertheless during this research, only equipment to The experimental setup consisted of two identical and independent reactors connected to an influent-effluent hydraulic line (thick black line) and interconnected through a recirculation hydraulic line (dashed thick black line). Reactors were equipped with a tubing system (blue line) to provide aeration and drag gaseous emissions to the 320E Teledyne N_2O analyser for nitrification experiments only. Sensors and equipment to measure N_2O in liquid and gaseous phases are represented as green lines and boxes. These instruments were connected to a computer for online data recording. **Figure 6.4**. shows a photograph of the two bioreactors used in this study. The bioreactor on the left is completely mixed, while the one on the right is sediment sludge.

Figure 6.2. Activated sludge in BNR reactors at Mangere Wastewater Treatment Plant, New Zealand

Prior to initialisation of each culture, half a litre of seed sludge was washed twice with tap water, diluted to a volume of 2.7 L, with an adjusted volatile suspended solids (VSS) concentration of 1.1 g/L and stripped with pure N_2 gas for 5 minutes to remove dissolved oxygen. Batch cultures were initialized by enriching the diluted sludge with 0.3 L of concentrated phosphate buffer growth medium with the following composition: $NaNO_3$ (3 g/L), NaOH (40 g/L), KH_2PO_4 (13.7 g/L), $FeSO_4$-$7H_2O$ (0.02 g/L) and commercial milk powder (0.1 g/L) as a micronutrient source. Sodium acetate was added as a carbon source at concentrations of 0.7 or 0.25 grams per litre of culture to obtain initial chemical oxygen demands (COD) of 541 or 196 g/L. The resulting mixed liquor had an initial nitrate (NO_3^--N) concentration of 49±3 mg-N/L (3.5±0.2 mmol-N/L), VSS of 1±0.13 g/L, pH of 7.5±0.1 and COD/N ratios of 11 or 4, depending on the initial acetate concentration. Cultures were thoroughly mixed with a magnetic stirrer and run at room temperature (from 22 to 25ºC) until NO_3^--N consumption stopped. N_2O production was triggered by perturbing (spiking) the culture with 5 mL of a concentrated NO_2^--N solution (1.2 M, $NaNO_2$) during the reaction phase (NO_3^--N reduction phase). Each experimental condition (i.e. cultures with COD/N ratio of 11 or 4 with and without an NO_2^- spike) was tested in triplicate by running three identical batch cultures (**Table 6.1**).

Table 6.1. Tested conditions in denitrifying cultures

COD/N=11, control	COD/N=11 with NO_2^- spike
COD/N=4, control	COD/N=4 with NO_2^- spike

Denitrifying culture performance was monitored in triplicate using IntelliCAL ISENO318101 Nitrate Ion Selective Electrode by Hach Company,USA, by measuring the mixed liquor's NO_3^--N concentration every 15 minutes or 12 hours, depending on the NO_3^--N depletion rate. Mixed liquor NO_2^--N and liquid phase N_2O-N concentration were respectively measured in real time with biosensors and Clark-type microsensors (**Figure 6.4.**) connected to a multimeter (Unisense, Aarhus, Denmark, **Figure 6.5.**). Immediately after NO_3^--N readings, 30 mL of mixed liquor was sampled to measure total and volatile suspended solids (TSS and VSS) in accordance with Standard Methods (APHA, 1995). Soluble chemical oxygen demand (sCOD) was measured by collecting 10 mL of filtrate from solids analysis and re-filtered with a 0.45 µm pore size fiberglass syringe filter; and then analysed in triplicate following the dichromate colorimetric method following the Standard Methods (APHA, 1995). Soluble protein concentration was measured as an indicator of microbial biomass concentration in the following way: 10 of the original 30 mL sample were sonicated for 15 minutes and centrifuged at 4000 r.p.m. for 10 minutes; the pellet was re-suspended in 2 mL of sodium hydroxide solution (0.2 M), incubated at 98±1 ºC for 20 minutes, cooled on ice and centrifuged at 5000 r.p.m. for 5 minutes to eliminate possible precipitates. The supernatant was then used to measure total soluble protein by Bradford colorimetric micro plate assays (Bio-Rad protein assay dye reagent and bovine serum albumin (Sigma A7906) as standard).

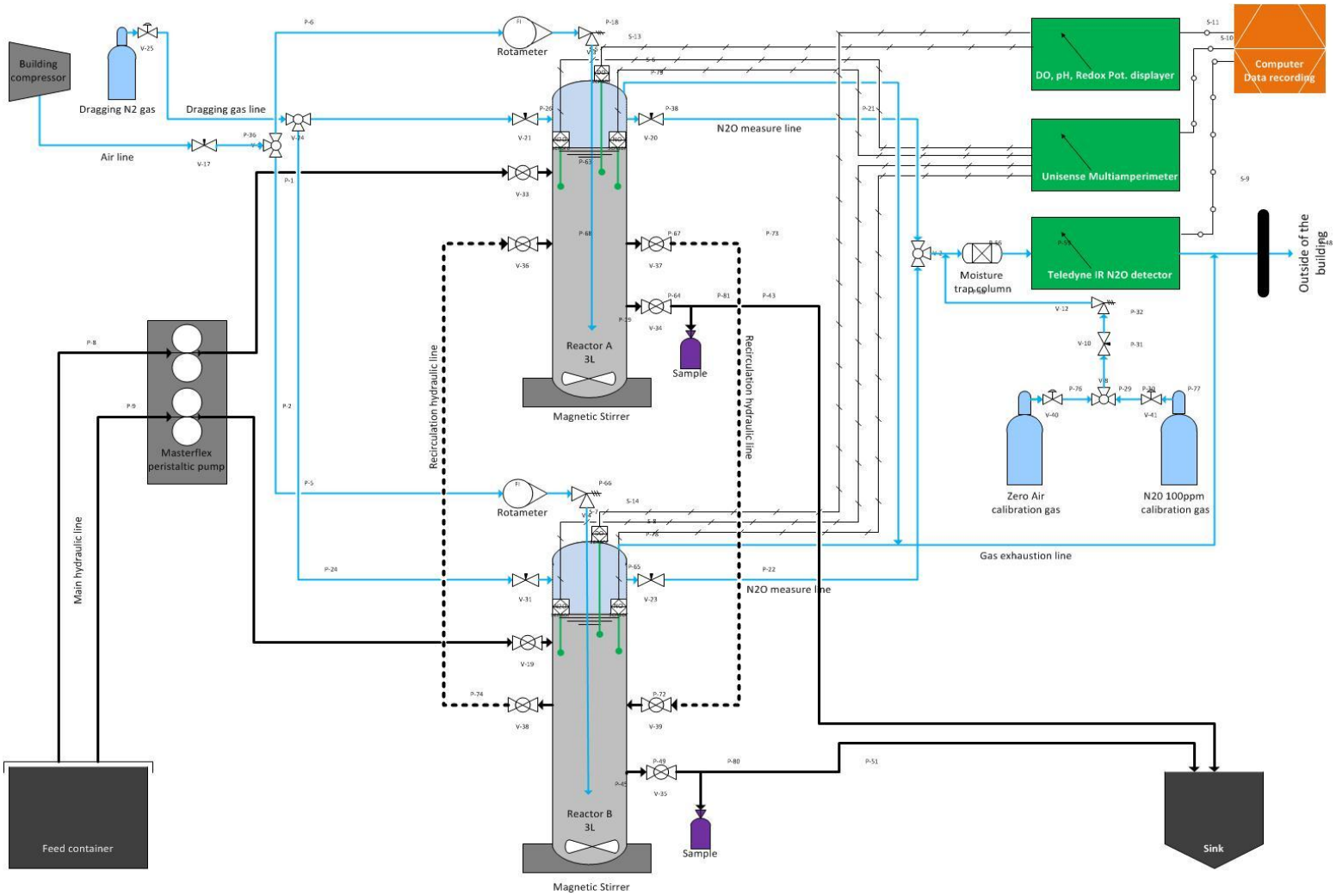

Figure 6.3. Diagram of experimental setup for N_2O measurements in BNR processes

Figure 6.4 Bioreactors for 3 litres of denitrifying cultures

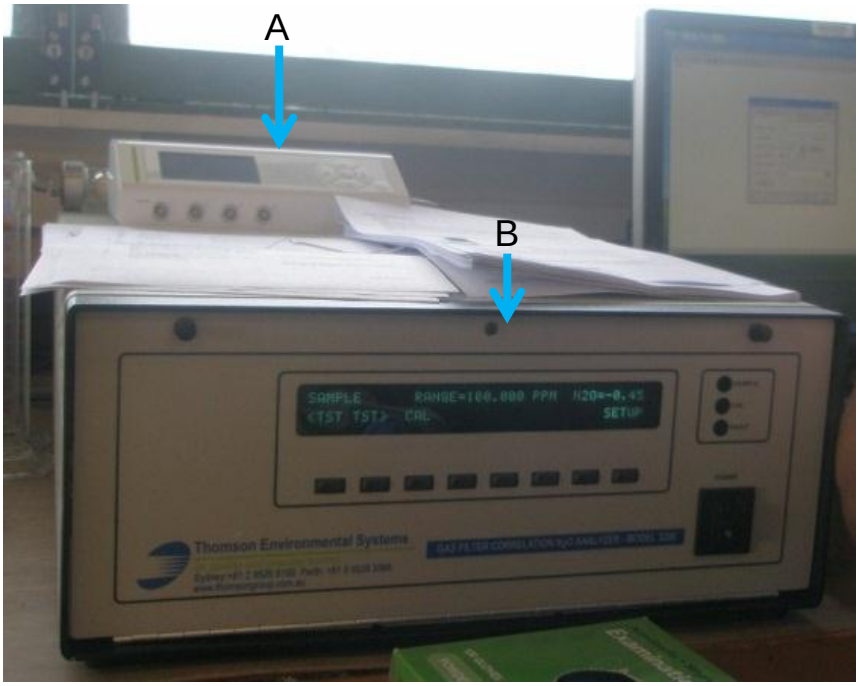

Figure 6.5. NO and N_2O detection equipment
A) Unisense Microsensor Multimeter used to process signal from NO_2^- and N_2O microsensors; B) The 320E Teledyne Infra-Red gas filter correlation N_2O analyser. Both instruments were connected to a PC for variable online monitoring.

Figure 6.6. Unisense Clark type N_2O microsensors

6.2.2. Metabolic profile of mixed liquor biomass

Relative abundance of the intracellular metabolites in the cultures was measured following the protocol described in Smart et al (2010), developed in the Metabolomics Laboratory of The University of Auckland and adapted to process mixed liquor samples. During the NO_3^--N oxidation phase, after adding NO_2^--N perturbation, two 25mL samples were taken from the bioreactor and each filtered immediately using a vacuum filtration system with 0.45 µm pore-size cellulose acetate filter. Biomass quenching was done by rapidly washing the pellet on the filter with 10mL of saline solution (0.9 % (wt/vol) NaCl) at 4 ºC. Thirty milligrams of pelletized biomass was recovered and placed in a 50 mL centrifuge tube containing 2.5 mL of cold methanol-water solution (1:1 (vol/vol)) at -30 ºC. The internal standard 2,3,3,3-d_4-alanine (0.5 µmol/sample) was added to each sample and vigorously mixed with vortex for 30 seconds. Intracellular extracts were stored at -80 ºC for two to four weeks to wait further processing. Intracellular metabolite extraction was done by subjecting samples to freeze-thaw cycles as described in Smart et al (2010). Cell debris from this metabolite extraction step was used to quantify biomass (as a soluble protein) by using the Bradford method. Sample extracts were concentrated by adding 10 mL of cold (4 ºC) bidistilled water, freezing the diluted extracts to -80 ºC and then freeze-drying them. Freeze-dried samples were re-suspended in 200 µL of NaOH (1 N) and then derivatized using the methyl chloroformate (MCF) protocol (Smart et al., 2010). The MCF derivatives were analysed by GC-MS (Agilnet GC7890 coupled with MSD597) operated following the equipment setup specified in Smart et al (2010). In total six samples were analysed for each experimental condition. In other words, each culture was sampled in duplicate and each of the conditions was reproduced in triplicate cultures.

Metabolites from each analysed sample were identified by deconvoluting GC-MS chromatograms with AMDIS software (NIST, Boulder, CO, USA) and identifying metabolites using The Metabolomics Laboratory MCF MS library. Metabolite identification was based on both the MS spectrum of the derivatized metabolite and its respective chromatographic retention time. **Figures 6.7.** and **6.8.** are screenshots of AMDIS software showing a chromatogram and a MS spectra from an analysed sample. The relative abundance of identified metabolites was determined with the ChemStation software (Agilent), using the GC base-peak value of a selected reference ion. Metabolites detected in one sample alone were excluded from the analysis. The relative abundance values were normalized by the biomass content in each sample as well as by the abundance of the internal standard 2,3,3,3-d_4-alanine. Normalized relative abundance values of the metabolites were auto-scaled with the formula $\tilde{x}_{ij} = (x_{ij} - \bar{X}_i)/std_i$ in order to compare all relative abundances with the same scale (van den Berg et al., 2006). In this formula, $\tilde{x}_{ij}$ is the autoscaled relative abundance value of metabolite i in sample j; x_{ij} is the relative abundance value (in this case, already normalized by internal standard abundance and sample's biomass content) of metabolite i in sample j; $\bar{X}_i$ is the mean of metabolite i relative abundance in all samples; and std_i is the standard deviation of metabolite i relative abundance in all samples.

6.2.3. Analysis of metabolite profile data

An initial exploration of differences between sample relative abundances was performed with Partial Least Squares Discriminant Analysis (PLS-DA), PLS-DA cross validation was done by estimating the goodness of fit of the linear model in the first three components using the coefficient of determination (R^2), and by estimating the predictive ability of the model with Q^2 scores. Following this, a univariate analysis of variance (ANOVA and Tukey HSD tests) was applied to determine whether the relative abundance of each identified metabolite was significantly different between culture conditions. Where these differences were significant (at $\alpha = 0.05$), they were plotted with a heatmap using the R software (R Development Core Team, 2010). The Pathway Activity Profiling (PAPi) algorithm (Aggio et al., 2010) was used to predict and compare the relative activity of different metabolic pathways in denitrifying biomass during the conditions tested. The PAPi programme connects to the KEGG online database (http://www.kegg.com) and uses the number of metabolites identified from each pathway and their relative abundances to predict which metabolic pathway is likely to be active in the cell.

6.2.4. Metabolic reaction rate estimation with the SMN model

A SMN model of denitrification was developed to estimate fluxes of reactions in carbon assimilation and nitrogen respiration pathways. The model was based on stoichiometric equations of metabolic reactions occurring in four species with denitrifying capabilities, i.e. *Acidovorax ebreus*, *Azoarcus* sp. KH32C, *Paracoccus denitrificans* and *Pseudomonas aeruginosa*. These species were selected to cover the reaction diversity in denitrifier metabolism and due they have been detected on the activated sludge used to seed the batch experiments (Biswas et al., 2009; Brown, 2010). The

denitrifier SMN model included pathways for assimilation (oxidation) of acetate, ethanol, glucose, common organic acids (C2 to C4), and common amino acids, as well as for synthesis of all the 20 common amino acids and the reduction/oxidation pathways of saturated fatty acids, unsaturated fatty acids, glycerolipids and phosphoglycerolipids. The complete network consisted of 351 metabolites and 485 metabolic reactions. Assimilation pathways of single carbon compounds (methanol, methane) were not included as acetate was the model carbon source used on experiments. **Figure 6.9**. presents the network formed by the model's metabolites (circle nodes) and reactions (small square shaped nodes). The black square shape nodes at the network periphery represent reactions for uptake and secretion of inorganic substrates (e.g. nitrogenous compounds) and organic substrates (e.g. carbohydrates and amino acids).

Intracellular fluxes in each experimental condition where calculated as follows. Pathways with high A_S scores in the PAPi analysis were allowed to carrion flux, while in pathways with A_S scores of zero the flux was blocked. Estimated substrate consumption rates of nitrate and acetate (measured as COD) were used as the model's input values. Once the constraints described above were set for the model, flux balance analysis (FBA) simulations were launched using the COBRA toolbox v2.0 (Orth et al., 2010; Schellenberger et al., 2011) running in MATLAB® 7 R2010b (The MathWorks Inc, Massachusetts, USA).

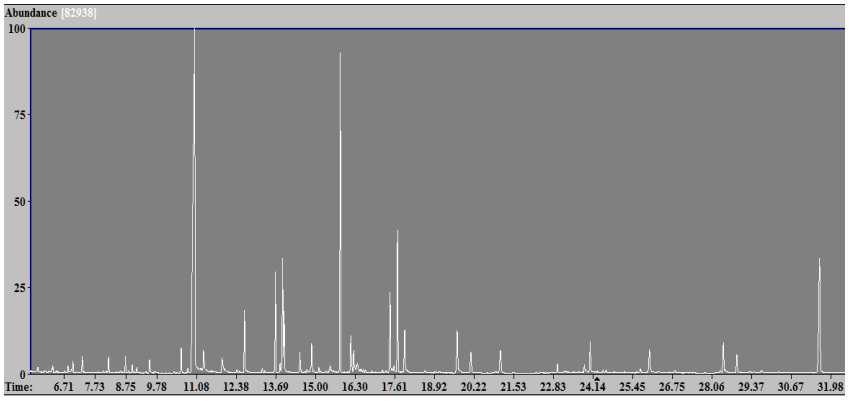

Figure 6.7. Screen shots of AMDIS software showing a chromatogram of an analysed sample

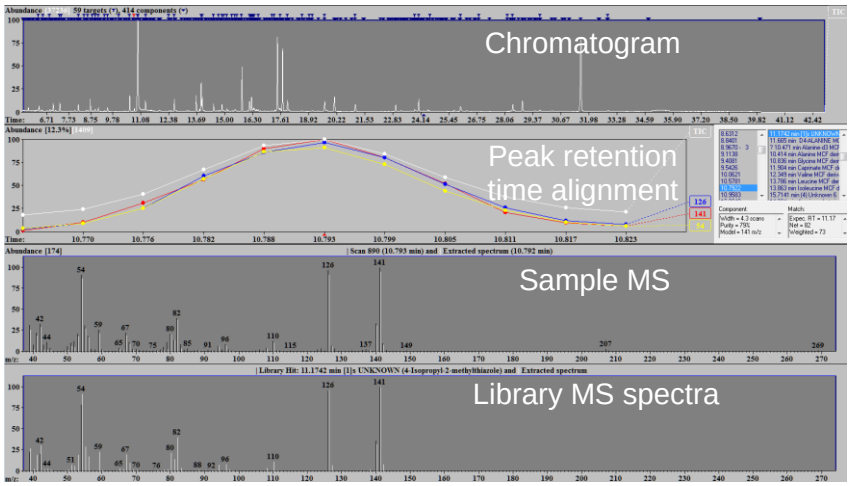

Figure 6.8. Screen shots of AMDIS software identifying a metabolic compound by comparing chromatogram peak retention time and MS spectra.

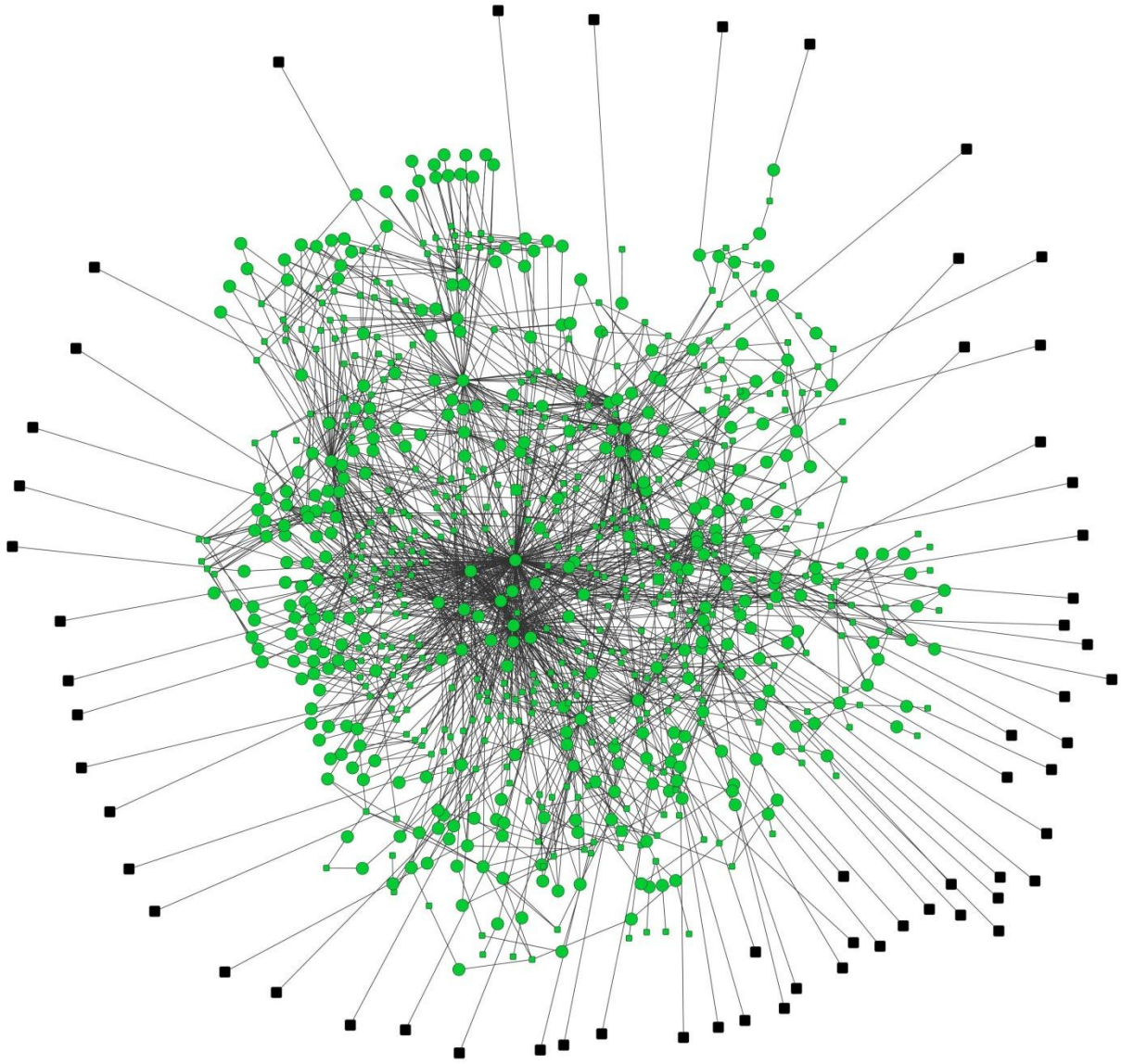

Figure 6.9. Metabolic network constructed with biochemical information of denitrifying microbes The complete list of reaction equations and metabolic compounds that form the complete SMN model can be found in the Appendix Three of this document.

6.3. Results and Discussion

6.3.1. N_2O production by denitrifying cultures

Culture medium COD/N ratio and NO_2^- spikes had an effect on the amount of N_2O accumulated in denitrifying cultures, shown in **Figure 6.10.** Independently of culture medium COD/N ratio, N_2O was detected only in cultures that were spiked with NO_2^-. Where the NO_2^- perturbation was applied, N_2O immediately began to accumulate (indicated as an arrow in the plots in **Figure 6.10.**), while none of the control cultures without NO_2^- perturbation accumulated N_2O. After their NO_2^- spike, cultures on medium with low COD/N ratio (4) accumulated N_2O to a maximum concentration of 0.47±0.045 mmol-N/L, which is significantly more than cultures on medium with high COD/N ratio (11), which reached a maximum N_2O concentration of 0.14±0.037 mmol-N/L. On the other hand, cultures on medium with COD/N = 4 had a lower N_2O production rate (0.03±0.002 mmol-N/gVSS*h) than cultures with COD/N = 11 medium (0.12±0.002 mmol-N/gVSS*h), after NO_2^- perturbation. **Table 6.2** presents a summary of the metabolic rates measured on cultures when producing N_2O.

NO_3^- and sCOD consumption in batch cultures on COD/N = 11 medium was faster than that for experiments on COD/N = 4 medium (X axis on graphs of **Figure 6.10**), even though all cultures had a similar initial biomass concentration (1±0.13 g/L of VSS). Cultures on medium with COD/N = 11 completely consumed the initial NO_3^- in less than 2.5 hours, while cultures on COD/N = 4 medium failed to reach complete NO_3^- removal even though experiments were prolonged for 90 hours. During the reaction phase (at t = 24 h) and before applying NO_2^- perturbation, cultures on medium with COD/N = 11 presented a NO_3^- consumption rate of 2.3±0.73 mmol-N/gVSS*h, while for cultures on medium with COD/N = 4 it was 0.11±0.027 mmol-N/gVSS*h. Because of these differences in NO_3^- consumption rate, NO_2^- perturbation was applied at t = 1 h in cultures on COD/N = 11 medium, while on COD/N = 4 cultures it was applied at = 24 h. In all tested conditions, culture VSS and soluble protein concentration did not change significantly over time (according to ANOVA test at α=0.05), indicating a non-significant change of microbial biomass concentration. Cultures with COD/N = 11 had an average VSS of 968±78 mg/L and soluble protein of 582±107 mg/L, while for cultures with COD/N = 4, the average VSS was 793±153 mg/L and soluble protein 592±87 mg/L.

Table 6.2. Summary of main results from denitrifying cultures

Culture	Experiment duration (h)	NO_3^- consumption rate (mmol-N /gDW*h)	sCOD consumption rate (mmol-Ac /gDW*h)	N_2O production rate (mmol-N /gDW*h)	Maximum N_2O accumulation (mmol-N/L)	Total N_2O-N produced (mmol-N)
COD/N = 11 with NO_2^- spike	2.5	1.73±0.08	0.7±0.3	0.15±0.002	0.14±0.03	0.57±0.12
COD/N = 4 with NO_2^- spike	96	0.11±0.022	0.08±0.054	0.024±0.007	0.47±0.045	1.47±0.29

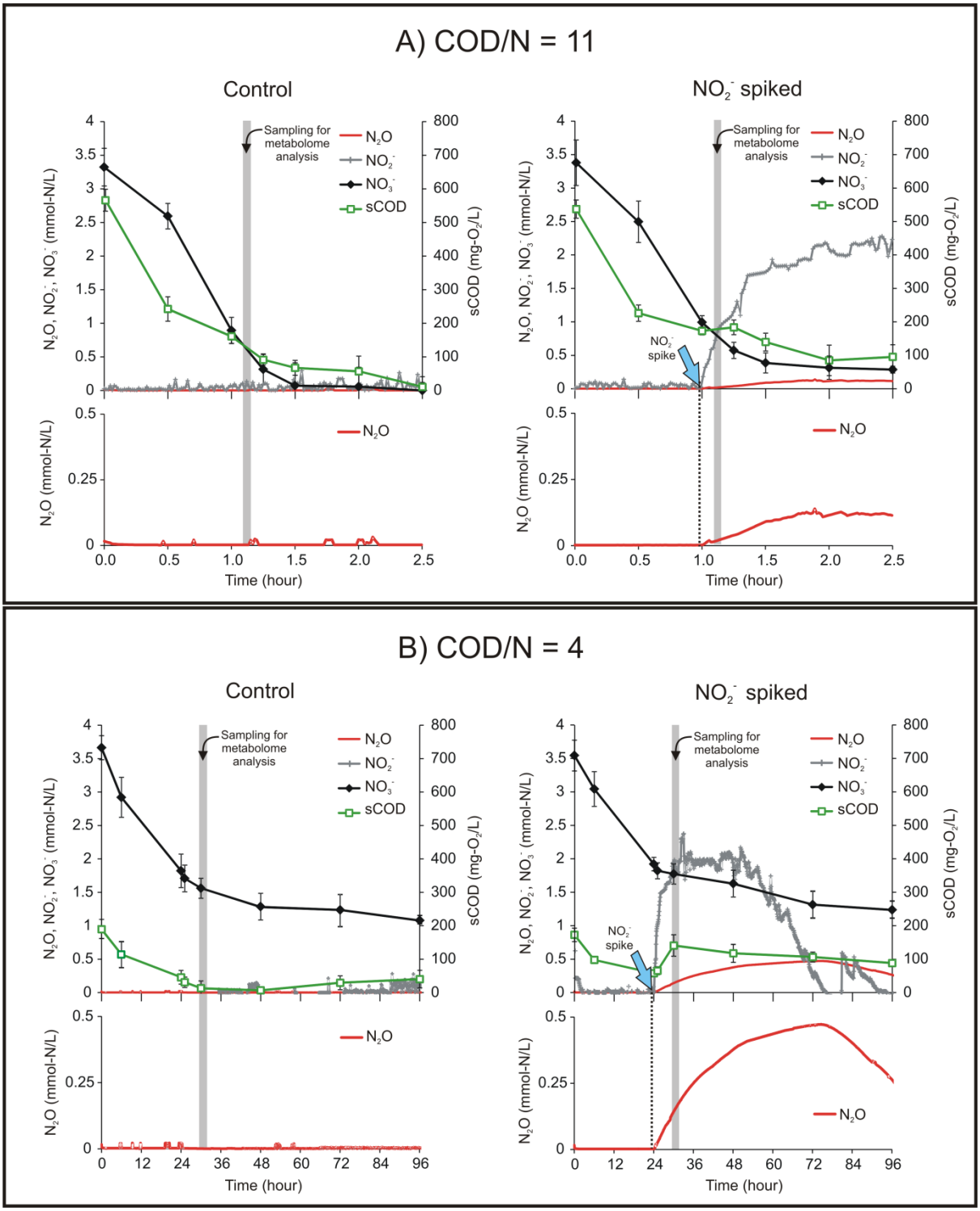

Figure 6.10 Nitrogenous compounds concentration curves observed in denitrifying cultures on growth medium with COD/N ratio of 11 and 4

6.3.2. Intracellular metabolite profiles of denitrifying cultures

A total of 53 intracellular metabolites were identified in 24 biomass samples from denitrifying cultures, although metabolite relative abundance was affected by culture medium COD/N ratio and NO_2^- spikes, as illustrated in **Figures 6.11** and **6.12**. In general metabolite relative abundances of COD/N=4 cultures were lower than that of COD/N=11 cultures indicating that cells in COD/N=4 cultures were limited of carbon substrate presented low metabolic activity. Out of the 53 identified metabolites, fourteen were common amino acids, twenty one were fatty acids (thirteen saturated and eight unsaturated), four were di- carboxylic organic acids, five were tricarboxylic acid cycle (TCA) intermediates and nine were intermediates of amino acid metabolism. However, among the 53 detected metabolites, only 39 presented a relative abundance with significant difference between experimental conditions, according to ANOVA and (p-value < 0.05). Interestingly, relative abundance of lactic and as well as all the di- carboxilic acids (levulinc, pimelic, suberic and azelaic) was not significantly different between experimental conditions, suggesting a group of pathways active in all the conditions.

The scatter plot of **Figure 6.11.A.** shows spheres, representing samples from each culture condition, which clustered together but clearly distinguishing different culture condition. Samples with most distinct metabolite profile were those from COD/N = 4 and COD/N = 11 medium, evidencing a clear difference between the metabolic state of cells in these two experimental conditions. For instance, metabolite abundance in samples from COD/N = 4 cultures were significantly lower than those in COD/N = 11 cultures according to PLS-DA (**Figure 6.11.A**.). PLS-DA also identified key differences between metabolite profiles of control experiments from those in NO_2^- spiked experiments (**Figure 6.11.A**.). However, differences between control and NO_2^- spiked samples were not as significant as those observed between COD/N=4 and COD/N=11 samples, due the fact that there is not a clear separation between control and NO_2^- samples. In PLS-DA cross validation (**Figure 6.11 .B**.), the high R^2 and Q^2 values obtained for the three first components indicate that PLS-DA was discriminating sample data correctly. However, component 2 showed a lower predictive ability (Q^2=0.45) than component 1 (Q^2=0.82), involving a degree of uncertainty in the separation between control and NO_2^- spiked samples.

The heatmap in **Figure 6.12**. shows all the metabolites detected with significant relative abundance differences according to ANOVA test at $\alpha = 0.05$. Similarly as in PLS-DA plot, in general all detected metabolites had lower relative abundance in samples from COD/N = 4 cultures compared to those from COD/N = 11 cultures. This suggests that in cultures with low COD/N ratio there is low metabolic activity through catabolic and anabolic pathways per unit of biomass. The columns dendrogram on top of the heatmap separates metabolite profiles of COD/N = 11 cultures from those of COD/N = 4 cultures. The heatmap shows average relative abundance values (after normalization and auto-scaled data pre-treatment) of identified metabolites in each of the tested conditions. Relative abundance values below -1 (light green) or above 1 (bright red) indicate that the metabolite abundance in that specific condition (column) is below or above the mean of that of all the samples by more than one standard deviation. Values near zero (black) indicate an average relative abundance.

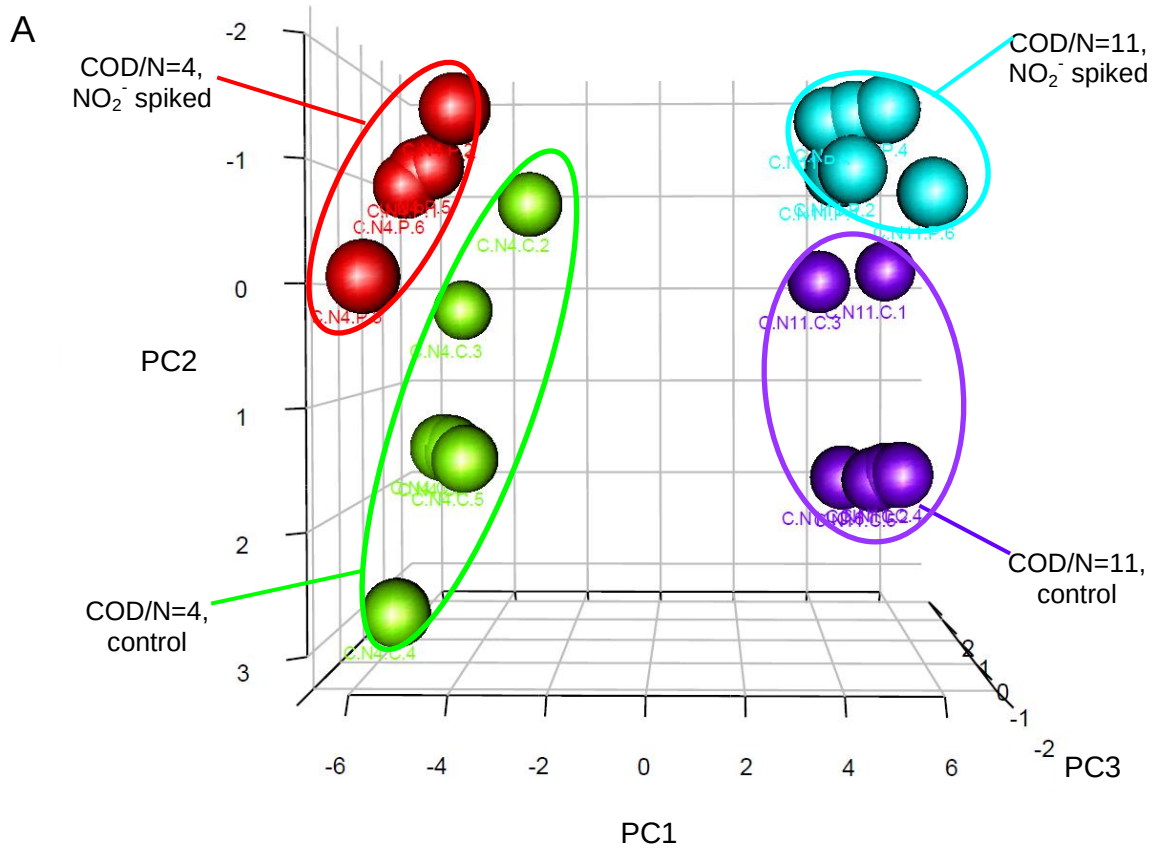

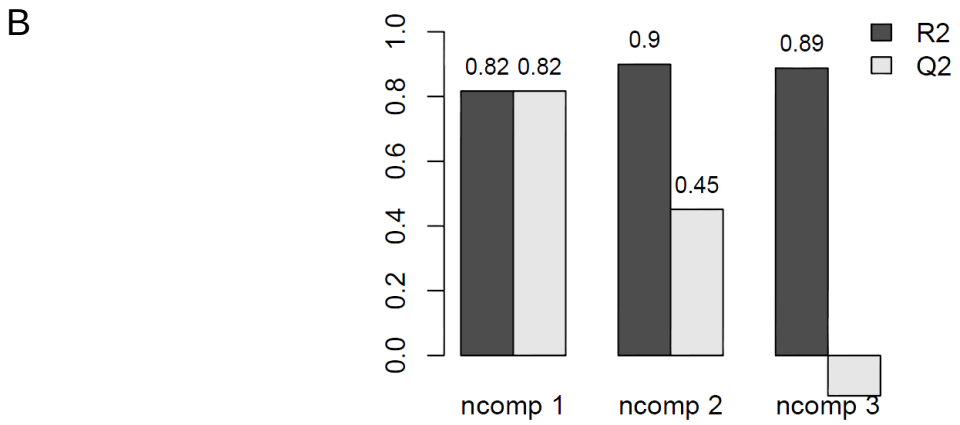

Figure 6.11. PLS-DA between metabolites relative abundance measurements in biomass samples from denitrifying cultures. (A) Scatter plot of samples grouped according to the first three components. (B) Bar graph of R^2 and Q^2 values obtained for the first three components.

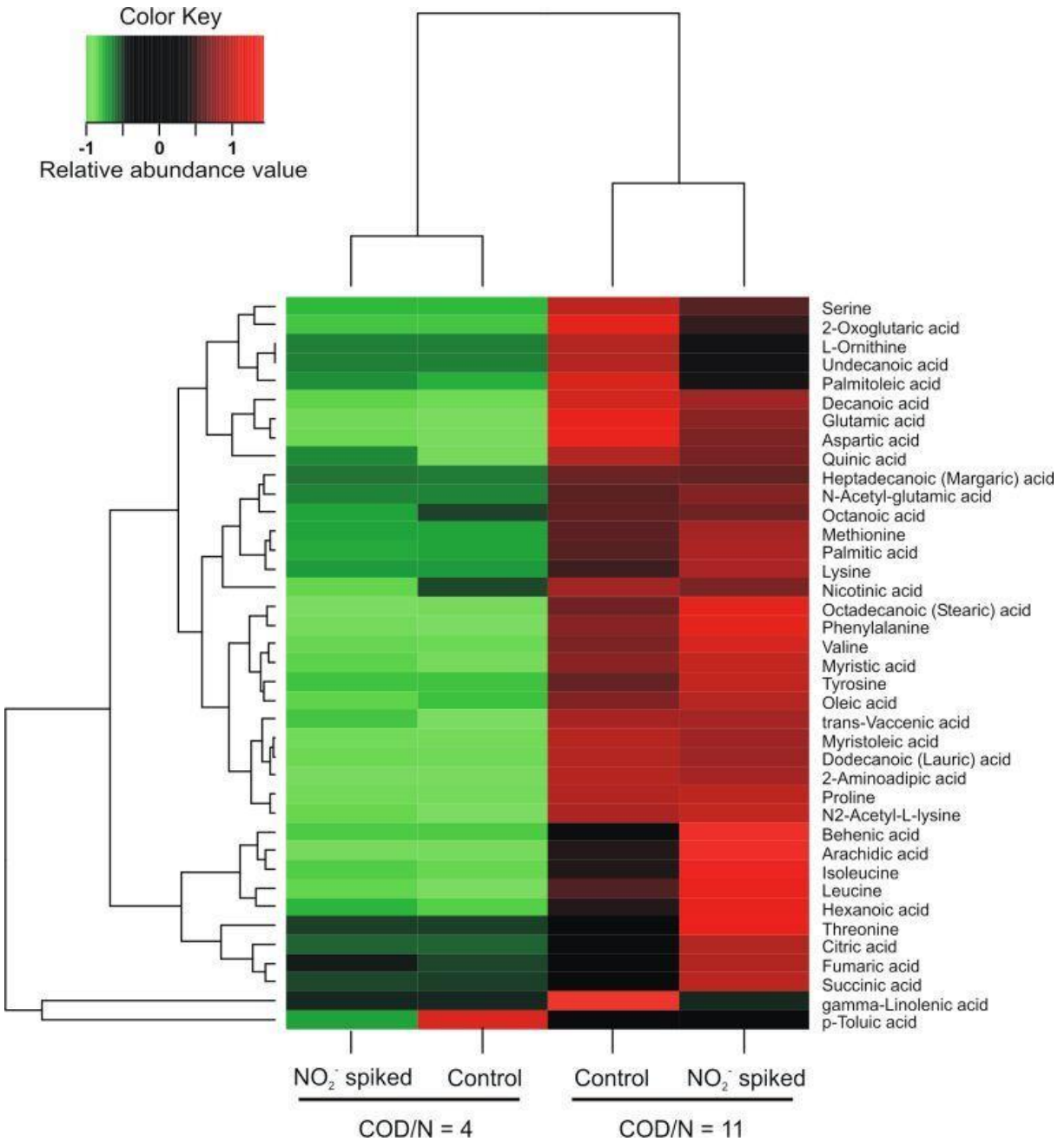

Figure 6.12. Heatmap of average relative abundance of intracellular metabolites in biomass samples from denitrifying cultures on medium with COD/N ratio of 4 and 11

Heatmap of **Figure 6.12**. also shows that TCA intermediates (citric, fumaric and succinic acids), amino acids, intermediaries of amino acid metabolism (L-ornithine, benzoic acid, nicotinic acid, N-acetyl-glutamic acid, putrescine, pyroglutamic and p-toluic acid) and saturated fatty acids were detected in the 24 samples. The heatmap in **Figure 6.12**. illustrates that cultures on COD/N=11 medium had significantly higher abundance of amino acids and fatty acids than cultures on COD/N=4 medium. This indicates that in COD/N=11 cultures, the carbon source was used to build up amino and fatty acids; and that electron equivalents to reduce NO_3 to N_2 were generated on the TCA cycle pathway. Conversely, cultures on COD/N=4 medium were carbon-source starved and not synthesizing amino and fatty acids.

Metabolite profiles of control cultures on COD/N = 11 medium were different than those on NO_2^- spiked cultures at the same COD/N ratio; relative abundance of saturated dicarboxylic acids, TCA intermediates, eleven out of fourteen amino acids, and nine out of thirteen saturated monocarboxylic fatty acids increased in NO_2^- spiked samples. In contrast, Metabolite profiles of control and NO_2^- perturbed cultures on COD/N = 4 did not have any particular significant difference. Common amino acids were detected at low relative abundance (below one standard deviation of the mean relative abundance of all samples) in samples from COD/N = 4 cultures, indicating no accumulation of these compounds in those cultures. Long chain fatty acids (i.e. palmitoleic, undecanoic, margaric, octanoic, palmitic, and gamma-linolenic acids) were detected at average relative abundances (values near to the mean relative abundance of all samples), indicating the presence of storage compounds and therefore of potential electron donors. It is therefore possible that cultures on COD/N= 4 medium were slowly oxidizing inner carbon storage compounds (such as fatty acids) to incompletely reduce NO_3 to N_2, therefore accumulating high quantities of N_2O.

6.3.3. Predicted metabolic pathway activity

The Pathway Activity Profiling (PAPi) algorithm estimated higher activity (per unit of biomass) for the majority of metabolic pathways in cells from cultures in COD/N=11 medium compared to cells on COD/N=4 medium (**Figure 6.13.).** As with metabolite profiles, predicted activity in biosynthetic pathways was down-regulated on cultures on COD/N = 4 medium. **Figure 6.13**. shows those metabolic pathways with statistically significant (p-value <0.05) changes in S_A scores. Twenty out of twenty four metabolic pathways were up-regulated in denitrifying cells growing on COD/N = 11 medium. This means that the denitrifying cultures that produced more N_2O (those on COD/N = 4 medium) had lower metabolic activity on pathways related to amino acids biosynthesis and metabolism, nitrogen respiration and fatty acid biosynthesis; and that cells on cultures on COD/N = 4 were depleted of carbon-rich metabolites and therefore of electron equivalents. Interestingly, the S_A scores for pathways: pyruvate metabolism and glycolysis/gluconeogenesis where not significantly different in all the conditions except for cultures on NO_2^- spiked-COD/N = 11 cultures, which suggest high activity in the central carbon pathways in those cultures and therefore delivery of electrons for nitrogen reduction via succinate, NADH or lactate oxidation.

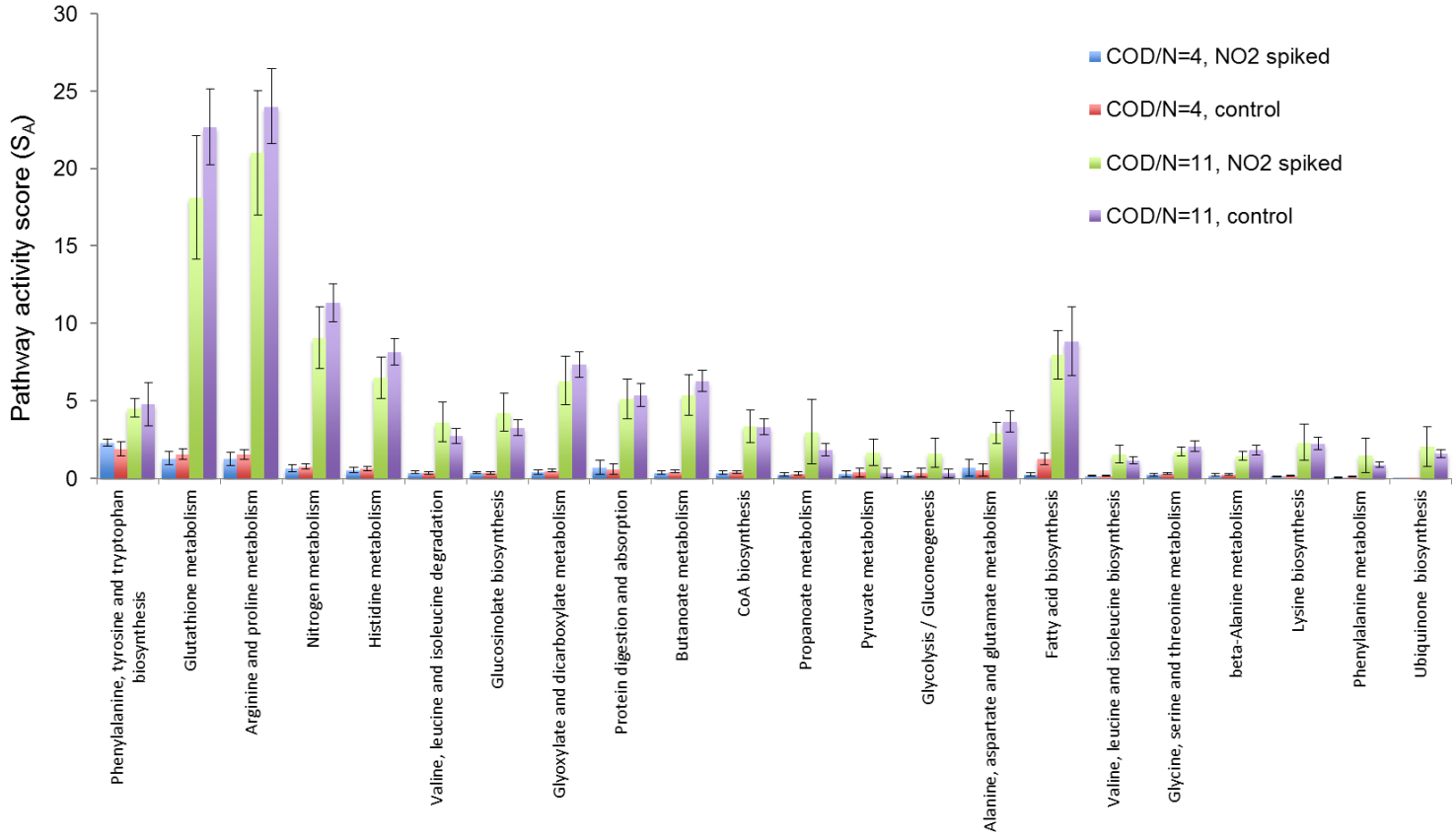

Figure 6.13. Comparative metabolic activities in denitrifying cells based on intracellular metabolite profiling data as predicted by Pathway Activity Profiling (PAPi) software.

The PAPi algorithm estimates an Activity Score (S_A), which represents potential metabolic pathway activity and allows its comparison between conditions (Aggio et al., 2010). In this algorithm each identified pathway receives a score based on the abundance/relative abundance of the metabolite to which it is linked and the number of metabolites with which it is associated. For instance, the pathway "arginine and proline metabolism" obtained high S_A scores on COD = 11 cultures because many metabolites participating in that pathway (proline, putrescine, aspartate, N-acetyl glutamic acid) were detected at high relative abundances in those cultures. The same applies for the fatty acid biosynthesis pathway, relative abundances of hexanoic, octanoic, palmitic and stearic acids (including others), contribute to the high S_A score of that pathway in COD = 11 cultures.

6.3.4. Flux balance analysis interpretation of metabolite profiles

An SMN model for denitrifier organisms and flux balance analysis was used to estimate metabolic fluxes that satisfy the observed physiological state of denitrifying cultures, i.e. the NO_3^- and acetate uptake rates and PAPi activity predictions. The metabolites identified in metabolites profiles were mapped onto the reconstructed metabolic network via PAPi algorithm. Computed FBA solutions can also be presented on the network map and compared with PAPi solution, thus FBA solution reflect predicted pathway activity.

Figure 6.13. presents two simplified networks of carbon assimilation and nitrogen respiration pathways in denitrifying cells and estimated fluxes using the SMN model. The flux distribution shown is a snapshot flux estimation carried out immediately after cultures were spiked with the NO_2^- solution. FBA was only performed to estimate fluxes of NO_2^- spiked cultures. The estimated fluxes presented in **Figure 6.13.** illustrate that cells of N_2O producing cultures on COD/N = 11 medium delivered electrons to nitrogen reduction reactions through central carbon pathways; while cells of cultures on COD/N = 4 medium delivered electrons to nitrogen reduction reactions through fatty acids degradation pathway. These electron delivery differences affected the rate of N_2O production but, most importantly, the total mass accumulated as N_2O-N per mass of NO_3^--N consumed. The rate of N_2O production after NO_2^- addition in COD/N = 4 cultures was lower than that observed in COD/N = 11 (0.024±0.007 and 0.15±0.002 mmol-N/gCOD*h, respectively) (**Table 6.2.**). However, cultures on COD/N = 4 medium accumulated 21.3% of the consumed NO_3^--N mass as N_2O-N, while cultures on COD/N = 11 medium accumulated 6.8%. Hence, cultures on COD/N = 4 medium yielded a large N_2O concentration at 0.47±0.045 mmol-N/L.

As shown in **Figure 6.13.**, cells of cultures on COD/N = 11 medium assimilated acetate and nitrate at a high rate (0.7±0.3 mmol-Ac/gCOD*h and 1.73±0.08 mmol-n/gCOD*h). These cells presented flux through biosynthetic pathways for amino acids and fatty acid synthesis. Results from the PAPi analysis were comparable. The central carbon pathway was active and, by reducing ubiquinone-8 (UQ8) to ubiquinol-8 ($UQ8H_2$), delivered electron equivalents to the electron transport chain as succinate, NADH and $FADH_2$, at rates of 1.41, 3.50 and 0.06 mmol/gCOD*h, respectively. In contrast,

cells of cultures on COD/N = 4 medium assimilated acetate and nitrate slowly (0.133±0.05 mmol-Ac/gCOD*h and 0.11±0.022 mmol-n/gCOD*h). Although the central carbon pathway was active, it delivered electrons to denitrification reactions at low rates (0.04 mmol/gCOD*h) through succinate oxidation to fumarate only. However, fatty acid oxidation (i.e. oactadecanoic and hexadecanoic acid oxidation) was active and delivered electrons to denitrifying reactions through NADH and $FADH_2$ oxidation at rates of 0.17 and 0.14 mmol/gCOD*h.

The SMN model is based on biochemical information from four species of denitrifying bacteria. These species are commonly and abundantly detected in denitrifying bioreactors (Daims and Wagner, 2010) and have been detected in the sludge from Mangere Wastewater Treatment Plant in previous studies (Biswas et al., 2009). The SMN model for denitrifying organisms (**Figure 6.9.**) was constructed using a lumped approach. The model's core reactions were common for the four reference organisms, but the model also contained reactions particular to each of the reference species. The modelled metabolic network, which was based on biochemical information for denitrifying bacteria, did not contain pathways for some of the secondary metabolites identified on GC-MS metabolite profiles. Those not included were N2-acetyl-L-lysine, L-ornithine, benzoic acid, nicotinic acid, N-Acetyl-glutamic acid, putrescine, pyroglutamic acid, quinic acid, p-toluic acid.

PAPi and FBA predictions of pathway activity based on metabolite profiles indicate that greater production of N_2O observed in acetate-starved cultures (COD/N = 4) was due potentially to the utilization of intracellular carbonaceous compounds (i.e. fatty acids) as electron donors for the reduction of nitrogenous compound (**Figure 6.13.** and **6.14.**). Because intracellular fatty acid oxidation is low in comparison to other carbon sources (Tchobanoglous et al., 2003), electron equivalents were delivered to nitrogen reduction reactions (N) at a low rate for a prolonged period of time. Electrons were therefore scarce, and insufficient to completely reduce NO_3^- and NO_2^-, induced by the spike to N_2 in NirK, qNor and Nos reactions. This state of chronic electron scarcity on denitrifying cells propitiated continuous competition for electrons between qNor and Nos reactions, resulting in a high accumulation of N_2O (0.47±0.045 mmol-N/L). Chronic electron scarcity did not occur in cells on acetate abundant cultures COD/N = 11. N_2O production in these cultures was sharp (at high rates of 0.15±0.002 mmol-N/gCOD*h) and transient, yielding a maximum accumulation of 0.14±0.03 mmol-N/gCOD*h.

Independently of growth medium COD/N ratio, N_2O did not accumulate on cultures not spiked with NO_2^- solution. FBA of these cultures indicated that in non-spiked cultures the acetate assimilated by cells provided enough electron equivalents for the complete reduction of NO_3^- to N_2, with the effect that no accumulation of N_2O was apparent. When cultures were spiked with NO_2^--saturated solution, growth medium COD/N ratio in fact decreased. In this case, available carbon source (acetate) was not enough to provide electron equivalents to completely reduce the available NO_3^- and NO_2^- to N_2, resulting therefore in the presence of N_2O accumulation.

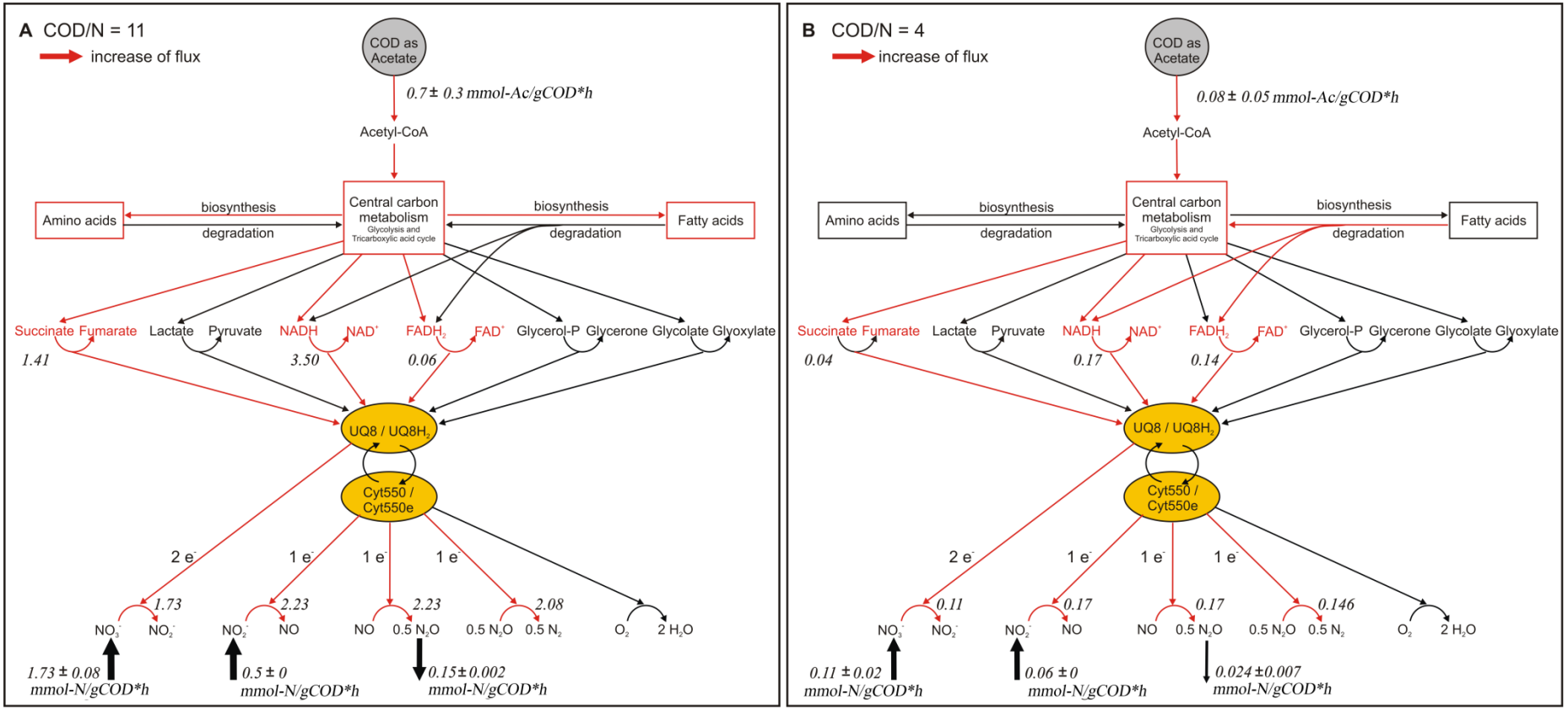

Figure 6.14. Simplified metabolic network and predicted fluxes of the electron transfer system in cells of denitrifying cultures. The figures depicts metabolic rate calculations (in mmol/gCOD*h) during the period maximum N_2O productivity of cultures (indicated as the sampling point on Figure 6.10.).

6.4. Concussions

This chapter describes how metabolite profiling and SMN modelling were used to illustrate the metabolic state of microbial cells in denitrifying cultures producing N_2O. The application of both techniques provided a powerful combination of experimental and computational approaches to quantifying metabolic activity in microbial cultures. In this case N_2O production in denitrification was studied experimentally in laboratory conditions, as opposed to the previous computational studies on N_2O production in nitrification described on Chapters 4 and 5. The most significant conclusions drawn from this experimental-computational research are the following:

- Denitrifying biomass consuming carbon substrates at a low rate is susceptible to the production of more N_2O than biomass with a high carbon substrate consumption rate.

- High nitrite concentrations trigger N_2O accumulation in denitrifying cultures because available electron donors (carbon source) are too limited to completely reduce NO_3^- and NO_2^- to N_2.

- Denitrifying cultures operated at low COD/N ratio produce more N_2O, and for longer periods of time, than cultures operated at high COD/N ratio.

- Denitrifying cultures operated at low COD/N ratio are susceptible to N_2O production after an environmental perturbation, due a lack of electron equivalents to completely reduce NO_3^- to N_2.

- Low COD/N ratio conditions minimize amino and fatty acid concentration in denitrifying cells, and under these conditions cells are depleted of carbon-rich metabolites and therefore electron equivalent donors. Even though long chain fatty acids (i.e. palmitoleic, undecanoic, margaric, octanoic, palmitic, and gamma-linolenic acids) are detected, indicating the presence of storage compounds and therefore of potential electron donors.

- Electron competition between denitrifying enzymes and subsequent N_2O accumulation is enhanced by the utilization of slow, degradable, carbon sources, such as fatty acids.

CHAPTER SEVEN
Discussion and conclusions

The principal aim of this doctoral research was to establish a relationship between the activity of N_2O production pathways and operational parameters of BNR processes. This aim was successfully achieved through an integrated computational and experimental research approach investigating N_2O production in nitrifying and denitrifying microbial cultures.

The importance of this research lies in the generation of a deeper understanding of why environmental conditions in nitrification and denitrification processes lead to N_2O emissions; and in providing a theoretical foundation for developing guidelines to minimize N_2O emission from BNR processes in wastewater treatment plants (WWTPs). The value of reducing N_2O emissions from WWTPs lies in its environmental benefits, i.e. reducing greenhouse gas (GHG) emissions, a plant's carbon footprint and nitrogenous water pollutants (NH_4^+ and NO_3^-); and generating GHG credits that can also offset plant operational or upgrade costs. We know that the amount N_2O-N emitted from BNR processes in full-scale WWTPs is estimated at between 0.6 and 20% of influent N load, averaging 3.7±2.7% (Ahn et al., 2010; Foley et al., 2010). N_2O emissions of only 1% will increase a WWTP's carbon footprint by 30% (de Hass and Hartley, 2004). It follows that at average values (3.7%), N_2O emissions would double the carbon footprint generated by WWTP operation. Under a GHG emission credit scheme, such as the one proposed by (Wang et al., 2011), Mangere WWTP (Auckland City wastewater treatment facility) could obtain from $90,000 to $360,000 US dollars per year for reducing its N_2O emission to less than 0.1% (0.001 kg N_2O-N/kg $N_{influent}$), depending on the market price of GHG credits (nowadays ranging between 10 and 40 USD/ton CO_2 equivalent).

Microbial metabolism is the most significant process in N_2O emission from soils (Wuebbles, 2009). Agricultural soil is the largest source of N_2O emissions in New Zealand and makes up 15% of the total greenhouse gasses emitted per year (N.Z. MfE, 2013). The relevance of this research lies in the fact that the knowledge derived from it can be adapted to design management or fertilization strategies for soils in agriculture. It is evident then that there is real potential to reduce soil N_2O emission by manipulating nitrification and denitrification processes.

In addition, this research introduces SMN modelling and metabolomics (metabolic profiling) into environmental engineering practice. It uses computational and analytical methods to investigate complex metabolic phenomena in biological processes. SMN modelling formalizes vast quantities of biological data into flexible mathematical models; while metabolomics provides analytical measurements of hundreds of metabolic compounds. Therefore, these powerful techniques provide meaningful and accurate information about true cell phenotype.

7.1. Linking BNR operation parameters to microbial N_2O production

From the simulation and experimental studies of this research, it can be concluded that different operational conditions of BNR processes that lead to changes in environmental availability of electron donors or acceptors cause an imbalance between production and consumption of electron equivalents in microbial nitrifying and denitrifying cells, and promotes N_2O production or accumulation as a consequent by-product of the metabolic adjustment to those imbalances. In nitrification processes, an excess of electron equivalent production leads to N_2O formation and subsequent emission. In contrast, for denitrification processes, insufficient electron equivalent production results in N_2O accumulation and subsequent emission.

Figure 7.1. is a plot of the specific N_2O production rate (sN_2OPR) observed in all BNR cultures analysed (n=15) related to the ratio between electrons equivalents (e^- eq.) produced and consumed by culture biomass (mmol e^- $eq._{produced}$/mmol e^- $eq._{consumed}$) during respiration of nitrogenous compounds. This ratio is obtained by dividing the rate of consumption of electron donor by the rate of consumption of final acceptor (O_2 or NO_3^-) observed in cultures, each rate of consumption having been multiplied by the theoretical amount of electron equivalents that each donor/acceptor can produce or consume in the oxidation or reduction process (in units mmol e^- $eq/mmol_{substrate}$). (See Equation 7.1):

$$Ratio = \frac{sUR_{donor} * \left({}^{mmol\ e^- eq}/_{mmol_{donor}} \right)}{sUR_{acceptor} * \left({}^{mmol\ e^- eq}/_{mmol_{acceptor}} \right)} \qquad (7.1)$$

From Figure 7.1 it can be appreciated that high N_2O productivity by nitrifying cultures (shown as diamonds) is related to a ratio higher than one (mmol e^- $eq._{produced}$/mmol e^- $eq._{consumed}$ > 1)., meaning that N_2O is produced and emitted when the respiratory machinery in cells produces more electrons than the ones that the available electron acceptor (O_2) is able to receive. Conversely, positive sN_2OPR are only observed in denitrifying cultures when the e^- eq production/acceptance ratio is less than one (mmol e^- $eq._{produced}$/ mmol e^- $eq._{cunsumed}$ <1). Ratio values close to one would indicate a balanced, non-stressed state and no N_2O production. Although the amount of data used in **Figure 7.1.** is not large, it is promising and coherent with the experimental measurements from the research, our current knowledge of BNR microbes metabolism and reaction stoichiometry and energetics. Further, this data is in line with conclusions of other authors related to N_2O emission as an indicator of a stressed BNR system (Ahn et al., 2011; Yu et al., 2010); and about BNR processes with high N removal efficiency emitting low amounts of N_2O (Ahn et al., 2010; Foley et al., 2010)

A summary of the electron donor and acceptor uptake rates observed from the analysis of the BNR cultures is presented in **Table 7.1.** The estimated rates correspond to the moment of maximum N_2O production of the culture. The table also presents the specific N_2O production rates (sN_2OPR) that are plotted in **Figure 7.1.**, along with the electron equivalents produced and accepted and the e^- $eq._{produced}$/e^- $eq._{consumed}$ ratio. It is interesting to note that the highest sN_2OPR values were observed

from nitrifying cultures under transient anoxic-oxic conditions (green boxes in **Table 7.1.**), whilst data points from non-perturbed conditions were lower, suggesting that significant electron equivalent imbalance exists in cells in transient condition.

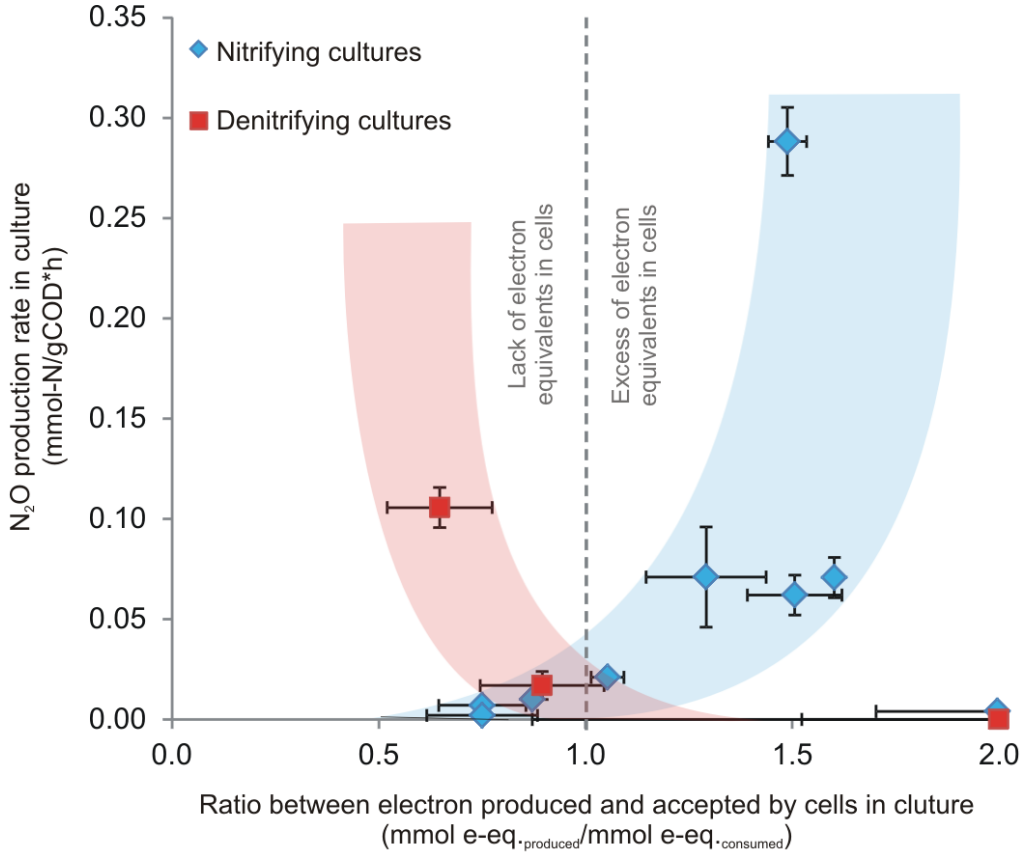

Figure 7.1. N_2O production rate related to the ratio between electrons produced and accepted by the cultured cells

Causes of electron donor and acceptor imbalance could be due the availability of enzymes involved on nitrogen respiration and energy generation but most importantly on the bio-kinetic properties of such enzymes. Enzyme availability would be related to genetic, transcriptional and post transcriptional regulation, while kinetic properties would be related to substrate concentrations and affinity constants to enzyme's substrates. In AOB, NOB and denitrifying cells, N_2O is formed on the essential pathways of energy generation. Therefore enzymes of such pathways would be always present in live cells and constantly synthetized independently of the given environmental condition. Consequently gene expression or protein presence patters would not be directly related to electron imbalances. In contrast kinetic properties of enzymes would be playing a determining role on electron availability imbalances and therefore on N_2O formation under a given environmental condition. Particularly the

electron affinity constant of terminal oxidizes in AOB, NOB and denitrifying microbes would be key to explain correlations between N_2O formation rates and environmental conditions. Due the above argument, experimental efforts should focus on determine the bio-kinetic properties of such enzymes in microbial populations.

Table 7.2 and **Figure 7.2** are graphic and written summaries of the main findings of the three research studies designed to achieve the three main research objectives. They are described in Chapters Four, Five and Six, respectively. The conclusions derived from these studies are described below.

7.1.1. N_2O production pathways in pure AOB cultures

The first research objective was to understand how operational parameters regulate N_2O production pathways in AOB. Flux balance analysis (FBA) of *Nitrosomonas europaea* pure cultures revealed that N_2O production and emission occur as an electron sink mechanism in ammonia oxidizing cells. The unlimited availability of electron donors (NH_4^+) combined with a lack of electron acceptors (O_2) triggers nitrifier denitrification as an electron sink pathway. When electron donor depletion is accompanied with a decrease in electron acceptor concentration such that the intracellular electron equivalents generated are not enough to activate nitrifier denitrification pathway, NO/N_2O production through the hydroxylamine oxidoreductase pathway can be expected. In the transition to anoxic conditions, a leak of NO from the HAO-mediated reaction occurs due to limited availability of electron acceptors to completely oxidize NO to HNO_2. The transition from anoxic to oxic conditions results in baseline N_2O production via the hydroxylamine oxidoreductase pathway, but the total amount of N_2O emission is dependent upon activation of the nitrifier denitrification pathway. The FBA of *N. europaea* metabolism also indicated that NO and N_2O emissions are partially mitigated by the NO oxidation to NO_2^- reaction catalysed by cytochrome P460.

Table 7.1. List of analysed experimental microbial cultures and substrate uptake rates observed at the moment of the culture's maximum N_2O production. Data in the grey columns is plotted in **Figure 7.1.** Data in the green boxes corresponds to the anoxic-oxic transition condition

BNR process	Experimental culture reference	e^-donor uptake rate mmol/gCOD*h	e^- acceptor uptake rate mmol/gCOD*h	sN_2OPR mmol/gCOD*h	mol e^- eq /mol_{donor}	e^- eq. produced	e^- eq. accepted	Ratio e^- $eq._{produced}$ / e^- $eq._{accepted}$
NH_4^+ oxidation to NO_2^-	Previously published by (Yu et al., 2010)	2.619±0.18	3.144±0.3	0.2882±0.017	6	18.719±1.08	12.575±1.2	1.489±0.04
	Previously published by (Yu et al., 2010)	1.1789±0.09	1.5719±0.1	0.0707±0.01	6	10.074±0.55	6.288±1.4	1.602±0.01
	Previously published by (Ahn et al., 2011)	2.13±0.84	2.72±1.6	0.017±0.014	6	19.32±5.04	8.52±6.4	2.268±0.1
	Previously published by (Law et al., 2012)	10.2±0.106	5.43±0.33	0.010±0.0017	6	35.580±0.6	40.80±1.32	0.872±0.01
	Previously published by (Law et al., 2012)	10.25±0.049	6.7±0.54	0.021±0.0013	6	43.2±0.29	41.0±2.16	1.054±0.04
	Previously published by (Law et al., 2012)	11.73±0.042	11.28±1.12	0.062±0.01	6	70.68±0.25	46.92±4.48	1.506±0.11
NH_4^+ oxidation to NO_3^-	Previously published by (Ahn et al., 2011)	2.82±0.35	2.44±0.81	0.004±0.0028	8	22.520±2.8	11.280±3.24	1.996±0.29
	Previously published by (Ahn et al., 2011)	2.81±0.32	1.44±0.11	0.071±0.025	8	14.520±2.56	11.240±0.44	1.292±0.14
	Previously published by (Wunderlin et al., 2013)	0.26±0.003	0.1±0.01	0.002±0.002	8	3.80±0.024	1.040±0.04	3.654±0.09
NO_2^- oxidation to NO_3^-	Previously published by (Wunderlin et al., 2013)	0.06±0	0.09±0.01	0.007±0.0002	2	0.180±0	0.240±0.04	0.750±0.10
NH_2OH oxidation to NO_x	Previously published by (Wunderlin et al., 2013)	0.04±0.004	0.03±0.013	0.002±0.004	4	0.12±0.016	0.160±0.052	0.750±0.13
NO_3^- reduction to N_2	Experiment performed as part of this doctoral research	3.1655±0.2	1.6831±0.028	0.0000±0.001	8	25.324±0.8	8.415±0.14	3.009±0.47
	Experiment performed as part of this doctoral research	0.4930±0.3	1.2183±0.08	0.1056±0.005	8	3.94±1.2	6.092±0.4	0.647±0.12
	Experiment performed as part of this doctoral research	0.1877±0.2	0.0922±0.02	0.0000±0.001	8	1.5±0.2	0.461±0.1	3.259±2.38
	Experiment performed as part of this doctoral research	0.0563±0.0014	0.0775±0.022	0.0169±0.007	8	0.451±0.022	0.50±0.11	0.89±0.14

7.1.2. N_2O production in nitrifying mixed microbial cultures

After studying the basic mechanism of N_2O production in pure cultures of AOB, the relationship between N_2O production and operational parameters in nitrifying mixed cultures was investigated applying a model simulation approach. The reconstruction of eight SMN models (four for AOB and four for NOB species) highlighted that genomes of all the species modelled contain copies of the *nirK*, *cyp*, *hmp* genes, which encode for enzymes with nitric oxide oxidase activity (NO oxidation to NO_2^-), suggesting that this reaction is an important mechanism to deal with NO accumulation in nitrifying microbial communities. The SMN of each species modelled was used to formulate a nitrifying community model using a multi-compartment approach. Monte Carlo random sampling simulations using the community model indicated that activation of NO oxidation reactions satisfy the mass and energy balance of nitrifying mixed cultures performing ammonia oxidation to nitrate and nitrite. In view of this, NO oxidation to NO_2^- reactions were allowed to occur without constraints for the rest of the simulation. Afterwards, the model was used to define expected sN_2OPR with respect to electron donor and acceptor uptake rates. The range of N_2O production rates estimated for ammonia oxidation to nitrate processes was from 0 to 0.02 mmol-N/gCOD*h, maximum value being expected only at NH_4^+ concentrations above 35 mg-N/L. In contrast, the range of N_2O production rate estimated for ammonia oxidation to nitrite processes was from 0 to 0.13 mmol-N/gCOD*h, with expected maximum value only at NH_4^+ concentrations above 30 mg-N/L. From this data it was concluded that by consuming NO_2^- and NO produced by AOB, NOB cells have the ability to contribute to the reduction of N_2O formation in full nitrification processes. In this case, both molecules would be used as electron donors in NOB metabolism. Independently of process operation conditions, AOB and NOB species richness and abundance profiles were found to affect the amount of N_2O produced in a given nitrification process.

An important conclusion from the second study was that in ammonia oxidation to nitrite processes, the N_2O production rate was correlated in positive linear fashion to the cell's ammonium uptake rate, in line with the correlations found by (Law et al., 2012). However, the intercept to y axis value of the line formed with this correlation is inversely related to oxygen uptake rates. This means that the oxygen uptake rate affects this correlation by modifying the minimum value of the ammonium uptake rate required before N_2O production begins to be observed. For example, at an oxygen uptake rate of 2 mmol-O_2/gCOD*h, N_2O production starts at an ammonium uptake rate of 0.5 mmol-N/gCOD*h. Whereas, at an oxygen uptake rate of 15 mmol-O_2/gCOD*h, N_2O production starts at an ammonium uptake rate of 10 mmol-N/gCOD*h.

7.1.3. N_2O accumulation in denitrifying mixed microbial cultures

In the third study on experimental denitrifying cultures and metabolite profiles, of culture biomass was used to investigate the production of N_2O in denitrification as a function of medium carbon to nitrogen ratios (COD/N) and high nitrite concentrations. Metabolite profiling and FBA of denitrifying cultures revealed that N_2O accumulation and emission occur due to an electron equivalent depletion state in

denitrifying cells. Medium COD/N ratios below 4 impose a condition where the lack of electron donors yields an incomplete nitrate/nitrite reduction to N_2, leading to N_2O accumulation in the culture. Interestingly, an increase of nitrite concentration does in fact decrease the medium COD/N ratio, therefore accentuating the imbalance between the low electron equivalent production and high electron acceptor availability, once again yielding an incomplete nitrate/nitrite reduction to N_2.

Denitrifying biomass consuming carbon substrates at low a COD/N ratio tends to produce more N_2O than biomass with a high carbon substrate consumption rate. Not only do these denitrifying cultures produce more N_2O, they also produce it for longer periods of time than cultures operated at high COD/N ratios. This is due to a chronic lack of electron equivalents to completely reduce NO_3^- to N_2. However, at high COD/N ratios, sN_2OPR is higher than at low COD/N ratios. Metabolite profiles revealed that relative abundances of TCA intermediates i.e. citric, fumaric and succinic acids, remained at similar levels in all tested conditions. Moreover, posterior PAPi analysis highlighted that central carbon and glycolysis pathways remained active in all these conditions. The metabolite profiles also revealed that low COD/N conditions minimise amino acid abundance in denitrifying cells. Under these conditions cells are almost depleted of carbon-rich metabolites. However, long-chain fatty acids (palmitoleic, undecanoic, margaric, octanoic, palmitic and gamma-linolenic) are detected at higher relative abundances than amino acids, indicating the presence of storage compounds and, therefore, of potential electron donors. FBA of a SMN model of carbon assimilation pathways in denitrifying microbes was applied to explore whether the utilization of fatty acids as electron donors satisfies the observed substrate uptake and N_2O production rates. FBA confirmed that it is possible to match the rate values measured in experiments by providing fatty acids (palmitic and linolenic) as a carbon source. It can be concluded from this study that electron competition between denitrifying enzymes and subsequent N_2O accumulation is enhanced by the utilization of slow, degradable, carbon sources, such as long-chain fatty acids. In deed storage compounds such as these long-chain fatty acids and PHB's are known to have a low metabolic oxidation rate (Marshall et al., 2013).

7.1.4. Summary of operational conditions and N_2O production pathways

Figure 7.2. and **Table 7.2.** summarise the conclusions from this research on the relationship between BNR operational conditions and dominant N_2O production pathway. To aid interpretation of **Table 7.2.**, the four N_2O production pathways of BNR microbes are listed below:

(i) Aerobic hydroxylamine oxidation pathway in ammonia oxidizers (also known as the HAO mediated NO production pathway)

(ii) Dissimilatory nitrite reduction pathway in ammonia oxidizers (also known as the nitrifier denitrification pathway)

(iii) Dissimilatory nitrite reduction pathway in denitrifiers (also known as incomplete denitrification)

(iv) NO detoxification pathway in ammonia and nitrite oxidizers (can be reductive or oxidative NO oxidation to NO_2^-)

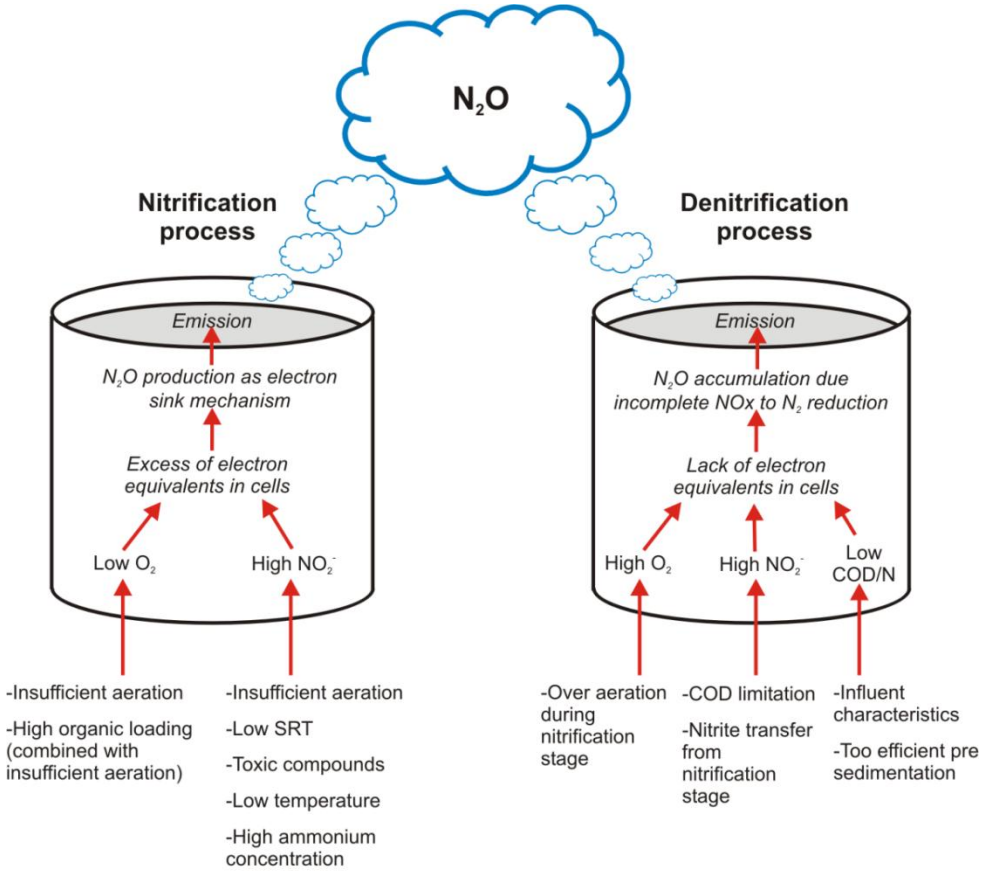

Figure 7.2. Effect of operational parameters on the activation of microbial N_2O production pathways

Table 7.2. Summary of operational conditions, metabolic mechanisms and pathways associated with N_2O emission

Process	Operational parameter/condition	Metabolic mechanism	Dominant N_2O production pathway
Nitrification	Low dissolved oxygen	NO leaks from NO reaction due low rate of terminal oxidize with respect to AMO. Not enough electron equivalent for NirK	HAO mediated NO production pathway
	Anoxic-oxic transition	AMO rate is high with respect to terminal oxidize rate Cyt_{aa3}	Nitrifier denitrification pathway, HAO mediated NO production, and NO detoxification
	High ammonium	High availability of electron equivalents. N_2O production as electron sink mechanism	Nitrifier denitrification pathway HAO mediated NO production, and NO detoxification
	High nitrite	NO_3^- and NirK competes with O_2 and Cyt_{aa3} for electron equivalents	Nitrifier denitrification pathway
	Presence of NOB	NOB consumes NO_{2-} and NO as electron donors	HAO mediated NO production and NO detoxification
Denitrification	High dissolved oxygen	Electron donor, incomplete NO_3^- reduction to N_2	Incomplete denitrification
	High nitrite	Increase of electron acceptor leads to depletion of electron equivalents. Incomplete NO_3^- reduction to N_2	Incomplete denitrification
	Low COD/N ratio	Lack of electron donor. Incomplete NO_3^- reduction to N_2. Use of storage compounds as electron donor	Incomplete denitrification

The research approach allowed us to generate a mechanistic hypothesis of how N_2O is produced in relationship to changes of bioreactor's electron donor and acceptor availability (as described in Section 7.1.). Such mechanistic hypothesis was systematically developed by fitting the SMN models to experimental data in order to quantify metabolic reaction rates. The next step of this research workflow would be to test this hypothesis, validate the proposed relationship between N_2O production and environmental conditions and then use the generated knowledge to design reactor operation strategies to reduce N_2O emissions. For instance, practical implications about reactor operation strategies found during this thesis are following illustrated with three examples:

- From the objective two of this doctoral thesis (about quantification of N_2O production pathways in AOB cells) we now know that it is possible to minimize the production of N_2O triggered by NH_4^+ loading shocks if bioreactor's O_2 set point is determined according to influents NH_4^+ and bioreactors biomass concentrations. So the implementation of operational strategies of bioreactors based on the concept of dynamic O_2 set point can be used to mitigate N_2O emissions.
- Various previously published experiments showed that full nitrification processes produce less N_2O than partial nitrification process. From the results generated during the objective three of this thesis (about modelling nitrifying microbial communities, i.e. Figures 5.7. and 5.8.) we now have a clearer picture of how much more N_2O (from 250 to 500% more) can be produced from partial nitrification in comparison to full nitrification. This information can be used to support decision making procedures about which process implement on a full scale treatment system.
- From the fourth objective (investigating the effect of medium COD/N ratio on N_2O production by denitrifiers) we now know that at limiting or low COD/N ratios do not necessary make denitrifiers produce N_2O but put them on a susceptible metabolic state to do so. In this case process operation strategies would again really on maintain a balance between carbon and nitrogen substrates in reactor considering its concentration of biomass

7.2. Importance of gene expression and enzyme kinetics

The estimated rates of metabolic reaction highlight that uptake rates for electron acceptor and donor molecules determine the amount of N_2O produced in the nitrification and denitrification process. However, it is important to emphasize that metabolic reaction occurrence is governed by the following biological conditions:

(i) substrate and enzyme availability
(ii) mass and charge conservation in the network
(iii) reaction thermodynamics
(iv) amount of biomass present in culture
(v) gene expression of catalytic enzyme and
(vi) enzyme kinetic properties (defined with the parameters affinity constant to substrate (K_s) and maximum reaction rate (v_j^{max} or μ_j^{max}));

As described in the following paragraphs, SMN models capture the effect of the first four conditions. However, additional equations and parameters must be added to models in order to capture the effect of the last two conditions.

Metabolic reactions only occur if substrates are present in the microenvironment of the cells or if they are produced from other reactions. This condition is captured by the SMN models by entering the initial uptake rates of substrates and nutrients. The enzyme availability condition is satisfied since SMNs are reconstructed from genetic information that validates the existence of gene encoding for the catalytic enzyme in the modelled species. Mass conservation further limits the possible reaction products and their stoichiometry; and thermodynamics constrains reaction directionality (Lewis et al., 2012).

The amount of active biomass in a culture is captured in the SMN models by normalizing all reaction rates by the amount of total biomass in the simulated culture, so that all model estimations provide rates per unit of biomass (gDW, gCOD or gVSS), thus facilitating the interpretation of estimated data. The rate of biomass reaction provides an estimation of growth rate due to the fact that this reaction drains exactly 1.0 g of metabolite mass (i.e.. the total amount of protein, DNA, RNA, carbohydrate, lipid and other components in biomass) from the system, and the resulting biomass flux equals the growth rate (in units of $hour^{-1}$) (Oberhardt et al., 2009).

In the context of this research, the amount of biomass present in a given BNR culture is crucial to understanding N_2O emission. Much variability has been observed in the amount of N_2O emitted from BNR (measured as kg N_2O-N/kg $N_{influent}$) (Ahn et al., 2010; Foley et al., 2010). However, in order to quantitatively relate the effect of operational conditions to the amount of N_2O emitted, it is important to take into account the quantity of biomass that is exposed to those conditions and producing N_2O. For example, a process that emits 0.01 kg N_2O-N/kg $N_{influent}$ and has 2 gCOD of biomass is more efficient on mitigating environmental changes than a process that emits the same amount of N_2O, but has 0.5 gCOD of biomass. Clearly, the biomass in the second system is more stressed than that in the first.

As regards the gene expression of catalytic enzymes, the SMN models developed in this research assume that all the enzymes that catalyse for the metabolic reactions modelled were available in cells of the analysed cultures. This assumption is not necessarily true, however, as it is not known whether the cell gene and protein expression patterns of catalytic enzymes are consistent with the predicted pathway usage. Therefore, quantification of the expression of genes and proteins of respiratory enzymes in AOB, NOB and DEN cells are required in order to increase the certainty of the model's predictions. This can be achieved through methods such as q-RT-PCR and transcriptomics (e.g. microarrays) and proteomics (e.g. 2-D electrophoresis and LC-MS) (Ahn et al., 2011; Lewis et al., 2010; Yu et al., 2010). SMN models can capture gene and protein expression information by including gene–protein-reaction (GPR) relationships with the AND/OR associations of Boolean logic (Oberhardt

et al., 2009). The inclusion of the GPR relationships facilitates the characterization of the genotype to phenotype relationship. Reactions in the *S* matrix are linked to genes that encode the associated enzymes. This association allows for the analysis of the effects of gene knockouts and transcriptional regulation of metabolism. For example, in Boolean logic terms, Isozymes have an "OR" relationship as they can catalyse independently. Subunits of a protein complex can be associated with an "AND" relationship, as both subunits are required to catalyse a specific reaction. Once GPR relationships are included in the model, simulation algorithms, such as parsimonious FBA (pFBA), can be used to run simulations incorporating experimental transcriptomics and proteomic information (Lewis et al., 2010). Omics data sets and the computed solutions can be compared in the context of network functions. Transcripts, proteins and metabolites found in the omics data sets can be mapped onto the reconstructed SMN. Computed SMN model solutions can also be represented on the network map and compared with the omics data. Comparative statistical analysis can then be performed (Lewis et al., 2010).

The kinetic properties of enzymes that directly use nitrogenous compounds or oxygen as substrates determine the amount of N_2O produced in relation to a given substrate concentration. Kinetic properties specifically refer to substrate affinity constants (K_s) and maximum reaction rates (v_j^{max}). Previous simulation studies, based on AS modelling and Monod kinetics in N_2O production in nitrification processes, showed that v_{HAO}^{max} of hydroxylamine oxidoreductase (HAO) and the affinity constant for oxygen (K_{O2}) by the terminal oxidase cytochrome aa3 (Cyt_{aa3}) are key parameters for predicting liquid phase N_2O concentration (Ni et al., 2011; Ni et al., 2013). The affinity constant for electron equivalents $K_{e.eq.}$ and v_{Nos}^{max} of nitrous oxide reductase (Nos) were shown to be crucial parameters to predict N_2O accumulation in the denitrifying process (Pan et al., 2013). The research findings presented in this thesis were in line with these studies in highlighting that the rates of reactions (and the proportions within them) catalysed by HAO, Cytaa3 and Nos are key determinants of the amount of N_2O produced in BNR processes. However, in the SMN models the rate of metabolic reaction was not mathematically related to substrate concentration present in the cultures analysed, except in the simulation study described in Chapter Five. Nonetheless, v_j^{max} values can be directly incorporated into SMN models as reaction rate constraints α_j or β_j, but the inclusion of an affinity constant requires the extension of the SMN model with Monod kinetic equations.

7.3. SMN models and metabolomics of microbial communities

SMN modelling techniques were applied throughout this research to estimate the metabolic behaviour of microbial communities in BNR processes. Knowledge of the most important microbial guilds involved in the performance of a given mixed microbial culture is a prerequisite to modelling with SMN. Once the functional guild or species is identified, whole-genome sequences in conjunction with detailed physiological experiments enable SMN models to be generated for the organisms or guilds of interest. Determining the abundance of individual microbial guilds in BNR processes is essential to the development of SMN models for microbial communities. Abundance quantification can be

achieved more directly with techniques like fluorescent in situ hybridization (FISH), real time polymerase chain ration (qPCR) and reverse transcriptase qPCR (q-RT-PCR) (Daims et al., 2006; Wagner et al., 2002). Cultivation-independent approaches, such as metagenomics, metatranscriptomics and metaproteomics, target the community as a whole and can also provide insights into species abundance, but they have limited resolution at the species or strain level (Zengler and Palsson, 2012).

The starting point for SMN modelling is information on species genome and gene functions. However, it is important to keep in mind that genome annotations in databases may have errors, and that identifying genes that encode for catalytic enzymes it is not always straight forward. Furthermore, any genome will contain a good portion of genes of unknown function, and large parts of the genome encode proteins involved in processes other than metabolism, such as macromolecule synthesis, transcriptional and translational regulation, replication, signalling, adhesion and repair (Zengler and Palsson, 2012).

SMN modelling efforts of microbes in BNR systems should also focus on identifying suitable objective functions in addition to constraints obtained from experiments (e.g., through gene expression patterns). The solution space of a given model is not entirely an inherent feature of network structure, but also a function of the arbitrarily chosen objectives function and constraints. SMN modelling uses optimization principles to estimate reaction rates of a given metabolic network. Therefore it is important to acknowledge that no single objective can predict experimental data from a cell culture under all possible environmental conditions, then it is important to identify the most relevant objective for each condition. For cultures under nutrient scarcity, cell metabolism normally supports efficient biomass formation with respect to the limiting nutrient. This operational state appears to have evolved under the objective to maximize either the ATP or biomass yield (synonymous to the frequently used maximization of growth rate objective). For cultures under conditions that allow unlimited growth, in contrast, energy production is clearly not optimized *per se* because cells secrete or accumulate large amounts of organic compounds, instead of using them for energy generation (Schuetz et al., 2007). As demonstrated in chapter four, carefully chosen objectives achieve intrinsically good prediction not only of growth physiology, but also of intracellular fluxes without preconditioning the system through additional constraints apart from the experimentally determined substrate uptake and growth rate. Model preconditioning through additional and potentially artificial constraints is not necessary if the appropriate objective function is chosen for a given condition. Invoking additional constraints for suitable objectives achieved only subtle improvements or avoided alternative optima in few cases. In other hand, when combined with particular constraints, even suboptimal objectives could be forced to yield equally accurate predictions for some conditions. Setting of these additional constraints, however, is condition- and objective specific, thus requires considerable *a priori* knowledge or further computational assessment (trough e.g. sensitivity analysis) to be biologically meaningful. In some cases, alternate flux optima are responsible for the apparent discrepancy and in others it is primarily

the specific combination of chosen constraints that explain why good physiology predictions can be achieved with suboptimal objectives.

The metabolite profiling of biomass in wastewater BNR processes yields useful information about the metabolic state of cells in bioreactors, more so than microbial community composition. To the best of the author's knowledge, this research reports for the first time on the application of metabolomic techniques to analyse BNR processes. Microbial community metabolomics (also known as meta metabolomics or environmental metabolomics) applied in this research provided information about the actual metabolic compounds and their concentrations present in the BNR process. Metabolomic measurements report on the actual functional status of the microbial community organisms. These can, in principle, be mechanistically related to organism phenotype, that is, a higher level of biological organization within a single organism. In practical terms, though, such relationships are usually not straightforward and several data analysis steps must be followed before meaningful information can be obtained. Metabolomics focuses more on questions than hypotheses. This approach can lead to the discovery of unexpected relationships and metabolite responses, which in turn can encourage hypothesis generation (Bundy et al., 2009). It follows that an increasing number of applications is being found for metabolomics in the environmental sciences. For example, understanding organismal responses to abiotic stressors, including natural factors like temperature and anthropogenic factors, such as pollution, as well as biomarker development, risk assessment of toxicant, environmental monitoring and investigation of ecological interactions (Bundy et al., 2009; de Lorenzo, 2008; Villas-Bôas and Bruheim, 2007).

The appropriate, rigorous calibration performed on the model means it can be assumed with a high level of confidence that the rates of metabolic reactions estimated with the SMN models developed are a valid representation of the metabolic activity of the cultures analysed. This calibration involved: a) accurate definition of stoichiometric equations based strictly on proven biochemical data by which the chemical compounds and capabilities of mass transformations of the system are defined; b) correct definition of objective function(s) and the solving method of the optimization problem; and c) obtaining high fitness between observed experimental data and model predictions - the model must mimic at least the consumption and production rates of compounds observed in cultures. Most estimated rates of metabolic reactions cannot be measured experimentally and therefore cannot be validated directly. Nonetheless, data from transcriptomics, proteomics, metabolomics and 13C-based metabolic flux analysis (13C-MFA) methods can be used to reduce uncertainty and increase the accuracy of the model's predictions.

Methods for SMN modelling are evolving in the direction of two main fields: a) the modelling of cellular communities; and b) the modelling of the whole cell (Bordbar et al., 2014; Ishii et al., 2004; Zengler and Palsson, 2012). The first has been reviewed and discussed in detail in this thesis. The latter involves the computational encoding of transcriptional, translational and regulatory signal processes, as well protein structures and cell molecular crowding (Palsson, 2009; Zengler and Palsson, 2012).

As the SMN modelling and metabolomic fields become more and more established, the standards, protocols and quality controls that will without doubt be put in place will make these technologies even more accessible and powerful. SMN modelling and metabolomics of microbial communities are tools that have the ability to afford a better understanding of microbial cells and communities. Their potential for application to environmental engineering, and the wastewater treatment industry in particular, is immense, as is already being seen in the pharmaceutical and bio-refinery industries. For instance new strains have been developed using model driven metabolic engineering to increase productivities of eicosapentaenoic acid, docosahexaenoic acid, butanol, etc. of microalgae and bacteria cultures (Oberhardt et al., 2009; Orth et al., 2010; Feist et al., 2009),

7.4. Future research

This research provides a theoretical foundation that explains N_2O formation in nitrification and denitrification processes. Although the objectives of the current study were achieved, there remains considerable scope for basic and applied research to further advance the understanding of N_2O formation in nitrification and denitrification processes and to improve the methods used in this research.

7.4.1 Experimental hypothesis test of sAUR vs sOUR

The relationship between N_2O production rate and the ratio between specific electron donor uptake rate and specific electron acceptor uptake rate requires experimental verification. The FBA of the BNR cultures undertaken in this research highlights the ratio between specific electron donor uptake rate and specific electron acceptor uptake rate as being the causative factor in N_2O production observed in the experiments. This conclusion was derived from analysing 15 independent experimental cultures. However, further specific experiments need to be undertaken to confirm these findings. As explained in section 7.1., causes of electron donor and acceptor imbalance would be determined by the kinetic properties of each enzyme in the nitrogen respiration pathways. Particularly the electron affinity constant of terminal oxidizes in AOB, NOB and denitrifying microbes. Therefore experimental efforts should focus on determining the bio-kinetic properties of such enzymes operation under environmental conditions resembling real BNR processes.

For the sake of practical application mixed-species, nitrifying, continuous cultures would be the best way to experimentally test such biokinetic properties. For example, culture aeration introduces noise in the quantification of liquid-phase N_2O, as N_2O sensors are sensitive to vigorous aeration and N_2O is quickly air-stripped. To resolve this problem a chamber to saturate the culture's feed with oxygen can be coupled to the nitrifying culture vessel operated without aeration. Dissolved oxygen can be regulated in the culture vessel by means of its working volume and air flow in the pre-aeration chamber.

It is important to stress that quantification of ammonia oxidizing, nitrite oxidizing or denitrifying biomass is key to performing the required mass and energy balances to differentiate between N_2O production pathways. A precise quantification of active biomass of specific groups of organisms and guilds can be achieved with molecular techniques, such as q-RT-PCR, FISH or MAR-FISH.

7.4.2. Detection and quantification of NO oxidation genes and transcripts

In order to confirm the participation of enzymatic NO oxidation as an N_2O emission mitigation mechanism, it will be necessary to detect the expression of genes and proteins for cytochrome P460 (C_{P460}), flavohemoglobins (Hmp) and copper-containing nitrite oxidoreductase (NirK) enzyme in AOB and NOB cells in nitrifying cultures. Primers will need to be designed in order to detect these genes in cultures. Full gene sequences of these genes in specific species of AOB and NOB can be obtained from the NCBI internet database.

7.4.3. Environmental metabolomics

As a newcomer to the field of environmental engineering, environmental metabolomics has abundant potential for research. Ground work in standardisation of sampling and sample pre-processing protocols is an early requirement. Standardising these methods will homogenize noise or error at the moment of mass spectrometry analysis of samples and increase statistical robustness of datasets. These protocols must be developed not only for mixed liquor samples, but for sludge, sediment, soil and aqueous samples as well.

Absolute quantification of metabolite concentration will significantly improve the ability of metabolite profiling methods to provide a true picture of the metabolic states in cells. During this research we quantified metabolite abundance in relation to a known concentration of an internal standard. This information was limited to providing insights into cell metabolism. Further insight can be gained by applying absolute metabolite concentration data directly into the SMN modelling framework via Network Embedded Thermodynamic (NET) analysis. This will open the door to robust flux distribution estimation and identification of reactions that are subject to allosteric or genetic regulation (Kümmel et al., 2006a; Kümmel et al., 2006b).

Finally, libraries and mass spectral databases must be built for environmental organic pollutants, such as personal care products, agrochemicals and oil derivatives. The existence of such libraries will speed up the high-throughput identification of microbial transformation products of organic micropollutants and their classification chemical and hazardous properties, so treatment strategies can be improved. The key feature of metabolomic analysis - and metabolite profiling in particular - is the untargeted identification and quantification of small molecules that are the product of cell metabolism. Groups of compounds can then be identified in a single chromatography injection, allowing the discovery of novel undetected compounds.

7.4.4. Dynamic-SMN model of BNR processes

The next step in the development of a computational platform of BNR processes based on SMN models will be to extend the SMN models developed in this study with kinetic equations. This extension will allow us to predict dynamic behaviours and compound concentrations in BNR processes. By definition, FBA of SMN models predicts rates of metabolic reactions at a specific steady state, but it has two major limitations (Mahadevan et al., 2002):

- compound concentrations are not considered and calculated; and
- rates and concentrations cannot be predicted across time.

To deal with this significant limitation it is possible to associate specific reactions within the network to kinetic equations that link compound concentration to a specific rate of the associated reaction (Hjersted et al., 2005; Mahadevan et al., 2002). This method is called Dynamic FBA (dFBA) (Mahadevan et al., 2002). Dynamic simulation of SMN models is commonly performed using a Static Optimization Approach (SOA) (Mahadevan et al., 2002). The analysed time period is divided into several time intervals. An instantaneous optimization problem is solved at the beginning of each time interval, followed by integration over the time period. The optimization problem is solved using linear programming repeatedly during the course of the time period obtain the flux distribution at a particular time interval. The SOA approach for DFBA simulation has been applied successfully to study bioremediation processes with mixed microbial population (Zhuang et al 2011).

Figure 7.3. is a conceptual diagram of the proposed dynamic-SMN model for BNR. The dynamic model is formed with differential and Monod kinetic equations, whereas the stoichiometric model is formulated as a S matrix. The number of microbial and metabolic species appearing in the diagram is arbitrary. The maximum number of microbial and metabolic species depends on the capacity of the computational hardware. Simulation length (hrs.) and simulation step size (hrs.) must be defined. The following sub routines are executed during each simulation step: (i) the metabolite concentrations $[X_j]$ along with the kinetic parameters v_j^{max} and K_j are used in Monod kinetic equations to estimate uptake rate of substratesv_{upatek}; (ii) this rate is used as a constraint of the FBA problem to obtain the flux distribution of the SMN mode; (iii) rates for products and biomass estimated from FBA simulation are used in the differential equations to obtain the change in concentration of metabolites, $\Delta[X_j]$. Only the rates of change of external metabolites are integrated, since all internal metabolites still follow the internal steady state assumption; and (iv) the new concentration $[X]_j^{new}$ at the end of the simulation step is calculated by adding $\Delta[X_j]$ to the original concentration$[X]_j^{old}$. This continues until the simulation length is reached. At each time interval, the flux constraints for each organism vary based on the substrate concentration at that particular time, leading to dynamic variations in the growth rate.

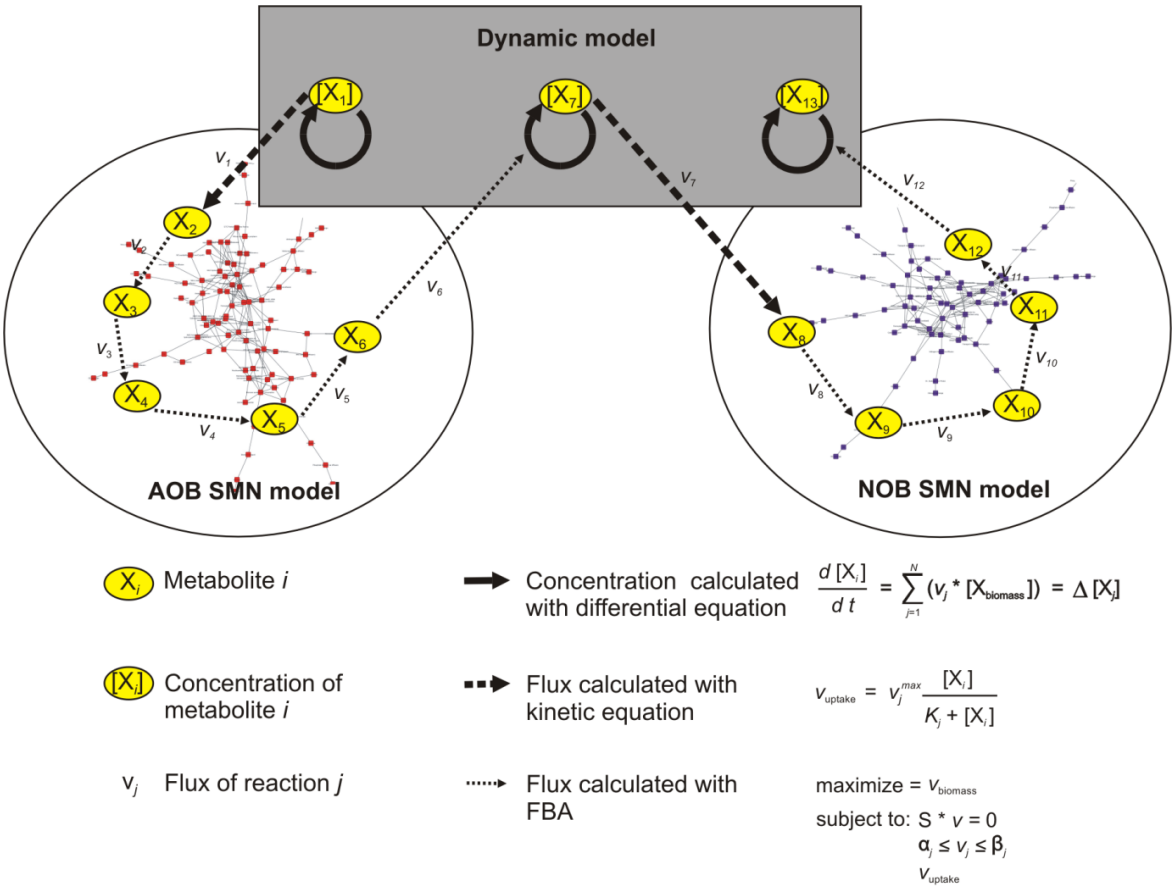

Figure 7.3. Concept of dynamic-SMN model for BNR process

The design of BNR processes requires an understanding of how microorganisms interact not only with each other, but also with their environment (Mahadevan et al., 2011). Hydrological, oxygen transfer and temperature models for bioreactors are well developed and can be implemented on the computational platform. The sequence of flow of data between these models would be as follows:

1. Temperature model (i.e. modified Arrhenius);
2. Oxygen transfer model. (i.e. two-film physical mass transfer);
3. Bioprocess Dynamic model (i.e. Monod and differential equations);
4. Bioprocesses Stoichiometric model (i.e. microbial community SMN); and
5. Hydrodynamic mixing model (i.e. continuous stirred tank reactor (CSRT)).

In conclusion, this research study has undertaken to advance another step in modelling the metabolism of nitrifying and denitrifying microbes. However, additional research is needed if dynamic simulation of BNR microbes into MATLAB®, ASIM® or Biowin® software codes is to be achieved. Validation with experimental datasets would need to be performed to ensure certainty and robustness. This dynamic-SMN computational platform would have the ability to run in real-time on a computer connected to a data-logger, capturing signals from NH_4^+, NO_3^-, NO_2^- and N_2O quantification probes in a BNR reactor. The outcome would be the capacity to provide reliable, online rate measurement and prediction of metabolic reactions of BNR microbes.

References

Aggio RBM, Ruggiero K, Villas-Bôas SG. 2010. Pathway activity profiling (papi): From the metabolite profile to the metabolic pathway activity. Bioinformatics 26:2969-2976.

Agler MT, Wrenn BA, Zinder SH, Angenent LT. 2011. Waste to bioproduct conversion with undefined mixed cultures: the carboxylate platform. Trends Biotechnol 29:70-78.

Ahn JH, Kim S, Park H, Rahm B, Pagilla K, Chandran K. 2010. N2O emissions from activated sludge processes, 2008-2009: Results of a national monitoring survey in the united states. Environmental Science and Technology 44:4505-4511.

Ahn JH, Kwan T, Chandran K. 2011. Comparison of partial and full nitrification processes applied for treating high-strength nitrogen wastewaters: Microbial ecology through nitrous oxide production. Environmental Science and Technology 45:2734-2740.

Ahn JH, Yu R, Chandran K. 2008. Distinctive microbial ecology and biokinetics of autotrophic ammonia and nitrite oxidation in a partial nitrification bioreactor. Biotechnol Bioeng 100:1078-1087.

Allison SD, Martiny JBH. 2008. Resistance, resilience, and redundancy in microbial communities. Proc Natl Acad Sci U S A 105:11512-11519.

APHA. 1995. Standard Methods for Examination of Water and Wastewater. Washington, D.C.:American Public Health Association.

Arp DJ, Sayavedra-Soto LA, Hommes NG. 2002. Molecular biology and biochemistry of ammonia oxidation by Nitrosomonas europaea. Arch Microbiol 178:250-255.

Arp DJ, Stein LY. 2003. Metabolism of Inorganic N Compounds by Ammonia-Oxidizing Bacteria. Crit Rev Biochem Mol Biol 38:471-495.

Beaumont HJE, Hommes NG, Sayavedra-Soto LA, Arp DJ, Arciero DM, Hooper AB, Westerhoff HV, Van Spanning RJM. 2002. Nitrite reductase of Nitrosomonas europaea is not essential for production of gaseous nitrogen oxides and confers tolerance to nitrite. J Bacteriol 184:2557-2560.

Becker SA, Feist AM, Mo ML, Hannum G, Palsson BØ, Herrgard MJ. 2007. Quantitative prediction of cellular metabolism with constraint-based models: The COBRA Toolbox. Nature Protocols 2:727-738.

Begon M, Townsend C,R., Harper J,L. 2005. Ecology: from individuals to ecosystems. Oxford, UK:Blackwell Publishing Ltd.

Biswas K, Kumarsingham S, Turner S. 2009. Effects of an oligocheate blom on the bacterial compositoin in municipal activated sludge reactor. Poster presentation at EXPOSURE

Bordbar A, Monk JM, King ZA, Palsson BO. 2014. Constraint-based models predict metabolic and associated cellular functions. Nature Reviews Genetics 15:107-120.

Brown CE. 2010. The microbial ecology of*Acidovorax temperans*in activated sludge. PhD thesis. The University of Auckland. Access No. THESIS 11-336

Bundy JG, Davey MP, Viant MR. 2009. Environmental metabolomics: A critical review and future perspectives. Metabolomics 5:3-21.

Cabail MZ, Pacheco AA. 2003. Selective one-electron reduction of Nitrosomonas europaea hydroxylamine oxidoreductase with nitric oxide. Inorg Chem 42:270-272.

Çalik P, Sahin M, Taspinar H, Soyaslan ES, Inankur B. 2011. Dynamic flux balance analysis for pharmaceutical protein production by Pichia pastoris: Human growth hormone. Enzyme Microb Technol 48:209-216.

Cantera JJL, Stein LY. 2007. Role of nitrite reductase in the ammonia-oxidizing pathway of Nitrosomonas europaea. Arch Microbiol 188:349-354.

Cascante M, Marin S. 2008. Metabolomics and fluxomics approaches. Essays Biochem 45:67-81.

Chaganti SR, Kim D-, Lalman JA. 2011. Flux balance analysis of mixed anaerobic microbial communities: Effects of linoleic acid (LA) and pH on biohydrogen production. Int J Hydrogen Energy 36:14141-14152.

Chain P, Lamerdin J, Larimer F, Regala W, Lao V, Land M, Hauser L, Hooper A, Klotz M, Norton J, Sayavedra-Soto L, Arciero D, Hommes N, Whittaker M, Arp D. 2003. Complete genome sequence of the ammonia-oxidizing bacterium and obligate chemolithoautotroph Nitrosomonas europaea. J Bacteriol 185:2759-2773.

Chandran K, Stein LY, Klotz MG, Van Loosdrecht MCM. 2011. Nitrous oxide production by lithotrophic ammonia-oxidizing bacteria and implications for engineered nitrogen-removal systems. Biochem Soc Trans 39:1832-1837.

Chubukov V, Gerosa L, Kochanowski K, Sauer U. 2014. Coordination of microbial metabolism. Nature Reviews Microbiology 12:327-340.

Colliver BB, Stephenson T. 2000. Production of nitrogen oxide and dinitrogen oxide by autotrophic nitrifiers. Biotechnol Adv 18:219-232.

Daims H, Wagner M. 2010. The microbiology of nitrogen removal. In: Seviour RJ and Nielsen PH, editors. Microbial Ecology of Activated Sludge. London:IWA Publishing. p 259-280.

Daims H, Taylor MW, Wagner M. 2006. Wastewater treatment: a model system for microbial ecology. Trends Biotechnol 24:483-489.

de Hass D, Hartley KJ. 2004. Greenhouse gas emissions from BNR plant - dowe have the right focus? 5-7.

de Lorenzo V. 2008. Systems biology approaches to bioremediation. Curr Opin Biotechnol 19:579-589.

De Vries S, Suharti, Pouvreau LAM. 2007. Nitric Oxide Reductase: Structural Variations and Catalytic Mechanism. Biology of the Nitrogen Cycle 57-66.

Dias JML, Oehmen A, Serafim LS, Lemos PC, Reis MAM, Oliveira R. 2008. Metabolic modelling of polyhydroxyalkanoate copolymers production by mixed microbial cultures. BMC Systems Biology 2:

Dias JML, Serafim LS, Lemos PC, Reis MAM, Oliveira R. 2005. Mathematical modelling of a mixed culture cultivation process for the production of polyhydroxybutyrate. Biotechnol Bioeng 92:209-222.

Dorian PM. 1995. Bioprocess Engineering Principles. London, UK:Academic Press.

Durot M, Bourguignon P-, Schachter V. 2009. Genome-scale models of bacterial metabolism: Reconstruction and applications. FEMS Microbiol Rev 33:164-190.

Edwards JS, Ibarra RU, Palsson BO. 2001. In silico predictions of Escherichia coli metabolic capabilities are consistent with experimental data. Nat Biotechnol 19:125-130.

Elmore BO, Bergmann DJ, Klotz MG, Hooper AB. 2007. Cytochromes P460 and c'-beta; A new family of high-spin cytochromes c. FEBS Lett 581:911-916.

Endler L, Rodriguez N, Juty N, Chelliah V, Laibe C, Li C, Le Novère N. 2009. Designing and encoding models for synthetic biology. Journal of the Royal Society Interface 6:S405-S417.

Feist AM, Herrgård MJ, Thiele I, Reed JL, Palsson BØ. 2009. Reconstruction of biochemical networks in microorganisms. Nature Reviews Microbiology 7:129-143.

Ferguson SJ. 1998. The*Paracoccus denitrificans*electron transport system: Aspects of organisation, structures and biogenesis. In: Canters GW and Vijgenboom E, editors. Biological Electron Transport Chains: Genetics, Composition and Mode of Operation. Kluwer Academic Publisher. p 77.

Ferguson SJ, Richardson DJ, Van Spanning RJM. 2007. Biochemistry and Molecular Biology of Nitrification. Biology of the Nitrogen Cycle 209-222.

Foladori P, Bruni L, Tamburini S, Ziglio G. 2010. Direct quantification of bacterial biomass in influent, effluent and activated sludge of wastewater treatment plants by using flow cytometry. Water Res 44:3807-3818.

Foley J, de Haas D, Yuan Z, Lant P. 2010. Nitrous oxide generation in full-scale biological nutrient removal wastewater treatment plants. Water Res 44:831-844.

Grady CPLJ, Daugger GT, Lim HC. 1999. Biological wastewater treatment. New York:Marcel Dekker.

Hanaki K, Hong Z, Matsuo T. 1992. Production of nitrous oxide gas during denitrification of wastewater. Water Science and Technology 26:1027-1036.

Helbling DE, Hollender J, Kohler H-E, Singer H, Fenner K. 2010. High-throughput identification of microbial transformation products of organic micropollutants. Environmental Science and Technology 44:6621-6627.

Hjersted J, Henson MA, Mahadevan R. 2005. Dynamic Flux Balance Analysis of Yeast Primary Metabolism in Fed-Batch Culture. AIChE Annual Meeting, Conference Proceedings 9169-9170.

Hollocher TC, Kumar S, Nicholas DJD. 1982. Respiration-dependent proton translocation in Nitrosomonas europaea and its apparent absence in Nitrobacter agilis during inorganic oxidations. J Bacteriol 149:1013-1020.

Hooper AB. 1991. Spectroscopic and rapid kinetic studies of reduction of cytochrome c554 by hydroxylamine oxidoreductase from nitrosomonas europaea. Biochemistry 30:11466-11472.

Hooper AB, Vannelli T, Bergmann DJ, Arciero DM. 1997. Enzymology of the oxidation of ammonia to nitrite by bacteria. Antonie van Leeuwenhoek, International Journal of General and Molecular Microbiology 71:59-67.

IPCC. 2013. Climate Change 2013: The Physical Science Basis. Contribution of Working Group I to the Fifth Assessment Report of the Intergovernmental Panel on Climate Change. Cambridge, United Kingdom and New York, NY, USA:Cambridge University Press.

IPCC. 2001. Climate Change 2001: The Scientific Basis. Cambridge, United Kingdom and New York, NY, USA:Cambridge University Press.

Ishii N, Robert M, Nakayama Y, Kanai A, Tomita M. 2004a. Toward large-scale modeling of the microbial cell for computer simulation. J Biotechnol 113:281-294.

Ishii N, Robert M, Nakayama Y, Kanai A, Tomita M. 2004b. Toward large-scale modeling of the microbial cell for computer simulation. J Biotechnol 113:281-294.

Jorgensen BB. 2000. Bacterial and Marine Biogeochemistry. In: Schulz HD and Zabel M, editors. Marine Geochemistry. Berlin:Springer.

Kaelin D, Manser R, Rieger L, Eugster J, Rottermann K, Siegrist H. 2009. Extension of ASM3 for two-step nitrification and denitrification and its calibration and validation with batch tests and pilot scale data. Water Res 43:1680-1692.

Kampschreur MJ, Picioreanu C, Tan N, Kleerebezem R, Jetten MSM, Van Loosdrecht MCM. 2007. Unraveling the source of nitric oxide emission during nitrification. Water Environ Res 79:2499-2509.

Kampschreur MJ, Tan NCG, Kleerebezem R, Picioreanu C, Jetten MSM, Van Loosdrecht MCM. 2008. Effect of dynamic process conditions on nitrogen oxides emission from a nitrifying culture. Environmental Science and Technology 42:429-435.

Kampschreur MJ, Temmink H, Kleerebezem R, Jetten MSM, van Loosdrecht MCM. 2009. Nitrous oxide emission during wastewater treatment. Water Res 43:4093-4103.

Kaufman DE, Smith RL. 1998. Direction choice for accelerated convergence in hit-and-run sampling. Oper Res 46:84-95.

Kell DB. 2006. Systems biology, metabolic modelling and metabolomics in drug discovery and development. Drug Discov Today 11:1085-1092.

Kim TY, Sohn SB, Kim YB, Kim WJ, Lee SY. 2012. Recent advances in reconstruction and applications of genome-scale metabolic models. Curr Opin Biotechnol 23:617-623.

Kindaichi T, Ito T, Okabe S. 2004. Ecophysiological Interaction between Nitrifying Bacteria and Heterotrophic Bacteria in Autotrophic Nitrifying Biofilms as Determined by Microautoradiography-Fluorescence In Situ Hybridization. Appl Environ Microbiol 70:1641-1650.

Kishida N, Kim JH, Kimochi Y, Nishimura O, Sasaki H, Sudo R. 2004. Effect of C/N ratio on nitrous oxide emission from swine wastewater treatment process. Water Science and Technology 49:359-365.

Kitano H. 2002. Computational systems biology. Nature 420:206-210.

Kleerebezem R, van Loosdrecht MC. 2007. Mixed culture biotechnology for bioenergy production. Curr Opin Biotechnol 18:207-212.

Klitgord N, Segrè D. 2010. Environments that induce synthetic microbial ecosystems. PLoS Computational Biology 6:

Klotz MG, Arp DJ, Chain PSG, El-Sheikh AF, Hauser LJ, Hommes NG, Larimer FW, Malfatti SA, Norton JM, Poret-Peterson AT, Vergez LM, Ward BB. 2006. Complete genome sequence of the marine, chemolithoautotrophic, ammonia-oxidizing bacterium Nitrosococcus oceani ATCC 19707. Appl Environ Microbiol 72:6299-6315.

Kohlstedt M, Becker J, Wittmann C. 2010. Metabolic fluxes and beyond-systems biology understanding and engineering of microbial metabolism. Appl Microbiol Biotechnol 88:1065-1075.

Kostera J, Youngblut MD, Slosarczyk JM, Pacheco AA. 2008. Kinetic and product distribution analysis of NO• reductase activity in Nitrosomonas europaea hydroxylamine oxidoreductase. Journal of Biological Inorganic Chemistry 13:1073-1083.

Kumar S, Nicholas DJD. 1982. A protonmotive force-dependent adenosine-5' triphosphate synthesis in spheroplasts of Nitrosomonas europaea. FEMS Microbiol Lett 14:21-25.

Kümmel A, Panke S, Heinemann M. 2006a. Putative regulatory sites unraveled by network-embedded thermodynamic analysis of metabolome data. Molecular Systems Biology 2:

Kümmel A, Panke S, Heinemann M. 2006b. Systematic assignment of thermodynamic constraints in metabolic network models. BMC Bioinformatics 7:

Law Y, Lant P, Yuan Z. 2011. The effect of pH on N2O production under aerobic conditions in a partial nitritation system. Water Res 45:5934-5944.

Law Y, Ni B, Lant P, Yuan Z. 2012. N2O production rate of an enriched ammonia-oxidising bacteria culture exponentially correlates to its ammonia oxidation rate. Water Res 46:3409-3419.

Lee JM, Gianchandani EP, Papin JA. 2006. Flux balance analysis in the era of metabolomics. Briefings in Bioinformatics 7:140-150.

Lewis NE, Hixson KK, Conrad TM, Lerman JA, Charusanti P, Polpitiya AD, Adkins JN, Schramm G, Purvine SO, Lopez-Ferrer D, Weitz KK, Eils R, König R, Smith RD, Palsson BØ. 2010. Omic data from evolved E. coli are consistent with computed optimal growth from genome-scale models. Molecular Systems Biology 6:

Lewis NE, Nagarajan H, Palsson BO. 2012. Constraining the metabolic genotype-phenotype relationship using a phylogeny of in silico methods. Nature Reviews Microbiology 10:291-305.

Li C, Fang HHP. 2007. Fermentative hydrogen production from wastewater and solid wastes by mixed cultures. Crit Rev Environ Sci Technol 37:1-39.

Lovley DR. 2003. Cleaning up with genomics: applying molecular biology to bioremediation. Nature reviews.Microbiology 1:35-44.

Lu H, Chandran K. 2010. Factors promoting emissions of nitrous oxide and nitric oxide from denitrifying sequencing batch reactors operated with methanol and ethanol as electron donors. Biotechnol Bioeng 106:390-398.

Lu H, Chandran K, Stensel D. 2014. Microbial ecology of denitrification in biological wastewater treatment. Water Res 64:237-254.

Lücker S, Nowka B, Rattei T, Spieck E, Daims H. 2013. The genome of Nitrospina gracilis illuminates the metabolism and evolution of the major marine nitrite oxidizer. Frontiers in Microbiology 4:

Lücker S, Wagner M, Maixner F, Pelletier E, Koch H, Vacherie B, Rattei T, Damsté JSS, Spieck E, Le Paslier D, Daims H. 2010a. A Nitrospira metagenome illuminates the physiology and evolution of globally important nitrite-oxidizing bacteria. Proc Natl Acad Sci U S A 107:13479-13484.

Lücker S, Wagner M, Maixner F, Pelletier E, Koch H, Vacherie B, Rattei T, Damsté JSS, Spieck E, Le Paslier D, Daims H. 2010b. A Nitrospira metagenome illuminates the physiology and evolution of globally important nitrite-oxidizing bacteria. Proc Natl Acad Sci U S A 107:13479-13484.

Mahadevan R, Edwards JS, Doyle FJ. 2002a. Dynamic flux balance analysis of diauxic growth in Escherichia coli. Biophys J 83:1331.

Mahadevan R, Edwards JS, Doyle III FJ. 2002b. Dynamic Flux Balance Analysis of diauxic growth in Escherichia coli. Biophys J 83:1331-1340.

Mahadevan R, Palsson BØ, Lovley DR. 2011. In situ to in silico and back: Elucidating the physiology and ecology of Geobacter spp. using genome-scale modelling. Nature Reviews Microbiology 9:39-50.

Makinia J. 2010. Mathematical Modelling and Computer Simulation of Activated Sludge Systems. London, U.K.:IWA publishing.

Marshall CW, LaBelle EV, May HD. 2013. Production of fuels and chemicals from waste by microbiomes. Curr Opin Biotechnol 24:391-397.

Miller LD, Mosher JJ, Venkateswaran A, Yang ZK, Palumbo AV, Phelps TJ, Podar M, Schadt CW, Keller M. 2010. Establishment and metabolic analysis of a model microbial community for understanding trophic and electron accepting interactions of subsurface anaerobic environments. BMC Microbiology 10:

N.Z. MfE. 2013a. Climate change. New Zealand's Ministry for the Environment (MfE). 2014:

N.Z. MfE. 2013b. New Zealand's Greenhouse Gas Inventory 1990-2011. ME 1113 ubmitted to the United Nations Framework Convention on Climate Change. Wellington:Ministry for the Environment (MfE).

Ni B-, Ruscalleda M, Pellicer-Nàcher C, Smets BF. 2011. Modeling nitrous oxide production during biological nitrogen removal via nitrification and denitrification: Extensions to the general ASM models. Environmental Science and Technology 45:7768-7776.

Ni B-, Ye L, Law Y, Byers C, Yuan Z. 2013a. Mathematical modeling of nitrous oxide (N2O) emissions from full-scale wastewater treatment plants. Environmental Science and Technology 47:7795-7803.

Ni B-, Yuan Z, Chandran K, Vanrolleghem PA, Murthy S. 2013b. Evaluating four mathematical models for nitrous oxide production by autotrophic ammonia-oxidizing bacteria. Biotechnol Bioeng 110:153-163.

Norton JM, Klotz MG, Stein LY, Arp DJ, Bottomley PJ, Chain PSG, Hauser LJ, Land ML, Larimer FW, Shin MW, Starkenburg SR. 2008. Complete genome sequence of Nitrosospira multiformis, an ammonia-oxidizing bacterium from the soil environment. Appl Environ Microbiol 74:3559-3572.

Numata M, Saito T, Yamazaki T, Fukumori Y, Yamanaka T. 1990. Cytochrome P-460 of Nitrosomonas europaea: Further purification and further characterization. J Biochem 108:1016-1021.

Oberhardt MA, Chavali AK, Papin JA. 2009. Flux balance analysis: Interrogating genome-scale metabolic networks. Methods in Molecular Biology 500:61-80.

Oehmen A, Carvalho G, Lopez-Vazquez CM, van Loosdrecht MCM, Reis MAM. 2010. Incorporating microbial ecology into the metabolic modelling of polyphosphate accumulating organisms and glycogen accumulating organisms. Water Res 44:4992-5004.

Orth JD, Thiele I, Palsson BO. 2010. What is flux balance analysis? Nat Biotechnol 28:245-248.

Palsson B. 2009. Metabolic systems biology. FEBS Lett 583:3900-3904.

Pan Y, Ni B-, Bond PL, Ye L, Yuan Z. 2013a. Electron competition among nitrogen oxides reduction during methanol-utilizing denitrification in wastewater treatment. Water Res 47:3273-3281.

Pan Y, Ni B-, Yuan Z. 2013b. Modeling electron competition among nitrogen oxides reduction and N 2O accumulation in denitrification. Environmental Science and Technology 47:11083-11091.

Pan Y, Ye L, Ni B-, Yuan Z. 2012. Effect of pH on N 2O reduction and accumulation during denitrification by methanol utilizing denitrifiers. Water Res 46:4832-4840.

Pardelha F, Albuquerque MGE, Carvalho G, Reis MAM, Dias JML, Oliveira R. 2013. Segregated flux balance analysis constrained by population structure/function data: The case of PHA production by mixed microbial cultures. Biotechnol Bioeng 110:2267-2276.

Pardelha F, Albuquerque MGE, Reis MAM, Dias JML, Oliveira R. 2012. Flux balance analysis of mixed microbial cultures: Application to the production of polyhydroxyalkanoates from complex mixtures of volatile fatty acids. J Biotechnol 162:336-345.

Park JH, Lee SY, Kim TY, Kim HU. 2008. Application of systems biology for bioprocess development. Trends Biotechnol 26:404-412.

Park JM, Kim TY, Lee SY. 2009. Constraints-based genome-scale metabolic simulation for systems metabolic engineering. Biotechnol Adv 27:979-988.

Perez-Garcia O, Villas-Boas SG, Swift S, Chandran K, Singhal N. 2014. Clarifying the regulation of NO/N2O production in Nitrosomonas europaea during anoxic–oxic transition via flux balance analysis of a metabolic network model. Water Res 60:267-277.

Poughon L, Dussap C-, Gros J-. 2001. Energy model and metabolic flux analysis for autotrophic nitrifiers. Biotechnol Bioeng 72:416-433.

Pramanik J, Trelstad PL, Schuler AJ, Jenkins D, Keasling JD. 1999. Development and validation of a flux-based stoichiometric model for enhanced biological phosphorus removal metabolism. Water Res 33:462-476.

Price ND, Schellenberger J, Palsson BO. 2004. Uniform Sampling of Steady-State Flux Spaces: Means to Design Experiments and to Interpret Enzymopathies. Biophys J 87:2172-2186.

R Development Core Team. 2010. R: A language and environment for statistical computing. Vienna, Austria:R Foundation for Statistical Computing.

Rassamee V, Sattayatewa C, Pagilla K, Chandran K. 2011. Effect of oxic and anoxic conditions on nitrous oxide emissions from nitrification and denitrification processes. Biotechnol Bioeng 108:2036-2045.

Ravishankara AR, Daniel JS, Portmann RW. 2009. Nitrous oxide (N2O): The dominant ozone-depleting substance emitted in the 21st century. Science 326:123-125.

Richardson D, Felgate H, Watmough N, Thomson A, Baggs E. 2009. Mitigating release of the potent greenhouse gas N2O from the nitrogen cycle - could enzymic regulation hold the key? Trends Biotechnol 27:388-397.

Rocha BS, Gago B, Barbosa RM, Laranjinha J. 2010. Diffusion of nitric oxide through the gastric wall upon reduction of nitrite by red wine: Physiological impact. Nitric Oxide - Biology and Chemistry 22:235-241.

Rodríguez J, Kleerebezem R, Lema JM, Van Loosdrecht MCM. 2006. Modeling product formation in anaerobic mixed culture fermentations. Biotechnol Bioeng 93:592-606.

Rodriguez-Caballero A, Ribera A, Balcázar JL, Pijuan M. 2013. Nitritation versus full nitrification of ammonium-rich wastewater: Comparison in terms of nitrous and nitric oxides emissions. Bioresour Technol 139:195-202.

Saltelli A, Ratto M, Andres T, Campolongo F, Carboni J, Gatelli D, Saisana M, Tarantola S. 2008. Global Sensitivity Analysis. The Primer. West Sussex, England:Johon Wiley and Sons, Ltd.

Sauer U. 2006. Metabolic networks in motion: 13C-based flux analysis. Molecular Systems Biology 2:

Savinell JM, Palsson BO. 1992. Optimal selection of metabolic fluxes for in vivo measurement. I. Development of mathematical methods. J Theor Biol 155:201-214.

Sayavedra-Soto LA, Arp DJ. 2011. Ammonia-oxidizing bacteria: Their biochemistry and molecular biology
. In: Ward BB, et al., editor. Nitrification. Washington, DC:ASM Press. p 11.

Schalk-Otte S, Seviour RJ, Kuenen JG, Jetten MSM. 2000. Nitrous oxide (N2O) production by Alcaligenes faecalis during feast and famine regimes. Water Res 34:2080-2088.

Scheibe TD, Mahadevan R, Fang Y, Garg S, Long PE, Lovley DR. 2009. Coupling a genome-scale metabolic model with a reactive transport model to describe in situ uranium bioremediation. Microbial Biotechnology 2:274-286.

Schellenberger J, Palsson BØ. 2009. Use of randomized sampling for analysis of metabolic networks. J Biol Chem 284:5457-5461.

Schellenberger J, Que R, Fleming RMT, Thiele I, Orth JD, Feist AM, Zielinski DC, Bordbar A, Lewis NE, Rahmanian S, Kang J, Hyduke DR, Palsson BØ. 2011. Quantitative prediction of cellular metabolism with constraint-based models: The COBRA Toolbox v2.0. Nature Protocols 6:1290-1307.

Schmidt I. 2008. Nitric Oxide: Interaction with the Ammonia Monooxygenase and Regulation of Metabolic Activities in Ammonia Oxidizers. Methods in Enzymology 440:121-135.

Schreiber F, Wunderlin P, Udert KM, Wells GF. 2012. Nitric oxide and nitrous oxide turnover in natural and engineered microbial communities: Biological pathways, chemical reactions, and novel technologies. Frontiers in Microbiology 3:

Schuetz R, Kuepfer L, Sauer U. 2007. Systematic evaluation of objective functions for predicting intracellular fluxes in Escherichia coli. Molecular Systems Biology 3:

Smart KF, Aggio RBM, Van Houtte JR, Villas-Bôas SG. 2010. Analytical platform for metabolome analysis of microbial cells using methyl chloroformate derivatization followed by gas chromatography-mass spectrometry. Nature Protocols 5:1709-1729.

Starkenburg SR, Spieck E, Bottomley PJ. 2011. Metabolism and genomics of nitrite oxidizing bacteria: Emphasis on studies of pure cultures and of *Nitrobacter* species. In: Ward BB, et al., editor. Washington, D.C:ASM Press. p 267-2963.

Starkenburg SR, Arp DJ, Bottomley PJ. 2008a. Expression of a putative nitrite reductase and the reversible inhibition of nitrite-dependent respiration by nitric oxide in Nitrobacter winogradskyi Nb-255. Environ Microbiol 10:3036-3042.

Starkenburg SR, Chain PSG, Sayavedra-Soto LA, Hauser L, Land ML, Larimer FW, Malfatti SA, Klotz MG, Bottomley PJ, Arp DJ, Hickey WJ. 2006. Genome sequence of the chemolithoautotrophic nitrite-oxidizing bacterium Nitrobacter winogradskyi Nb-255. Appl Environ Microbiol 72:2050-2063.

Starkenburg SR, Larimer FW, Stein LY, Klotz MG, Chain PSG, Sayavedra-Soto LA, Poret-Peterson AT, Gentry ME, Arp DJ, Ward B, Bottomley PJ. 2008b. Complete genome sequence of Nitrobacter hamburgensis X14 and comparative genomic analysis of species within the genus Nitrobacter. Appl Environ Microbiol 74:2852-2863.

Stein LY. 2011. Heterotrophic nitrification and nitrifier denitrification<*br* />. In: Ward BB, et al., editor. Nitrification<*br* /> . Washington, DC:ASM Press. p 95.

Stein LY. 2010. Surveying N2O-producing pathways in bacteria. Methods in Enzymology 486:131-152.

Stein LY, Arp DJ, Berube PM, Chain PSG, Hauser L, Jetten MSM, Klotz MG, Larimer FW, Norton JM, Op Den Camp HJM, Shin M, Wei X. 2007. Whole-genome analysis of the ammonia-oxidizing bacterium, Nitrosomonas eutropha C91: Implications for niche adaptation. Environ Microbiol 9:2993-3007.

Stein LY, Yung YL. 2003. Production, isotopic composition, and atmospheric fate of biologically produced nitrous oxide. Annual Review of Earth and Planetary Sciences 31:329-356.

Stolyar S, Van Dien S, Hillesland KL, Pinel N, Lie TJ, Leigh JA, Stahl DA. 2007. Metabolic modeling of a mutualistic microbial community. Molecular systems biology 3:92.

Taffs R, Aston JE, Brileya K, Jay Z, Klatt CG, McGlynn S, Mallette N, Montross S, Gerlach R, Inskeep WP, Ward DM, Carlson RP. 2009. In Silico approaches to study mass and energy flows in microbial consortia: A syntrophic case study. BMC Systems Biology 3:

Tallec G, Garnier J, Billen G, Gousailles M. 2006. Nitrous oxide emissions from secondary activated sludge in nitrifying conditions of urban wastewater treatment plants: Effect of oxygenation level. Water Res 40:2972-2980.

Tchobanoglous G, Burton FL, Stensel HD. 2003. Wastewater Engineering. Treatment and Reuse. New York:Mc Graw Hill.

Terry KR, Hooper AB. 1970. Polyphosphate and orthophosphate content of Nitrosomonas europaea as a function of growth. J Bacteriol 103:199-206.

Thiele I. 2009. A stoichiometric model of Escherichia coli 's macromolecular synthesis machinery and its
integration with metabolism. UC San Diego Electronic Theses and Dissertations

Thiele I, Palsson BØ. 2010. A protocol for generating a high-quality genome-scale metabolic reconstruction. Nature Protocols 5:93-121.

Thiele I, Price ND, Vo TD, Palsson BØ. 2005. Candidate metabolic network states in human mitochondria. Impact of diabetes, ischemia, and diet. J Biol Chem 280:11683-11695.

Thomas DD, Liu X, Kantrow SP, Lancaster Jr. JR. 2001. The biological lifetime of nitric oxide: implications for the perivascular dynamics of NO and O2. Proc Natl Acad Sci U S A 98:355-360.

Tzamali E, Poirazi P, Tollis IG, Reczko M. 2011. A computational exploration of bacterial metabolic diversity identifying metabolic interactions and growth-efficient strain communities. BMC Systems Biology 5:

U.S. EPA. 2014. Inventory of U.S. Greenhouse Gas Emission and Sinks: 1990-2012. Washington, DC, USA.:U.S. Environmental Protection Agency.

U.S. EPA. 2010. Methane and Nitrous Oxide Emission From Natural Sources. Washington, DC, USA.:U.S. Environmental Protection Agency.

Vadivelu VM, Keller J, Yuan Z. 2006. Stoichiometric and kinetic characterisation of Nitrosomonas sp. in mixed culture by decoupling the growth and energy generation processes. J Biotechnol 126:342-356.

Vallero DA. 2010. Environmental Biotechnology: A Biosystems Approach. San Diego:Academic Press. 1 p.

van den Berg RA, Hoefsloot HCJ, Westerhuis JA, Smilde AK, van der Werf MJ. 2006. Centering, scaling, and transformations: Improving the biological information content of metabolomics data. BMC Genomics 7:

van Loosdrecht MCM, Ekama GA, Wentzel MC, Brdjanovic D, Hooijmans CM. 2008. Modelling activated sludge processes. In: Henze M, et al., editor. Biological Wastewater Treatment. Principles, Modelling and Design. London, UK:IWA Publishing. p 361.

van Spanning RJM, Richardson DJ, Ferguson SJ. 2007. Introduction to the biochemistry and molecular biology of denitrification. In: Bothe H, et al., editor. Biology of the nitrogen cycle. Elsevier B.V.

Varma A, Palsson BO. 1994a. Metabolic flux balancing: Basic concepts, scientific and practical use. Bio/Technology 12:994-998.

Varma A, Palsson BO. 1994b. Stoichiometric flux balance models quantitatively predict growth and metabolic by-product secretion in wild-type Escherichia coli W3110. Appl Environ Microbiol 60:3724-3731.

Vilchez-Vargas R, Junca H, Pieper DH. 2010. Metabolic networks, microbial ecology and 'omics' technologies: Towards understanding in situ biodegradation processes. Environ Microbiol 12:3089-3104.

Villas-Bôas SG, Bruheim P. 2007. The potential of metabolomics tools in bioremediation studies. OMICS A Journal of Integrative Biology 11:305-313.

Villas-Bôas SG, Mas S, Åkesson M, Smedsgaard J, Nielsen J. 2005. Mass spectrometry in metabolome analysis. Mass Spectrom Rev 24:613-646.

Wagner M, Loy A. 2002. Bacterial community composition and function in sewage treatment systems. Curr Opin Biotechnol 13:218-227.

Wagner M, Loy A, Nogueira R, Purkhold U, Lee N, Daims H. 2002. Microbial community composition and function in wastewater treatment plants. Antonie van Leeuwenhoek, International Journal of General and Molecular Microbiology 81:665-680.

Wang JS, Hamburg SP, Pryor DE, Chandran K, Daigger GT. 2011. Emissions credits: Opportunity to promote integrated nitrogen management in the wastewater sector. Environmental Science and Technology 45:6239-6246.

Weckwerth W, Morgenthal K. 2005. Metabolomics: From pattern recognition to biological interpretation. Drug Discov Today 10:1551-1558.

Werner JJ, Knights D, Garcia ML, Scalfone NB, Smith S, Yarasheski K, Cummings TA, Beers AR, Knight R, Angenent LT. 2011. Bacterial community structures are unique and resilient in full-scale bioenergy systems. Proc Natl Acad Sci U S A 108:4158-4163.

Whittaker M, Bergmann D, Arciero D, Hooper AB. 2000. Electron transfer during the oxidation of ammonia by the chemolithotrophic bacterium Nitrosomonas europaea. Biochimica et Biophysica Acta - Bioenergetics 1459:346-355.

Wuebbles DJ. 2009. Nitrous oxide: No laughing matter. Science 326:56-57.

Wunderlin P, Lehmann MF, Siegrist H, Tuzson B, Joss A, Emmenegger L, Mohn J. 2013. Isotope signatures of N2O in a mixed microbial population system: Constraints on N2O producing pathways in wastewater treatment. Environmental Science and Technology 47:1339-1348.

Wunderlin P, Mohn J, Joss A, Emmenegger L, Siegrist H. 2012. Mechanisms of N2O production in biological wastewater treatment under nitrifying and denitrifying conditions. Water Res 46:1027-1037.

Yu R, Chandran K. 2010. Strategies of nitrosomonas europaea 19718 to counter low dissolved oxygen and high nitrite concentrations. BMC Microbiology 10:

Yu R, Kampschreur MJ, Van Loosdrecht MCM, Chandran K. 2010. Mechanisms and specific directionality of autotrophic nitrous oxide and nitric oxide generation during transient anoxia. Environmental Science and Technology 44:1313-1319.

Zengler K, Palsson BO. 2012. A road map for the development of community systems (CoSy) biology. Nature Reviews Microbiology 10:366-372.

Zhuang K, Izallalen M, Mouser P, Richter H, Risso C, Mahadevan R, Lovley DR. 2011. Genome-scale dynamic modeling of the competition between Rhodoferax and Geobacter in anoxic subsurface environments. ISME Journal 5:305-316.

Zomorrodi AR, Islam MM, Maranas CD. 2014. D-OptCom: Dynamic Multi-level and Multi-objective Metabolic Modeling of Microbial Communities. ACS Synthetic Biology 3:247-257.

Zomorrodi AR, Maranas CD. 2012. OptCom: A multi-level optimization framework for the metabolic modeling and analysis of microbial communities. PLoS Computational Biology 8:

APPENDIX ONE

SMN model of nitrogen reparation metabolism *in Nitrosomonas europaea*. (Single species model).

	Equations of reactions *j*
Ammonium exchange	[e] : nh4 <==>
O2 exchange	[e] : o2 <==>
Nitrite exchange	[e] : no2 <==>
nitrous oxide exchange	[e] : n2o <==>
nitric oxide exchange	[e] : no <==>
Biomass exchange	[e] : biomass <==>
Phosphate exchange	[e] : pi <==>
dinitrogen exchange	[e] : n2 <==>
H2O exchange	[e] : h2o <==>
Hydrogen exchange	[e] : h <==>
Hydrogen exchange to cytoplasm	[c] : h <==>
Nitrite pool	[p] : hno2 <==>
Hydroxylamine pool	[p] : nh2oh <==>
Cytochrome pool	[p] : cyt552e <==>
Ubiquinol-8 pool	[c] : q8h2[c] <==>
H2O transport via diffusion	h2o[p] <==> h2o[e]
O2 transport via diffusion	o2[p] <==> o2[e]
Phosphate transport via diffusion	pi[p] <==> pi[e]
Ammonium transport via diffusion	nh4[p] <==> nh4[e]
Hidrogen transport via diffusion	h[p] <==> h[e]
niric oxide transport via diffusion	no[p] <==> no[e]
dinitrogen transport via diffusion	n2[p] <==> n2[e]
nitrous oxide transport via diffusion	n2o[p] <==> n2o[e]
Nitrite transport via diffusion	hno2[p] <==> no2[e] + h[e]
Biomass transport	biomass[c] <==> biomass[e]
O2 transport (diffusion)	o2[c] <==> o2[p]
Inorganic phosphate exchange, diffusion	pi[c] <==> pi[p]
Hydrogen transport	h[c] <==> h[p]
NH4 transport (diffusion)	nh3[c] + h[c] <==> nh4[p]
H2O transport via diffusion	h2o[c] <==> h2o[p]
Combination of 2 molecules of NO2 to form N2O4	2 hno2[p] <==> n2o4[p]
Deprotonation of ammonia	nh3[p] + h[p] <==> nh4[p]
AMO Ammonia oxidation to hydroxylamine using ubiquinol as e donor	nh3[p] + o2[p] + q8h2[c] --> nh2oh[p] + h2o[c] + q8[c]
HAO Hydroxylamine oxidation to nitrite 1	nh2oh[p] + cyt554[p] --> noh[p] + cyt554e[p] + 2 h[p]
HAO Hydroxylamine oxidation to nitrite 2	noh[p] + 0.5 cyt554[p] --> no1[p] + h[p] + 0.5 cyt554e[p]
HAO Hydroxylamine oxidation to nitrite 3	no1[p] + h2o[p] + 0.5 cyt554[p] --> hno2[p] + h[p] + 0.5 cyt554e[p]
ETC Partion of electron flow by cyt554	cyt554e[p] + cyt552[c] --> cyt552e[c] + cyt554[p]
ETC Ubiquinone to ubiquinol for AMO	q8[c] + cyt552e[c] + 2 h[p] --> q8h2[c] + cyt552[c]
ETC NADH production by NADH-ubiquinone reductase using ubiquinol	nad[c] + q8h2[c] + 4 h[p] --> nadh[c] + q8[c] + 6 h[c]
ETC proton pump by CytCbc1 reductase using ubiquinol	q8h2[c] + 2 cyt552[p] + 2 h[c] --> 4 h[p] + q8[c] + 2 cyt552e[p]
ETC proton pump by Cytaa3, Oxygen as final electron acceptor OXIC	.5 o2[c] + 4 h[c] + 2 cyt552e[p] --> h2o[c] + 2 h[p] + 2 cyt552[p]
NO2 synthesis from NH2OH + NO	0.5 nh2oh[p] + 0.5 no[p] + 2.5 cyt552[p] + h2o[p] --> hno2[p] + 2.5 cyt552e[p] + 2.5 h[p]
NO availability to NOR and Cytp460	no1[p] --> no[p]

R1 - NIR Nitrite reduction to nitric oxide	hno2[p] + cyt552e[p] + h[p] --> no[p] + cyt552[p] + h2o[p]
R2 - NOR Nitric oxide reduction to nitrous oxide	no[p] + cyt552e[p] + h[p] --> 0.5 n2o[p] + cyt552[p] + 0.5 h2o[p]
ETC ATP transmembrane synthesis (four protons per ATP)	adp[c] + pi[c] + 6.8 h[p] --> atp[c] + h2o[c] + 4.8 h[c]
Protein synthesis from ammonia	2.244 atp[c] + nh3[c] --> 2.244 adp[c] + 2.244 pi[c] + 2.244 h[c] + 0.25 protein[c]
Maintenance ATP consumption (non-growth associated energy consumption)	atp[c] + h2o[c] --> adp[c] + pi[c] + h[c] + m[c]
Biomass synthesis ATP consumption	15 atp[c] + 12 nadh[c] + 0.25 protein[c] + 32 m[c] <==> 15 adp[c] + 12 nad[c] + 15 pi[c] + 15 h[c] + biomass[c]

Metabolite description	Metabolite *i*
Ammonium	nh4[e]
Ammonium	nh4[p]
Ammonia	nh3[p]
Ammonia	nh3[c]
Nitric oxide	no[e]
Nitric oxide HAO	no1[p]
Nitric oxide pool in periplasm	no[p]
Nitrite	no2[e]
Nitrous acid	hno2[p]
Nitrous oxide	n2o[e]
Nitrous oxide pool in periplasm	n2o[p]
O2	o2[e]
O2	o2[p]
O2	o2[c]
H+, Hydrogen Ion/ Proton	h[e]
H+	h[p]
H+	h[c]
H2O	h2o[e]
H2O	h2o[p]
H2O	h2o[c]
Phosphate	pi[e]
Phosphate	pi[p]
Phosphate	pi[c]
Hydroxylamine	nh2oh[p]
Dinitrogen tetroxide	n2o4[p]
Ferrocytochrome c (reduced)	cyt554e[p]
Ferricytochrome c (oxidized)	cyt554[p]
Ubiquinone-8 (oxidized)	q8[c]
Ubiquinol-8 (reduced)	q8h2[c]
Membrane Ferrocytochrome c (reduced)	cyt552e[c]
Membrane Ferricytochrome c (oxidized)	cyt552[c]
Ferrocytochrome c (reduced)	cyt552e[p]
Ferricytochrome c (oxidized)	cyt552[p]
Nicotinamide adenine dinucleotide	nad[c]
Nicotinamide adenine dinucleotide - reduced	nadh[c]
ATP	atp[c]
ADP	adp[c]
dinitrogen	n2[e]
dinitrogen	n2[p]
Nitroxyl	noh[p]
biomass	biomass[e]
biomass	biomass[c]
protein	protein[c]
membrane ensemble	m[c]

APPENDIX TWO

Multi-species SMN model of nitrifying community metabolism. (Multi compartment model).

Reaction description	Equation of reaction *j*
EX. NH4	nh4[e] <==>
EX. O2	o2[e] <==>
EX. NO2	no2[e] <==>
EX. NO3	no3[e] <==>
EX. N2O	n2o[e] <==>
EX. NO	no[e] <==>
EX. N2	n2[e] <==>
EX. NH2OH	nh2oh[e] <==>
EX. Biomass	biomass[e] <==>
EX. Pi	pi[e] <==>
EX. H2O	h2o[e] <==>
EX. CO2	co2[e] <==>
EX. H	h[e] <==>
ECO. Tr1	nh4[e] <==> nh4[a]
ECO. Tr2	nh4[e] <==> nh4[b]
ECO. Tr3	nh4[e] <==> nh4[c]
ECO. Tr4	nh4[e] <==> nh4[d]
ECO. Tr5	nh4[e] <==> nh4[f]
ECO. Tr6	nh4[e] <==> nh4[g]
ECO. Tr7	nh4[e] <==> nh4[h]
ECO. Tr8	nh4[e] <==> nh4[i]
ECO. Tr9	o2[e] <==> o2[a]
ECO. Tr10	o2[e] <==> o2[b]
ECO. Tr11	o2[e] <==> o2[c]
ECO. Tr12	o2[e] <==> o2[d]
ECO. Tr13	o2[e] <==> o2[f]
ECO. Tr14	o2[e] <==> o2[g]
ECO. Tr15	o2[e] <==> o2[h]
ECO. Tr16	o2[e] <==> o2[i]
ECO. Tr17	no2[e] <==> no2[a]
ECO. Tr18	no2[e] <==> no2[b]
ECO. Tr19	no2[e] <==> no2[c]
ECO. Tr20	no2[e] <==> no2[d]
ECO. Tr21	no2[e] <==> no2[f]
ECO. Tr22	no2[e] <==> no2[g]
ECO. Tr23	no2[e] <==> no2[h]
ECO. Tr24	no2[e] <==> no2[i]
ECO. Tr25	no3[e] <==> no3[b]
ECO. Tr26	no3[e] <==> no3[d]
ECO. Tr27	no3[e] <==> no3[f]
ECO. Tr28	no3[e] <==> no3[g]
ECO. Tr29	no3[e] <==> no3[h]
ECO. Tr30	no3[e] <==> no3[i]
ECO. Tr31	n2o[e] <==> n2o[a]
ECO. Tr32	n2o[e] <==> n2o[b]

ECO. Tr33	n2o[e] <==> n2o[c]
ECO. Tr34	n2o[e] <==> n2o[d]
ECO. Tr35	n2o[e] <==> n2o[f]
ECO. Tr36	n2o[e] <==> n2o[h]
ECO. Tr37	no[e] <==> no[a]
ECO. Tr38	no[e] <==> no[b]
ECO. Tr39	no[e] <==> no[c]
ECO. Tr40	no[e] <==> no[d]
ECO. Tr41	no[e] <==> no[f]
ECO. Tr42	no[e] <==> no[g]
ECO. Tr43	no[e] <==> no[h]
ECO. Tr44	no[e] <==> no[i]
ECO. Tr45	n2[e] <==> n2[c]
ECO. Tr46	n2[e] <==> n2[d]
ECO. Tr47	nh2oh[e] <==> nh2oh[a]
ECO. Tr48	nh2oh[e] <==> nh2oh[b]
ECO. Tr49	nh2oh[e] <==> nh2oh[c]
ECO. Tr50	nh2oh[e] <==> nh2oh[d]
ECO. Tr51	biomass[e] <==> biomass[a]
ECO. Tr52	biomass[e] <==> biomass[b]
ECO. Tr53	biomass[e] <==> biomass[c]
ECO. Tr54	biomass[e] <==> biomass[d]
ECO. Tr55	biomass[e] <==> biomass[i]
ECO. Tr56	biomass[e] <==> biomass[f]
ECO. Tr57	biomass[e] <==> biomass[g]
ECO. Tr58	biomass[e] <==> biomass[h]
ECO. Tr59	pi[e] <==> pi[a]
ECO. Tr60	pi[e] <==> pi[b]
ECO. Tr61	pi[e] <==> pi[c]
ECO. Tr62	pi[e] <==> pi[d]
ECO. Tr63	pi[e] <==> pi[i]
ECO. Tr64	pi[e] <==> pi[f]
ECO. Tr65	pi[e] <==> pi[g]
ECO. Tr66	pi[e] <==> pi[h]
ECO. Tr67	h2o[e] <==> h2o[a]
ECO. Tr68	h2o[e] <==> h2o[b]
ECO. Tr69	h2o[e] <==> h2o[c]
ECO. Tr70	h2o[e] <==> h2o[d]
ECO. Tr71	h2o[e] <==> h2o[i]
ECO. Tr72	h2o[e] <==> h2o[f]
ECO. Tr73	h2o[e] <==> h2o[g]
ECO. Tr74	h2o[e] <==> h2o[h]
ECO. Tr75	co2[e] <==> co2[a]
ECO. Tr76	co2[e] <==> co2[b]
ECO. Tr77	co2[e] <==> co2[c]
ECO. Tr78	co2[e] <==> co2[d]
ECO. Tr79	co2[e] <==> co2[i]
ECO. Tr80	co2[e] <==> co2[f]
ECO. Tr81	co2[e] <==> co2[g]
ECO. Tr82	co2[e] <==> co2[h]
ECO. Tr83	h[e] <==> h[a]
ECO. Tr84	h[e] <==> h[b]
ECO. Tr85	h[e] <==> h[c]
ECO. Tr86	h[e] <==> h[d]
ECO. Tr87	h[e] <==> h[i]
ECO. Tr88	h[e] <==> h[f]
ECO. Tr89	h[e] <==> h[g]
ECO. Tr90	h[e] <==> h[h]

NEU. Tr1	nh4[a] <==> nh3[j] + h[j]
NEU. Tr2	o2[a] <==> o2[j]
NEU. Tr3	no2[a] + h[a] <==> hno2[j]
NEU. Tr4	n2o[a] <==> n2o[j]
NEU. Tr5	no[a] <==> no[j]
NEU. Tr6	nh2oh[a] <==> nh2oh[j]
NEU. Tr7	biomass[a] <==> biomass[j]
NEU. Tr8	pi[a] <==> pi[j]
NEU. Tr9	h2o[a] <==> h2o[j]
NEU. Tr10	co2[a] <==> co2[j]
NEU. Tr11	h[a] <==> h[j]
NEU. Tr12	h[a] <==> h[r]
NEU. Tr13	nh3[j] <==> nh3[r]
NEU. Tr14	o2[j] <==> o2[r]
NEU. Tr15	biomass[j] <==> biomass[r]
NEU. Tr16	pi[j] <==> pi[r]
NEU. Tr17	h2o[j] <==> h2o[r]
NEU. Tr18	co2[j] <==> co2[r]
NEU. Tr19	h[j] <==> h[r]
NEU. AMO Ammonia oxidation to hydroxylamine using ubiquinol as e donor	nh3[j] + o2[j] + q8h2[r] --> nh2oh[j] + h2o[r] + q8[r]
NEU. HAO Hydroxylamine oxidation to nitrite 1	nh2oh[j] + cyt554[j] --> noh[j] + cyt554e[j] + 2 h[j]
NEU. HAO Hydroxylamine oxidation to nitrite 2	noh[j] + 0.5 cyt554[j] --> no1[j] + h[j] + 0.5 cyt554e[j]
NEU. HAO Hydroxylamine oxidation to nitrite 3	no1[j] + h2o[j] + 0.5 cyt554[j] --> hno2[j] + h[j] + 0.5 cyt554e[j]
NEU. ETC division of electron flow by cyt554	cyt554e[j] + cyt552[r] --> cyt552e[r] + cyt554[j]
NEU. ETC Ubiquinone to ubiquinol for AMO	q8[r] + cyt552e[r] + 2 h[j] --> q8h2[r] + cyt552[r]
NEU. ETC NADH production by NADH-ubiquinone reductase using ubiquinol	nad[r] + q8h2[r] + 4 h[j] --> nadh[r] + q8[r] + 6 h[r]
NEU. ETC proton pump by CytCbc1 reductase using ubiquinol	q8h2[r] + 2 cyt552[j] + 0 h[r] --> 2 h[j] + q8[r] + 2 cyt552e[j]
NEU. ETC proton pump by Cytaa3, Oxygen as final electron acceptor OXIC	.5 o2[r] + 4 h[r] + 2 cyt552e[j] --> h2o[r] + 2 h[j] + 2 cyt552[j]
NEU. CytP460 NO2 synthesis from NH2OH + NO	0.5 nh2oh[j] + 0.5 no[j] + 2 cyt552[j] + h2o[j] --> hno2[j] + 2 cyt552e[j] + 3 h[j]
NEU. NO availability to NOR and Cytp460	no1[j] --> no[j]
NEU. R1 - NIR Nitrite reduction to nitric oxide	hno2[j] + cyt552e[j] + h[j] --> no[j] + cyt552[j] + h2o[j]
NEU. R2 - NOR Nitric oxide reduction to nitrous oxide	no[j] + cyt552e[j] + h[j] --> 0.5 n2o[j] + cyt552[j] + 0.5 h2o[j]
NEU. Nitric oxide activity by cytochrome C554	no[j] + h[j] + 0.5 cyt554e[j] --> 0.5 n2o[j] + 0.5 cyt554[j] + 0.5 h2o[j]
NEU. ATP production	adp[r] + pi[r] + 6.8 h[j] --> atp[r] + h2o[r] + 4.8 h[r]
NEU. Protein synthesis	2.244 atp[r] + nh3[r] + 4 co2[r] --> 2.244 adp[r] + 2.244 pi[r] + 2.244 h[r] + 0.25 protein[r]
NEU. ATP maintenance consumption	atp[r] + h2o[r] --> adp[r] + pi[r] + h[r] + m[r]
NEU. Biomass synthesis.	15 atp[r] + 12 nadh[r] + 0.25 protein[r] + 32 m[r] --> 15 adp[r] + 12 nad[r] + 15 pi[r] + 15 h[r] + biomass[r]
NET. Tr1	nh4[b] <==> nh3[k] + h[k]
NET. Tr2	no2[b] + h[b] <==> hno2[k]
NET. Tr3	no2[b] + no2[b] <==> n2o4[k]
NET. Tr4	o2[b] <==> o2[k]
NET. Tr5	n2o[b] <==> n2o[k]
NET. Tr6	no[b] <==> no[k]
NET. Tr7	nh2oh[b] <==> nh2oh[k]
NET. Tr8	no3[b] <==> no3[k]
NET. Tr9	biomass[b] <==> biomass[k]
NET. Tr10	pi[b] <==> pi[k]
NET. Tr11	h2o[b] <==> h2o[k]
NET. Tr12	co2[b] <==> co2[k]
NET. Tr13	h[b] <==> h[k]
NET. Tr14	h[b] <==> h[s]
NET. Tr15	nh3[k] <==> nh3[s]
NET. Tr16	o2[k] <==> o2[s]
NET. Tr17	no[k] <==> no[s]

NET. Tr18	no3[k] <==> no3[s]
NET. Tr19	n2o[k] <==> n2o[s]
NET. Tr20	biomass[k] <==> biomass[s]
NET. Tr21	pi[k] <==> pi[s]
NET. Tr22	h2o[k] <==> h2o[s]
NET. Tr23	co2[k] <==> co2[s]
NET. Tr24	h[k] <==> h[s]
NET. AMO Ammonia oxidation to hydroxylamine using ubiquinol as e donor	nh3[k] + o2[k] + q8h2[s] --> nh2oh[k] + h2o[s] + q8[s]
NET. AMO-ANX Ammonia oxidation to hydroxylamine using ubiquinol as e donor	nh3[k] + n2o4[k] + q8h2[s] --> nh2oh[k] + h2o[s] + q8[s] + 2 no[k]
NET. HAO Hydroxylamine oxidation to nitrite 1	nh2oh[k] + cyt554[k] --> noh[k] + cyt554e[k] + 2 h[k]
NET. HAO Hydroxylamine oxidation to nitrite 2	noh[k] + 0.5 cyt554[k] --> no1[k] + h[k] + 0.5 cyt554e[k]
NET. HAO Hydroxylamine oxidation to nitrite 3	no1[k] + h2o[k] + 0.5 cyt554[k] --> hno2[k] + h[k] + 0.5 cyt554e[k]
NET. ETC division of electron flow by cyt554	cyt554e[k] + cyt552[s] --> cyt552e[s] + cyt554[k]
NET. ETC Ubiquinone to ubiquinol for AMO	q8[s] + cyt552e[s] + 2 h[k] --> q8h2[s] + cyt552[s]
NET. ETC NADH production by NADH-ubiquinone reductase using ubiquinol	nad[s] + q8h2[s] + 4 h[k] --> nadh[s] + q8[s] + 6 h[s]
NET. ETC proton pump by CytCbc1 reductase using ubiquinol	q8h2[s] + 2 cyt552[k] + 0 h[s] --> 2 h[k] + q8[s] + 2 cyt552e[k]
NET. ETC proton pump by Cytaa3, Oxygen as final electron acceptor OXIC	.5 o2[s] + 4 h[s] + 2 cyt552e[k] --> h2o[s] + 2 h[k] + 2 cyt552[k]
NET. CytP460 NO2 synthesis from NH2OH + NO	0.5 nh2oh[k] + 0.5 no[k] + 2 cyt552[k] + h2o[k] --> hno2[k] + 2 cyt552e[k] + 3 h[k]
NET. NO availability to NOR and Cytp460	no1[k] --> no[k]
NET. R1 - NIR Nitrite reduction to nitric oxide	hno2[k] + cyt552e[k] + h[k] --> no[k] + cyt552[k] + h2o[k]
NET. R2 - NOR Nitric oxide reduction to nitrous oxide	no[k] + cyt552e[k] + h[k] --> 0.5 n2o[k] + cyt552[k] + 0.5 h2o[k]
NET. Nitric oxide activity by cytochrome C554	no[k] + h[k] + 0.5 cyt554e[k] --> 0.5 n2o[k] + 0.5 h2o[k]
NET. Nitric oxide oxidoreductase, flavohemoglobin involved in nitric oxide detoxification	no[s] + o2[s] + 0.5 nadh[s] --> no3[s] + 0.5 nad[s] + 0.5 h[s]
NET. Nitric oxide oxidoreductase, flavohemoglobin involved in nitric oxide detoxification	no[s] + 0.5 nadh[s] --> n2o[s] + 0.5 nad[s] + 0.5 h[s]
NET. ATP production	adp[s] + pi[s] + 6.8 h[k] --> atp[s] + h2o[s] + 4.8 h[s]
NET. Protein synthesis	2.244 atp[s] + nh3[s] + 4 co2[s] --> 2.244 adp[s] + 2.244 pi[s] + 2.244 h[s] + 0.25 protein[s]
NET. ATP maintenance consumption	atp[s] + h2o[s] --> adp[s] + pi[s] + h[s] + m[s]
NET. Biomass synthesis.	15 atp[s] + 12 nadh[s] + 0.25 protein[s] + 32 m[s] --> 15 adp[s] + 12 nad[s] + 15 pi[s] + 15 h[s] + biomass[s]
NMU. Tr1	nh4[c] <==> nh3[l] + h[l]
NMU. Tr2	no2[c] + h[c] <==> hno2[l]
NMU. Tr3	o2[c] <==> o2[l]
NMU. Tr4	n2o[c] <==> n2o[l]
NMU. Tr5	no[c] <==> no[l]
NMU. Tr6	nh2oh[c] <==> nh2oh[l]
NMU. Tr7	n2[c] <==> n2[l]
NMU. Tr8	biomass[c] <==> biomass[l]
NMU. Tr9	pi[c] <==> pi[l]
NMU. Tr10	h2o[c] <==> h2o[l]
NMU. Tr11	co2[c] <==> co2[l]
NMU. Tr12	h[c] <==> h[l]
NMU. Tr13	h[c] <==> h[t]
NMU. Tr14	nh3[l] <==> nh3[t]
NMU. Tr15	hno2[l] <==> h[t] + no2[t]
NMU. Tr16	n2[l] <==> n2[t]
NMU. Tr17	o2[l] <==> o2[t]
NMU. Tr18	biomass[l] <==> biomass[t]
NMU. Tr19	pi[l] <==> pi[t]
NMU. Tr20	h2o[l] <==> h2o[t]
NMU. Tr21	co2[l] <==> co2[t]
NMU. Tr22	h[l] <==> h[t]

NMU. AMO Ammonia oxidation to hydroxylamine using ubiquinol as e donor	nh3[l] + o2[l] + q8h2[t] --> nh2oh[l] + h2o[t] + q8[t]
NMU. HAO Hydroxylamine oxidation to nitrite 1	nh2oh[l] + cyt554[l] --> noh[l] + cyt554e[l] + 2 h[l]
NMU. HAO Hydroxylamine oxidation to nitrite 2	noh[l] + 0.5 cyt554[l] --> no1[l] + h[l] + 0.5 cyt554e[l]
NMU. HAO Hydroxylamine oxidation to nitrite 3	no1[l] + h2o[l] + 0.5 cyt554[l] --> hno2[l] + h[l] + 0.5 cyt554e[l]
NMU. ETC Partion of electron flow by cyt554	cyt554e[l] + cyt552[t] --> cyt552e[t] + cyt554[l]
NMU. ETC Ubiquinone to ubiquinol for AMO	q8[t] + cyt552e[t] + 2 h[l] --> q8h2[t] + cyt552[t]
NMU. ETC NADH production by NADH-ubiquinone reductase using ubiquinol	nad[t] + q8h2[t] + 4 h[l] --> nadh[t] + q8[t] + 6 h[t]
NMU. ETC proton pump by CytCbc1 reductase using ubiquinol	q8h2[t] + 2 cyt552[l] + 0 h[t] --> 2 h[l] + q8[t] + 2 cyt552e[l]
NMU. ETC proton pump by Cytaa3, Oxygen as final electron acceptor OXIC	.5 o2[t] + 4 h[t] + 2 cyt552e[l] --> h2o[t] + 2 h[l] + 2 cyt552[l]
NMU. ETC proton pump by cytaa3, nitrite as final electron acceptor ANOXIC	no2[t] + 3 h[t] + 3 cyt552e[l] --> 0.5 n2[t] + 2 h2o[t] + 3 cyt552[l]
NMU. NO availability to NOR and Cytp460	no1[l] --> no[l]
NMU. R1 - NIR Nitrite reduction to nitric oxide	hno2[l] + cyt552e[l] + h[l] --> no[l] + cyt552[l] + h2o[l]
NMU. R2 - NOR Nitric oxide reduction to nitrous oxide	no[l] + cyt552e[l] + h[l] --> 0.5 n2o[l] + cyt552[l] + 0.5 h2o[l]
NMU. ATP production	adp[t] + pi[t] + 6.8 h[l] --> atp[t] + h2o[t] + 4.8 h[t]
NMU. Protein synthesis	2.244 atp[t] + nh3[t] + 4 co2[t] --> 2.244 adp[t] + 2.244 pi[t] + 2.244 h[t] + 0.25 protein[t]
NMU. ATP maintenance consumption	atp[t] + h2o[t] --> adp[t] + pi[t] + h[t] + m[t]
NMU. Biomass synthesis.	15 atp[t] + 12 nadh[t] + 0.25 protein[t] + 32 m[t] --> 15 adp[t] + 12 nad[t] + 15 pi[t] + 15 h[t] + biomass[t]
NOC. Tr1	nh4[d] <==> nh3[m] + h[m]
NOC. Tr2	no2[d] + h[d] <==> hno2[m]
NOC. Tr3	o2[d] <==> o2[m]
NOC. Tr4	n2o[d] <==> n2o[m]
NOC. Tr5	no[d] <==> no[m]
NOC. Tr6	nh2oh[d] <==> nh2oh[m]
NOC. Tr7	n2[d] <==> n2[m]
NOC. Tr8	no3[d] <==> no3[m]
NOC. Tr9	biomass[d] <==> biomass[m]
NOC. Tr10	pi[d] <==> pi[m]
NOC. Tr11	h2o[d] <==> h2o[m]
NOC. Tr12	co2[d] <==> co2[m]
NOC. Tr13	h[d] <==> h[m]
NOC. Tr14	h[d] <==> h[u]
NOC. Tr15	nh3[m] <==> nh3[u]
NOC. Tr16	hno2[m] <==> h[u] + no2[u]
NOC. Tr17	no3[m] <==> no3[u]
NOC. Tr18	n2o[m] <==> n2o[u]
NOC. Tr19	n2[m] <==> n2[u]
NOC. Tr20	o2[m] <==> o2[u]
NOC. Tr21	no[m] <==> no[u]
NOC. Tr22	biomass[m] <==> biomass[u]
NOC. Tr23	pi[m] <==> pi[u]
NOC. Tr24	h2o[m] <==> h2o[u]
NOC. Tr25	co2[m] <==> co2[u]
NOC. Tr26	h[m] <==> h[u]
NOC. AMO Ammonia oxidation to hydroxylamine using ubiquinol as e donor	nh3[m] + o2[m] + q8h2[u] --> nh2oh[m] + h2o[u] + q8[u]
NOC. HAO Hydroxylamine oxidation to nitrite 1	nh2oh[m] + cyt554[m] --> noh[m] + cyt554e[m] + 2 h[m]
NOC. HAO Hydroxylamine oxidation to nitrite 2	noh[m] + 0.5 cyt554[m] --> no1[m] + h[m] + 0.5 cyt554e[m]
NOC. HAO Hydroxylamine oxidation to nitrite 3	no1[m] + h2o[m] + 0.5 cyt554[m] --> hno2[m] + h[m] + 0.5 cyt554e[m]
NOC. ETC division of electron flow by cyt554	cyt554e[m] + cyt552[u] --> cyt552e[u] + cyt554[m]
NOC. ETC Ubiquinone to ubiquinol for AMO	q8[u] + cyt552e[u] + 2 h[m] --> q8h2[u] + cyt552[u]
NOC. ETC NADH production by NADH-ubiquinone reductase using ubiquinol	nad[u] + q8h2[u] + 4 h[m] --> nadh[u] + q8[u] + 6 h[u]
NOC. ETC proton pump by CytCbc1 reductase using ubiquinol	q8h2[u] + 2 cyt552[m] + 0 h[u] --> 2 h[m] + q8[u] + 2 cyt552e[m]
NOC. ETC proton pump by Cytaa3, Oxygen as	.5 o2[u] + 4 h[u] + 2 cyt552e[m] --> h2o[u] + 2 h[m] + 2 cyt552[m]

final electron acceptor OXIC	
NOC. ETC proton pump by cytaa3, nitrite as final electron acceptor ANOXIC	no2[u] + 3 h[u] + 3 cyt552e[m] --> 0.5 n2[u] + 2 h2o[u] + 3 cyt552[m]
NOC. NO availability to NOR and Cytp460	no1[m] --> no[m]
NOC. R1 - NIR Nitrite reduction to nitric oxide	hno2[m] + cyt552e[m] + h[m] --> no[m] + cyt552[m] + h2o[m]
NOC. R2 - NOR Nitric oxide reduction to nitrous oxide	no[m] + cyt552e[m] + h[m] --> 0.5 n2o[m] + cyt552[m] + 0.5 h2o[m]
NOC. Nitric oxide oxidoreductase, flavohemoglobin involved in nitric oxide detoxification	no[u] + o2[u] + 0.5 nadh[u] --> no3[u] + 0.5 nad[u] + 0.5 h[u]
NOC. Nitric oxide oxidoreductase, flavohemoglobin involved in nitric oxide detoxification	no[u] + 0.5 nadh[u] --> n2o[u] + 0.5 nad[u] + 0.5 h[u]
NOC. ATP production	adp[u] + pi[u] + 6.8 h[m] --> atp[u] + h2o[u] + 4.8 h[u]
NOC. Protein synthesis	2.244 atp[u] + nh3[u] + 4 co2[u] --> 2.244 adp[u] + 2.244 pi[u] + 2.244 h[u] + 0.25 protein[u]
NOC. ATP maintenance consumption	atp[u] + h2o[u] --> adp[u] + pi[u] + h[u] + m[u]
NOC. Biomass synthesis.	15 atp[u] + 12 nadh[u] + 0.25 protein[u] + 32 m[u] --> 15 adp[u] + 12 nad[u] + 15 pi[u] + 15 h[u] + biomass[u]
NDE. Tr1	nh4[f] <==> nh3[n] + h[n]
NDE. Tr2	o2[f] <==> o2[n]
NDE. Tr3	no2[f] <==> no2[n]
NDE. Tr4	no3[f] <==> no3[n]
NDE. Tr5	no[f] <==> no[n]
NDE. Tr6	n2o[f] <==> n2o[n]
NDE. Tr7	biomass[f] <==> biomass[n]
NDE. Tr8	pi[f] <==> pi[n]
NDE. Tr9	h2o[f] <==> h2o[n]
NDE. Tr10	co2[f] <==> co2[n]
NDE. Tr11	h[f] <==> h[n]
NDE. Tr12	h[f] <==> h[v]
NDE. Tr13	nh3[n] <==> nh3[v]
NDE. Tr14	o2[n] <==> o2[v]
NDE. Tr15	biomass[n] <==> biomass[v]
NDE. Tr16	no[n] <==> no[v]
NDE. Tr17	n2o[n] <==> n2o[v]
NDE. Tr18	pi[n] <==> pi[v]
NDE. Tr19	h2o[n] <==> h2o[v]
NDE. Tr20	co2[n] <==> co2[v]
NDE. Tr21	h[n] <==> h[v]
NDE. Transport mediated NO2 transport	no2[n] --> no2[v]
NDE. Transport mediated NO3 transport	no3[v] --> no3[n]
NDE. NXR Periplasmic Nitrite oxidation to nitrate	no2[n] + 2 cyt550[v] + h2o[n] --> no3[n] + 2 cyt550e[v] + 2 h[n]
NDE. Terminal oxidase Cytbd, Oxygen as final electron acceptor OXIC	0.5 o2[v] + 2 h[v] + 2 cyt550e[v] --> h2o[v] + 2 cyt550[v]
NDE. ETC proton pump by CytCbc1 reductase using ubiquinol	q8[v] + 2 cyt550e[v] + 4 h[n] --> q8h2[v] + 2 cyt550[v] + 2 h[v]
NDE. ETC NADH production by NADH-ubiquinone reductase using ubiquinol	nad[v] + q8h2[v] + 2 h[n] + 2 h[v] --> nadh[v] + q8[v] + 5 h[v]
NDE. ETC ferredoxin production	nadh[v] + 2 fe[v] <==> nad[v] + 2 fee[v] + h[v]
NDE. Nitrite reductase nitric oxide forming	no2[n] + cyt550e[v] + 2 h[n] --> no[n] + cyt550[v] + h2o[n]
NDE. Dissimilatory reduction of Nitrate to Nitrite NXR	no3[n] + nadh[v] + h[v] --> no2[n] + nad[v] + h2o[v]
NDE. Assimilatory reduction of Nitrite to Ammonia	no2[v] + 4 h[v] + 3 nadh[v] --> nh3[v] + 2 h2o[v] + 3 nad[v]
NDE. Assimilatory reduction of Nitrite to Ammonia	no2[v] + 6 fee[v] + 7 h[v] --> nh3[v] + 2 h2o[v] + 6 fe[v]
NDE. Nitric oxide oxidoreductase, flavohemoglobin involved in nitric oxide detoxification	no[v] + o2[v] + 0.5 nadh[v] --> no3[v] + 0.5 nad[v] + 0.5 h[v]
NDE. Nitric oxide oxidoreductase, flavohemoglobin involved in nitric oxide detoxification	no[v] + 0.5 nadh[v] --> n2o[v] + 0.5 nad[v] + 0.5 h[v]
NDE. ETC ATP transmembrane synthesis (four protons per ATP)	adp[v] + pi[v] + 3 h[n] --> atp[v] + h2o[v] + 3 h[v]
NDE. Protein synthesis from ammonia	2.244 atp[v] + nh3[v] + 4 co2[v] --> 2.244 adp[v] + 2.244 pi[v] + 2.244 h[v] + 0.25 protein[v]

NDE. Maintenance ATP consumption (non-growth associated energy consumption)	atp[v] + h2o[v] --> adp[v] + pi[v] + h[v] + m[v]
NDE. Biomass synthesis ATP consumption	15 atp[v] + 12 nadh[v] + 0.25 protein[v] + 200 m[v] --> 15 adp[v] + 12 nad[v] + 15 pi[v] + 15 h[v] + biomass[v]
NWI. TR1	o2[g] <==> o2[o]
NWI. TR2	nh4[g] <==> nh3[o] + h[o]
NWI. TR3	no2[g] <==> no2[o]
NWI. TR4	no3[g] <==> no3[o]
NWI. TR5	no[g] <==> no[o]
NWI. TR6	biomass[g] <==> biomass[o]
NWI. TR7	pi[g] <==> pi[o]
NWI. TR8	h2o[g] <==> h2o[o]
NWI. TR9	co2[g] <==> co2[o]
NWI. TR10	h[g] <==> h[o]
NWI. TR11	h[g] <==> h[w]
NWI. TR12	nh3[o] <==> nh3[w]
NWI. TR13	o2[o] <==> o2[w]
NWI. TR14	biomass[o] <==> biomass[w]
NWI. TR15	pi[o] <==> pi[w]
NWI. TR16	h2o[o] <==> h2o[w]
NWI. TR17	co2[o] <==> co2[w]
NWI. TR18	h[o] <==> h[w]
NWI. Transport mediated NO2 transport	no2[o] <==> no2[w]
NWI. Transport mediated NO3 transport	no3[o] <==> no3[w]
NWI. NXR Periplasmic Nitrite oxidation to nitrate	no2[w] + 2 cyt550[w] + h2o[w] <==> no3[w] + 2 cyt550e[w] + 2 h[o]
NWI. Terminal oxidase Cytbd, Oxygen as final electron acceptor OXIC	0.5 o2[w] + 4 h[w] + 2 cyt550e[w] --> h2o[w] + 2 h[o] + 2 cyt550[w]
NWI. ETC proton pump by CytCbc1 reductase using ubiquinol	q8[w] + 2 cyt550e[w] + 4 h[o] --> q8h2[w] + 2 cyt550[w] + 2 h[w]
NWI. ETC NADH production by NADH-ubiquinone reductase using ubiquinol	nad[w] + q8h2[w] + 2 h[o] + 2 h[w] --> nadh[w] + q8[w] + 5 h[w]
NWI. Nitrite reductase nitric oxide forming	no2[o] + cyt550e[w] + 2 h[o] --> no[o] + cyt550[w] + h2o[o]
NWI. Nitric oxide reductase NADH forming	no[o] + 0.5 nad[w] + h2o[w] --> no2[o] + 0.5 nadh[w] + 1.5 h[o]
NWI. Dissimilatory reduction of Nitrate to Nitrite NXR mediated	no3[o] + nadh[w] + h[w] --> no2[o] + nad[w] + h2o[w]
NWI. Dissimilatory reduction of Nitrate to Nitrite NAR mediated	no3[o] + q8h2[w] --> no2[o] + q8[w] + h2o[o]
NWI. Assimilatory reduction of Nitrite to Ammonia by NAR	no2[w] + 4 h[w] + 3 nadh[w] --> nh3[w] + 2 h2o[w] + 3 nad[w]
NWI. ETC ATP transmembrane synthesis (four protons per ATP)	adp[w] + pi[w] + 3 h[o] --> atp[w] + h2o[w] + 3 h[w]
NWI. Protein synthesis from ammonia	2.244 atp[w] + nh3[w] + 4 co2[w] --> 2.244 adp[w] + 2.244 pi[w] + 2.244 h[w] + 0.25 protein[w]
NWI. Maintenance ATP consumption (non-growth associated energy consumption)	atp[w] + h2o[w] --> adp[w] + pi[w] + h[w] + m[w]
NWI. Biomass synthesis ATP consumption	15 atp[w] + 12 nadh[w] + 0.25 protein[w] + 200 m[w] --> 15 adp[w] + 12 nad[w] + 15 pi[w] + 15 h[w] + biomass[w]
NHA. Tr1	o2[h] <==> o2[p]
NHA. Tr2	nh4[h] <==> nh3[p] + h[p]
NHA. Tr3	no2[h] <==> no2[p]
NHA. Tr4	no3[h] <==> no3[p]
NHA. Tr5	no[h] <==> no[p]
NHA. Tr6	n2o[h] <==> n2o[p]
NHA. Tr7	biomass[h] <==> biomass[p]
NHA. Tr8	pi[h] <==> pi[p]
NHA. Tr9	h2o[h] <==> h2o[p]
NHA. Tr10	co2[h] <==> co2[p]
NHA. Tr11	h[h] <==> h[p]
NHA. Tr12	h[h] <==> h[x]
NHA. Tr13	nh3[p] <==> nh3[x]
NHA. Tr14	o2[p] <==> o2[x]
NHA. Tr15	biomass[p] <==> biomass[x]
NHA. Tr16	pi[p] <==> pi[x]

NHA. Tr17	h2o[p] <==> h2o[x]
NHA. Tr18	co2[p] <==> co2[x]
NHA. Tr19	h[p] <==> h[x]
NHA. Transport mediated NO2 transport	no2[p] <==> no2[x]
NHA. Transport mediated NO3 transport	no3[p] <==> no3[x]
NHA. NXR Periplasmic Nitrite oxidation to nitrate	no2[x] + 2 cyt550[x] + h2o[x] <==> no3[x] + 2 cyt550e[x] + 2 h[p]
NHA. Terminal oxidase Cytbd, Oxygen as final electron acceptor OXIC	0.5 o2[x] + 4 h[x] + 2 cyt550e[x] --> h2o[x] + 2 h[p] + 2 cyt550[x]
NHA. ETC proton pump by CytCbc1 reductase using ubiquinol	q8[x] + 2 cyt550e[x] + 4 h[p] --> q8h2[x] + 2 cyt550[x] + 2 h[x]
NHA. ETC NADH production by NADH-ubiquinone reductase using ubiquinol	nad[x] + q8h2[x] + 2 h[p] + 2 h[x] --> nadh[x] + q8[x] + 5 h[x]
NHA. ETC ferredoxin production	nadh[x] + 2 fe[x] <==> nad[x] + 2 fee[x] + h[x]
NHA. P460 NO2 synthesis from NH2OH + NO	no[p] + cyt550[x] + h2o[x] --> no2[p] + cyt550e[x] + 2 h[p]
NHA. NOR Nitric oxide reduction to nitrous oxide	no[p] + cyt550e[x] + h[p] --> 0.5 n2o[p] + cyt550[x] + 0.5 h2o[p]
NHA. Assimilatory reduction of Nitrite to Ammonia by NAR	no2[x] + 6 fee[x] + 7 h[x] --> nh3[x] + 2 h2o[x] + 6 fe[x]
NHA. Nitrite reductase nitric oxide forming	no2[p] + cyt550e[x] + 2 h[p] --> no[p] + cyt550[x] + h2o[p]
NHA. Dissimilatory reduction of Nitrate to Nitrite NXR mediated	no3[o] + nadh[w] + h[w] --> no2[o] + nad[w] + h2o[w]
NHA. Assimilatory reduction of Nitrite to Ammonia by NAR	no2[x] + 4 h[x] + 3 nadh[x] --> nh3[x] + 2 h2o[x] + 3 nad[x]
NHA. ETC ATP transmembrane synthesis (four protons per ATP)	adp[x] + pi[x] + 3 h[p] --> atp[x] + h2o[x] + 3 h[x]
NHA. Protein synthesis from ammonia	2.244 atp[x] + nh3[x] + 4 co2[x] --> 2.244 adp[x] + 2.244 pi[x] + 2.244 h[x] + 0.25 protein[x]
NHA. Maintenance ATP consumption (non-growth associated energy consumption)	atp[x] + h2o[x] --> adp[x] + pi[x] + h[x] + m[x]
NHA. Biomass synthesis ATP consumption	15 atp[x] + 12 nadh[x] + 0.25 protein[x] + 200 m[x] --> 15 adp[x] + 12 nad[x] + 15 pi[x] + 15 h[x] + biomass[x]
NSP. Tr1	o2[i] <==> o2[q]
NSP. Tr2	nh4[i] <==> nh3[q] + h[q]
NSP. Tr3	no2[i] <==> no2[q]
NSP. Tr4	no3[i] <==> no3[q]
NSP. Tr5	no[i] <==> no[q]
NSP. Tr6	biomass[i] <==> biomass[q]
NSP. Tr7	pi[i] <==> pi[q]
NSP. Tr8	h2o[i] <==> h2o[q]
NSP. Tr9	co2[i] <==> co2[q]
NSP. Tr10	h[i] <==> h[q]
NSP. Tr11	h[i] <==> h[y]
NSP. Tr12	nh3[q] <==> nh3[y]
NSP. Tr13	o2[q] <==> o2[y]
NSP. Tr14	biomass[q] <==> biomass[y]
NSP. Tr15	pi[q] <==> pi[y]
NSP. Tr16	h2o[q] <==> h2o[y]
NSP. Tr17	co2[q] <==> co2[y]
NSP. Tr18	h[q] <==> h[y]
NSP. Transport mediated NO2 transport	no2[q] <==> no2[y]
NSP. NXR Periplasmic Nitrite oxidation to nitrate	no2[q] + 2 cyt550[y] + h2o[q] --> no3[q] + 2 cyt550e[y] + 2 h[q]
NSP. Terminal oxidase Cytbd, Oxygen as final electron acceptor OXIC	0.5 o2[y] + 4 h[y] + 2 cyt550e[y] --> h2o[y] + 2 h[q] + 2 cyt550[y]
NSP. ETC proton pump by CytCbc1 reductase using ubiquinol	q8[y] + 2 cyt550e[y] + 4 h[q] --> q8h2[y] + 2 cyt550[y] + 2 h[y]
NSP. ETC NADH production by NADH-ubiquinone reductase using ubiquinol	nad[y] + q8h2[y] + 2 h[q] + 2 h[y] --> nadh[y] + q8[y] + 5 h[y]
NSP. ETC ferredoxin production	nadh[y] + 2 fe[y] <==> nad[y] + 2 fee[y] + h[y]
NSP. NO2 synthesis from NH2OH + NO	no[q] + cyt550[y] + h2o[y] --> no2[q] + cyt550e[y] + 2 h[p]
NSP. Assimilatory reduction of Nitrite to Ammonia by NAR	no2[y] + 6 fee[y] + 7 h[y] --> nh3[y] + 2 h2o[y] + 6 fe[y]
NSP. Nitrite reductase nitric oxide forming	no2[q] + cyt550e[y] + 2 h[q] --> no[q] + cyt550[y] + h2o[q]
NSP. ETC ATP transmembrane synthesis (four protons per ATP)	adp[y] + pi[y] + 3 h[q] --> atp[y] + h2o[y] + 3 h[y]
NSP. Protein synthesis from ammonia	2.244 atp[y] + nh3[y] + 4 co2[y] --> 2.244 adp[y] + 2.244 pi[y] + 2.244 h[y] + 0.25 protein[y]

NSP. Maintenance ATP consumption (non-growth associated energy consumption)	atp[y] + h2o[y] --> adp[y] + pi[y] + h[y] + m[y]
NSP. Biomass synthesis ATP consumption	15 atp[y] + 12 nadh[y] + 0.25 protein[y] + 200 m[y] --> 15 adp[y] + 12 nad[y] + 15 pi[y] + 15 h[y] + biomass[y]

Metabolite description	Metabolite *i*
EX.Ammonium	nh4[e]
EX.Oxygen	o2[e]
EX.Nitrite	no2[e]
EX.Nitrate	no3[e]
EX.Nitrous oxide	n2o[e]
EX.Nitric oxide	no[e]
EX.Nitrogen	n2[e]
EX.Hydroxylamine	nh2oh[e]
EX.Biomass	biomass[e]
EX.Orthophosphate	pi[e]
EX.Water	h2o[e]
EX.Carbon dioxide	co2[e]
EX.Hydrogen, Proton	h[e]
NEU.Ammonium	nh4[a]
NET.Ammonium	nh4[b]
NMU.Ammonium	nh4[c]
NOC.Ammonium	nh4[d]
NDE.Ammonium	nh4[f]
NWI.Ammonium	nh4[g]
NHA.Ammonium	nh4[h]
NSP.Ammonium	nh4[i]
NEU.Oxygen	o2[a]
NET.Oxygen	o2[b]
NMU.Oxygen	o2[c]
NOC.Oxygen	o2[d]
NDE.Oxygen	o2[f]
NWI.Oxygen	o2[g]
NHA.Oxygen	o2[h]
NSP.Oxygen	o2[i]
NEU.Nitrite	no2[a]
NET.Nitrite	no2[b]
NMU.Nitrite	no2[c]
NOC.Nitrite	no2[d]
NDE.Nitrite	no2[f]
NWI.Nitrite	no2[g]
NHA.Nitrite	no2[h]
NSP.Nitrite	no2[i]
NET.Nitrate	no3[b]
NOC.Nitrate	no3[d]
NDE.Nitrate	no3[f]
NWI.Nitrate	no3[g]
NHA.Nitrate	no3[h]
NSP.Nitrate	no3[i]
NEU.Nitrous oxide	n2o[a]
NET.Nitrous oxide	n2o[b]
NMU.Nitrous oxide	n2o[c]
NOC.Nitrous oxide	n2o[d]
NDE.Nitrous oxide	n2o[f]
NHA.Nitrous oxide	n2o[h]
NEU.Nitric oxide	no[a]

NET.Nitric oxide	no[b]
NMU.Nitric oxide	no[c]
NOC.Nitric oxide	no[d]
NDE.Nitric oxide	no[f]
NWI.Nitric oxide	no[g]
NHA.Nitric oxide	no[h]
NSP.Nitric oxide	no[i]
NMU.Nitrogen	n2[c]
NOC.Nitrogen	n2[d]
NEU.Hydroxylamine	nh2oh[a]
NET.Hydroxylamine	nh2oh[b]
NMU.Hydroxylamine	nh2oh[c]
NOC.Hydroxylamine	nh2oh[d]
NEU.Biomass	biomass[a]
NET.Biomass	biomass[b]
NMU.Biomass	biomass[c]
NOC.Biomass	biomass[d]
NDE.Biomass	biomass[f]
NWI.Biomass	biomass[g]
NHA.Biomass	biomass[h]
NSP.Biomass	biomass[i]
NEU.Hydroxilamine	pi[a]
NET.Hydroxilamine	pi[b]
NMU.Hydroxilamine	pi[c]
NOC.Hydroxilamine	pi[d]
NDE.Hydroxilamine	pi[f]
NWI.Hydroxilamine	pi[g]
NHA.Hydroxilamine	pi[h]
NSP.Hydroxilamine	pi[i]
NEU.Water	h2o[a]
NET.Water	h2o[b]
NMU.Water	h2o[c]
NOC.Water	h2o[d]
NDE.Water	h2o[f]
NWI.Water	h2o[g]
NHA.Water	h2o[h]
NSP.Water	h2o[i]
NEU.Carbon dioxide	co2[a]
NET.Carbon dioxide	co2[b]
NMU.Carbon dioxide	co2[c]
NOC.Carbon dioxide	co2[d]
NDE.Carbon dioxide	co2[f]
NWI.Carbon dioxide	co2[g]
NHA.Carbon dioxide	co2[h]
NSP.Carbon dioxide	co2[i]
NEU.Hydrogen	h[a]
NET.Hydrogen	h[b]
NMU.Hydrogen	h[c]
NOC.Hydrogen	h[d]
NDE.Hydrogen	h[i]
NWI.Hydrogen	h[f]
NHA.Hydrogen	h[g]
NSP.Hydrogen	h[h]
NEU.O2	o2[j]
NEU.Ammonia	nh3[j]
NEU.Nitrous acid	hno2[j]
NEU.Nitrous oxide	n2o[j]
NEU.Nitric oxide	no[j]

NEU.Hydroxylamine	nh2oh[j]
NEU.Nitric oxide HAO	no1[j]
NEU.biomass	biomass[j]
NEU.Phosphate	pi[j]
NEU.H2O	h2o[j]
NEU.Carbon dioxide	co2[j]
NEU.H+, Hydrogen Ion/ Proton	h[j]
NEU.Ferrocytochrome c (reduced)	cyt554e[j]
NEU.Ferricytochrome c (oxidized)	cyt554[j]
NEU.Ferrocytochrome c (reduced)	cyt552e[j]
NEU.Ferricytochrome c (oxidized)	cyt552[j]
NEU.Nitroxyl	noh[j]
NEUc.O2	o2[r]
NEUc.Phosphate	pi[r]
NEUc.H2O	h2o[r]
NEUc.Carbon dioxide	co2[r]
NEUc.H+, Hydrogen Ion/ Proton	h[r]
NEUc.Ammonia	nh3[r]
NEUc.Ubiquinone-8 (oxidized)	q8[r]
NEUc.Ubiquinol-8 (reduced)	q8h2[r]
NEUc.Membrane Ferrocytochrome c (reduced)	cyt552e[r]
NEUc.Membrane Ferricytochrome c (oxidized)	cyt552[r]
NEUc.Nicotinamide adenine dinucleotide	nad[r]
NEUc.Nicotinamide adenine dinucleotide - reduced	nadh[r]
NEUc.ATP	atp[r]
NEUc.ADP	adp[r]
NEUc.biomass	biomass[r]
NEUc.protein	protein[r]
NEUc.membrane ensamble	m[r]
NETp.O2	o2[k]
NETp.Ammonia	nh3[k]
NETp.Nitrous acid	hno2[k]
NETp.Nitrous oxide	n2o[k]
NETp.Nitric oxide	no[k]
NETp.Nitric oxide HAO	no1[k]
NETp.Hydroxylamine	nh2oh[k]
NETp.Nitrate	no3[k]
NETp.Hydrazine	n2o4[k]
NETp.Nitroxyl	noh[k]
NETp.biomass	biomass[k]
NETp.Phosphate	pi[k]
NETp.H2O	h2o[k]
NETp.Carbon dioxide	co2[k]
NETp.H+, Hydrogen Ion/ Proton	h[k]
NETp.Ferrocytochrome c (reduced)	cyt554e[k]
NETp.Ferricytochrome c (oxidized)	cyt554[k]
NETp.Ferrocytochrome c (reduced)	cyt552e[k]
NETp.Ferricytochrome c (oxidized)	cyt552[k]
NETc.O2	o2[s]
NETc.Phosphate	pi[s]
NETc.H2O	h2o[s]
NETc.Carbon dioxide	co2[s]
NETc.H+, Hydrogen Ion/ Proton	h[s]
NETc.Ammonia	nh3[s]
NETc.Nitrate	no3[s]
NETc.Nitrous oxide	n2o[s]
NETc.Nitric oxide	no[s]
NETc.Ubiquinone-8 (oxidized)	q8[s]

NETc.Ubiquinol-8 (reduced)	q8h2[s]
NETc.Membrane Ferrocytochrome c (reduced)	cyt552e[s]
NETc.Membrane Ferricytochrome c (oxidized)	cyt552[s]
NETc.Nicotinamide adenine dinucleotide	nad[s]
NETc.Nicotinamide adenine dinucleotide - reduced	nadh[s]
NETc.ATP	atp[s]
NETc.ADP	adp[s]
NETc.biomass	biomass[s]
NETc.protein	protein[s]
NETc.membrane ensamble	m[s]
NMUp.O2	o2[l]
NMUp.Ammonia	nh3[l]
NMUp.Nitrous acid	hno2[l]
NMUp.Nitrous oxide	n2o[l]
NMUp.Nitric oxide	no[l]
NMUp.Nitric oxide HAO	no1[l]
NMUp.Hydroxylamine	nh2oh[l]
NMUp.Nitrogen	n2[l]
NMUp.Nitroxyl	noh[l]
NMUp.biomass	biomass[l]
NMUp.Phosphate	pi[l]
NMUp.H2O	h2o[l]
NMUp.Carbon dioxide	co2[l]
NMUp.H+, Hydrogen Ion/ Proton	h[l]
NMUp.Ferrocytochrome c (reduced)	cyt554e[l]
NMUp.Ferricytochrome c (oxidized)	cyt554[l]
NMUp.Ferrocytochrome c (reduced)	cyt552e[l]
NMUp.Ferricytochrome c (oxidized)	cyt552[l]
NMUc.O2	o2[t]
NMUc.Phosphate	pi[t]
NMUc.H2O	h2o[t]
NMUc.Carbon dioxide	co2[t]
NMUc.H+, Hydrogen Ion/ Proton	h[t]
NMUc.Ammonia	nh3[t]
NMUc.Nitrite	no2[t]
NMUc.Nitrogen	n2[t]
NMUc.Ubiquinone-8 (oxidized)	q8[t]
NMUc.Ubiquinol-8 (reduced)	q8h2[t]
NMUc.Membrane Ferrocytochrome c (reduced)	cyt552e[t]
NMUc.Membrane Ferricytochrome c (oxidized)	cyt552[t]
NMUc.Nicotinamide adenine dinucleotide	nad[t]
NMUc.Nicotinamide adenine dinucleotide - reduced	nadh[t]
NMUc.ATP	atp[t]
NMUc.ADP	adp[t]
NMUc.biomass	biomass[t]
NMUc.protein	protein[t]
NMUc.membrane ensamble	m[t]
NOCp.O2	o2[m]
NOCp.Ammonia	nh3[m]
NOCp.Nitrous acid	hno2[m]
NOCp.Nitrous oxide	n2o[m]
NOCp.Nitric oxide	no[m]
NOCp.Nitric oxide HAO	no1[m]
NOCp.Hydroxylamine	nh2oh[m]
NOCp.Nitrogen	n2[m]
NOCc.Nitrate	no3[m]
NOCp.Nitroxyl	noh[m]
NOCp.biomass	biomass[m]

NOCp.Phosphate	pi[m]
NOCp.H2O	h2o[m]
NOCp.Carbon dioxide	co2[m]
NOCp.H+, Hydrogen Ion/ Proton	h[m]
NOCp.Ferrocytochrome c (reduced)	cyt554e[m]
NOCp.Ferricytochrome c (oxidized)	cyt554[m]
NOCp.Ferrocytochrome c (reduced)	cyt552e[m]
NOCp.Ferricytochrome c (oxidized)	cyt552[m]
NOCc.O2	o2[u]
NOCc.Phosphate	pi[u]
NOCc.H2O	h2o[u]
NOCc.Carbon dioxide	co2[u]
NOCc.H+, Hydrogen Ion/ Proton	h[u]
NOCc.Ammonia	nh3[u]
NOCc.Nitrate	no3[u]
NOCc.Nitrous oxide	n2o[u]
NOCc.Nitric oxide	no[u]
NOCc.Nitrite	no2[u]
NOCc.Nitrogen	n2[u]
NOCc.Ubiquinone-8 (oxidized)	q8[u]
NOCc.Ubiquinol-8 (reduced)	q8h2[u]
NOCc.Membrane Ferrocytochrome c (reduced)	cyt552e[u]
NOCc.Membrane Ferricytochrome c (oxidized)	cyt552[u]
NOCc.Nicotinamide adenine dinucleotide	nad[u]
NOCc.Nicotinamide adenine dinucleotide - reduced	nadh[u]
NOCc.ATP	atp[u]
NOCc.ADP	adp[u]
NOCc.biomass	biomass[u]
NOCc.protein	protein[u]
NOCc.membrane ensamble	m[u]
NDEp.O2	o2[n]
NDEp.Nitrite	no2[n]
NDEp.Nitrate	no3[n]
NDEp.Nitrous oxide	n2o[n]
NDEp.Nitric oxide	no[n]
NDEp.biomass	biomass[n]
NDEp.Phosphate	pi[n]
NDEp.H2O	h2o[n]
NDEp.Carbon dioxide	co2[n]
NDEp.H+, Hydrogen Ion/ Proton	h[n]
NDEp.Ammonia	nh3[n]
NDEc.O2	o2[v]
NDEc.Phosphate	pi[v]
NDEc.H2O	h2o[v]
NDEc.Carbon dioxide	co2[v]
NDEc.H+, Hydrogen Ion/ Proton	h[v]
NDEc.Ammonia	nh3[v]
NDEc.Nitrous oxide	n2o[v]
NDEc.Nitrite	no2[v]
NDEc.Nitrate	no3[v]
NDEc.Nitric oxide	no[v]
NDEc.Ubiquinone-8 (oxidized)	q8[v]
NDEc.Ubiquinol-8 (reduced)	q8h2[v]
NDEc.Membrane Ferrocytochrome c (reduced)	cyt550e[v]
NDEc.Membrane Ferricytochrome c (oxidized)	cyt550[v]
NDEc.Nicotinamide adenine dinucleotide	nad[v]
NDEc.Nicotinamide adenine dinucleotide - reduced	nadh[v]
NDEc.Ferredoxin reduced	fee[v]

NDEc.Ferredoxin oxidized	fe[v]
NDEc.ATP	atp[v]
NDEc.ADP	adp[v]
NDEc.biomass	biomass[v]
NDEc.protein	protein[v]
NDEc.membrane ensamble	m[v]
NWIp.O2	o2[o]
NWIp.Nitrite	no2[o]
NWIp.Nitrate	no3[o]
NWIp.Nitric oxide	no[o]
NWIp.biomass	biomass[o]
NWIp.Phosphate	pi[o]
NWIp.H2O	h2o[o]
NWIp.Carbon dioxide	co2[o]
NWIp.H+, Hydrogen Ion/ Proton	h[o]
NWIp.Ammonia	nh3[o]
NWIc.O2	o2[w]
NWIc.Phosphate	pi[w]
NWIc.H2O	h2o[w]
NWIc.Carbon dioxide	co2[w]
NWIc.H+, Hydrogen Ion/ Proton	h[w]
NWIc.Ammonia	nh3[w]
NWIc.Nitrous oxide	n2o[w]
NWIc.Nitrite	no2[w]
NWIc.Nitrate	no3[w]
NWIc.Ubiquinone-8 (oxidized)	q8[w]
NWIc.Ubiquinol-8 (reduced)	q8h2[w]
NWIc.Membrane Ferrocytochrome c (reduced)	cyt550e[w]
NWIc.Membrane Ferricytochrome c (oxidized)	cyt550[w]
NWIc.Nicotinamide adenine dinucleotide	nad[w]
NWIc.Nicotinamide adenine dinucleotide - reduced	nadh[w]
NWIc.ATP	atp[w]
NWIc.ADP	adp[w]
NWIc.biomass	biomass[w]
NWIc.protein	protein[w]
NWIc.membrane ensamble	m[w]
NHAp.O2	o2[p]
NHAp.Nitrite	no2[p]
NHAp.Nitrate	no3[p]
NHAp.Nitrous oxide	n2o[p]
NHAp.Nitric oxide	no[p]
NHAp.biomass	biomass[p]
NHAp.Phosphate	pi[p]
NHAp.H2O	h2o[p]
NHAp.Carbon dioxide	co2[p]
NHAp.H+, Hydrogen Ion/ Proton	h[p]
NHAp.Ammonia	nh3[p]
NHAc.O2	o2[x]
NHAc.Phosphate	pi[x]
NHAc.H2O	h2o[x]
NHAc.Carbon dioxide	co2[x]
NHAc.H+, Hydrogen Ion/ Proton	h[x]
NHAc.Ammonia	nh3[x]
NHAc.Nitrite	no2[x]
NHAc.Nitrate	no3[x]
NHAc.Ubiquinone-8 (oxidized)	q8[x]
NHAc.Ubiquinol-8 (reduced)	q8h2[x]
NHAc.Membrane Ferrocytochrome c (reduced)	cyt550e[x]

NHAc.Membrane Ferricytochrome c (oxidized)	cyt550[x]
NHAc.Ferredoxin reduced	fee[x]
NHAc.Ferredoxin oxidized	fe[x]
NHAc.Nicotinamide adenine dinucleotide	nad[x]
NHAc.Nicotinamide adenine dinucleotide - reduced	nadh[x]
NHAc.ATP	atp[x]
NHAc.ADP	adp[x]
NHAc.biomass	biomass[x]
NHAc.protein	protein[x]
NHAc.membrane ensamble	m[x]
NSPp.O2	o2[q]
NSPp.Nitrite	no2[q]
NSPp.Nitrate	no3[q]
NSPp.Nitric oxide	no[q]
NSPp.biomass	biomass[q]
NSPp.Phosphate	pi[q]
NSPp.H2O	h2o[q]
NSPp.Carbon dioxide	co2[q]
NSPp.H+, Hydrogen Ion/ Proton	h[q]
NSPp.Ammonia	nh3[q]
NSPc.O2	o2[y]
NSPc.Phosphate	pi[y]
NSPc.H2O	h2o[y]
NSPc.Carbon dioxide	co2[y]
NSPc.H+, Hydrogen Ion/ Proton	h[y]
NSPc.Ammonia	nh3[y]
NSPc.Nitrite	no2[y]
NSPc.Ubiquinone-8 (oxidized)	q8[y]
NSPc.Ubiquinol-8 (reduced)	q8h2[y]
NSPc.Membrane Ferrocytochrome c (reduced)	cyt550e[y]
NSPc.Membrane Ferricytochrome c (oxidized)	cyt550[y]
NSPc.Ferredoxin reduced	fee[y]
NSPc.Ferredoxin oxidized	fe[y]
NSPc.Nicotinamide adenine dinucleotide	nad[y]
NSPc.Nicotinamide adenine dinucleotide - reduced	nadh[y]
NSPc.ATP	atp[y]
NSPc.ADP	adp[y]
NSPc.biomass	biomass[y]
NSPc.protein	protein[y]
NSPc.membrane ensamble	m[y]

APPENDIX THREE

SMN model of denitrifying metabolims. (Lumped model).

Rxn description	Formula
Biomass exchange	biomass <=>
Oxyge exchange	cpd00007 <=>
Nitrate exchange	cpd00209[p] <=>
Nitrite exchange	cpd00075[p] <=>
Nitric oxide exchange	cpd00418[p] <=>
Nitrous oxide exchange	cpd00659[p] <=>
Nitrogen exchange	cpd00528[p] <=>
Ammonium exchange	cpd00013 <=>
Hydroxilamine exchange	cpd00165 <=>
ADP exchnage	cpd00008 <=>
ATP exchange	cpd00002 <=>
OrthoPhosphate exchange	cpd00009 <=>
Proton exchange	cpd00067 <=>
H2O exchange	cpd00001 <=>
H2O exchange	cpd00001[p] <=>
CO2 exchange	cpd00011 <=>
Acetate exchange	cpd00029 <=>
L-Lactate exchange	cpd00159 <=>
Pyruvate exchange	cpd00020 <=>
Glucose exchange	cpd00027 <=>
Ethanol exchange	cpd00363 <=>
Citrate exchange	cpd00137 <=>
Isocitrate exchange	cpd00260 <=>
Oxaloacetate exchange	cpd00032 <=>
2-Oxoglutarate exchange	cpd00024 <=>
Succinyl-CoA exchange	cpd00078 <=>
Succinate exchange	cpd00159 <=>
Fumarate exchange	cpd00106 <=>
Malate exchange	cpd00130 <=>
Hydrogen H2 exchange	cpd11640 <=>
Hydrogen-sulfide	cpd00239 <=>
L-Tryptophan exchange	cpd03114 <=>
L-Cysteine exchange	cpd00084 <=>
L-Glycine exchange	cpd00033 <=>
L-Threonine exchange	cpd00161 <=>
L-Glutamate exchange	cpd00023 <=>
L-Glutamine exchnage	cpd00053 <=>
L-Alanine exchange	cpd00035 <=>
L-Aspartate exchange	cpd00041 <=>
L-Arginine exchange	cpd00051 <=>
L-Asparagine exchange	cpd00132 <=>
L-Proline exchange	cpd00129 <=>
L-Isoleucine exchnage	cpd00322 <=>
L-Valine exchange	cpd00156 <=>
L-Leucine exchange	cpd00107 <=>
L-Lysine exchange	cpd00039 <=>
L-Histidine	cpd00119 <=>

L-Serine	cpd00054 <=>
L-Methionine	cpd00060 <=>
L-Phenylalanine	cpd00066 <=>
L-Tyrosine	cpd00069 <=>
Maltose exchange	cpd00179 <=>
Agmatine exchange	cpd00152 <=>
N-Acetyl-L-glutamate exchnage	cpd00477 <=>
Cadaverine exchange	cpd01155 <=>
N2-acetyl-lysine	cpd01770 <=>
Decanoic acid exchange	cpd01107 <=>
Tetradecanoic acid exchange	cpd03847 <=>
Glycerol-3-Phosphate exchange	cpd00080[p] <=>
Hexadecanoic acid exchange	cpd00214[p] <=>
Octadecanoic acid exchange	cpd01080[p] <=>
Undecanoate exchange	cpd01741odd <=>
Hexadecanoate transport via proton symport	cpd00214[c] <=> cpd00214[p]
Octadecanoate transport via proton symport	cpd01080[c] <=> cpd01080[p]
Urea transport via facilitate diffusion	cpd00073 <=>
sn-Glycerol ABC transport	cpd00001[c] + cpd00002[c] + cpd00080[p] <=> cpd00008[c] + cpd00009[c] + cpd00067[c] + cpd00080[c]
Indol exchange	cpd00359 <=>
Homocysteine exchange	cpd00135 <=>
2-Oxobutyrate exchange	cpd00094 <=>
5,10-Methylene-THF exchange	cpd00125 <=>
Tetrahydrofolate exchange	cpd00087 <=>
GTP	cpd00038 <=>
IMP	cpd00114 <=>
GDP	cpd00031 <=>
Adenylosuccinate	cpd02375 <=>
Citrulline	cpd00274 <=>
L-Argininosuccinate	cpd02152 <=>
ACP	cpd11493 <=>
Carbamoylphosphate	cpd00146 <=>
Pyrroloquinoline-quinone	cpd00097 <=>
Quinate	cpd00248 <=>
PQQH2	cpd00986 <=>
H2S2O3	cpd00268 <=>
trdrd	cpd11421 <=>
trdox	cpd11420 <=>
Sulfite	cpd00081 <=>
5-Methyltetrahydrofolate	cpd00345 <=>
5-Methyltetrahydropteroyltri-L-glutamate	cpd02738 <=>
Tetrahydropteroyltri-L-glutamate	cpd02555 <=>
AICAR	cpd02851 <=>
Formamide	cpd00378 <=>
Formate	cpd00047 <=>
Niacin Nicotinic	cpd00218 <=>
Maltose alpha-D-glucosylmutase	cpd00179 <=> cpd00089
alpha-D-Glucose 1-phosphate 1,6-phosphomutase	cpd00089 <=> cpd00079
D-Glucose-6-phosphate ketol-isomerase	cpd00079 <=> cpd00072
alpha-D-Glucose 6-phosphate ketol-isomerase	cpd00079 <=> cpd00863
beta-D-Glucose 6-phosphate ketol-isomerase	cpd00863 <=> cpd00072
ATP:D-glucose 6-phosphotransferase	cpd00002 + cpd00027 --> cpd00008 + cpd00079
alpha-D-Glucose 1-epimerase	cpd00027 <=> cpd00190
ATP:D-glucose 6-phosphotransferase	cpd00002 + cpd00190 --> cpd00008 + cpd00863
ATP:D-fructose-6-phosphate 1-phosphotransferase	cpd00002 + cpd00072 --> cpd00008 + cpd00290
D-Fructose-1,6-bisphosphate 1-phosphohydrolase	cpd00001 + cpd00290 --> cpd00009 + cpd00067 + cpd00072
D-Fructose-1,6-bisphosphate D-glyceraldehyde-3-phosphate-lyase	cpd00290 <=> cpd00095 + cpd00102

D-Glyceraldehyde-3-phosphate ketol-isomerase	cpd00102 <=> cpd00095
D-Glyceraldehyde-3-phosphate:NAD+ oxidoreductasephosphorylating	cpd00003 + cpd00009 + cpd00102 <=> cpd00004 + cpd00203
ATP:3-phospho-D-glycerate 1-phosphotransferase	cpd00008 + cpd00203 <=> cpd00002 + cpd00067 + cpd00169
2-Phospho-D-glycerate 2,3-phosphomutase	cpd00482 <=> cpd00169
2-Phospho-D-glycerate hydro-lyase	cpd00482 <=> cpd00001 + cpd00061
ATP:pyruvate O2-phosphotransferase	cpd00002 + cpd00020 <=> cpd00008 + cpd00061
ATP:oxaloacetate carboxy-lyase transphosphorylating	cpd00002 + cpd00032 + cpd00067 --> cpd00008 + cpd00011 + cpd00061
pyruvate:thiamin diphosphate acetaldehydetransferase	cpd00020 + cpd00056 + cpd00067 --> cpd00011 + cpd03049
2-alpha-Hydroxyethylthiamine diphosphate:lipoamide	cpd00213 + cpd03049 --> cpd00056 + cpd00836
acetyl-CoA:enzyme N6-dihydrolipoyllysine S-acetyltransferase	cpd00022 + cpd00449 <=> cpd00010 + cpd00836
Acetate:CoA ligase AMP-forming	cpd00002 + cpd00010 + cpd00029 + cpd00067 <=> cpd00009 + cpd00008 + cpd00022
Acetaldehyde:NAD+ oxidoreductase	cpd00001 + cpd00003 + cpd00071 --> cpd00004 + cpd00029 + 2 cpd00067
rxn00544	cpd00056 + cpd00071 <=> cpd03049
Ethanol:NAD+ oxidoreductase	cpd00003 + cpd00363 <=> cpd00004 + cpd00067 + cpd00071
Pyruvate ferredoxin oxidoreductase	cpd00010 + cpd00020 + cpd11621 <=> cpd00011 + cpd00022 + cpd00067 + cpd11620
S-Lactate:NAD+ oxidoreductase	cpd00003 + cpd00159 <=> cpd00004 + cpd00020 + cpd00067
L-Lactate dehydrogenase ubiquinone	cpd00159[c] + cpd15560[p] --> cpd00020[c] + cpd15561[p]
L-Lactate oxidoreductase Ferricytochrome-c 2	2 cpd00109[p] + cpd00159[c] <=> cpd00020[c] + 2 cpd00067[p] + 2 cpd00110[p]
L-Lactate dehydrogenase menaquinone	cpd00159[c] + cpd15500[p] --> cpd00020[c] + cpd15499[p]
Acetyl-CoA:orthophosphate acetyltransferase	cpd00009 + cpd00022 + cpd00067 <=> cpd00010 + cpd00196
ATP:acetate phosphotransferase	cpd00002 + cpd00029 + cpd00067 <=> cpd00008 + cpd00196
Pyruvate:carbon-dioxide ligase ADP-forming	cpd00002 + cpd00020 + cpd00242 <=> cpd00008 + cpd00009 + cpd00032 + cpd00067
Citrate oxaloacetate-lyase pro-3S-CH2COO- -> acetyl-CoA	cpd00001 + cpd00022 + cpd00032 --> cpd00010 + cpd00067 + cpd00137
Citrate oxaloacetate-lyase pro-3S-CH2COO- -->acetate	cpd00137 <=> cpd00029 + cpd00032
citrate hydro-lyase	cpd00137 <=> cpd00001 + cpd00331
isocitrate hydro-lyase	cpd00260 <=> cpd00001 + cpd00331
Isocitrate:NADP+ oxidoreductase decarboxylating	cpd00003 + cpd00260 <=> cpd00004 + cpd00067 + cpd03187
Oxalosuccinate:NADP+ oxidoreductase decarboxylating	cpd00067 + cpd03187 <=> cpd00011 + cpd00024
2-Oxoglutarate:Thiamin diphosphate 2-oxidoreductasedecarboxylating	cpd00024 + cpd00056 + cpd00067 --> cpd00011 + cpd03189
3-Carboxy-1-hydroxypropyl-ThPP:lipoamde	cpd00213 + cpd03189 <=> cpd00056 + cpd00860
succinyl-CoA:enzyme N6-dihydrolipoyllysine S-succinyltransferase	cpd00010 + cpd00860 <=> cpd00078 + cpd00449
Dihydrolipoamide:NAD+ oxidoreductase	cpd00003 + cpd00449 <=> cpd00004 + cpd00067 + cpd00213
Succinate:CoA ligase ADP-forming	cpd00008 + cpd00009 + cpd00078 <=> cpd00002 + cpd00010 + cpd00036
S-Malate hydro-lyase	cpd00001 + cpd00106 <=> cpd00130
S-malate:NAD+ oxidoreductase	cpd00003 + cpd00130 <=> cpd00004 + cpd00032 + cpd00067
NADH dehydrogenase ubiquinone-8 . No proton translocation	cpd00004[c] + cpd00067[c] + cpd15560[p] --> cpd00003[c] + cpd15561[p]
NADH dehydrogenase ubiquinone-8 & 3.5 protons	cpd00004[c] + 4.5 cpd00067[c] + cpd15560[p] <=> cpd00003[c] + 3.5 cpd00067[p] + cpd15561[p]
NADH dehydrogenase ubiquinone-8 & 3 protons periplasm	cpd00004 + 4 cpd00067 + cpd15560[p] <=> cpd00003 + 3 cpd00067[p] + cpd15561[p]
NADH dehydrogenase demethylmenaquinone-8 & 0 protons No proton translocation	cpd00004 + cpd00067 + cpd15352[p] --> cpd00003 + cpd15353[p]
NADH dehydrogenase menaquinone-8 & 0 protonsNo proton translocation	cpd00004 + cpd00067 + cpd15500[p] --> cpd00003 + cpd15499[p]
fumarate reductase	cpd00036 + cpd15500[p] <=> cpd00106 + cpd15499[p]
fumarate reductase	cpd00036[c] + cpd15352[p] <=> cpd00106[c] + cpd15353[p]
Succinate dehydrogenase irreversible	cpd00036[c] + cpd15560[p] --> cpd00106[c] + cpd15561[p]
Succinate:acceptor oxidoreductase	cpd00015[c] + cpd00036[c] <=> cpd00106[c] + cpd00982[c]
Succinate dehyrdogenase	cpd00982[c] + cpd15560[p] --> cpd00015[c] + cpd15561[p]
Glycolate oxidase	cpd00139[c] + cpd15560[p] <=> cpd00040[c] + cpd15561[p]
Glycolate oxidase	cpd00139[c] + cpd15500[p] --> cpd00040[c] + cpd15499[p]
Glycolate oxidase	cpd00139 + cpd15352[p] --> cpd00040 + cpd15353[p]

Hydrogenase ubiquinone-8: 2 protons	2 cpd00067 + cpd11640 + cpd15560[p] --> 2 cpd00067[p] + cpd15561[p]
glycerol-3-phosphate dehydrogenase ubiquinone-8	cpd00080 + cpd15560[p] --> cpd00095 + cpd15561[p]
glycerol-3-phosphate dehydrogenase menaquinone-8	cpd00080 + cpd15500[p] --> cpd00095 + cpd15499[p]
glycerol-3-phosphate dehydrogenase demethylmenaquinone-8	cpd00080 + cpd15352[p] --> cpd00095 + cpd15353[p]
ubiquinol---cytochrome-c reductase	2 cpd00109[p] + cpd15561[p] <=> 2 cpd00067[p] + 2 cpd00110[p] + cpd15560[p]
ubiquinol---paeudo azurin reductase	2 cpd12711[p] + cpd15561[p] <=> 2 cpd00067[p] + 2 cpd12712[p] + cpd15560[p]
cytochrome oxygen oxidase bo3 ubiquinol-8: 2.5 protons	0.5 cpd00007 + 2.5 cpd00067 + cpd15561[p] --> cpd00001 + 2.5 cpd00067[p] + cpd15560[p]
cytochrome-c oxygen oxidase H+/e- = 2	0.5 cpd00007 + 6 cpd00067 + 2 cpd00110[p] --> cpd00001 + 4 cpd00067[p] + 2 cpd00109[p]
Ferrocytochrome-c:oxygen oxidoreductase No gain of Proton potential	cpd00007 + 4 cpd00067 + 4 cpd00110[p] --> 2 cpd00001 + 4 cpd00109[p]
ATP synthase four protons for one ATP periplasm	cpd00008[c] + cpd00009[c] + 4 cpd00067[p] --> cpd00001[c] + cpd00002[c] + 3 cpd00067[c]
Nitrate reductase Ubiquinol-8 Membrane bounded, two proton pumped	2 cpd00067 + cpd00209 + cpd15561[p] --> cpd00001 + 2 cpd00067[p] + cpd00075 + cpd15560[p]
Nitrate reductase Menaquinol-8	2 cpd00067 + cpd00209 + cpd15499[p] --> cpd00001 + 2 cpd00067[p] + cpd00075 + cpd15500[p]
Nitrate reductase Ubiquinol-8 Periplasmic bounded, dissimilatory. No proton pumped	cpd00209[p] + cpd15561[p] <=> cpd00001[p] + cpd00075[p] + cpd15560[p]
Nitrite oxidoreductase. Ferrocytochrome-c	2 cpd00067[p] + cpd00075[p] + cpd00110[p] <=> cpd00001[p] + cpd00109[p] + cpd00418[p]
Nitrite oxidoreductase. Reduced azurin	2 cpd00067[p] + cpd00075[p] + cpd12712[p] <=> cpd00001[p] + cpd00418[p] + cpd12711[p]
Nitrite reductase NH4 forming NADPH	3 cpd00005 + 5 cpd00067 + cpd00075 --> 2 cpd00001 + 3 cpd00006 + cpd00013
Nitrite reductase NH4 forming NADH	3 cpd00004 + 5 cpd00067 + cpd00075 --> 2 cpd00001 + 3 cpd00003 + cpd00013
Nitric oxide reduction to nitrous oxide, Cytochrome C	cpd00418[p] + cpd00110[p] + cpd00067[p] --> 0.5 cpd00659[p] + cpd00109[p] + 0.5 cpd00001[p]
Nitrogen production from nitrous oxide. Cytochtome c	0.5 cpd00659[p] + cpd00110[p] + cpd00067[p] --> 0.5 cpd00528[p] + cpd00109[p] + 0.5 cpd00001[p]
Nitrogen production from nitrous oxide. Azurin	cpd00659[p] + 2 cpd12712[p] + 2 cpd00067[p] --> cpd00528[p] + 2 cpd12711[p] + cpd00001[p]
Nitrogen fixation	8 cpd11620[c] + 8 cpd00067[c] + cpd00528[p] + 16 cpd00002[c] + 16 cpd00001[c] --> 8 cpd11621[c] + cpd11640[c] + 2 cpd00013[c] + 16 cpd00008[c] + 16 cpd00009[c]
Hydroxilamine recutase NH4 forming NADH	cpd00165 + cpd00004 --> cpd00013 + cpd00003 + cpd00001
Transport mediated NO2 transport	cpd00075 --> cpd00075[p]
Transport mediated NO3 transport	cpd00209[p] --> cpd00209
Isocitrate glyoxylate-lyase	cpd00260 <=> cpd00036 + cpd00040
L-Malate glyoxylate-lyase CoA-acetylating	cpd00001 + cpd00022 + cpd00040 --> cpd00010 + cpd00067 + cpd00130
Glycolate:NAD+ oxidoreductase	cpd00003 + cpd00139 <=> cpd00004 + cpd00040 + cpd00067
Glycolate:NADP+ oxidoreductase	cpd00006 + cpd00139 <=> cpd00005 + cpd00040 + cpd00067
S-2-Hydroxy-acid:oxygen 2-oxidoreductase	cpd00007 + cpd00139 --> cpd00025 + cpd00040
hydrogen-peroxide:hydrogen-peroxide oxidoreductase	2 cpd00025 --> 2 cpd00001 + cpd00007
Aminoacetic acid:oxygen oxidoreductase deaminating	cpd00001 + cpd00007 + cpd00033 --> cpd00013 + cpd00025 + cpd00040
ATP:R-glycerate 3-phosphotransferase	cpd00002 + cpd00223 <=> cpd00008 + cpd00169
D-Glycerate:NADP+ 2-oxidoreductase	cpd00003 + cpd00223 <=> cpd00004 + cpd00067 + cpd00145
3-Phospho-D-glycerate:NAD+ 2-oxidoreductase	cpd00003 + cpd00169 <=> cpd00004 + cpd00067 + cpd02069
3-Phosphoserine:2-oxoglutarate aminotransferase	cpd00024 + cpd00738 <=> cpd00023 + cpd02069
L-O-Phosphoserine phosphohydrolase	cpd00001 + cpd00738 --> cpd00009 + cpd00054 + cpd00067
L-serine ammonia-lyase	cpd00054 --> cpd00013 + cpd00020
L-Serine hydro-lyase adding indoleglycerol-phosphate	cpd00054 + cpd00359 <=> cpd00001 + cpd00065
L-Serine hydro-lyase adding homocysteine	cpd00054 + cpd00135 <=> cpd00001 + cpd00424
L-Cystathionine Lysteine-lyase deaminating	cpd00001 + cpd00424 --> cpd00013 + cpd00084 + cpd00094
serine O-acetyltransferase	cpd00022 + cpd00054 --> cpd00010 + cpd00722
O3-Acetyl-L-serine acetate-lyase adding hydrogen sulfide	cpd00239 + cpd00722 --> cpd00029 + cpd00067 + cpd00084
cysteine synthase Thiosulfate	cpd00268 + cpd00722 + cpd11421 <=> cpd00029 + cpd00081 + cpd00084 + cpd11420
L-Cysteine L-homocysteine-lyase deaminating	cpd00001 + cpd00084 --> cpd00013 + cpd00020 + cpd00239

5,10-Methylenetetrahydrofolate:glycine hydroxymethyltransferase	cpd00001 + cpd00033 + cpd00125 <=> cpd00054 + cpd00087
L-Threonine acetaldehyde-lyase	cpd00161 <=> cpd00033 + cpd00071
L-Glutamate:NADP+ oxidoreductase deaminating	cpd00005 + cpd00013 + cpd00024 + cpd00067 --> cpd00001 + cpd00006 + cpd00023
L-Glutamate:NAD+ oxidoreductase deaminating	cpd00004 + cpd00013 + cpd00024 + cpd00067 --> cpd00001 + cpd00003 + cpd00023
L-Glutamate:NADP+ oxidoreductase transaminating	cpd00005 + cpd00024 + cpd00053 + cpd00067 --> cpd00006 + 2 cpd00023
L-Glutamate:NAD+ oxidoreductase transaminating	cpd00004 + cpd00024 + cpd00053 + cpd00067 --> cpd00003 + 2 cpd00023
L-Glutamate:ammonia ligase ADP-forming	cpd00002 + cpd00013 + cpd00023 --> cpd00008 + cpd00009 + cpd00053 + cpd00067
L-Glutamine amidohydrolase	cpd00001 + cpd00053 --> cpd00013 + cpd00023
L-Alanine:2-oxoglutarate aminotransferase	cpd00024 + cpd00035 <=> cpd00020 + cpd00023
L-Alanine:glyoxylate aminotransferase	cpd00035 + cpd00040 <=> cpd00020 + cpd00033
L-Alanine:NAD+ oxidoreductase deaminating	cpd00001 + cpd00003 + cpd00035 <=> cpd00004 + cpd00013 + cpd00020 + cpd00067
L-Aspartate ammonia-lyase	cpd00041 <=> cpd00013 + cpd00106
IMP:L-aspartate ligase GDP-forming	cpd00038 + cpd00041 + cpd00114 --> cpd00009 + cpd00031 + 2 cpd00067 + cpd02375
N6-1,2-DicarboxyethylAMP AMP-lyase	cpd02375 <=> cpd00018 + cpd00106
L-Citrulline:L-aspartate ligase AMP-forming	cpd00002 + cpd00041 + cpd00274 <=> cpd00012 + cpd00018 + cpd02152
N-L-Argininosuccinate arginie-lyase	cpd02152 <=> cpd00051 + cpd00106
L-aspartate:L-glutamine amido-ligase AMP-forming	cpd00001 + cpd00002 + cpd00041 + cpd00053 --> cpd00012 + cpd00018 + cpd00023 + cpd00132
L-Asparagine amidohydrolase	cpd00001 + cpd00132 --> cpd00013 + cpd00041
L-Aspartate:2-oxoglutarate aminotransferase	cpd00024 + cpd00041 <=> cpd00023 + cpd00032
L-Aspartic acid:oxygen oxidoreductase deaminating	cpd00001 + cpd00007 + cpd00041 --> cpd00013 + cpd00025 + cpd00032
D-Glyceraldehyde:NAD+ oxidoreductase	cpd00001 + cpd00003 + cpd00448 <=> cpd00004 + 2 cpd00067 + cpd00223
Glycerol:NAD+ oxidoreductase	cpd00003 + cpd00100 <=> cpd00004 + cpd00067 + cpd00448
ATP:glycerol 3-phosphotransferase	cpd00002 + cpd00100 <=> cpd00008 + cpd00080
Acetyl-CoA:carbon-dioxide ligase ADP-forming	cpd00002 + cpd00022 + cpd00242 <=> cpd00008 + cpd00009 + cpd00067 + cpd00070
acetyl-CoA:[acyl-carrier-protein] S-acetyltransferase	cpd00022 + cpd11493 <=> cpd00010 + cpd11494
Acetyl-CoA:carbon-dioxide ligase ADP-forming	cpd00022 + cpd12543 <=> cpd00070 + cpd12848
biotin-carboxyl-carrier-protein:carbon-dioxide ligase ADP-forming	cpd00002 + cpd00242 + cpd12848 <=> cpd00008 + cpd00009 + cpd00067 + cpd12543
malonyl-ACP:[acyl-carrier-protein] transferase	cpd00070 + cpd11493 <=> cpd00010 + cpd11492
Acyl-[acyl-carrier-protein]:malonyl-[acyl-carrier-protein]	cpd00067 + cpd11492 + cpd11494 --> cpd00011 + cpd11488 + cpd11493
3R-3-Hydroxybutanoyl-[acyl-carrier protein]:NADP+ oxidoreductase	cpd00006 + cpd11478 <=> cpd00005 + cpd00067 + cpd11488
3R-3-Hydroxybutanoyl-[acyl-carrier-protein] hydro-lyase	cpd11478 <=> cpd00001 + cpd11465
Butyryl-[acyl-carrier protein]:malonyl-CoA	cpd00004 + cpd00067 + cpd11465 --> cpd00003 + cpd11464
butyryl-[acyl-carrier protein]:malonyl-[acyl-carrier-protein]	cpd00067 + cpd11464 + cpd11492 --> cpd00011 + cpd11486 + cpd11493
3R-3-Hydroxyhexanoyl-[acyl-carrier-protein]:NADP+ oxidoreductase	cpd00006 + cpd11479 <=> cpd00005 + cpd00067 + cpd11486
3R-3-Hydroxybutanoyl-[acyl-carrier-protein] hydro-lyase	cpd11479 <=> cpd00001 + cpd11473
Hexanoyl-[acyl-carrier protein]:malonyl-CoA	cpd00004 + cpd00067 + cpd11473 --> cpd00003 + cpd11472
hexanoyl-[acyl-carrier protein]:malonyl-[acyl-carrier-protein]	cpd00067 + cpd11472 + cpd11492 --> cpd00011 + cpd11490 + cpd11493
3R-3-Hydroxyoctanoyl-[acyl-carrier-protein]:NADP+ oxidoreductase	cpd00006 + cpd11483 <=> cpd00005 + cpd00067 + cpd11490
3R-3-Hydroxybutanoyl-[acyl-carrier-protein] hydro-lyase	cpd11483 <=> cpd00001 + cpd11471
Octanoyl-[acyl-carrier protein]:malonyl-CoA	cpd00004 + cpd00067 + cpd11471 --> cpd00003 + cpd11470
Fatty-acyl-ACP hydrolase	cpd00001 + cpd11470 --> cpd00067 + cpd03846 + cpd11493
Octanoyl-[acyl-carrier protein]:malonyl-[acyl-carrier-protein]	cpd00067 + cpd11470 + cpd11492 --> cpd00011 + cpd11487 + cpd11493
3R-3-Hydroxydecanoyl-[acyl-carrier-protein]:NADP+ oxidoreductase	cpd00006 + cpd11482 <=> cpd00005 + cpd00067 + cpd11487
3R-3-Hydroxybutanoyl-[acyl-carrier-protein] hydro-lyase	cpd11482 <=> cpd00001 + cpd11475
Decanoyl-[acyl-carrier protein]:malonyl-CoA	cpd00004 + cpd00067 + cpd11475 --> cpd00003 + cpd11474

fatty-acyl-ACP hydrolase	cpd00001 + cpd11474 --> cpd00067 + cpd01107 + cpd11493
Decanoyl-[acyl-carrier protein]:malonyl-[acyl-carrier-protein]	cpd00067 + cpd11474 + cpd11492 --> cpd00011 + cpd11489 + cpd11493
3R-3-Hydroxydodecanoyl-[acyl-carrier-protein]:NADP+ oxidoreductase	cpd00006 + cpd11480 <=> cpd00005 + cpd00067 + cpd11489
3R-3-Hydroxybutanoyl-[acyl-carrier-protein] hydro-lyase	cpd11480 <=> cpd00001 + cpd11469
Dodecanoyl-[acyl-carrier protein]:malonyl-CoA	cpd00004 + cpd00067 + cpd11469 --> cpd00003 + cpd11468
Dodecanoyl-[acyl-carrier-protein] hydrolase	cpd00001 + cpd11468 --> cpd00067 + cpd01741 + cpd11493
dodecanoyl-[acyl-carrier-protein]:malonyl-[acyl-carrier-protein]	cpd00067 + cpd11468 + cpd11492 --> cpd00011 + cpd11491 + cpd11493
3R-3-Hydroxytetradecanoyl-[acyl-carrier-protein]:NADP+	cpd00006 + cpd11484 <=> cpd00005 + cpd00067 + cpd11491
3R-3-Hydroxypalmitoyl-[acyl-carrier-protein] hydro-lyase	cpd11484 <=> cpd00001 + cpd11467
Tetradecanoyl-[acyl-carrier protein]:malonyl-CoA	cpd00004 + cpd00067 + cpd11467 --> cpd00003 + cpd11466
Myristic fatty-acyl-ACP hydrolase	cpd00001 + cpd11466 --> cpd00067 + cpd03847 + cpd11493
Tetradecanoyl-[acyl-carrier protein]:malonyl-[acyl-carrier-protein]	cpd00067 + cpd11466 + cpd11492 --> cpd00011 + cpd11485 + cpd11493
3R-3-Hydroxypalmitoyl-[acyl-carrier-protein]:NADP+ oxidoreductase	cpd00006 + cpd11481 <=> cpd00005 + cpd00067 + cpd11485
3R-3-Hydroxypalmitoyl-[acyl-carrier-protein] hydro-lyase	cpd11481 <=> cpd00001 + cpd11477
Hexadecanoyl-[acyl-carrier protein]:malonyl-CoA	cpd00004 + cpd00067 + cpd11477 --> cpd00003 + cpd11476
Palmitic fatty-acyl-ACP hydrolase	cpd00001 + cpd11476 --> cpd00067 + cpd00214 + cpd11493
3-Oxooctodecanoyl-ACP:malonyl-[acyl-carrier-protein] C-acyltransferase decarboxylating	cpd00067 + cpd11476 + cpd11492 --> cpd00011 + cpd11493 + cpd11570
3-Hydroxyoctodecanoyl-ACP:NADP+ oxidoreductase	cpd00006 + cpd11571 <=> cpd00005 + cpd00067 + cpd11570
trans-Octodec-2-enoyl-ACP hydro-lyase	cpd11571 <=> cpd00001 + cpd11572
trans-Octodec-2-enoyl-ACP:NAD+ oxidoreductase A-specific	cpd00004 + cpd00067 + cpd11572 --> cpd00003 + cpd11573
Stearic fatty-acyl-ACP hydrolase	cpd00001 + cpd11573 --> cpd00067 + cpd01080 + cpd11493
Tetradecanoyl-ACP:[acyl-carrier-protein] transferase	cpd00010 + cpd11466 <=> cpd01695 + cpd11493
Hexadecanoyl-ACP:[acyl-carrier-protein] transferase	cpd00010 + cpd11476 <=> cpd00134 + cpd11493
Hexadecenoyl-ACP:[acyl-carrier-protein] transferase	cpd00010 + cpd15239 <=> cpd15238 + cpd11493
Octadecanoyl-ACP:[acyl-carrier-protein] transferase	cpd00010 + cpd11573 <=> cpd00327 + cpd11493
Octadecenoyl-ACP:[acyl-carrier-protein] transferase	cpd00010 + cpd11825 <=> cpd15274 + cpd11493
Palimitate synthesis	cpd00001 + cpd00134 --> cpd00010 + cpd00067 + cpd00214
Stearate synthesis	cpd00001 + cpd00327 --> cpd00010 + cpd00067 + cpd01080
3oxoacyl-acp synthase c20:0	2 cpd00067 + cpd00327 + cpd00070 + cpd00004 + cpd00005 --> cpd00011 + cpd01393 + cpd00010 + cpd00003 + cpd00006
Arachidic-[acyl-carrier-protein] hydrolase	cpd00001 + cpd01393 --> cpd03848 + cpd00010
3oxoacyl-acp synthase c22:0	2 cpd00067 + cpd01393 + cpd00070 + cpd00004 + cpd00005 --> cpd00011 + cpd16343 + cpd00010 + cpd00003 + cpd00006
Behenic-[acyl-carrier-protein] hydrolase	cpd00001 + cpd16343 --> cpd05196 + cpd00010
Myristoyl-ACP desaturase delta-9 desaturase	cpd00007 + cpd11466 + cpd00005 --> 2 cpd00001 + cpd15294 + cpd00006
Myristoleoyl fatty-acyl-ACP hydrolase	cpd00001 + cpd15294 --> cpd00067 + cpd15298 + cpd11493
Palmitoyl-ACP desaturase delta-9 desaturase	cpd00007 + cpd11476 + cpd00005 --> 2 cpd00001 + cpd15239 + cpd00006
Palmitoleoyl-ACP fatty-acyl-ACP hydrolase	cpd00001 + cpd15239 --> cpd00067 + cpd15237 + cpd11493
Stearoyl-CoA desaturase delta-9 desaturase	cpd00007[c] + cpd00327[c] + 2 cpd00110[p] --> 2 cpd00001[c] + cpd15274[c] + 2 cpd00109[p]
Oleoyl-CoA fatty-acyl-ACP hydrolase	cpd00001 + cpd15274 --> cpd00067 + cpd15269 + cpd11493
Octadecenoyl-CoA fatty-acyl-ACP hydrolase	cpd00001 + cpd15274 --> cpd00067 + cpd152691 + cpd11493
Octadecenoyl-CoAdesaturase delta-9, 12 and 6 desaturase	2 cpd00007 + cpd15274 + 4 cpd00110[p] --> 4 cpd00001 + cpd03849c + 4 cpd00109[p]
gamma Linonlenic-CoA fatty-acyl-ACP hydrolase	cpd00001 + cpd03849c --> cpd00067 + cpd03849 + cpd11493
Decanoyl-[acyl-carrier protein]:acetyl-[acyl-carrier-protein]	2 cpd00067 + cpd11474 + cpd11494 + cpd00004 + cpd00005 --> cpd00011 + cpd11468odd + cpd11493 + cpd00003 + cpd00006
Undecanoyl-[acyl-carrier-protein] hydrolase	cpd00001 + cpd11468odd --> cpd01741odd + cpd11493
Dodecanoyl-[acyl-carrier protein]:acetyl-[acyl-carrier-protein]	2 cpd00067 + cpd11468 + cpd11494 + cpd00004 + cpd00005 --> cpd00011 + cpd11466odd + cpd11493 + cpd00003 + cpd00006
Tridecanoyl-[acyl-carrier-protein] hydrolase	cpd00001 + cpd11466odd --> cpd03847odd + cpd11493
Tetraecanoyl-[acyl-carrier protein]:acetyl-[acyl-carrier-protein]	2 cpd00067 + cpd11466 + cpd11494 + cpd00004 + cpd00005 --> cpd00011 + cpd11476odd + cpd11493 + cpd00003 + cpd00006
Pentadecanoyl-[acyl-carrier-protein] hydrolase	cpd00001 + cpd11476odd --> cpd00214odd + cpd11493
Hexadecanoyl-[acyl-carrier protein]:acetyl-[acyl-carrier-protein]	2 cpd00067 + cpd11476 + cpd11494 + cpd00004 + cpd00005 --> cpd00011 + cpd11573odd + cpd11493 + cpd00003 + cpd00006

Pentadecanoyl-[acyl-carrier-protein] hydrolase	cpd00001 + cpd11573odd --> cpd01080odd + cpd11493
Myristic:CoA ligase tetradecanoate	cpd00002 + cpd00010 + cpd00067 + cpd03847 --> cpd00012 + cpd00018 + cpd01695
Palmitic:CoA ligase AMP-forming	cpd00002 + cpd00010 + cpd00067 + cpd00214 --> cpd00012 + cpd00018 + cpd00134
Stearic:CoA ligase octadecanoate	cpd01080 --> cpd00327
Oleic:CoA ligase octadecenoate	cpd00002 + cpd00010 + cpd00067 + cpd15269 --> cpd00012 + cpd00018 + cpd15274
Palmitoleic--CoA ligase hexadecenoate, peroxisomal	cpd00002 + cpd00010 + cpd00067 + cpd15237 --> cpd00012 + cpd00018 + cpd15238
FACOAL17iso	cpd00002 + cpd00010 + cpd00067 + cpd11431 --> cpd00012 + cpd00018 + cpd11432
FACOAL17anteiso	cpd00002 + cpd00010 + cpd00067 + cpd11433 --> cpd00012 + cpd00018 + cpd11434
FACOAL14iso	cpd00002 + cpd00010 + cpd00067 + cpd11430 --> cpd00012 + cpd00018 + cpd11435
FACOAL15iso	cpd00002 + cpd00010 + cpd00067 + cpd11436 --> cpd00012 + cpd00018 + cpd11437
FACOAL15anteiso	cpd00002 + cpd00010 + cpd00067 + cpd11438 --> cpd00012 + cpd00018 + cpd11439
FACOAL16iso	cpd00002 + cpd00010 + cpd00067 + cpd11440 --> cpd00012 + cpd00018 + cpd11441
FACOAL14iso	cpd03847 --> cpd11430
FACOAL16iso	cpd00214 --> cpd11440
FACOAL15iso	cpd00214odd --> cpd11436
FACOAL15anteiso	cpd00214odd --> cpd11438
FACOAL17iso	cpd01080odd --> cpd11431
FACOAL17anteiso	cpd01080odd --> cpd11433
glycerol-3-phosphate acyltransferase C12:0	cpd00080 + cpd11468 --> cpd11493 + cpd15325
1-tetradecanoyl-sn-glycerol 3-phosphate O-acyltransferase n-C12:0	cpd11468 + cpd15325 --> cpd11493 + cpd15521
glycerol-3-phosphate acyltransferase C14:0	cpd00080 + cpd11466 --> cpd11493 + cpd15331
1-tetradecanoyl-sn-glycerol 3-phosphate O-acyltransferase n-C14:0	cpd11466 + cpd15331 --> cpd11493 + cpd15522
glycerol-3-phosphate acyltransferase C14:1	cpd00080 + cpd15294 --> cpd11493 + cpd15330
1-tetradec-7-enoyl-sn-glycerol 3-phosphate O-acyltransferase n-C14:1	cpd15294 + cpd15330 --> cpd11493 + cpd15523
glycerol-3-phosphate acyltransferase C16:0	cpd00080 + cpd11476 --> cpd11493 + cpd15327
1-hexadecanoyl-sn-glycerol 3-phosphate O-acyltransferase n-C16:0	cpd11476 + cpd15327 --> cpd11493 + cpd15524
glycerol-3-phosphate acyltransferase C16:1	cpd00080 + cpd15239 --> cpd11493 + cpd15326
1-hexadec-7-enoyl-sn-glycerol 3-phosphate O-acyltransferase n-C16:1	cpd15239 + cpd15326 --> cpd11493 + cpd15525
glycerol-3-phosphate acyltransferase C18:0	cpd00080 + cpd11573 --> cpd11493 + cpd15329
1-octadecanoyl-sn-glycerol 3-phosphate O-acyltransferase n-C18:0	cpd11573 + cpd15329 --> cpd11493 + cpd15526
glycerol-3-phosphate acyltransferase C18:1	cpd00080 + cpd11825 --> cpd11493 + cpd15328
1-octadec-7-enoyl-sn-glycerol 3-phosphate O-acyltransferase n-C18:1	cpd11825 + cpd15328 --> cpd11493 + cpd15527
palmitoyl-glycerol-3-phosphate O-acyltransferase	cpd00080 + cpd00134 --> cpd00010 + cpd15327
palmitoyl-1-acylglycerol-3-phosphate O-acyltransferase	cpd00134 + cpd15327 --> cpd00010 + cpd15524
myristoyl-glycerol-3-phosphate O-acyltransferase	cpd00080 + cpd01695 --> cpd00010 + cpd15331
myristoyl-1-acylglycerol-3-phosphate O-acyltransferase	cpd01695 + cpd15331 --> cpd00010 + cpd15522
stearoyl-glycerol-3-phosphate O-acyltransferase	cpd00080 + cpd00327 --> cpd00010 + cpd15329
stearoyl-1-acylglycerol-3-phosphate O-acyltransferase	cpd00327 + cpd15329 --> cpd00010 + cpd15526
isoheptadecanoyl-glycerol-3-phosphate O-acyltransferase	cpd00080 + cpd11432 --> cpd00010 + cpd15671
isoheptadecanoyl-1-acylglycerol-3-phosphate O-acyltransferase	cpd11432 + cpd15671 --> cpd00010 + cpd15677
anteisoheptadecanoyl-glycerol-3-phosphate O-acyltransferase	cpd00080 + cpd11434 --> cpd00010 + cpd15672
anteisoheptadecanoyl-1-acylglycerol-3-phosphate O-acyltransferase	cpd11434 + cpd15672 --> cpd00010 + cpd15678
isotetradecanoyl-glycerol-3-phosphate O-acyltransferase	cpd00080 + cpd11435 --> cpd00010 + cpd15673
isotetradecanoyl-1-acylglycerol-3-phosphate O-acyltransferase	cpd11435 + cpd15673 --> cpd00010 + cpd15679
isopentadecanoyl-glycerol-3-phosphate O-	cpd00080 + cpd11437 --> cpd00010 + cpd15674

acyltransferase	
isopentadecanoyl-1-acylglycerol-3-phosphate O-acyltransferase	cpd11437 + cpd15674 --> cpd00010 + cpd15680
anteisopentadecanoyl-glycerol-3-phosphate O-acyltransferase	cpd00080 + cpd11439 --> cpd00010 + cpd15675
anteisopentadecanoyl-1-acylglycerol-3-phosphate O-acyltransferase	cpd11439 + cpd15675 --> cpd00010 + cpd15681
isohexadecanoyl-glycerol-3-phosphate O-acyltransferase	cpd00080 + cpd11441 --> cpd00010 + cpd15676
isohexadecanoyl-1-acylglycerol-3-phosphate O-acyltransferase	cpd11441 + cpd15676 --> cpd00010 + cpd15682
Stearoyl-CoA:oxygen 2-oxidoreductase	cpd00015 + cpd00327 <=> cpd00982 + cpd03126b
S-3-Hydroxyhexadecanoyl-CoA hydro-lyase	cpd03113b <=> cpd00001 + cpd03126b
S-3-Hydroxyhexadecanoyl-CoA:NAD+ oxidoreductase	cpd00003 + cpd03113b <=> cpd00004 + cpd00067 + cpd03114b
myristoyl-CoA:acetylCoA C-myristoyltransferase	cpd00022 + cpd00134 <=> cpd00010 + cpd03114b
Palmitoyl-CoA:oxygen 2-oxidoreductase	cpd00015 + cpd00134 <=> cpd00982 + cpd03126
S-3-Hydroxyhexadecanoyl-CoA hydro-lyase	cpd03113 <=> cpd00001 + cpd03126
S-3-Hydroxyhexadecanoyl-CoA:NAD+ oxidoreductase	cpd00003 + cpd03113 <=> cpd00004 + cpd00067 + cpd03114
myristoyl-CoA:acetylCoA C-myristoyltransferase	cpd00022 + cpd01695 <=> cpd00010 + cpd03114
acyl-CoA dehydrogenase tetradecanoyl-CoA	cpd00004 + cpd00067 + cpd03127 --> cpd00003 + cpd01695
Miristoyl-CoA:acceptor 2,3-oxidoreductase	cpd00015 + cpd01695 --> cpd00982 + cpd03127
S-3-Hydroxytetradecanoyl-CoA hydro-lyase	cpd03115 <=> cpd00001 + cpd03127
S-3-Hydroxytetradecanoyl-CoA:NAD+ oxidoreductase	cpd00003 + cpd03115 <=> cpd00004 + cpd00067 + cpd12689
Lauroyl-CoA:acetyl-CoA C-acyltransferase	cpd00022 + cpd01260 <=> cpd00010 + cpd12689
acyl-CoA dehydrogenase dodecanoyl-CoA	cpd00004 + cpd00067 + cpd02060 --> cpd00003 + cpd01260
Lauroyl-CoA:acceptor 2,3-oxidoreductase	cpd00015 + cpd01260 <=> cpd00982 + cpd02060
S-3-Hydroxydodecanoyl-CoA hydro-lyase	cpd03116 <=> cpd00001 + cpd02060
S-3-Hydroxydodecanoyl-CoA:NAD+ oxidoreductase	cpd00003 + cpd03116 <=> cpd00004 + cpd00067 + cpd03117
Decanoyl-CoA:acetyl-CoA C-acyltransferase	cpd00022 + cpd03128 <=> cpd00010 + cpd03117
acyl-CoA dehydrogenase decanoyl-CoA	cpd00004 + cpd00067 + cpd03129 --> cpd00003 + cpd03128
Decanoyl-CoA:acceptor 2,3-oxidoreductase	cpd00015 + cpd03128 <=> cpd00982 + cpd03129
S-Hydroxydecanoyl-CoA hydro-lyase	cpd03118 <=> cpd00001 + cpd03129
S-Hydroxydecanoyl-CoA:NAD+ oxidoreductase	cpd00003 + cpd03118 <=> cpd00004 + cpd00067 + cpd03119
Octanoyl-CoA:acetyl-CoA C-acyltransferase	cpd00022 + cpd01335 <=> cpd00010 + cpd03119
acyl-CoA dehydrogenase octanoyl-CoA	cpd00004 + cpd00067 + cpd03130 --> cpd00003 + cpd01335
Octanoyl-CoA:oxygen 2-oxidoreductase	cpd00015 + cpd01335 <=> cpd00982 + cpd03130
S-Hydroxyoctanoyl-CoA hydro-lyase	cpd03120 <=> cpd00001 + cpd03130
S-Hydroxyoctanoyl-CoA:NAD+ oxidoreductase	cpd00003 + cpd03120 <=> cpd00004 + cpd00067 + cpd03121
Hexanoyl-CoA:acetyl-CoA C-acyltransferase	cpd00022 + cpd03124 <=> cpd00010 + cpd03121
acyl-CoA dehydrogenase hexanoyl-CoA	cpd00004 + cpd00067 + cpd03125 --> cpd00003 + cpd03124
Hexanoyl-CoA:oxygen 2-oxidoreductase	cpd00015 + cpd03124 <=> cpd00982 + cpd03125
S-Hydroxyhexanoyl-CoA hydro-lyase	cpd03122 <=> cpd00001 + cpd03125
S-Hydroxyhexanoyl-CoA:NAD+ oxidoreductase	cpd00003 + cpd03122 <=> cpd00004 + cpd00067 + cpd03123
Acetyl-CoA:acetyl-CoA C-acetyltransferase	cpd00022 + cpd00120 <=> cpd00010 + cpd03123
Butanoyl-CoA:acceptor 2,3-oxidoreductase	cpd00004 + cpd00067 + cpd00650 --> cpd00003 + cpd00120
Butanoyl-CoA:oxygen 2-oxidoreductase	cpd00015 + cpd00120 <=> cpd00982 + cpd00650
S-3-Hydroxybutanoyl-CoA hydro-lyase	cpd00842 <=> cpd00001 + cpd00650
S-3-Hydroxybutanoyl-CoA:NAD+ oxidoreductase	cpd00003 + cpd00842 <=> cpd00004 + cpd00067 + cpd00279
Acetyl-CoA:acetyl-CoA C-acetyltransferase	2 cpd00022 <=> cpd00010 + cpd00279
Acetyl-CoA:L-glutamate N-acetyltransferase	cpd00022 + cpd00023 --> cpd00010 + cpd00067 + cpd00477
ATP:N-acetyl-L-glutamate 5-phosphotransferase	cpd00002 + cpd00067 + cpd00477 <=> cpd00008 + cpd02552
N-Acetyl-L-glutamate-5-semialdehyde:NADP+ 5-oxidoreductase	cpd00005 + cpd02552 --> cpd00006 + cpd00009 + cpd00918
N2-Acetyl-L-ornithine:2-oxoglutarate aminotransferase	cpd00024 + cpd00342 <=> cpd00023 + cpd00918
N2-Acetyl-L-ornithine amidohydrolase	cpd00001 + cpd00342 <=> cpd00029 + cpd00064
N2-Acetyl-L-ornithine:L-glutamate N-acetyltransferase	cpd00023 + cpd00342 <=> cpd00064 + cpd00477
L-Ornithine carboxy-lyase	cpd00064 + cpd00067 --> cpd00011 + cpd00118
L-Ornithine ammonia-lyasecyclizing	cpd00064 --> cpd00013 + cpd00067 + cpd00129
L-1-Pyrroline-5-carboxylate:NAD+ oxidoreductase	2 cpd00001 + cpd00003 + cpd02431 <=> cpd00004 + cpd00023 + cpd00067
L-Glutamate 5-semialdehyde:NAD+ oxidoreductase	cpd00001 + cpd00003 + cpd00858 <=> cpd00004 + cpd00023 + 2 cpd00067

L-Proline:NADP+ 5-oxidoreductase	cpd00006 + cpd00129 <=> cpd00005 + cpd00067 + cpd02431
1-Pyrroline-5-carboxylate	cpd00858 <=> cpd02431
ATP:L-glutamate 5-phosphotransferase	cpd00002 + cpd00023 + cpd00067 <=> cpd00008 + cpd02097
L-Glutamate-5-semialdehyde:NADP+ 5-oxidoreductase phosphorylationg	cpd00005 + cpd02097 --> cpd00006 + cpd00009 + cpd00858
Carbamoyl-phosphate:L-ornithine carbamoyltransferase	cpd00064 + cpd00146 --> cpd00009 + 2 cpd00067 + cpd00274
L-Arginine iminohydrolase	cpd00001 + cpd00051 --> cpd00013 + cpd00274
L-Ornithine:2-oxo-acid aminotransferase	cpd00024 + cpd00064 <=> cpd00023 + cpd00858
L-Arginine amidinohydrolase	cpd00001 + cpd00051 --> cpd00064 + cpd00073
Urea amidohydrolase	cpd00001 + 2 cpd00067 + cpd00073 --> cpd00011 + 2 cpd00013
L-Arginine carboxy-lyase	cpd00051 + cpd00067 --> cpd00011 + cpd00152
L-threonine ammonia-lyase	cpd00161 --> cpd00013 + cpd00094
S-2-Aceto-2-hydroxybutanoate pyruvate-lyase carboxylating	cpd00094 + cpd03049 <=> cpd00056 + cpd00498
S-2-Aceto-2-hydroxybutanoate:NADP+ oxidoreductase isomerizing	cpd00498 <=> cpd10162
R-2,3-Dihydroxy-3-methylpentanoate:NADP+ oxidoreductase	cpd00006 + cpd02535 <=> cpd00005 + cpd00067 + cpd10162
R-2,3-Dihydroxy-3-methylpentanoate hydro-lyase	cpd02535 --> cpd00001 + cpd00508
L-Isoleucine:2-oxoglutarate aminotransferase	cpd00024 + cpd00322 <=> cpd00023 + cpd00508
L-Isoleucine:NAD+ oxidoreductasedeaminating	cpd00001 + cpd00003 + cpd00322 <=> cpd00004 + cpd00013 + cpd00067 + cpd00508
2-Acetolactate pyruvate-lyase carboxylating	cpd00056 + cpd00668 <=> cpd00020 + cpd03049
2-Acetolactate methylmutase	cpd00668 <=> cpd02569
R-2,3-Dihydroxy-3-methylbutanoate:NADP+ oxidoreductase	cpd00006 + cpd02498 <=> cpd00005 + cpd00067 + cpd02569
2,3-Dihydroxy-3-methylbutanoate hydro-lyase	cpd02498 --> cpd00001 + cpd00123
L-Valine:2-oxoglutarate aminotransferase	cpd00024 + cpd00156 <=> cpd00023 + cpd00123
L-Valine:NAD+ oxidoreductasedeaminating	cpd00001 + cpd00003 + cpd00156 <=> cpd00004 + cpd00013 + cpd00067 + cpd00123
L-Valine:pyruvate aminotransferase	cpd00020 + cpd00156 <=> cpd00035 + cpd00123
3-Carboxy-3-hydroxy-4-methylpentanoate 3-methyl-2-oxobutanoate-lyase	cpd00001 + cpd00022 + cpd00123 --> cpd00010 + cpd00067 + cpd01646
2-Isopropylmalate hydro-lyase	cpd01646 <=> cpd00001 + cpd01710
3-Isopropylmalate hydro-lyase	cpd02693 <=> cpd00001 + cpd01710
3-Isopropylmalate:NAD+ oxidoreductase	cpd00003 + cpd02693 <=> cpd00004 + cpd00067 + cpd02605
2-Oxo-4-methyl-3-carboxypentanoate decarboxylation	cpd00067 + cpd02605 --> cpd00011 + cpd00200
L-Leucine:2-oxoglutarate aminotransferase	cpd00024 + cpd00107 <=> cpd00023 + cpd00200
L-leucine:NAD+ oxidoreductasedeaminating	cpd00001 + cpd00003 + cpd00107 <=> cpd00004 + cpd00013 + cpd00067 + cpd00200
ATP:L-aspartate 4-phosphotransferase	cpd00002 + cpd00041 + cpd00067 <=> cpd00008 + cpd01977
L-Aspartate-4-semialdehyde:NADP+ oxidoreductase phosphorylating	cpd00005 + cpd01977 --> cpd00006 + cpd00009 + cpd00346
L-Homoserine:NAD+ oxidoreductase	cpd00003 + cpd00227 <=> cpd00004 + cpd00067 + cpd00346
L-Aspartate-4-semialdehyde hydro-lyase adding pyruvate and	cpd00020 + cpd00346 + cpd00004 + cpd00067 --> 2 cpd00001 + cpd02465 + cpd00003
Succinyl-CoA:2,3,4,5-tetrahydropyridine-2,6-dicarboxylate	2 cpd00001 + cpd00078 + cpd02465 + cpd00023 <=> cpd00010 + cpd00024 + cpd00036 + cpd00516
meso-2,6-Diaminoheptanedioate carboxy-lyase	cpd00067 + cpd00516 --> cpd00011 + cpd00039
N2-Acyl-L-lysine amidohydrolase	cpd00001 + cpd01770 <=> cpd00029 + cpd00039
L-Lysine carboxy-lyase	cpd00039 + cpd00067 --> cpd00011 + cpd01155
Phosphoenolpyruvate:D-erythrose-4-phosphate	cpd00001 + cpd00061 + cpd00236 --> cpd00009 + cpd00067 + cpd02857
2-Dehydro-3-deoxy-D-arabino-heptonate 7-phosphate phosphate-lyase	cpd02857 --> cpd00009 + cpd00067 + cpd00699
Quinate:pyrroloquinoline-quinone 5-oxidoreductase	cpd00097 + cpd00248 <=> cpd00699 + cpd00986
3-Dehydroquinate hydro-lyase	cpd00699 --> cpd00001 + cpd01716
Shikimate:NADP+ 5-oxidoreductase	cpd00006 + cpd00383 <=> cpd00005 + cpd00067 + cpd01716
ATP:shikimate 3-phosphotransferase	cpd00002 + cpd00383 <=> cpd00008 + cpd02030
Phosphoenolpyruvate:3-phosphoshikimate	cpd00061 + cpd02030 <=> cpd00009 + cpd00067 + cpd00932
5-O-1-Carboxyvinyl-3-phosphoshikimate phosphate-lyase	cpd00932 --> cpd00009 + cpd00067 + cpd00216
Chorismate pyruvate-lyase amino-accepting	cpd00013 + cpd00216 --> cpd00001 + cpd00020 + cpd00067 + cpd00093
N-5-Phospho-D-ribosylanthranilate:pyrophosphate	cpd00093 + cpd00103 --> cpd00012 + cpd02642

N-5-Phospho-beta-D-ribosylanthranilate ketol-isomerase	cpd02642 <=> cpd00956
1-2-Carboxyphenylamino-1-deoxy-D-ribulose-5-phosphate	cpd00067 + cpd00956 --> cpd00001 + cpd00011 + cpd02210
L-Serine hydro-lyase adding indoleglycerol-phosphate	cpd00054 + cpd02210 <=> cpd00001 + cpd00065 + cpd00102
1S,2R-1-C-indol-3-ylglycerol 3-phosphate	cpd02210 <=> cpd00102 + cpd00359
Chorismate pyruvatemutase	cpd00216 --> cpd00219
Prephenate hydro-lyase decarboxylating	cpd00067 + cpd00219 --> cpd00001 + cpd00011 + cpd00143
L-Phenylalanine:2-oxoglutarate aminotransferase	cpd00024 + cpd00066 <=> cpd00023 + cpd00143
Prephenate:NAD+ oxidoreductasedecarboxylating	cpd00003 + cpd00219 --> cpd00004 + cpd00011 + cpd00868
Prephenate:NADP+ oxidoreductasedecarboxylating	cpd00006 + cpd00219 --> cpd00005 + cpd00011 + cpd00868
L-Tyrosine:2-oxoglutarate aminotransferase	cpd00024 + cpd00069 <=> cpd00023 + cpd00868
D-Fructose 6-phosphate:D-glyceraldehyde-3-phosphate glycolaldehyde	cpd00072 + cpd00102 <=> cpd00198 + cpd00236
Sedoheptulose-7-phosphate:D-glyceraldehyde-3-phosphate	cpd00102 + cpd00238 <=> cpd00072 + cpd00236
D-Ribulose-5-phosphate 3-epimerase	cpd00171 <=> cpd00198
D-Ribose-5-phosphate ketol-isomerase	cpd00101 <=> cpd00171
Sedoheptulose-7-phosphate:D-glyceraldehyde-3-phosphate	cpd00102 + cpd00238 <=> cpd00101 + cpd00198
ATP:D-ribose-5-phosphate pyrophosphotransferase	cpd00002 + cpd00101 <=> cpd00018 + cpd00103
Acetyl-CoA:L-homoserine O-acetyltransferase	cpd00022 + cpd00227 --> cpd00010 + cpd00790
O-Acetyl-L-homoserine acetate-lyase adding methanethiol	cpd00268 + cpd00790 + cpd11421 <=> cpd00029 + cpd00081 + cpd00135 + cpd11420
O-Acetyl-L-homoserine acetate-lyase adding methanethiol	cpd00239 + cpd00790 --> cpd00029 + cpd00067 + cpd00135
5-Methyltetrahydrofolate:L-homocysteine S-methyltransferase	cpd00135 + cpd00345 <=> cpd00060 + cpd00087
5-Methyltetrahydropteroyltri-L-glutamate:L-homocysteine	cpd00135 + cpd02738 <=> cpd00060 + cpd02555
1-5-Phospho-D-ribosyl-ATP:pyrophosphate phosphoribosyl-transferase	cpd00002 + cpd00103 --> cpd00012 + cpd01775
Phosphoribosyl-ATP pyrophosphohydrolase	cpd00001 + cpd01775 --> cpd00012 + cpd01777
1-5-phospho-D-ribosyl-AMP 1,6-hydrolase	cpd00001 + cpd01777 <=> cpd02979
N-5'-Phospho-D-ribosylformimino-5-amino-1-	cpd02979 <=> cpd02991
Imidazole-glycerol-3-phosphate synthase	cpd00053 + cpd02991 --> cpd00023 + cpd00067 + cpd02843 + cpd02851
D-erythro-1-Imidazol-4-ylglycerol 3-phosphate hydro-lyase	cpd02843 --> cpd00001 + cpd00930
5-Amino-2-oxopentanoate:2-oxoglutarate aminotransferase	cpd00024 + cpd00807 <=> cpd00023 + cpd00930
L-Histidinol-phosphate phosphohydrolase	cpd00001 + cpd00807 --> cpd00009 + cpd00067 + cpd00641
L-Histidinol:NAD+ oxidoreductase	cpd00003 + cpd00641 <=> cpd00004 + cpd00067 + cpd01324
L-Histidinal:NAD+ oxidoreductase	cpd00001 + cpd00003 + cpd01324 <=> cpd00004 + 2 cpd00067 + cpd00119
L-Histidine ammonia-lyase	cpd00119 --> cpd00013 + cpd00581
4,5-Dihydro-4-oxo-5-imidazolepropanoate hydro-lyase	cpd02311 <=> cpd00001 + cpd00581
4-imidazolone-5-propanoate amidohydrolase	cpd00001 + cpd02311 --> cpd00344
N-Formimino-L-glutamate formiminohydrolase	cpd00001 + cpd00344 <=> cpd00023 + cpd00378
N-Formimino-L-glutamate iminohydrolase	cpd00001 + cpd00344 <=> cpd00013 + cpd00770
N-Formyl-L-glutamate amidohydrolase	cpd00001 + cpd00770 <=> cpd00023 + cpd00047
L-aspartate oxidase	cpd00007 + cpd00041 --> cpd00025 + cpd00067 + cpd03470
quinolinate synthase	cpd00095 + cpd03470 --> 2 cpd00001 + cpd00009 + cpd00067 + cpd02333
Nicotinate-nucleotide:pyrophosphate phosphoribosyltransferase	2 cpd00067 + cpd00103 + cpd02333 --> cpd00011 + cpd00012 + cpd00873
Nicotinate D-ribonucleotide:pyrophosphate phosphoribosyltransferase	cpd00012 + cpd00873 <=> cpd00067 + cpd00103 + cpd00218
ATP:nicotinamide-nucleotide adenylyltransferase	cpd00002 + cpd00873 <=> cpd00012 + cpd00638
Deamino-NAD+:ammonia ligase AMP-forming	cpd00002 + cpd00013 + cpd00638 --> cpd00003 + cpd00012 + cpd00018
Deamido-NAD+:L-glutamine amido-ligase AMP-forming	cpd00001 + cpd00002 + cpd00053 + cpd00638 --> cpd00003 + cpd00012 + cpd00018 + cpd00023
ATP:NAD+ 2'-phosphotransferase	cpd00002 + cpd00003 <=> cpd00006 + cpd00008
Membrane asamble. Phospholypids consumption	0.045946 cpd15521 + 0.02106 cpd15522 + 0.045946 cpd15523 + 0.02106 cpd15524 + 0.045946 cpd15525 + 0.02106 cpd15526 + 0.045946 cpd15527 + 3.8 cpd00002 --> membrane + 3.8 cpd00008

	+ 3.8 cpd00009
Protein asamble	0.29579 cpd0051 + 0.21579 cpd00054 + 0.056843 cpd00065 + 0.09158 cpd00084 + 0.61264 cpd00033 + 0.25369 cpd00161 + 0.26316 cpd00023 + 0.26316 cpd00053 + 0.51369 cpd00035 + 0.24105 cpd00041 + 0.24105 cpd00132 + 0.094738 cpd00119 + 0.22106 cpd00129 + 0.29053 cpd00322 + 0.42316 cpd00156 + 0.45053 cpd00107 + 0.34316 cpd00039 + 0.18527 cpd00066 + 0.1379 cpd00069 + 0.15369 cpd00060 + 35 cpd00002 + 35 cpd00001 --> protein + 35 cpd00008 + 35 cpd00009
Biomass production	6.7 cpd00002 + protein + membrane + 6.7 cpd00001 --> biomass + 6.7 cpd00008 + 6.7 cpd00009

Metabolite description	Metabolite *i*
H2O	cpd00001
H2O	cpd00001[p]
ATP	cpd00002
NAD	cpd00003
NADH	cpd00004
NADPH	cpd00005
NADP	cpd00006
O2	cpd00007
ADP	cpd00008
Phosphate	cpd00009
CoA	cpd00010
CO2	cpd00011
PPi	cpd00012
NH3	cpd00013
FAD	cpd00015
AMP	cpd00018
Pyruvate	cpd00020
Acetyl-CoA	cpd00022
L-Glutamate	cpd00023
2-Oxoglutarate	cpd00024
H2O2	cpd00025
D-Glucose	cpd00027
Acetate	cpd00029
Oxaloacetate	cpd00032
L-Glycine	cpd00033
L-Alanine	cpd00035
Succinate	cpd00036
Glyoxalate	cpd00040
L-Aspartate	cpd00041
L-Arginine	cpd00051
L-Glutamine	cpd00053
L-Serine	cpd00054
TPP, Thiaminediphosphate	cpd00056
Phosphoenolpyruvate	cpd00061
Ornithine	cpd00064
L-Tryptophan	cpd00065
H+	cpd00067
H+	cpd00067[p]
Acetaldehyde	cpd00071
D-fructose-6-phosphate	cpd00072
Urea	cpd00073
Nitrite	cpd00075
Nitrite	cpd00075[p]
Succinyl-CoA	cpd00078
D-glucose-6-phosphate	cpd00079
Glycerol-3-phosphate	cpd00080
L-Cysteine	cpd00084
Tetrahydrofolate	cpd00087
Glucose-1-phosphate	cpd00089
2-Oxobutyrate (Oxobutanoate)	cpd00094
Glycerone-phosphate	cpd00095
Glycerol	cpd00100
Glyceraldehyde3-phosphate	cpd00102
Fumarate	cpd00106

Cytochrome c3+ 550 (oxydized) Ferricytochrome	cpd00109[p]
Cytochrome c2+ 550 (reduced) Ferrocytochrome	cpd00110[p]
D-Alanine	cpd00117
Putrescine	cpd00118
5-10-Methylenetetrahydrofolate	cpd00125
L-Proline	cpd00129
L-Malate	cpd00130
L-Asparagine	cpd00132
Homocysteine	cpd00135
Citrate	cpd00137
Glycolate	cpd00139
Hydroxypyruvate	cpd00145
Carbamoylphosphate	cpd00146
Agmatine	cpd00152
Maltose	cpd00179
L-Lactate	cpd00159
L-Threonine	cpd00161
Hydroxylamine	cpd00165
3-Phosphoglycerate	cpd00169
D-Glutamate	cpd00186
beta-D-Glucose	cpd00190
Acetylphosphate	cpd00196
1,3-Bisphospho-D-glycerate	cpd00203
Nitrate	cpd00209
Nitrate	cpd00209[p]
Lipoamide	cpd00213
Glycerate	cpd00223
H2S	cpd00239
H2CO3	cpd00242
Isocitrate	cpd00260
Citrulline	cpd00274
D-fructose-1,6-bisphosphate	cpd00290
cis-Aconitate	cpd00331
N-Acetylornithine	cpd00342
indol	cpd00359
Ethanol	cpd00363
NO	cpd00418[p]
Cystathionine	cpd00424
D-Glyceraldehyde	cpd00448
Dihydrolipoamide	cpd00449
N-Acetyl-L-glutamate	cpd00477
2-Phospho-D-glycerate	cpd00482
N2	cpd00528[p]
Nitrous oxide	cpd00659[p]
O-Acetyl-L-serine	cpd00722
phosphoserine	cpd00738
S-Acetyldihydrolipoamide	cpd00836
L-Glutamate5-semialdehyde	cpd00858
S-Succinyldihydrolipoamide	cpd00860
beta-D-Glucose 6-phosphate	cpd00863
2-Acetamido-5-oxopentanoate	cpd00918
FADH2	cpd00982
3-Phosphonooxypyruvate	cpd02069
L-Glutamyl 5-phosphate	cpd02097
1-Pyrroline-5-carboxylate	cpd02431
n-acetylglutamyl-phosphate	cpd02552
2-Hydroxyethyl-ThPP	cpd03049
Oxalosuccinate	cpd03187
3-Carboxy-1-hydroxypropyl-ThPP	cpd03189
2-Aceto-2-hydroxybutanoate	cpd00498
(R)-3-Hydroxy-3-methyl-2-oxopentanoate	cpd10162
2,3-Dihydroxy-3-methylvalerate	cpd02535
3MOP	cpd00508
L-Isoleucine	cpd00322
ALCTT	cpd00668
2-Oxo-3-hydroxyisovalerate	cpd02569
2,3-Dihydroxy-isovalerate	cpd02498
3-Methyl-2-oxobutanoate	cpd00123
L-Valine	cpd00156
2-Isopropylmalate	cpd01646
2-Isopropylmaleate	cpd01710

3-Isopropylmalate	cpd02693
2-isopropyl-3-oxosuccinate	cpd02605
4MOP	cpd00200
L-Leucine	cpd00107
4-Phospho-L-aspartate	cpd01977
L-Aspartate4-semialdehyde	cpd00346
tetrahydrodipicolinate	cpd02465
meso-2,6-Diaminopimelate	cpd00516
L-Lysine	cpd00039
Cadaverine	cpd01155
N2-acetyl-lysine	cpd01770
D-Erythrose4-phosphate	cpd00236
DAHP	cpd02857
5-Dehydroquinate	cpd00699
Pyrroloquinoline-quinone	cpd00097
Quinate	cpd00248
PQQH2	cpd00986
3-Dehydroshikimate	cpd01716
Shikimate	cpd00383
3-phosphoshikimate	cpd02030
5-O--1-Carboxyvinyl-3-phosphoshikimate	cpd00932
Chorismate	cpd00216
Anthranilate (Vitamin L1)	cpd00093
PRPP	cpd00103
N-5-phosphoribosyl-anthranilate	cpd02642
1-(2-carboxyphenylamino)-1-deoxyribulose 5-phosphat	cpd00956
Indoleglycerol phosphate	cpd02210
Prephenate	cpd00219
Phenylpyruvate	cpd00143
L-Phenylalanine	cpd00066
p-hydroxyphenylpyruvate	cpd00868
L-Tyrosine	cpd00069
D-Xylulose5-phosphate	cpd00198
Sedoheptulose7-phosphate	cpd00238
D-Ribulose5-phosphate	cpd00171
ribose-5-phosphate	cpd00101
L-Homoserine	cpd00227
O-Acetyl-L-homoserine	cpd00790
H2S2O3	cpd00268
trdrd	cpd11421
trdox	cpd11420
Sulfite	cpd00081
5-Methyltetrahydrofolate	cpd00345
L-Methionine	cpd00060
5-Methyltetrahydropteroyltri-L-glutamate	cpd02738
Tetrahydropteroyltri-L-glutamate	cpd02555
Phosphoribosyl-ATP	cpd01775
Phosphoribosyl-AMP	cpd01777
phosphoribosylformiminoaicar-phosphate	cpd02979
phosphoribulosylformimino-AICAR-phosphate	cpd02991
AICAR	cpd02851
D-erythro-imidazol-glycerol-phosphate	cpd02843
imidazole acetol-phosphate	cpd00930
L-histidinol-phosphate	cpd00807
L-Histidinol	cpd00641
L-Histidinal	cpd01324
L-Histidine	cpd00119
Urocanate	cpd00581
4-Imidazolone-5-propanoate	cpd02311
N-Formimino-L-glutamate	cpd00344
Formamide	cpd00378
N-Formyl-L-glutamate	cpd00770
Formate	cpd00047
Iminoaspartate	cpd03470
Quinolinate	cpd02333
Nicotinate ribonucleotide	cpd00873
Niacin (Nicotinic)	cpd00218
Deamido-NAD	cpd00638
Reducedferredoxin	cpd11620
Oxidizedferredoxin	cpd11621
H2	cpd11640

Oxidized azurin	cpd12711[p]
Reduced azurin	cpd12712[p]
2-Demethylmenaquinone 8	cpd15352[p]
2-Demethylmenaquinol 8	cpd15353[p]
Menaquinol 8	cpd15499[p]
Menaquinone 8	cpd15500[p]
Ubiquinone-8	cpd15560[p]
Ubiquinol-8	cpd15561[p]
GTP	cpd00038
IMP	cpd00114
GDP	cpd00031
Adenylosuccinate	cpd02375
L-Argininosuccinate	cpd02152
ACP	cpd11493
Acetyl-ACP	cpd11494
Malonyl-ACP	cpd11492
Malonyl-CoA	cpd00070
Carboxybiotin-carboxyl-carrier protein	cpd12543
Holo-[carboxylase]	cpd12848
Acetoacetyl-ACP	cpd11488
D-3-Hydroxybutanoyl-ACP	cpd11478
But-2-enoyl-ACP	cpd11465
Butyryl-ACP	cpd11464
3-Oxohexanoyl-ACP	cpd11486
D-3-Hydroxyhexanoyl-ACP	cpd11479
(2E)-Hexenoyl-ACP	cpd11473
Hexanoyl-ACP	cpd11472
3-oxooctanoyl-ACP	cpd11490
D-3-Hydroxyoctanoyl-ACP	cpd11483
(2E)-Octenoyl-ACP	cpd11471
Octanoyl-ACP	cpd11470
Octanoate (Caprylic)	cpd03846
3-oxodecanoyl-ACP	cpd11487
D-3-Hydroxydecanoyl-ACP	cpd11482
(2E)-Decenoyl-ACP	cpd11475
Decanoyl-ACP	cpd11474
Decanoate (Capric)	cpd01107
3-oxododecanoyl-ACP	cpd11489
D-3-Hydroxydodecanoyl-ACP	cpd11480
(2E)-Dodecenoyl-ACP	cpd11469
Dodecanoyl-ACP	cpd11468
Dodecanoate (Lauric)	cpd01741
3-oxotetradecanoyl-ACP	cpd11491
D-3-Hydroxytetradecanoyl-ACP	cpd11484
(2E)-Tetradecenoyl-ACP	cpd11467
Myristoyl-ACP	cpd11466
Tetradecanoate (Myristic)	cpd03847
3-oxohexadecanoyl-ACP	cpd11485
D-3-Hydroxypalmitoyl-ACP	cpd11481
(2E)-Hexadecenoyl-ACP	cpd11477
Hexadecanoyl-ACP or Palmitoyl-ACP	cpd11476
Hexadecanoate (Palmitic)	cpd00214
3-Oxooctodecanoyl-ACP	cpd11570
D-3-Hydroxyoctodecanoyl-ACP	cpd11571
(2E)-Octodecanoyl-ACP	cpd11572
Octodecanoyl-ACP	cpd11573
Octadecanoate (Stearic)	cpd01080
Butyryl-CoA	cpd00120
Hexanoyl-CoA	cpd03124
Octanoyl-CoA	cpd01335
Decanoyl-CoA	cpd03128
Lauroyl-CoA	cpd01260
Myristoyl-CoA	cpd01695
Palmitoyl-CoA	cpd00134
Stearoyl-CoA	cpd00327
Arachidoyl-CoA	cpd01393
Hexadecenoyl-CoA	cpd15238
Behenoyl-CoA	cpd16343
Octadecenoyl-ACP	cpd11825
Eicosanoate (Arachidic)	cpd03848
Docosanoate (Behenic)	cpd05196

9Z-Tetradecenoyl-ACP	cpd15294
9Z-Tetradecenoate (Myristoleic)	cpd15298
9Z-Hexadecenoyl-ACP	cpd15239
9Z-Hexadecenoate (Palmitoleic)	cpd15237
9Z-Octadecenoyl-CoA	cpd15274
9Z-Octadecenoate (Oleic) cis	cpd15269
11E-Octadecenoic (trans-Vaccenic) acid	cpd152691
gamma-Linolenoyl-CoA	cpd03849c
gamma-Linolenic acid (Gamolenic)	cpd03849
1-dodecanoyl-sn-glycerol 3-phosphate	cpd15325
1,2-didodecanoyl-sn-glycerol 3-phosphate	cpd15521
1-tetradecanoyl-sn-glycerol 3-phosphate	cpd15331
1,2-ditetradecanoyl-sn-glycerol 3-phosphate	cpd15522
1-tetradec-7-enoyl-sn-glycerol 3-phosphate	cpd15330
1,2-ditetradec-7-enoyl-sn-glycerol 3-phosphate	cpd15523
Palmitoyl-ACP	cpd15277
1,2-dihexadecanoyl-sn-glycerol 3-phosphate	cpd15524
1-hexadec-9-enoyl-sn-glycerol 3-phosphate	cpd15326
1,2-dihexadec-9-enoyl-sn-glycerol 3-phosphate	cpd15525
1-octadecanoyl-sn-glycerol 3-phosphate	cpd15329
1,2-dioctadecanoyl-sn-glycerol 3-phosphate	cpd15526
1-octadec-11-enoyl-sn-glycerol 3-phosphate	cpd15328
1,2-dioctadec-11-enoyl-sn-glycerol 3-phosphate	cpd15527
1-hexadecanoyl-sn-glycerol 3-phosphate	cpd15327
fa11 (iso-C16:0)	cpd11431
fa11coa	cpd11432
1-isoheptadecanoyl-sn-glycerol 3-phosphate	cpd15671
1,2-diisoheptadecanoyl-sn-glycerol 3-phosphate	cpd15677
fa12 (Anteiso-C16:0)	cpd11433
fa12coa	cpd11434
1-anteisoheptadecanoyl-sn-glycerol 3-phosphate	cpd15672
1,2-dianteisoheptadecanoyl-sn-glycerol 3-phosphate	cpd15678
fa1 Tetradecanoate (Myristic)	cpd11430
fa1coa	cpd11435
1-isotetradecanoyl-sn-glycerol 3-phosphate	cpd15673
1,2-diisotetradecanoyl-sn-glycerol 3-phosphate	cpd15679
fa3 (Iso-C14:0)	cpd11436
fa3coa	cpd11437
1-isopentadecanoyl-sn-glycerol 3-phosphate	cpd15674
1,2-diisopentadecanoyl-sn-glycerol 3-phosphate	cpd15680
fa4 (Anteiso-C14:0)	cpd11438
fa4coa	cpd11439
1-anteisopentadecanoyl-sn-glycerol 3-phosphate	cpd15675
1,2-dianteisopentadecanoyl-sn-glycerol 3-phosphate	cpd15681
fa6 (Iso-15:0)	cpd11440
fa6coa	cpd11441
1-isohexadecanoyl-sn-glycerol 3-phosphate	cpd15676
1,2-diisohexadecanoyl-sn-glycerol 3-phosphate	cpd15682
(2E)-Octadecenoyl-CoA	cpd03126b
(S)-3-Hydroxyoctaadecanoyl-CoA	cpd03113b
3-Oxostearatoyl-CoA	cpd03114b
(2E)-Hexadecenoyl-CoA	cpd03126
(S)-3-Hydroxyhexadecanoyl-CoA	cpd03113
3-Oxopalmitoyl-CoA	cpd03114
(2E)-Tetradecenoyl-CoA	cpd03127
(S)-3-Hydroxytetradecanoyl-CoA	cpd03115
3-Oxotetradecanoyl-CoA	cpd12689
(2E)-Dodecenoyl-CoA	cpd02060
(S)-3-Hydroxydodecanoyl-CoA	cpd03116
3-Oxododecanoyl-CoA	cpd03117
(2E)-Decenoyl-CoA	cpd03129
(S)-Hydroxydecanoyl-CoA	cpd03118
3-Oxodecanoyl-CoA	cpd03119
(2E)-Octenoyl-CoA	cpd03130
(S)-Hydroxyoctanoyl-CoA	cpd03120
3-Oxooctanoyl-CoA	cpd03121
(2E)-Hexenoyl-CoA	cpd03125
3-Oxohexanoyl-CoA	cpd03123
(S)-Hydroxyhexanoyl-CoA	cpd03122
Crotonyl-CoA	cpd00650
(S)-3-Hydroxybutyryl-CoA	cpd00842

Acetoacetyl-CoA	cpd00279
Undecanoyl-ACP	cpd11468odd
Undecanoate	cpd01741odd
Tridecanoyl-ACP	cpd11466odd
Tridecanoate	cpd03847odd
Pentadecanoyl-ACP	cpd11476odd
Pentadecanoate	cpd00214odd
Heptadecanoyl-ACP	cpd11573odd
Heptadecanoate (Margaric)	cpd01080odd
membrane	membrane
protein	protein
biomass	biomass

APPENDIX FOUR

Details of nitrification experiments analysed with the nitrifying multispecies SMN model (Chapter 5)

A4.1. Details of (Ahn et al., 2011) experiments

Analysed experiments A, B and D were previously presented in (Ahn et al., 2011) publication. These experiments consisted of a single 11 litters bioreactor operated in continuous mode during 360 days; reactor's dissolved oxygen and Hydraulic retention time (HRT) were changed at specific days to impose different experimental conditions. The calculated experimental data sets A, B and D were generated from the bioreactors performance reported during the period of those experimental conditions. Bioreactor performance was monitored twice a week by measuring nitrogenous compounds concentrations subsequently reported as percentages of reactor removal and accumulation efficiency. Experimental conditions used to calculate the experimental datasets A, B and D are following enlisted:

Variable	Value (mean±std)			Units
Experiment ID	A	B	D	
Experimental process	NH_4^+ oxidation to NO_3^-	NH_4^+ oxidation to NO_3^- *	NH_4^+ oxidation to NO_2^-	
Reactor operation mode	Continuous	Continuous	Continuous	
Reactor working volume (V)	11	11	11	L
Hydraulic retention time (HRT)	1.1	1.1	1.1	d
Flow rate (Q)	10	10	10	L/d
Air flow rate	3	3	3	L/min
pH	7.5	7.5	7.5	
Dissolved oxygen	3.7	1.1	1.1	mg/L
Sludge retention time (SRT)	8.0	3.0	3.0	d
Analysed period from total experiment run	53 to 99	100 to 110	200 to 350	day of experiment
NH_4^+-N feed concentration	500	500	500	mg-N/L
Percentage of NH_4^+-N removed from feed	88.5±5.4	73.6±8.2	83.42±8.5	%
Percentage of N removed converted to NO_2^--N	0.15±0.12	67.6±19.8	91±4.6	%
Percentage of N removed converted to NO_3^--N	99.6±0.21	28.7±18.6	9.5±4.9	%
Percentage of N removed converted to N_2O-N	0.16±0.20	3.5±1.12	0.66±0.15	%
Percentage of N removed converted to NO-N	0.022±0.010	0.175±0.022	0.084±0.033	%
Oxygen uptake rate due NH_4^+ oxidation	2.26±0.34	2.22±0.34	2.33±0.75	$mmolO_2/gCOD*h$
Oxygen uptake rate due NO_2^- oxidation	0.55±0.11	0.58±0.03	0.05±0.15	$mmolO_2/gCOD*h$
AOB biomass concentration**	0.47±0.02	0.56±0.14	0.57±0.31	gCOD/L
NOB biomass concentration**	0.14±0.008	0.19±0.037	0.05±0.03	gCOD/L
Total biomass concentration**	0.54±0.19	0.68±011	0.61±0.32	gCOD/L

(*) Transition period (10 days) from NH_4^+ oxidation to NO_3^- to NH_4^+ oxidation to NO_2^-. Presence of NOB species
(**) Biomass concentrations in grams of COD were calculated by multiplying the number of 16SRNA gene copies for AOB, NOB and bacterial cells quantified by qPCR with the conversion factor $3.9x10^{-13}$ gCOD/16Scopy reported by (Ahn et al., 2008).

Reported NH_4^+-N feed concentrations and percentages of removed nitrogen converted to nitrogenous compounds were used to estimate absolute concentrations of nitrogenous compounds during the analysed period for each experiment. These nitrogenous compound concentrations (in mmol-N/L) were multiplied by bioreactor's flow rate (Q in L/h) and divided by bioreactor's AOB, NOB or total biomass (in gCOD) to obtain production and consumption rates of nitrogenous compounds in mmol-N/gCOD*h units.

A4.2. Details of (Wunderlin et al., 2013) experiments

Analysed experiments C, H and I were previously presented in (Wunderlin et al., 2013; Wunderlin et al., 2012) publications. Both publications reported the same set of 25 batch cultures experiments, each of them initialized by adding a specific amount of nitrogenous substrate; for our analysis; we chose three of these experiments on basis of two criteria: 1) different initial nitrogenous substrate and 2) availability experiment's concentration curves of nitrogenous compounds on publications. Experimental variables used to calculate the experimental datasets C, H and I are following enlisted:

Variable	Absolute value			Units
Experiment ID	C	H	I	
Experimental process	NH_4^+ oxidation to NO_3^-	NO_2^- oxidation to NO_3^-	NH_2OH oxidation to NO_x	
Reactor operation mode	Batch	Batch	Batch	
Reactor working volume (V)	6.9	6.9	6.9	L
Total suspended solids (TSS)	4.1	4.1	4.1	g/L
Air flow rate	1	1	1	L/min
pH	7.1	7.1	7.1	
Dissolved oxygen	1.9	1.1	1.1	mg/L
Nitrogenous substrate in feed	NH_4^+	NO_2^-	NH_2OH	d
N concentration in feed	25	15.5	9.8	mg-N/L
Experiment duration	180	120	360	min

Specific N_2O production rates were reported on (Wunderlin et al., 2012) publication. Nitrogenous substrate uptake rate and NO_2^--N, NO_3^--N production rates were estimated using the formula $rate = (C_1 - C_0)/(t_1 - t_0)$ along with the reported concentration data (C) observed at times t_1 and t_0 (in hours) (Dorian, 1995). In particular these rates were estimated for the reaction phase time period, where concentration curves of these three compounds presented a straight trend (constant slope) therefore indication a temporal steady state in the system. Specific oxygen uptake rates (sOUR) were estimated using the Activated Sludge (ASM) model "C" presented in (Law et al., 2012) (implemented in MS Excel® sheet) by fitting estimated NH_4^+ and NO_2^- and NO_3^+ concentration curves to the corresponding concentration data of experiments' C, H and I. All calculated rates were normalized by bioreactor's AOB, NOB or total biomass expressed as gCOD (measured in Wunderlin et al., (2013) and (2012) studies as TSS and converted to gCOD suing the factor 1.42gCOD/gTSS (Grady et al., 1999)).

A4.3. Details of (Law et al., 2012) experiments

Analysed experiments E, F and G were previously presented in (Law et al., 2011; Law et al., 2012) publications. These experiments consisted of batch cultures enriched with nitrifying biomass and initial ammonium concentration of 500mg-N/L; reactor pH and dissolved oxygen were changed at specific times of the reaction phase to impose different experimental conditions. The calculated experimental data sets E, F and G were generated from the bioreactors performance reported during the period of those experimental conditions. Bioreactor performance was monitored by measuring nitrogenous compounds concentrations. Experimental variables used to calculate the experimental datasets E, F and G are following enlisted:

Variable	Value (mean±std)			Units
Experiment ID	E	F	G	
Experimental process	NH_4^+ oxidation to NO_2^-	NH_4^+ oxidation to NO_2^-	NH_4^+ oxidation to NO_2^-	
Reactor operation mode	Batch	Batch	Batch	
Reactor working volume (V)	1.1	1.1	1.1	L
Volatile suspended solids (MLVSS)	750±50	750±50	750±50	mg/L
Air flow rate	2.5	2.5	2.5	L/min
pH	7	8	8	
Dissolved oxygen	0.55	0.55	1.25	mg/L
Initial NH_4^+-N concentration in feed	500	500	500	mg-N/L
Experimental condition duration	0.5	1.1	0.5	hours

Specific N_2O production and NH_4^+-N consumption rates were directly reported on Law et al., (2011) publication. NO_2^--N production rates were estimated using the formula $rate = (C_1 - C_0)/(t_1 - t_0)$ along with the reported concentration data (C) observed at times t_1 and t_0 (in hours) (Dorian, 1995). NO_2^--N production rates were estimated for the reaction phase time period, where concentration curves of this compound presented a straight trend (constant slope) therefore indication a temporal steady state in the system. Specific oxygen uptake rates (sOUR) were estimated using the Activated Sludge (ASM) model "C" presented in (Law et al., 2012) (implemented in MS Excel® sheet). All calculated rates were normalized by bioreactor's AOB, NOB or total biomass expressed as gCOD (measured in Law et al., 2012 and 2011 studies as MLVSS and converted to gCOD suing the factor 1.42gCOD/gVSS (Grady et al., 1999)).

A4.4. Definition experimental $\hat{X}$ and model estimated X datasets

In **Table A4.1.**, $\hat{X}_t$ is the experimentally observed mean value of the t^{th} variable; Cells in blank of **Table A4.1.** indicate that that variable couldn't be calculated for that particular experiment due lack of information on publication(s). Formulas to calculate variable value values using results of FBA or RS simulations are presented on the right column

Table A4.1. Definition of the 38 variables that describe the metabolic performance of microbial communities.

Variable t ID	Micro-bial popula-tion	Variable t definition and units	Variable values $\hat{X}_t$ in each experiment (mean±std)									Variable calculation formula
			A	B	C	D	E	F	G	H	I	
1	AOB	O_2/NH_4^+ molar yield (mmol-O_2/mmol-N)	2.4±1.03	3.524±0.5	1.459±0	2.406±2.1	1.85±0.096	1.43±0.042	0.98±0.04		0.419±0.1	$v_{ExO2}^{AOBnet}/v_{ExNH4}^{AOBnet}$
2		NO_2^-/NH_4^+ molar yield (mmol-N/mmol-N)	0.99±0.002	0.963±0.01	0.975±0.14	1.005±0.06		0.62±0.2	0.71±0		0.390±0.069	$v_{ExNO2}^{AOBnet}/v_{ExNH4}^{AOBnet}$
3		Cell/NH_4^+ molar yield (mmol-N/mmol-N)	0.032±0.016	0.053±0.006		0.048±0.02						$v_{ExCell}^{AOBnet}/v_{ExNH4}^{AOBnet}$
4		Specific O_2 uptake rate (mmol-O_2/gCOD*h)	2.26±0.34	2.225±0.34	0.203±0.03	2.111±0.7	10.20±0.1	10.25±0.05	11.73±0.042		0.019±0.002	v_{ExO2}^{AOBnet}
5		Specific NH_4^+ uptake rate (mmol-N/gCOD*h)	2.43±0.81	1.445±0.11	0.139±0	2.720±1.6	5.43±0.33	6.96±0.5	11.28±1.12		0.049±0.013	v_{ExNH4}^{AOBnet}
6		Specific N_2O production rate (mmol-N/gCOD*h)	0.004±0.003	0.071±0.02	0.002±0.0007	0.013±0.012	0.01±0.002	0.02±0.001	0.06±0.11		0.005±0.002	v_{ExN2O}^{AOBnet}
7		Specific NO production rate (mmol-N/gCOD*h)	0.0002±0.000			0.0002±0.0001						v_{ExNO}^{AOBnet}
8		Specific NO_2^- production rate (mmol-N/gCOD*h)	2.46±0.813	1.407±0.1	0.136±0.02	2.781±1.7	4.47±0.01	3.73±1.3	9.58±0		0.051±0.01	v_{ExNO2}^{AOBnet}
9	NOB	O_2/NO_2^- molar yield (mmol-O_2/mmol-N)	0.6±0.23		0.468±0.02	-0.394±0.9				0.413±0.12	0.493±0.15	$v_{ExO2}^{NOBnet}/v_{ExNO2}^{NOBnet}$
10		NO_3^-/NO_2^- molar yield (mmol-N/mmol-N)	0.99±0.002			1.635±1.5				0.956±0.17	1.077±0.12	$v_{ExNO3}^{NOBnet}/v_{ExNO2}^{NCBnet}$
11		Cell-N/NO_2^- molar yield (mmol-N/mmol-N)	0.011±0.006	0.047±0.023		0.053±0.05						$v_{ExCell}^{NOBnet}/v_{ExNO2}^{NOBnet}$
12		Specific O_2 uptake rate (mmol-O_2/gCOD*h)	0.55±0.11	0.582±0.032	0.060±0.003	0.019±0.015				0.057±0.008	0.021±0.004	v_{ExO2}^{NOBnet}
13		Specific NO_2^- uptake rate (mmol-N/gCOD*h)	2.3±0.81	0.303±0.26	0.129±0	0.131±0.23				0.151±0.039	0.047±0.017	v_{ExNO2}^{NOBnet}
14		Specific NO_3^- production rate (mmol-N/gCOD*h)	2.4±0.81	0.416±0.27	0.125±0.02	0.286±0.25				0.151±0.059	0.049±0.013	v_{ExNO3}^{NOBnet}
15	COM	Percentage of NH_4^+ oxidation to NO_2^- (%)	88.6±5.4	83.42±8.5	97.6±10	83.42±8.53	82.39±4.1	53.52±5.3	84.89±8		103.6±10.4	$(v_{ExNO2}^{COMnet}/v_{ExNH4}^{COMnet}) * 100$
16	(Full	Percentage of NH_4^+ oxidation to NO_3^- (%)	99.6±0.21	9.51±4.9	90.0±9	9.51±4.9				95.88±9	103.7±7.3	$(v_{ExNO3}^{COMnet}/v_{ExNH4}^{COMnet}) * 100$
17	communi ty)	NO_3^-/NH_4^+ molar yield (mmol-N/mmol-N)		0.29±0.19	0.900±0.14	0.10±0.05						$v_{ExNO3}^{COMnet}/v_{ExNH4}^{COMnet}$

18	NO_2^-/NH_4^+ molar yield (mmol-N/mmol-N)	0.002±0.001	0.68±0.2	0.075±0	0.91±0.05		0.62±0.21	0.71±0		0.060±0.1	$v_{ExNO2}^{COMnet}/v_{ExNH4}^{COMnet}$
19	N_2O/NH_4^+ molar yield (mmol-N/mmol-N)	0.002±0.002	0.05±0.02	0.016±0.001	0.01±0.01	0.0019±0.0002	0.003±0.0003	0.0055±0.0005		0.124±0.06	$v_{ExN2O}^{COMnet}/v_{ExNH4}^{COMnet}$
20	NO/NH_4^+ molar yield (mmol-N/mmol-N)	0.0002±0.0001	0.002±0.0002		0.0008±0.0006						$v_{ExNO}^{COMnet}/v_{ExNH4}^{COMnet}$
21	N_2O/NO_2^- molar yield (mmol-N/mmol-N)								0.100±0.059		$v_{ExN2O}^{COMnet}/v_{ExNO2}^{COMnet}$
22	O_2/N substrae molar yield (mmol-O_2/mmol-N)	2.99±1.19	4.45±0.47	1.892±0.018	2.42±2.3	1.9±1	1.43±0.04	0.98±0.04	0.413±0.12	0.869±0.12	$v_{ExO2}^{COMnet}/v_{ExN}^{COMnet}$
23	Cell-/N substrate molar yield (mmol-N/mmol-N)	0.04±0.02	0.06±0.004		0.05±0.03						$v_{ExCellN}^{COMnet}/v_{ExN}^{COMnet}$
24	Specific oxygen uptake rate (mmol-N/gCOD*h)	2.82±0.35	2.81±0.32	0.264±0.003	2.13±0.84	10.2±0.1	10.25±0.05	11.73±0.04	0.057±0	0.040±0.004	v_{ExO2}^{COMnet}
25	Specific N-substrate uptake rate (mmol-N/gCOD*h)	2.44±0.81	1.44±0.11	0.139±0	2.72±1.64	5.4±0.3	6.96±0.54	11.28±1.12	0.151±0.039	0.049±0.013	v_{ExNH4}^{COMnet}
26	Specific nitrate production rate (mmol-N/gCOD*h)	2.43±0.81	0.42±0.27	0.125±0.02	0.29±0.25				0.151±0.059	0.049±0.013	v_{ExNO3}^{COMnet}
27	Specific nitrite production rate (mmol-N/gCOD*h)	0.01±0.003		0.076±0.019	2.48±1.49	4.5±0.02	3.73±1.3	9.58±0		0.030±0.008	v_{ExNO2}^{COMnet}
28	Specific N_2O production rate (mmol-N/gCOD*h)	0.004±0.003	0.07±0.03	0.002±0	0.02±0.01	0.01±0.002	0.02±0.0012	0.06±0.1	0.013±0.004	0.005±0	v_{ExN2O}^{COMnet}
29	Specific NO production rate (mmol-N/gCOD*h)	0.001±0.000	0.003±0.0005		0.002±0.001						v_{ExNO}^{COMnet}
30	Specific biomass production rate (Cell-N/gCOD*h)	0.09±.001	0.09±0		0.09±0.0						$v_{ExCellN}^{COMnet}$
31	*N. europaea* biomass fraction (%)	52.6±5.3	52.6±5.3	20±2	60.0±6.0	80.24±8	80.24±8	80.24±8	20±2	20±2	$(v_{ExCellN}^{neu}/v_{ExcellN}^{COMnet}) * (100 - f^o)$
32	*N. eutropha* biomass fraction (%)				30.3±3.0	5.25±0.53	5.25±0.53	5.25±0.53			$(v_{ExCellN}^{net}/v_{ExcellN}^{COMnet}) * (100 - f^o)$
33	*N. multiformis* biomass fraction (%)			30±3		5.25±0.53	5.25±0.53	5.25±0.53	30±3	30±3	$(v_{ExCellN}^{nmu}/v_{ExcellN}^{COMnet}) * (100 - f^o)$
34	*N. oceani* biomass fraction (%)					5.25±0.53	5.25±0.53	5.25±0.53			$(v_{ExCellN}^{noc}/v_{ExcellN}^{COMnet}) * (100 - f^o)$
35	*N. defluvii* biomass fraction (%)			25±2.5		1.00±0.1	1.00±0.1	1.00±0.1	25±2.5	25±2.5	$(v_{ExCellN}^{nde}/v_{ExcellN}^{COMnet}) * (100 - f^o)$
36	*N. winogradskyi* biomass fraction (%)	9.7±1	9.7±1	12.5±1	4.5±0.4	1.00±0.1	1.00±0.1	1.00±0.1	12.5±1	12.5±1	$(v_{ExCellN}^{nwi}/v_{ExcellN}^{COMnet}) * (100 - f^o)$

37	*N. hamburgensis* biomass fraction (%)	9.7±1	9.7±1	12.5±1	4.5±0.4	1.00±0.1	1.00±0.1	1.00±0.1	12.5±1	12.5±1	$(v_{ExCellN}^{nha}/v_{ExcellN}^{COMnet}) * (100 - f^o)$
38	*N. gracilis* biomass fraction (%)					1.00±0.1	1.00±0.1	1.00±0.1			$(v_{ExCellN}^{nsp}/v_{ExcellN}^{COMnet}) * (100 - f^o)$
M	Number of variables in dataset	31	29	26	33	20	22	22	17	26	

$v_j^{AOBnet} = v_j^{neu} + v_j^{net} + v_j^{nmu} + v_j^{noc}$

$v_j^{NOBnet} = v_j^{nde} + v_j^{nwi} + v_j^{nha} + v_j^{nsp}$

$v_j^{COMnet} = v_j^{neu} + v_j^{net} + v_j^{nmu} + v_j^{noc} + v_j^{nde} + v_j^{nwi} + v_j^{nha} + v_j^{nsp}$

$f^o =$ biomass percentage fraction of non-nitrifying organism.

A4.5. Parameters used for FBA and RS simulation algorithms.

The objective function Z used in FBA was to maximize the total community biomass production rate ($v_{Ex-biomass}^{COM}$). In the case of RS simulations Monte-Carlo sampling of the solution space constrained by the reaction rate limits α_j^k and β_j^k was performed using the artificial centering hit-and-run algorithm to obtain a flux distribution matrix P $(n \times p)$, where p was the number of samples taken and n was the number of reactions for each sample (Kaufman and Smith, 1998; Price et al., 2004; Schellenberger and Palsson, 2009; Thiele et al., 2005), As shown in Figure 5.5., each row of the P matrix was a set of n rate values (v_j^k) that were used to analyse the estimated rates statistically by obtaining frequency distributions, median, mean, standard deviation and range values that where posteriorly compared against experimental rate values. To ensure a uniform sampling of the full solution space in each RS simulation, 50,000 feasible flux distributions were sampled with 200 iterations between them

APPENDIX FIVE

Copyright for Figures 2.5 and 2.6

NATURE PUBLISHING GROUP LICENSE
TERMS AND CONDITIONS

Aug 05, 2014

This is a License Agreement between The Unviersity of Auckland ("You") and Nature Publishing Group ("Nature Publishing Group") provided by Copyright Clearance Center ("CCC"). The license consists of your order details, the terms and conditions provided by Nature Publishing Group, and the payment terms and conditions.

All payments must be made in full to CCC. For payment instructions, please see information listed at the bottom of this form.

License Number	3442290987237
License date	Aug 05, 2014
Licensed content publisher	Nature Publishing Group
Licensed content publication	Nature Reviews Microbiology
Licensed content title	Constraining the metabolic genotype–phenotype relationship using a phylogeny of *in silico* methods
Licensed content author	Nathan E. Lewis, Harish Nagarajan, Bernhard O. Palsson
Licensed content date	Feb 27, 2012
Volume number	10
Issue number	4
Type of Use	reuse in a dissertation / thesis
Requestor type	academic/educational
Format	print and electronic
Portion	figures/tables/illustrations
Number of figures/tables /illustrations	1
High-res required	no
Figures	Figure 2 | The 'phylogeny' of constraint-based modelling methods
Author of this NPG article	no
Your reference number	None
Title of your thesis / dissertation	Metabolic network modelling and metabolomics to analyse nitrous oxide production in biological nitrogen removal processes
Expected completion date	Aug 2014
Estimated size (number of pages)	250
Total	0.00 USD
Terms and Conditions	

Terms and Conditions for Permissions

Nature Publishing Group hereby grants you a non-exclusive license to reproduce this material for this purpose, and for no other use,subject to the conditions below:

1. NPG warrants that it has, to the best of its knowledge, the rights to license reuse of this material. However, you should ensure that the material you are requesting is original to Nature Publishing Group and does not carry the copyright of another entity (as credited in the published version). If the credit line on any part of the material you have requested indicates that it was reprinted or adapted by NPG with permission from another source, then you should also seek permission from that source to reuse the material.

2. Permission granted free of charge for material in print is also usually granted for any electronic version of that work, provided that the material is incidental to the work as a

NATURE PUBLISHING GROUP LICENSE
TERMS AND CONDITIONS

Aug 05, 2014

This is a License Agreement between The Unviersity of Auckland ("You") and Nature Publishing Group ("Nature Publishing Group") provided by Copyright Clearance Center ("CCC"). The license consists of your order details, the terms and conditions provided by Nature Publishing Group, and the payment terms and conditions.

All payments must be made in full to CCC. For payment instructions, please see information listed at the bottom of this form.

License Number	3442300266840
License date	Aug 05, 2014
Licensed content publisher	Nature Publishing Group
Licensed content publication	Nature Protocols
Licensed content title	A protocol for generating a high-quality genome-scale metabolic reconstruction
Licensed content author	Ines Thiele, Bernhard Ø Palsson
Licensed content date	Jan 7, 2010
Volume number	5
Issue number	1
Type of Use	reuse in a dissertation / thesis
Requestor type	academic/educational
Format	print and electronic
Portion	figures/tables/illustrations
Number of figures/tables /illustrations	1
High-res required	no
Figures	Figure 7: Conversion of reconstruction into a condition-specific model.
Author of this NPG article	no
Your reference number	None
Title of your thesis / dissertation	Metabolic network modelling and metabolomics to analyse nitrous oxide production in biological nitrogen removal processes
Expected completion date	Aug 2014
Estimated size (number of pages)	250
Total	0.00 USD
Terms and Conditions	

Terms and Conditions for Permissions

Nature Publishing Group hereby grants you a non-exclusive license to reproduce this material for this purpose, and for no other use,subject to the conditions below:

1. NPG warrants that it has, to the best of its knowledge, the rights to license reuse of this material. However, you should ensure that the material you are requesting is original to Nature Publishing Group and does not carry the copyright of another entity (as credited in the published version). If the credit line on any part of the material you have requested indicates that it was reprinted or adapted by NPG with permission from another source, then you should also seek permission from that source to reuse the material.

2. Permission granted free of charge for material in print is also usually granted for any

electronic version of that work, provided that the material is incidental to the work as a whole and that the electronic version is essentially equivalent to, or substitutes for, the print version. Where print permission has been granted for a fee, separate permission must be obtained for any additional, electronic re-use (unless, as in the case of a full paper, this has already been accounted for during your initial request in the calculation of a print run). NB: In all cases, web-based use of full-text articles must be authorized separately through the 'Use on a Web Site' option when requesting permission.

3. Permission granted for a first edition does not apply to second and subsequent editions and for editions in other languages (except for signatories to the STM Permissions Guidelines, or where the first edition permission was granted for free).

4. Nature Publishing Group's permission must be acknowledged next to the figure, table or abstract in print. In electronic form, this acknowledgement must be visible at the same time as the figure/table/abstract, and must be hyperlinked to the journal's homepage.

5. The credit line should read:
   Reprinted by permission from Macmillan Publishers Ltd: [JOURNAL NAME] (reference citation), copyright (year of publication)
   For AOP papers, the credit line should read:
   Reprinted by permission from Macmillan Publishers Ltd: [JOURNAL NAME], advance online publication, day month year (doi: 10.1038/sj.[JOURNAL ACRONYM].XXXXX)

   Note: For republication from the *British Journal of Cancer*, the following credit lines apply.
   Reprinted by permission from Macmillan Publishers Ltd on behalf of Cancer Research UK: [JOURNAL NAME] (reference citation), copyright (year of publication)For AOP papers, the credit line should read:
   Reprinted by permission from Macmillan Publishers Ltd on behalf of Cancer Research UK: [JOURNAL NAME], advance online publication, day month year (doi: 10.1038/sj.[JOURNAL ACRONYM].XXXXX)

6. Adaptations of single figures do not require NPG approval. However, the adaptation should be credited as follows:

   Adapted by permission from Macmillan Publishers Ltd: [JOURNAL NAME] (reference citation), copyright (year of publication)

   Note: For adaptation from the *British Journal of Cancer*, the following credit line applies.
   Adapted by permission from Macmillan Publishers Ltd on behalf of Cancer Research UK: [JOURNAL NAME] (reference citation), copyright (year of publication)

7. Translations of 401 words up to a whole article require NPG approval. Please visit http://www.macmillanmedicalcommunications.com for more information. Translations of up to a 400 words do not require NPG approval. The translation should be credited as follows:

   Translated by permission from Macmillan Publishers Ltd: [JOURNAL NAME] (reference citation), copyright (year of publication).

   Note: For translation from the *British Journal of Cancer*, the following credit line applies.
   Translated by permission from Macmillan Publishers Ltd on behalf of Cancer Research UK: [JOURNAL NAME] (reference citation), copyright (year of publication)

We are certain that all parties will benefit from this agreement and wish you the best in the use of this material. Thank you.

Special Terms:

v1.1

You will be invoiced within 48 hours of this transaction date. You may pay your invoice by credit card upon receipt of the invoice for this transaction. Please follow instructions provided at that time.
To pay for this transaction now; please remit a copy of this document along with your payment. Payment should be in the form of a check or money order referencing your account number and this invoice number RLNK501369296.
Make payments to "COPYRIGHT CLEARANCE CENTER" and send to:

Copyright Clearance Center
Dept 001
P.O. Box 843006
Boston, MA 02284-3006
Please disregard electronic and mailed copies if you remit payment in advance.
Questions? customercare@copyright.com or +1-855-239-3415 (toll free in the US) or +1-978-646-2777.

Gratis licenses (referencing $0 in the Total field) are free. Please retain this printable license for your reference. No payment is required.